Solubility studies on ligands in supercritical carbon dioxide medium and their application to extraction of actinides

By

K CHINARAGA PITCHAIAH

Enrollment No: CHEM02201204002

Indira Gandhi Centre for Atomic Research, Kalpakkam

A thesis submitted to the

Board of Studies in Chemical Sciences

In partial fulfillment of requirements

for the Degree of

DOCTOR OF PHILOSOPHY

of

HOMI BHABHA NATIONAL INSTITUTE

February, 2018

Homi Bhabha National Institute

Recommendations of the Viva Voce Committee

As members of the Viva Voce Committee, we certify that we have read the dissertation prepared by **K Chinaraga Pitchaiah** entitled **"Solubility studies on ligands in supercritical carbon dioxide medium and their application to extraction of actinides"** and recommend that it may be accepted as fulfilling the thesis requirement for the award of Degree of Doctor of Philosophy.

Chairman - Prof. M. Joseph **Date:** 26/10/18

Guide / Convener – Prof. N. Sivaraman N. Sivaraman **Date:** 26.10.18

Examiner – Prof. Tamal Banerjee **Date:** 26/10/18

Member 1- Prof. K. Ananthasivan **Date:** 26/10/18

Member 2- Prof. B.S. Panigrahi Panigrahi **Date:** 26.10.18

Final approval and acceptance of this thesis is contingent upon the candidate's submission of the final copies of the thesis to HBNI.

I/We hereby certify that I/we have read this thesis prepared under my/our direction and recommend that it may be accepted as fulfilling the thesis requirement.

Date: Kalpakkam

Place: 26.10.18

N. Sivaraman 26.10.18
Prof. N. Sivaraman

STATEMENT BY AUTHOR

This dissertation has been submitted in partial fulfillment of requirements for an advanced degree at Homi Bhabha National Institute (HBNI) and is deposited in the Library to be made available to borrowers under rules of the HBNI.

Brief quotations from this dissertation are allowable without special permission, provided that accurate acknowledgement of source is made. Requests for permission for extended quotation from or reproduction of this manuscript in whole or in part may be granted by the Competent Authority of HBNI when in his or her judgment the proposed use of the material is in the interests of scholarship. In all other instances, however, permission must be obtained from the author.

25/10/2018

K Chinaraga Pitchaiah

DECLARATION

I, hereby declare that the investigation presented in the thesis has been carried out by me. The work is original and has not been submitted earlier as a whole or in part for a degree / diploma at this or any other Institution / University.

25|10|2018

K Chinaraga Pitchaiah

List of Publications arising from the thesis

---

1. Journal

[1] **K.C. Pitchaiah**, N. Lamba, J. Deepitha, N. Sivaraman, P.K. Mohapatra, Giridhar Madras, Experimental measurements and correlation of the solubility of *N,N*-dialkylamides in supercritical carbon dioxide, *J. Supercrit. Fluids,* 143 (2019) 162-170.

[2] **K.C. Pitchaiah**, N. Lamba, N. Sivaraman, Giridhar Madras, Solubility of trioctylmethylammonium chloride in supercritical carbon dioxide and the influence of co-solvents on the solubility behavior, *J. Supercrit. Fluids* 138 (2018) 102-114.

[3] **K.C. Pitchaiah**, C.V.S.B. Rao, N. Sivaraman, M. Joseph, Giridhar Madras, I. Brondz, Solubility of dialkylalkyl phosphonates in supercritical carbon dioxide: Experimental and modeling approach, *Fluid Phase Equilib.* 435 (2017) 88-97.

[4] **K.C. Pitchaiah**, N. Sivaraman, M. Joseph, P. Mohapatra, Giridhar Madras, Solubility of tri-iso-amyl phosphate in supercritical carbon dioxide and its application to selective extraction of uranium, *Sep. Sci. Technol.* 52 (2017) 2224-2237.

[5] **K.C. Pitchaiah**, N. Sivaraman, N. Lamba, Giridhar Madras, Experimental determination and model correlation for the solubilities of trialkyl phosphates in supercritical carbon dioxide, *RSC Adv.* 6 (2016) 51286-51295.

[6] **K.C. Pitchaiah**, K. Sujatha, C.V.S.B. Rao, S. Subramaniam, N. Sivaraman, P.R.V. Rao, Supercritical fluid extraction of uranium and thorium from nitric acid medium using organophosphorous compounds, *Radiochim. Acta* 103 (2015) 245-255.

[7] **K.C. Pitchaiah**, K. Sujatha, C.V.S.B. Rao, N. Sivaraman, T.G. Srinivasan, K. Nagarajan, P.R.V. Rao, Influence of co-solvent on the extraction behaviour of uranium and thorium nitrates with organophosphorous compounds, *Int. J. Anal. Mass. Spectrom. Cromatogr.* 2 (2014) 33-42.

[8] **K.C. Pitchaiah**, K. Sujatha, J. Deepitha, Suddhasattwa Ghosh, N. Sivaraman, Recovery of uranium and plutonium from pyrochemical salt matrix using supercritical fluid extraction, *J. Supercrit. Fluids (In press),* doi:10.1016/j.supflu.2018.10.015

2. Conferences

[1] **K.C. Pitchaiah**, J. Deepitha, C.V.S.B. Rao, N. Sivaraman, Solubility of H-phosphonates in supercritical carbon dioxide: Experimental and modeling approach, *Proc. of Symposium on Emerging Trends in Separation Science and Technology*, BITS-Pilani, Goa, May 23- 26, 2018, pp.208.

[2] **K.C. Pitchaiah**, N. Sivaraman, P.K. Mohapatra, Measurement and correlation of solubility of *N*,*N*-dihexyloctanamide in supercritical carbon dioxide, *Proc. of Symposium on Nuclear and Radiochemistry*, Bhubaneswar, February 6- 10, 2017.

[3] **K.C. Pitchaiah**, N. Sivaraman, Giridhar Madras, Experimental determination and correlation of solubility of *n*-trioctylmethylammonium chloride in supercritical carbon dioxide, *Proc. of Symposium on Emerging Trends in Separation Science and Technology* , Guwahati, May 17- 20, 2016, pp. 87.

[4] N. Sivaraman, **K.C. Pitchaiah**, A. Suresh, Giridhar Madras, Solubility of tri-*iso*-amyl phosphate in supercritical carbon dioxide: Experimental and modeling approach, *Proc. of Symposium on Emerging Trends in Separation Science and Technology*, Guwahati, May 17- 20, 2016, pp. 88.

[5] **K.C. Pitchaiah**, C.V.S.B. Rao, N. Sivaraman, P.R.V. Rao, Solubility of diamylamyl phosphonate in supercritical carbon dioxide, *Proc. of Symposium on Chemistry in Nuclear Technology* , Kalpakkam, July 30-31, 2015, pp. 22.

[6] **K.C. Pitchaiah**, K. Sujatha, C.V.S.B. Rao, N. Sivaraman, K. Nagarajan, P.R.V. Rao, Supercritical fluid extraction of uranium and thorium nitrates using carbon dioxide modified with phosphonates, *Proc. of Symposium on Emerging Trends in Separation Science and Technology*, Mumbai, February 25- 28, 2014, pp. 94.

[7] K. Sujatha, **K.C. Pitchaiah**, B.P. Reddy, N. Sivaraman, T.G. Srinivasan, K. Nagarajan, P.R.V. Rao, Supercritical fluid extraction and recovery of uranium from chloride salt matrix, *Proc. of International Nuclear Fuel Cycle Conference (Global)*, Salt Lake City, Utah, USA, Sept 29 – Oct 3, 2013.

25|10|2018

K Chinaraga Pitchaiah

ACKNOWLEDGEMENTS

I wish to express my sincere gratitude to my research supervisor ***Prof. N. Sivaraman*** who encouraged me to take up this work and under whose guidance this thesis took the present shape. I take great pleasure to thank him for his support, guidance, valuable suggestions and encouragement throughout the course of this work.

I am very grateful to ***Prof. Giridhar Madras, IISc, Bangalore***, for giving me an opportunity for interacting with his research group. His valuable suggestions and scientific discussions are highly stimulating throughout my research. I would like to thank my coworker and friend ***Ms. Neha Lamba, IISc, Bangalore,*** for all her support, collaboration and discussions on various chemical engineering aspects. I would like to thank ***Prof. P. K. Mohapatra, BARC, Mumbai,*** for his help in synthesis of amides for supercritical studies and many discussions.

I express my sincere gratitude to my doctorial committee chairman, ***Prof. M. Joseph*** and members, ***Prof. K. Ananthasivan***, ***Prof. B.S. Panigrahi*** and ***Prof. C. Mallika*** (formerly Doctoral committee chairman) for their valuable suggestions and constant encouragement.

I wish to express my special thanks to ***Prof. C.V.S. Brahmmanada Rao*** for his help and valuable suggestions. I would like to thank ***Dr. Suddhasattwa Ghosh, Prof. A. Suresh and Prof. V. Jayaraman*** for suggestions and corrections in thesis.

I would like to thank ***Dr. N. Ramanathan*** for IR spectra***,*** ***Dr. Satyabrata Mishra*** for GC analysis and ***Mr. Dhrubajyoti Das***, VIT University, Vellore for NMR and GC-MS data.

It is a pleasure to thank my friends, ***Dr. G.V.S Ashok Kumar, Dr. B. Sreenivasulu, Mr. Debasish Saha*** and ***Dr. K. Sujatha*** for their help and wishes. I am also grateful to all my sectional colleagues for their co-operation and support.

I am extremely thankful to my family for their support and encouragement.

25/10/2018

K Chinaraga Pitchaiah

CONTENTS

ABSTRACT

The recovery of actinides using solvent extraction technique involves use of diluent, leading to generation of secondary liquid waste. Literature data on the extraction and recovery of actinides using supercritical fluids are relatively scarce; data for the following is limited or not available: (i) recovery of actinides from a dissolver solution of spent nuclear fuel (ii) pre-concentration and recovery of actinides from aqueous waste stream (iii) selective extraction of uranium over thorium (iv) recovery of actinides such as plutonium and uranium from chloride salt waste of pyrochemical processing. The main objective of the present study is to develop supercritical fluid extraction (SFE) based methods (an alternate to solvent extraction technique) for the recovery of actinides from different matrices with minimum generation of liquid secondary waste.

The development of an SFE method for the recovery of actinide ions involves: (a) identification of actinide specific ligands (b) selection of ligand based on the nature of matrix, i.e. recovery of actinides from diverse matrices such as solid matrices (cellulose, pyrochemical inorganic salts) and liquid matrix (nitric acid medium) – this is quite crucial as recovery of actinides from various matrices depends on their interaction with the base material of the matrix (c) solubility of actinide specific ligands of interest in supercritical carbon dioxide (SCCO$_2$) medium and optimization of experimental conditions, namely, temperature, pressure, co-solvent composition and (d) use of SCCO$_2$ containing ligand for recovery of actinides.

In connection with the above, solubility of variety of ligands from the family of trialkyl phosphates, dialkylalkyl phosphonates, *N*,*N*-dialkylamides and quarternary ammonium based ionic liquids was measured as a function of pressure, temperature and in some cases as a function of co-solvent composition. These compounds were chosen

based on their ability to extract actinides as (i) neutral solvates (trialkyl phosphates), (ii) extraction from lean streams (stronger and more basic extractant, phosphonate based molecules), (iii) neutral solvates with better properties to radiation (amides) and (iv) extraction through ion-pair complexes (quarternary ammonium compound). The solubility data of ligands are correlated using various semi-empirical equations; new models were developed for the correlation of solubility of liquid solutes in $SCCO_2$ medium in the presence of co-solvents.

Based on these studies, SFE based methods were developed and demonstrated for the recovery of actinides from diverse matrices of the following (i) extraction of uranium, thorium from solid matrices as well as from acidic waste medium; (ii) selective extraction of uranium from thorium using $SCCO_2$ containing branched trialkyl phosphates (iii) selective extraction of uranium from representative fission products using $SCCO_2$ containing phosphonates and (iv) recovery of plutonium and uranium from chloride salt matrix using $SCCO_2$ containing trioctylmethylammonium chloride. Preliminary studies were also carried out towards scaling-up of a typical SFE method for the recovery of uranium from chloride salt matrix.

These studies have established promising applications of supercritical fluid based extraction based methods for the recovery of actinides from diverse matrices.

SYNOPSIS

The nuclear fuel cycle is associated with the series of process steps beginning from uranium mining, uranium enrichment, fuel fabrication, reactor operation, spent fuel reprocessing and waste management. Conventional methods such as liquid-liquid extraction, ion exchange and precipitation based techniques are extensively employed for separation and purification of actinides. However, use of these well-established methods lead to generation of secondary liquid waste. Therefore, there is strong impetus for the development of eco-friendly solvents that can reduce the waste generation and with reduced radiotoxic burden to the environment. The most prevalent of these solvent systems include supercritical fluids [1]. Supercritical fluid extraction (SFE) is a technique that uses a supercritical fluid (SCF) as a solvent for the extraction/recovery/separation of an analyte of interest from a matrix with minimum generation of liquid secondary waste, as CO_2 becomes gas after the extraction. SFE has many advantages over conventional liquid-liquid extraction and is a potential alternate technique to conventional liquid-liquid extraction [2].

SFE using carbon dioxide is widely employed for the extraction of a variety of compounds from both solid and liquid matrices. Several industrial plants are in operation for decaffeination of coffee, extraction of hop constituents, oils from leaves, fruits, seeds, spices etc. [3]. SFE of heavy metals, lanthanides and actinides from different matrices has been studied using $SCCO_2$ containing various ligands [4-6]. SFE based methods are also developed and demonstrated from our laboratory for the recovery of actinides [7]. The supercritical extraction of metal ions demands extensive knowledge on the solubility of ligands in $SCCO_2$ medium. The direct extraction of metal ions using neat $SCCO_2$ is not feasible because of weak solute-solvent interaction and charge neutralization requirements [8]. However, when metal ions are complexed with suitable ligands, the resulting metal-ligand complexes become quite soluble in $SCCO_2$ medium [9]. Thus, the solubility of ligand as well as that of metal complex in supercritical carbon dioxide medium plays an important role in designing a SFE process of metal ions.

Thus the use of SFE method for recovery of actinides can result in minimum generation of liquid secondary waste compared to traditional separation techniques. The literature data on the extraction and recovery of actinides ions using supercritical fluids are very limited. There is not enough SFE data in the literature for (a) recovery of actinides from dissolver solution of spent fuel and (b) for pre-concentration and recovery of actinides from aqueous waste stream. Use of pyrochemical-high temperature electrochemical process for recovery of actinides also results in the generation of salt waste containing precious actinides and there is no literature available for their recovery. Thus the motivation behind the work is to explore use of SFE based methods for the recovery of actinides from such waste streams and matrices.

The measurement of solubility of ligand in supercritical carbon dioxide is the first and fundamental step towards achieving the above objectives. Hence solubility of variety of ligands namely, trialkyl phosphates, dialkylalkyl phosphonates *N*,*N*-dialkylamides and quaternary ammonium based compounds are measured in $SCCO_2$ medium. The solubility data are correlated with various semi-empirical equations. Subsequently, $SCCO_2$ containing ligands are examined for the recovery of actinides from various waste matrices such as (i) recovery of uranium from nitric acid medium (ii) selective recovery of uranium from fission product elements and (iii) extraction and recovery of actinides from pyrochemical chloride salt matrix. The actinide specific ligands are chosen based on the solvent extraction literature data. Among the actinide specific ligands, further they are chosen based on the nature of matrix in which actinides are sorbed / complexed. For e.g. actinides in aqueous medium can be recovered using neutral extractants / ligands (trialkyl phosphates / dialkylalkyl phosphonates); actinides in lean streams can be pre-concentrated using stronger actinide specific dialkylalkyl phosphonate based ligands; recovery of actinides from chloride salt matrix demands use of ligands which are capable of forming ion-pair complex with actinides, e.g. quaternary ammonium ligands e.g. TOMAC. Thus appropriate ligands are chosen and employed for the recovery of actinides from diverse matrices.

Several semi-empirical models are available in the literature to correlate the solubilities of solid and liquid solutes in $SCCO_2$. However, models to correlate the solubility of liquid solutes in $SCCO_2$ in the presence of co-solvent are scarce. Two new models have been developed to correlate the solubilities of liquid solute in $SCCO_2$ in presence of co-solvents, using association theory based on Wilson and van Laar activity coefficient models. These new models have been successfully employed for the correlation of solubility of trioctylmethylammonium chloride (TOMAC) in $SCCO_2$ in presence of co-solvents.

This thesis is divided into eight chapters and a brief description of each chapter is given below

Chapter 1: Introduction

This chapter deals with the basic introduction about separation sciences, its significance in the nuclear industry and need for the development of green separation techniques. A brief introduction to supercritical fluids and their advantages over conventional extraction using organic solvents are presented. The emergence of supercritical fluid extraction based technique as an alternative to conventional separation techniques in nuclear fuel cycle is highlighted. The importance of theoretical and experimental aspects of supercritical fluids to develop a SFE process is discussed. The necessity for solubility measurements on actinide specific ligands and need for use of semi-empirical equations for solubility correlations are discussed. Current literature status on solubility measurements and SFE of actinides from various matrices are discussed.

The major motivation of the present study, i.e. developing supercritical fluid extraction based methods for recovery of actinides from diverse matrices is highlighted. The objectives, gap areas, and methodology followed towards achieving these are discussed.

Chapter 2: Experimental methods and semi-empirical models

Chapter 2 is composed of two sub chapters. Chapter 2(a) provides a brief overview of chemicals, instruments, experimental set-up and general experimental procedures adopted in the present study. The synthesis and characterization of various ligands employed in the present study are discussed. The general procedure adopted for the solubility measurements is discussed. Validation of experimental procedure employed for the solubility measurement is described. The methodologies for the estimation of actinides using high pressure liquid chromatograph (HPLC) and liquid scintillation counting (LSC) technique are presented. Various semi-empirical models employed for the solubility correlations are described. Chapter 2(b) deals with various semi-empirical models employed in this thesis for correlating experimental solubilities.

Chapter 3: Experimental determination and correlation of solubility of trialkyl phosphates in supercritical carbon dioxide

Chapter 3 deals with the experimental determination and mathematic modeling of solubilities of trialkyl phosphonates in $SCCO_2$. Trialkyl phosphates are candidate materials (ligands) in nuclear fuel reprocessing and hence the solubilities of a series of trialkyl phosphates in $SCCO_2$ medium were measured at 313- 333 K with pressure ranging from 10-25 MPa and the results are discussed. The experimental solubilities are correlated using different semi-empirical equations such as Chrastil equation, Mendez-Teja (MT) model and association theory based van Laar activity coefficient model and the results are presented. This approach provides an easy method to estimate unknown solubilities of other members of trialkyl phosphate series as well as to predict the solubilities of these compounds at different temperatures and pressures.

Chapter 4: Solubilities of dialkylalkyl phosphonates in supercritical carbon dioxide

Dialkylalkyl phosphonates have found renewed interest in the selective extraction of actinides from dilute waste streams. This chapter describes the solubilities of two dialkylalkyl phosphonates, namely, dibutylbutyl phosphonate (DBBP) and diamylamyl phosphonate (DAAP) in $SCCO_2$ medium and correlate solubilities using various fundamental properties of supercritical fluids. Solubilities of dialkylalkyl phosphonates are correlated using MT model, Chrastil equation, solution theory with Wilson activity coefficient model and association model based on van Laar activity coefficient model and results are explained in detail. Comparison among these models revealed that the association model with van Laar activity coefficient model provides better solubility predictions.

Chapter 5: Solubility of trioctylmethylammonium chloride in supercritical carbon dioxide with co-solvent and development of new models for ternary solubilities

Chapter 5 is divided into two sub chapters. Chapter 5(a) deals with the measurement of solubility of trioctylmethylammonium chloride (TOMAC) in $SCCO_2$ in the presence of different co-solvents. Recovery of actinides from complex salt mixture demands use of ion-pair reagents / ionic liquids and in this context, solubility studies on TOMAC in $SCCO_2$ are carried out at different temperatures and pressures. The influence of co-solvent and its concentration on the solubility behavior have been studied. The solubility of TOMAC in neat $SCCO_2$ medium is successfully correlated using semi-empirical models. Chapter 5(b) describes the development of new models for the correlation of solubility of liquid solutes in $SCCO_2$ in the presence of co-solvents (ternary solubilities) and two new models are derived.

Chapter 6: Solubility of *N,N*-dialkylamides in supercritical carbon dioxide: Experimental and modeling approach

The dialkylamides are potential alternate candidates to trialkyl phosphates for actinide recovery and extraction, as these ligands are resistant to hydrolysis and radiolysis, innocuous nature of their degradation products and possibility of complete incineration leading to reduction in the liquid secondary waste. Hence the solubility behavior of three straight chain amides (dihexylhexanamide, dihexyloctanamide and dihexylhexanamide) and three branched amides (di-2-ethylhexylacetamide, di-2-ethylhexyl-*iso*-butyramide and di-2-ethylhexylpivalamide) are examined in $SCCO_2$ medium. The experimental solubilities are correlated using various semi-empirical models.

Chapter 7: Supercritical fluid extraction studies of actinides from different matrices using modified supercritical carbon dioxide

The applications of SFE technique towards actinide recovery from various matrices are discussed. Actinides such as uranium, thorium and plutonium are to be recovered from aqueous medium to minimize the radiotoxicity on the liquid waste; similarly, separation of uranium from thorium is of primary importance in thorium fuel cycle; chloride salt waste arising from pyrochemical process contains residual actinides and these have to be removed in order to minimize the volume of high level liquid waste. An attempt has been made in this study to employ $SCCO_2$ containing ligands for recovery of actinides from these matrices.

This chapter consists of three sub chapters. Chapter 7(a) focuses on the extraction / recovery of actinides from nitric acid media Chapter 7(b) mainly emphasizes the use of TiAP and DAAP for the selective extraction of uranium from fission products. Chapter 7(c) deals with the recovery of actinides from pyrochemical salt matrix using $SCCO_2$ containing TOMAC. This chapter also describes the semi-preparative scale extraction of uranium from salt matrix. This study is first of its kind towards the recovery of actinides from chloride salt matrix.

Chapter 8: Conclusions and Discussions

This chapter consists of conclusions drawn from the present studies and discussions on future directions. The future scope of research in supercritical fluid based techniques has been highlighted, which includes measurement of solubility of actinide complexes in SCF medium. This chapter gives a brief outline about the possible outcomes and future directions that could be derived from the present work.

Reference

1. P. Pollet, E. A. Davey, E. E. Ureña-Benavides, C. A. Eckert and C. L. Liotta, *Green Chem.*, 2014, 16, 1034-1055.
2. M. A. McHugh and V. J. Krukonis, *Supercritical fluid extraction: principles and practice*, Butterworth-Heinemann, Boston, MA, 2nd edn., 1994.
3. Z. Kenz, E. Markocic, M. Leitgeb, M. Primozic, M. K. Hrnviv and M. Skerget, *Energy*, 2014, 77, 235-243.
4. Y. Lin, R. D. Brauer, K. E. Laintz and C. M. Wai, *Anal. Chem.*, 1993, 65, 2549-2551.
5. N. G. Smart, T. E. Carleson, S. Elshani, S. Wang and C. M. Wai, *Ind. Eng. Chem. Res.*, 1997, 36, 1819-1826.
6. B. J. Mincher, R. V. Fox, R. G. G. Holmes, R. A. Robbins and C. Boardman, *Radiochim. Acta*, 2001, 89, 613-617.
7. K. Sujatha, K. C. Pitchaiah, N. Sivaraman, K. Nagarajan, T. G. Srinivasan and P. R. V. Rao, *Desalin. Water Treat.*, 2013, 52, 470-475.
8. C. M. Wai, *Anal. Sci.*, 1995, 11, 165-167.
9. C. Erkey, *J. Supercrit. Fluids*, 2000, 17, 259-287.

LIST OF FIGURES

LIST OF TABLES

ABBREVIATIONS

Abbreviations	**Full name**
AARD	Average absolute relative deviation
AcAc	Acetylacetone
AIC	Akaike information criteria
AICc	Corrected Akaike information criteria
BPR	Back pressure regulator
CMPO	*n*-octylphenyl *N,N*-di-*iso*-butylcarbamoylmethyl phosphine oxide
CO_2	Carbon dioxide
D2EHAA	*N*,*N*-di-2-ethylhexylacetamide
D2EHIBA	*N*,*N*-di-2-ethylhexyl-*iso*-butyramide
D2EHPVA	*N*,*N*-di-2-ethylhexylpivalamide
DAAP	Diamylamyl phosphonate
DBBP	Dibutylbutyl phosphonate
DHDA	*N*,*N*-dihexyldecanamide
DHHA	*N*,*N*-dihexylhexanamide
DHOA	*N*,*N*-dihexyloctanamide
DOHP	Dioctylhydrogen phosphonate
DPO	Dioctylphosphine oxide
HDEHP	Di-(2-ethylhexyl)phosphoric acid
HLLW	High level liquid waste
HPLC	High pressure liquid chromatography
LSC	Liquid scintillation counting
MT	Mendez - Santiago and Teja
Pc	Critical pressure
PC88A	2-ethylhexyl phosphonic acid mono-2-ethylhexyl ester
RTIL	Room temperature ionic liquid
S	Solubility in g/L
$SCCO_2$	Supercritical carbon dioxide
SCF	Supercritical fluid
SFC	Supercritical fluid chromatography

SFE	Supercritical fluid extraction
SSQD	Slow suction quick delivery
TAP	Triamyl phosphate
TBP	Tributyl phosphate
Tc	Critical temperature
TEP	Triethyl phosphate
THP	Trihexyl phosphate
TiAP	Tri-*iso*-amyl phosphate
TMP	Trimethyl phosphate
TOA	Tri-*n*-octyl amine
TOMAC	Trioctylmethylammonium chloride
TOMAN	Trioctylmethylammonium nitrate
TOPO	Tri-*n*-octyl phosphine oxide
TsBP	Tri-*sec*-butyl phosphate
TTA	Thenoyltrifluoroacetone
y_2	Solubility in mole fraction units

Chapter 1

Introduction

1.1 Introduction to separation science and technology

Many major scientific and technological problems of concern to the scientists and engineers deal with the separation technology. This is especially in the areas such as energy production, pharmaceutical industry, food processing, fertilizer industries, recovery of metals, removal of contaminants from environment, fossil fuels and nuclear power [1, 2]. Other fields of study important to separation science and technology includes phase equilibrium thermodynamics, mass transfer and transport phenomenon, various aspects of chemical reactions, analytical chemistry etc. For example, burning of fossil fuel results in the generation of solid and gaseous waste that has to be removed from the environment. Recovery of various metal ions from the earth’s environment requires development of new and innovative separation techniques. Removal of various toxic substances from waste streams and pollutants from the environment is an important area of research in the environmental clean-up. In nuclear industry, production and recycling of nuclear material requires separation of fissile materials from highly radioactive fission products. Separation science and technology plays a key role in various areas of nuclear fuel cycle.

General separation techniques based on their principle/mechanism are shown in **Table 1.1.** Some of the commonly employed separation methods are solvent extraction [3], chromatography [4], membrane separations [5], ion exchange [6] and supercritical fluid extraction [7] etc. Amongst these techniques, solvent extraction is extensively employed for separation, enrichment and purification, from analytical scale to industrial process [3, 8, 9].

Table 1.1 General separation techniques [10]

Theory of separation	Separation techniques
Separations based phase addition or creation	Distillation Evaporation Crystallization Absorption Liquid-liquid extraction
Separation by barrier	Osmosis Ultrafiltration Gas permeation Liquid membrane
Separation by solid agents	Adsorption Ion exchange Chromatography
Separation by external field or gradient	Centrifugation Thermal diffusion Electrolysis Electrophoresis

1.2 Importance of separation science in nuclear fuel cycle

Nuclear power plants are one of the major sources of energy. Being one of the fast growing countries, India certainly needs huge amount of energy for its sustainable growth in terms of Gross Domestic Product. The total energy demand of India at 2050 is estimated to be around 1000 GWe [11, 12]. At present the nuclear energy contribution in India is only about 3% of the total energy production. In view of the limited source of fossil fuels, the contribution of nuclear energy to the total energy needs to be enhanced from the present 3% to about 25% for a sustained development of nation. Separation science plays a key role in the various process steps in the nuclear fuel cycle [13]. The nuclear fuel cycle involves a series of steps beginning from uranium mining, uranium enrichment, fuel fabrication, reactor operation, spent fuel reprocessing and waste management. Some of the important tasks are as follows:

(a) Front-end fuel cycle: The front-end of the nuclear fuel cycle consists of the process of mining and milling of fuel and fabrication of fuel into fuel rods. The waste originating from the mining, purification and fabrication of fuel process consists of different radioisotopes. The actinides namely uranium/thorium from the mining waste have to be recovered for safe management of nuclear waste. Separation and purification of uranium and thorium from their ores to obtain the nuclear grade uranium and thorium involves series of separation steps. Production of various nuclear grade structural materials also relies on the separation science, e.g. separation of Zr from Hf and Hf and Nb from Ta.

(b) Back-end fuel cycle:

Reprocessing of spent nuclear fuel: Recovery of fissile and fertile elements from the spent nuclear fuel and recycling back them into the reactor system is a key step in a closed nuclear fuel cycle. This process involves dissolution of spent nuclear fuel in nitric acid media and subsequent extraction U and Pu with 30% tributyl phosphate (TBP) in n-dodecane. U and Pu are separated and further purified [9].

Management of high level liquid waste (HLLW): HLLW obtained after the recovery of U and Pu from dissolver solution, consists of minor actinides (e.g. ^{237}Np, ^{241}Am, ^{243}Am & ^{245}Cm), long lived fission products and activation products of structural materials. Even though minor actinides are present in very small amounts (0.1%), they are long lived α-emitters and strong contributors to the hazards encountered in HLLW [14]. One of the options to handle the HLLW is the removal of minor actinides from fission products followed by the transmutation into the short lived isotopes [15].

(c) Radioactive laboratories: Handling of radioactive materials in fume hoods and glove boxes generate significant quantities of radioactive waste. These include various organic materials such as polymers, rubbers, cellulose, neoprene and surgical gloves. Separation techniques are used to decontaminate the laboratory radioactive waste before they are being disposed.

1.3 Need for the development of supercritical fluid based techniques

Several conventional techniques such as liquid-liquid extraction, ion-exchange, solid-phase extraction and chromatographic techniques are widely employed for the above applications. These conventional methods are well established; however, use of these techniques generally results in the generation of radioactive secondary liquid waste, which requires further treatment. Therefore, there is a strong impetus for the development of eco-friendly/green solvents that can reduce the waste generation and minimize the adverse effect on the environment.

The main objective of green chemistry is the development of eco-friendly processes for the synthesis of various molecules and utilization of green solvents for various applications [16-18]. The most prevalent of these solvent systems include ionic liquids (ILs), supercritical fluids (SCFs) and use of solvent less system [19-22]. ILs are organic salts that are composed of cations and anions with low melting points (<373 K) [21]. These ILs are non-volatile, less flammable, recyclable and can be classified as green solvents. ILs have unique properties such as good solvating power, miscibility and, chemical and thermal stability [21, 23]. ILs have attracted considerable interest over the last few years and have already successfully been applied as solvents in various chemical processes [24-26]. However use of ILs have some disadvantages such as difficulties in synthesis and theses are expensive. Use of solvent-less process is an important area of research with growing popularity as these processes involves in the reduction or elimination of toxic organic waste [27]. Combination of ILs and SCFs is a new and interesting aspect that can be used in several applications [28, 29].

In the recent years tremendous amount of attention has been paid to use of supercritical fluids based technique as an alternative to conventional method to address various issues relating to separation technology. Supercritical fluids find applications in mass-transfer processes, phase-transition processes, reactive systems, materials-related processes and nanostructured materials [30]. Some applications are already at industrial capacity, whereas others remain under development. SCFs are also successfully employed as green solvents in several industrial processes including food and pharmaceutical industries etc. [31, 32].

Use of SCF based techniques in the various process steps of nuclear industry, from mining to reprocessing of spent nuclear fuel and waste management can minimize the secondary waste generation compared to the one achieved with conventional methods using organic solvents. SCFs based methods are very attractive for the nuclear industry where the radioactive waste management is an important task; thus the major motivation behind the present study is to explore use of $SCCO_2$ containing ligands for the recovery of actinides from diverse matrices. The method development involves the following: (a) identification of actinide-specific ligands based on solvent extraction literature data and selection of ligand based on the nature of matrix - actinides are bound to the different matrices with different degree of interactions and hence appropriate ligands have to be selected depending on the nature matrix (b) measurement of solubility of ligands in $SCCO_2$ medium and optimization of experimental conditions (temperature, pressure, co-solvent composition etc.) (c) use of $SCCO_2$ containing appropriate ligand for recovery of actinides and (d) scaling-up of a typical SFE method.

1.4 Supercritical fluids

1.4.1 Introduction

In 1822 Baron Cagniard de la Tour [33] observed that above certain temperature and pressure, some substances can be no longer be classified as either liquid or gases but share the properties of both liquid and gas. This led to the discovery of critical point and the concept of SCFs. The ability to fine-tune the properties of SCFs for a variety of applications is now being explored in the analytical and industrial scale operations. The most commonly used analytical techniques that resulted from the SCFs are supercritical fluid extraction (SFE) and supercritical fluid chromatography (SFC).

A supercritical fluid (SCF) is any substance, temperature and pressure above its critical point. The critical point is defined by the critical pressure (P_c) and temperature (T_c), which are the characteristics of a given substance. T_c is the highest temperature above which a substance cannot be liquefied regardless of the pressure and the P_c is the minimum pressure required to liquefy the same at its critical temperature. SCF is a single phase that possesses the characteristics of both liquid and gas. The phase diagram represents where the substance exists as a solid, liquid and gas and at the triple point, all phases co-exist (**Figure 1.1)**. Along the vaporization curve, both liquid and vapor exists. As we increase the temperature and pressure along the vaporization curve, the density difference between the liquid and vapor decrease and the meniscus becomes less distinct. At the critical point, the curve comes to an end and the densities of two phases become identical and the substance is said to be supercritical fluid phase [34].

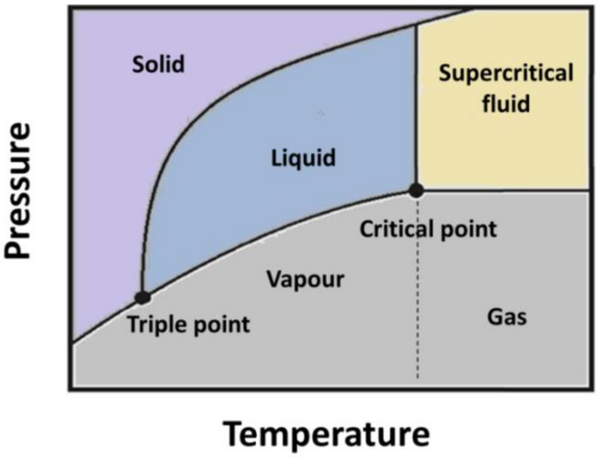

Figure 1.1 Phase diagram of a pure substance

1.4.2 Properties of supercritical fluids

The solvating power of the SCFs was first discovered by Hannay and Hogarth in 1879 [35]. SCFs have properties intermediate to that of liquids and gases. As there is no phase boundary between liquid and gas, these SCFs have no surface tension. **Table 1.2** compares physical properties of SCFs with liquids and gases. SCFs have densities that are comparable to those of liquids, which impart excellent solvent strength and act them as solvents [7, 34]. Due to their low viscosity and high diffusivity, supercritical fluids provide superior transport properties than liquids and easily penetrate into the solid matrices leading to a faster extraction. This unusual combination of physical properties can be advantageously exploited in new kind of solvent for various applications in green chemical processes. The solvating power of a SCF can be fine-tuned by altering its density, which in turn is dictated by the temperature and pressure. In principle, it is possible to avail a spectrum of solvent properties in single SCF by merely changing the pressure and temperature of the system. The properties of SCFs are very sensitive to the temperature and pressure in the vicinity of the critical point.

Table 1.2 Comparison of physical properties of liquids, gases and SCFs [36]

Property	Liquids	Supercritical fluids	Gases
Density (g/cc)	~1	0.1-0.8	~0.001
Viscosity (cP)	0.5-1	0.05-0.1	0.01
Diffusion coefficient (cm^2/s)	0.001	0.01-1	1-10

Table 1.3 Critical parameters of selected SCFs [37, 38]

Compound	Critical temperature (K)	Critical pressure (MPa)	Critical density (g/cc)
Ethylene	283.0	5.12	0.23
Carbon dioxide	304.1	7.39	0.47
Nitrous oxide	309.6	7.26	0.46
Propane	369.8	4.26	0.22
Sulfur hexafluoride	318.8	3.76	0.75
Methanol	513.4	7.99	0.27
Water	637.0	22.1	0.32
Ammonia	405.4	11.3	0.24
n-pentane	469.8	3.37	0.23
Xenon	289.7	5.92	1.10

1.4.3 Supercritical carbon dioxide

CO_2 is the most widely used SCF because of its moderate critical constants, inertness, availability in pure form, non-flammability and stability against radiation. Moreover, it is the second least expensive solvent after water. CO_2 is relatively good solvent for non-polar compounds as it is non-polar and has zero dipole moment. However, owing to its finite non-zero quadrupole moment it will dissolve moderately polar compounds. Addition of small amount of polar co-solvents e.g. methanol to CO_2 can enhance the solubility of polar compounds in supercritical carbon dioxide ($SCCO_2$). Critical parameters of commonly used SCFs are given in **Table 1.3**.

The phase diagram of CO_2 is shown in **Figure 1.2 [39]**. The triple point of CO_2 occurs at 216.6 K and 0.518 MPa. The triple point occurs at the intersection of three curves solid-liquid, solid-vapor and liquid-vapor. The vaporization curve terminates at critical point and corresponds to 304.2 K and 7.38 MPa. Beyond critical point CO_2 exists only in a single phase, known as $SCCO_2$ and is represented by shaded region (**Figure 1.2)**. The triple point pressure is well above the atmospheric pressure; therefore, at 0.101 MPa solid CO_2 sublimes directly to the vapor while maintaining a temperature of 194.6 K, the normal sublimation temperature.

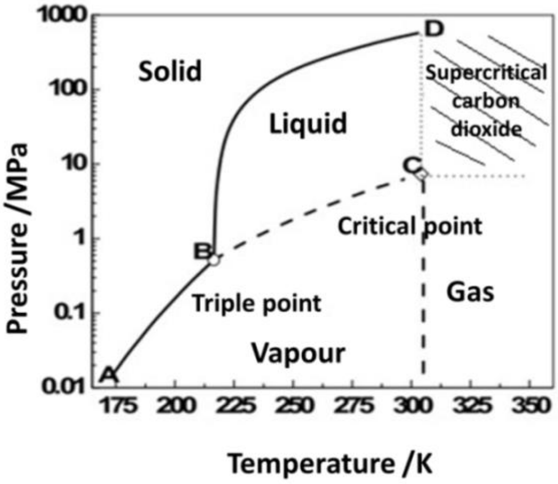

Figure 1.2 Phase diagram of carbon dioxide [40]

Figure 1.3 illustrates the variation of density of CO_2 as a function of pressure along different isotherms. In the vicinity of critical point, the density of CO_2 increases rapidly with the pressure. As the temperatures rises, the changes in density is less dramatic and moves to higher pressure. In the immediate vicinity of critical point, the density of $SCCO_2$ is about 400 kg.m^{-3}. At critical temperature, as the pressures rises, the density of $SCCO_2$ increases and comparable to that of liquid CO_2. The liquid like density enables many materials to solubilize into $SCCO_2$ medium. Density dependent properties (solubility, dielectric constant etc.) also exhibit similar dramatic and continuous variations in the critical region.

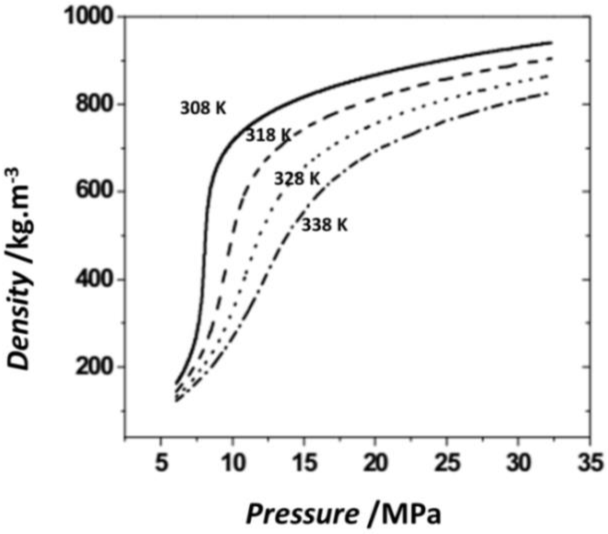

Figure 1.3 Density-pressure isotherms for CO_2 [40, 41]

The diffusion coefficient and viscosity of $SCCO_2$ determines rate of mass transfer in various $SCCO_2$ based techniques. The diffusion coefficient of $SCCO_2$ is influenced by the temperature, pressure and viscosity [42]. As the pressure increases, the density and viscosity of CO_2 increase with a corresponding decrease in the diffusion coefficient. At isobaric conditions, the diffusion coefficient increases with the temperature. Effect of temperature on the viscosity is not straightforward. At constant pressure, increase in the temperature reduces the fluid density and increases the intermolecular distance. Increase in the intermolecular distance facilitates the relative movement of molecules. As the temperature increases, the kinetic energy and collision rates of CO_2 molecule increase, hindering the movement of the molecules. Studies on the viscosity of several fluids such as CO_2, xenon, ethane, ethylene and nitrogen have shown an increase viscosity in the vicinity of critical point [43].

SCFs are considered as green solvents and the horizons of SCF based techniques have extended to wide variety of applications like extraction [44], chromatography [45], fractionation [46-48], synthesis of biodiesel [49], particle production [50], impregnation [51], reaction media [52], pharmaceutical and food industries [45], agricultural applications [53], energy applications [54, 55], petroleum industry [56] etc. Several industrial plants are in operation for decaffeination of coffee, extraction of oils from leaves, fruits, seeds and spices [31, 57, 58]. These applications continue to grow and spread to variety of industrial processes to produce high quality products with minimum impact on the environment.

1.5 Supercritical fluid extraction (SFE)

1.5.1 Introduction

SFE is a technique that uses a SCF as a solvent for the extraction or separation of a compound of interest from a matrix. SFE can be carried out from solid as well as liquid matrices and often employed as a sample preparation step for many analytical processes. It presents an alternative to conventional techniques such as solvent extraction and steam distillation because of its potential for minimizing the use of organic solvent waste. SCF allows the continuous modification of solvent strength by varying the density, which plays a major role in extraction and fractionation processes. SFE has the following advantages over conventional separation methods:

(a) SFE is an alternative technique to conventional liquid-liquid extraction, which use hexane, chloroform, dichloromethane etc. There will be always some residual organic solvent in the extract/matrix and leading to the contamination of the product. In contrast to that SFE utilizes $SCCO_2$ as a solvent and generally CO_2 becomes gas after extraction and leaving the extract in its clean form. Therefore SFE is green technique, which reduces the generation of toxic organic waste and provide cleaner extracts.

(b) The solvent strength of a SCF can be fine-tuned by altering the experimental temperature and pressure, resulting in the development of selective extraction/separation processes.

(c) SFE is diffusion based technique, in which, the SCF has to diffuse into the matrix and extract the compound of interest. SCF has diffusivities much faster than liquids and the extraction can occur at much faster rate. Moreover, SCFs have lower viscosities than liquid and zero surface tension, hence can easily penetrate into the pores of the matrix inaccessible to liquids.

(d) Thermally labile compounds can be extracted at low temperatures during SFE process

1.5.2 Basic principles of supercritical fluid extraction

The successful design and development of a SFE process relies on three important factors (i) solubility, (ii) diffusion and (iii) matrix [59]. The optimization of experimental parameters (temperature, pressure and flow rate etc.,) has to be carried out based on the above three factors.

For successful extraction/recovery of a compound using SFE technique, the analyte should have sufficient solubility in the SCF (**Figure 1.4**). This is particularly important in the initial phase of the extraction, where the kinetics of the extraction is faster. Secondly, the compound must be transported rapidly to the SCF phase from bulk/interior of the matrix. Transport generally happens by diffusion of the solute from bulk of the matrix and diffusion into the SCF phase. Third, the compound must be released from the matrix. This process involves desorption of analyte from the matrix and transfer into the SCF phase.

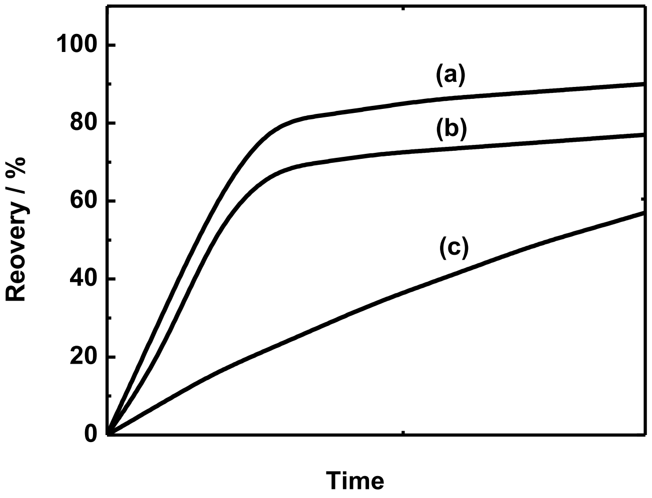

Figure 1.4 Examples of different types of extraction profiles: (a) diffusion controlled extraction behavior; (b) extraction with significant matrix effect; (c) solubility controlled extraction profile (a poorly soluble analyte) [59]

The rate of extraction/recovery of a compound from a matrix is a function of its solubility in SCF and mass transport rate across the sample matrix. In the case of poorly soluble analyte, the extraction efficiency can be improved by adding a co-solvent into the SCF. Assuming a compound is having sufficient solubility in SCF, then the rate determining step is the mass transport of the analyte from the sample matrix and there are four different types of transport mechanism

- Diffusion of the analyte through the internal volume of the sample
- Desorption of the analyte from the solute
- Diffusion of the analyte through a surface boundary layer
- Transport of analyte to the bulk of the sample

If rate determining step is the in-particle diffusion, then the rate of extraction can be enhanced by decreasing the particle size of the sample matrix. Desorption of the analyte from the surface can be accelerated with use of polar co-solvents and higher temperatures [38]. Transport of analyte to bulk of the sample depends on the diffusion coefficient of the analyte in the SCF medium.

1.5.3 Supercritical fluid extraction of metal ions

Extraction of metal ions using neat $SCCO_2$ is not feasible because of weak solute-solvent interactions and charge neutralization requirements [60, 61]. However, when the metal ions are complexed with suitable ligands, the resulting metal-ligand complexes become quite soluble in $SCCO_2$ medium [62]. Metal ions are converted into neutral CO_2 soluble species in two different methods:

(i) Online complexation: In this technique, suitable ligand is dissolved in $SCCO_2$ medium and the resultant $SCCO_2$ stream is directed for the extraction of metal ions (pre-loaded in high pressure extraction vessel).

(ii) Offline complexation: In this method, ligand is directly added to the matrix containing the metal ions and allowed to form stable complex. Then the metal-ligand complex is loaded into high pressure extraction vessel and neat $SCCO_2$ is continuously passed through the extraction vessel leading to the extraction of metal ion of interest.

The important parameters effecting the SFE of metal species are: (a) solubility of ligand, (b) solubility and stability of metal-ligand complex, (c) presence of water and pH, (d) temperature and pressure, (e) chemical form of metal bearing species and (f) matrix [63, 64]. Therefore, both, the solubility of ligand and that of metal complex plays a major role in designing a SFE process of metal ions. The SFE of metal ions mainly depends on the selection of suitable ligand. The ligand should have a sufficient solubility in $SCCO_2$ medium and should form a stable complex with metal ions of interest.

1.5.4 Solubility of ligands in supercritical carbon dioxide

Solubility is the most important parameter affecting the efficiency of supercritical fluid based processes. Solubility can have a direct impact on the rate, yield, design, and economy of a particular process. The determination of solubility of ligands in $SCCO_2$ medium is the first and fundamental step towards developing an efficient extraction process for the recovery of metal species from different environments. Optimization of supercritical experimental conditions, pressure, temperature and flow rate of $SCCO_2$ are carried out on the basis of solubility data.

Solubility in supercritical fluid is defined as "mole fraction or weight fraction of solute in the supercritical fluid, which is in equilibrium with bulk of the solute" [65]. Hildebrand and Scoot [66] introduced the solubility parameter (δ), defined as the square root of the cohesive energy density and is extensively used in the interpretation of the thermodynamic properties of the solution. The solubility parameter is defined as

$$\delta = \sqrt{C} = \frac{(\Delta H - RT)^{1/2}}{V} \qquad (1.1)$$

ΔH is heat of vaporization and V is the molar volume of the liquid. The δ values for gaseous carbon dioxide is essentially zero and the value for liquid carbon dioxide is similar to that of hydrocarbon e.g. *n*-pentane. For a supercritical fluid, the heat of vaporization is zero at the critical temperature and therefore above equation leads to a negative value of δ [67]. The equation was later modified and Giddings proposed an equation based on the studies in liquid chromatography using the van der Waals equation of state [68]. By assuming the equivalence of gases and liquids at a common density, the solubility parameter for SCF is defined as,

$$\delta = 1.25\sqrt{P_c}\,\frac{\rho_r}{\rho_{r,liq}} \qquad (1.2)$$

where, P_c is the critical pressure, ρ_r is the reduced density of the substance in supercritical state and $\rho_{r,\,liq}$ is reduced density of the liquid at its normal boiling point. To solubilize a particular solute in a supercritical solvent, the solubility parameters of both the solute and solvent need to have similar values. The solubility parameters of several compounds calculated from Eq., (1.6) are show in **Table 1.4**.

Table 1.4 solubility parameters of selected solvents [69]

Solvent	Solubility parameter (δ) $(cal.cm^{-3})^{1/2}$
Ammonia	13.2
Carbon dioxide	10.7
Nitrous oxide	10.6
Xenon	9.5
Propane	8.1
***n*-hexane**	7.0

1.6 Solubility of ligands in $SCCO_2$: a literature review

The solubility of various solid compounds in $SCCO_2$ has been studied in the past two decades including pharmaceutical compounds, environmental pollutants, dyes and organic reaction precursors [70]. A comprehensive list of phase equilibria systems in supercritical fluids is reported [71-75]. However, reports on the solubility/phase equilibria of liquid solutes, especially low volatile/high molecular weight compounds (organophosphorus, amides, ionic liquids etc.,) in $SCCO_2$ medium are very limited. The solubility data of these compounds are crucial in designing of SFE based methods for extraction and recovery of metal species, e.g. lanthanides and actinides.

Several studies have been reported on the extraction and spectroscopic behavior of metal-ligand complexes in $SCCO_2$ medium [76, 77]. Solubility of the ligand, dithiocarbamate has been extensively studied in the literature for the SFE of metal ions [60, 78]. The solubilities of dithiocarbamate based ligands are found to be very low and subsequently fluorinated dithiocarbamates were studied, which have higher solubilities in $SCCO_2$ medium. The solubility of TBP in $SCCO_2$ and phase equilibria of TBP-CO_2 system was investigated [79, 80]. The solubilities of different phosphine oxides and other organophosphorus compounds are reported [81-83]. Solubility behavior of macrocyclic compounds (e.g. Crown ethers) in $SCCO_2$ medium was studied [84]. Solubility of ionic liquids in $SCCO_2$ was determined by Wu *et al*. [85, 86]. Studies on the solubilities of primary amides and substituted amides were investigated [87, 88].

1.7 Modeling of solubility of ligands in $SCCO_2$: a literature review

Although several experimental techniques exist to determine the solubility of solutes in SCF, modeling of solubility is essential. Mathematical modeling of solubility data will provide a better understanding of the extraction process and also can be used to predict the solubility at various temperatures and pressures with experimental data generated. Different models have been used to correlate the solubility of solutes in SCFs [89-93]. In general, there are two types of models used to correlate and predict the solubility of solutes in SCFs. One is based on theoretical models such as equation of state (EOS); another one is based on semi-empirical models. The EOS based models require the knowledge of pure component properties such as solute critical parameters, acentric factor and sublimation pressures. These properties are not readily available and can be determined by group contribution theory methods or by experiments [89, 94]. However, semi-empirical models are based on simple error minimization and they only use available independent variables such as temperature, pressure and density of $SCCO_2$. Thus, empirical or semi-empirical models are preferably used for solubility determination [95]. Density based models are the most commonly used semi-empirical equations. Several empirical models have been reported in the literature for correlating the solubility of liquid and solid solutes in $SCCO_2$ [96-106]. Models are developed for the correlation of pharmaceutical compounds in $SCCO_2$ [107-111]. Different semi-empirical models have been reported in the literature to correlate the solubilities of solid solutes in $SCCO_2$ in the presence of co-solvents [103, 112-115]. Chrastil equation was modified by Gonzalez *et al*. [116] to correlate the solubility of compounds in $SCCO_2$ in the presence of co-solvents.

1.8 Literature review on supercritical fluid extraction of metal ions

(a) Supercritical fluid extraction of heavy metals

Laintz *et al.* first reported the SFE of metal ions [60]. This article describes the SFE of Cu^{2+} from aqueous media and silica surface using $SCCO_2$ saturated with lithium bis(trifluoroethyl)dithiocarbamate (FDDC). The extraction of heavy metals including, Cd^{2+}, Cu^{2+}, Hg^{2+}, Pb^{2+}, Co^{2+}, Zn^{2+} using $SCCO_2$ containing FDDCs as complexing agents is reported [117]. The solubility of Na–diethyldithiocarbamate (Na(DDC)) and Na(FDDC) were determined [78]. Solubility behavior of different metal complexes, (Na(DDC), $Ni(DDC)_2$, $Cu(DDC)_2$ $Co(DDC)_3$) $Cu(FDDC)_2$ and $Co(FDDC)_3$ etc. have been investigated [78, 118]. Solubility and SFE of metal-complexes of β-diketones, crown ethers and organophosphorus compounds was studied as function of temperature and pressure [84, 119-121]. Extraction and recovery of Cd^{2+}, Hg^{2+} and Pb^{2+} from spiked sand and filter paper samples were carried out using fluorinated β-diketones and dithiocarbamates [61]. Recovery of heavy elements from different matrices was demonstrated with $SCCO_2$ containing different organophosphorus ligands [83, 122]. Tributyl phosphate and hexafluoroacetylacetone were employed as ligands for extraction of gold and palladium [123]. SFE of heavy metals have been reviewed [124, 125].

(b) Supercritical fluid extraction of lanthanides

Extraction of lanthanides from nitric acid media was studied using $SCCO_2$ containing TBP and thenoyltrifluoroacetone (TTA) [126]. SFE of lanthanides (Nd and Gd) was carried from their oxides by using TBP-HNO_3 complex as ligand [127]. Extraction and recovery of lanthanides (La, Eu and Lu) from sand and filter paper samples were carried out using fluorinated β-diketones and TBP [119]. $SCCO_2$ modified with various ligands was employed for the extraction and separation of lanthanides from different matrices [128-132].

Table 1.5 Supercritical fluid extraction of actinides from different matrices using $SCCO_2$ containing following ligands

Actinide species	Matrix	Ligand	Reference
U	Cellulose filter paper	β-diketones	[133]
U	Nitric acid medium	TBP	[134-137]
U, Pu &Np	Oxide matrices	TTA, TBP	[127, 138-140]
U	TRISO coated fuel particles	TBP	[141]
U	Solid waste	TBP, TTA, TOPO	[139, 142]
U	Representative fission products	TBP-HNO_3	[135, 143]
U	Natural ore	PC88A, Cyanex 301	[144]
Pu and Am	Soil matrix	TTA, TBP	[145]
U, Pu & Am	Cellulose	TBP, AcAc, CMPO	[146, 147]
U and Pu	Teflon, glass and cellulose Neoprene, polyvinyl chloride and surgical gloves	AcAc, CMPO	[148, 149]
U, Pu, Np & Am	Acidic medium	TBP	[150]
U & Th	Nitric acid medium Cellulose matrix Oxide matrices	Dialkylamides TBP Crown ethers Calixaranes	[151-154]

TBP – Tributyl phosphate; TTA – Thenoyltrifluoroacetone; AcAc – Acetylacetone

CMPO - *n*-octylphenyl *N*,*N*-di-*iso*-butyl carbamoylmethylphosphine oxide;

TOPO – Trioctylphosphine oxide

(c) Supercritical fluid extraction of actinides

The recovery of actinides from solid and liquid matrices was reported [155-160]. SFE based methods were developed for the extraction of actinides from different matrices. Reviews appeared on the extraction of metal ions (heavy metal, lanthanides and actinides) using $SCCO_2$ modified with wide variety of ligands such as organophosphorus compounds, β-diketones, dithiocarbamates and macrocyclic compounds [63, 64, 117]. The literature on the extraction and recovery of actinides from different matrices is shown in **Table 1.5.**

1.9 Gap Areas and Objective of present study

Extraction and recovery of actinides from different process steps of nuclear fuel cycle is an important task. Use of supercritical fluid extraction method provides an opportunity to minimize generation of secondary liquid waste as CO_2 becomes gas after extraction. The literature data on the extraction and recovery of metal ions, especially of actinide ions are relatively scarce. There is not enough data in the literature for recovery of actinides from dissolver solution of spent fuel; similarly, there are not enough data available for pre-concentration and recovery of actinides from aqueous waste stream; use of pyrochemical-high temperature electrochemical process for recovery of actinides also results in the generation of salt waste containing precious actinides and there is no literature available for their recovery. Thus the motivation behind the work is to explore use of SFE based methods for the recovery of actinides from such waste streams and matrices.

Selection ligands for the SFE of actinides from different matrices can be done from (i) solvent extraction data and (ii) nature of the matrix to which actinides are bound. Neutral organophosphorus compound e.g. trialkyl phosphate has been used for solvent extraction of actinides. Hence series of trialkyl phosphates are examined in the present study for their solubility behavior in $SCCO_2$ medium; subsequently, $SCCO_2$ containing trialkyl phosphate has been explored for recovery of actinides from aqueous medium. The organophosphorous compounds exhibit extraction power through the basicity of the phosphoryl oxygen (P=O). The basicity of phosphoryl group can be enhanced by replacing the C-O-P group in the extractant by a C-P group. The extraction power of these molecules was found to be increasing in the order: phosphates < phosphonates < phosphinates < phosphine oxides [161-166]. Hence the stronger phosphonate based ligands are examined in the studies involving pre-concentration and recovery of uranium in the presence of fission product elements present in the aqueous medium.

Besides organophosphorus compounds, *N*,*N*-dialkyl amides are proposed as a potential alternative extractants to trialkyl phosphates for the extraction and recovery of actinides in the various process steps of nuclear industry [153, 167-173]. Hence *N*,*N*-dialkyl amides, which are resistant to hydrolysis and radiolysis compared to trialkyl phosphates are examined in the present study for their solubility behavior. *N*,*N*-dialkyl amides offer advantages over organophosphorus compounds like innocuous nature of their degradation products and possibility of complete incineration leading to reduction in the liquid secondary waste [169].

Another important research area in the recent past is use of pyrochemical based process for isolation of actinides from fission product elements such as lanthanides, transition metals, alkali and alkaline earth metal ions. This process employs LiCl-KCl or NaCl-CsCl eutectic mixture as an electrolyte for the recovery of actinides. In this process, disposal or reuse of molten salts is of important concern, besides recovery of precious actinides from salt matrix [174-176]. Since actinides are bound to a salt matrix, (relatively strong interacting matrix compared to cellulose or polymer matrix), there is a need for use of quarternary ammonium based ligand, which is capable of forming strong ion-pair complexes with actinides. Hence the solubility behavior of TOMAC was investigated and

$SCCO_2$ containing TOMAC was explored for recovery of plutonium and uranium from LiCl-KCl matrix.

Thus the solubility behavior of trialkyl phosphates, dialkylalkyl phosphonates, *N*,*N*-dialkylamides and ionic liquids in $SCCO_2$ medium were investigated as a preliminary step. Different semi-empirical models have been reported in the literature to correlate the solubilities of solid solutes in $SCCO_2$ in the presence of co-solvents. Despite the availability of models for correlating the solubilities of solid compounds in $SCCO_2$ in the presence of co-solvents, models correlating the solubilities of liquid solutes are scarce. To the best of our knowledge, no models are available in the literature for correlating the solubility of liquid solute in $SCCO_2$ in the presence of co-solvents with parameters for molecular interactions. Development of new models for correlating solubility of liquid solute in $SCCO_2$ in the presence of co-solvent is useful for solubility predictions at various pressures and temperatures. Two new model equations are developed for correlation of ternary solubilities ($SCCO_2$ + solute + co-solvent) using Wilson and van Laar activity coefficient models.

In summary, the thesis is mainly focused on the following to achieve the objectives, i.e. recovery of actinides from diverse matrices:

- Selection of actinide-specific ligands and experimental measurement of solubility of ligands in $SCCO_2$ medium at various experimental conditions
- Development of new models for the correlation of solubility of liquid solutes in $SCCO_2$ in the presence of co-solvents
- Optimization of experimental parameters for the recovery of actinides from different matrices (acidic aqueous medium and inorganic chloride salt matrices)
- Scaling-up of a typical SFE method to recover actinides from salt matrix.

Chapter 2

Experimental methods and semi-empirical equations

Chapter 2 (a)
Experimental methods

This chapter provides a brief over view of chemicals and instruments employed in the present study. The synthesis of various ligands employed in the present study is also discussed. This chapter also describes the experimental set-up and general experimental procedure adopted for the measurement on the solubility of compounds in supercritical fluids (SCFs) and supercritical fluid extraction (SFE) of actinides.

2.1.1 Materials

2.1.1.1 Chemicals

Detailed information of the chemical used in the present study has been summarized in **Table 2.1.**

Table 2.1 Specification of the chemicals used in the present study

Chemical Name	Source	Purity (%)	Purification method	Analysis method
Carbon dioxide	Sri Krishna Industrial Gases, India	99.9	Silica gel[a]	None
Phosphorus trichloride	Merck, India	99	None	None
Methanol	SD Fine Chem. Ltd. India	99.8	None	None
n-propanol	Merck, India	>99	None	None
1-butanol	Merck, India	99	None	None
n-pentanol	Merck, India	99	None	None
n-hexane	SD Fine Chem. Ltd. India.	99	None	None
n-bromobutane	Lancaster	99	None	None
n-bromopentane	Lancaster	99	None	None
α-hydroxy-*iso*-butyric acid	Alfa Aesar	99	None	None

(1S)-(+)-camphor-10-sulfonic acid	Alfa Aesar	98	None	None
Arsenazo (III)	TCI	98	None	None
Trimethyl phosphate	Koch Light Laboratories	99	None	None
Triethyl phosphate	Sigma Aldrich	99	None	None
Tributyl phosphate	Alfa	99	None	None
Tri-*sec*-butyl phosphate	Synthesis	99	VD[b]	GC[c]
Triamyl phosphate	Synthesis	98	VD	GC
Tri-*iso*-amyl phosphate	Synthesis	98	VD	GC
Trihexyl phosphate	Synthesis	96	VD	GC
Dibutylbutyl phosphonate	Synthesis	97	VD	GC-MS[d]
Diamylamyl phosphonate	Synthesis	98	VD	GC-MS
Dioctylhydrogen phosphonate	Synthesis	98	VD	GC-MS
Dioctylphosphine oxide	Synthesis	98	VD	GC-MS
Trioctylphosphine oxide	Merck, India	99	None	None
Di-(2-ethylhexyl)phosphoric acid	Sigma Aldrich	98	None	None
N,N-dihexylhexanamide	BARC[e], India	99	None	None
N,N-dihexyloctanamide	BARC, India	99	None	None
N,N-dihexyldecanamide	BARC, India	99	None	None
N,N -di-2-ethylhexylacetamide	BARC, India	99	None	None
N,N -di-2-ethylhexyl-*iso*-butyramide	BARC, India	99	None	None
N,N -di-2-ethylhexylpivalamide	BARC, India	99	None	None
Trioctylmethylammonium chloride	Alfa Aesar	99	CO_2 stripping[f]	None
Acetyl acetone	Lancaster	99	None	None

[a] CO_2 was passed through a silica gel column to remove the moisture
[b] vacuum distillation
[c] Gas chramogrpahy
[d] Gas chromatography coupled with mass spectrometry
[e] BARC- Bhabha Atomic Research Centre [177]
[f] supercritical carbon dioxide was continuously passed through trioctylmethylammonium chloride to remove the presence of any volatile impurities.

2.1.1.2 Preparation of trioctylmethylammonium nitrate

Trioctylmethylammonium chloride (TOMAC) was converted to its nitrate form, trioctylmethylammonium nitrate (TOMAN) by equilibrating with a solution of 4N $NaNO_3$; TOMAC was dissolved in chloroform and equilibrated with a solution of 4N $NaNO_3$ for 1 hour. The aqueous phase was rejected and the equilibration was continued with a fresh lot of $NaNO_3$ until the aqueous phase showed no chloride ions. Then the organic phase was washed with water and chloroform was removed by vacuum distillation.

2.1.1.3 Preparation of pyrochemical salt

The experimental set-up and procedure used for the preparation of pyrochemical salt is described elsewhere [178]. LiCl-KCl eutectic mixture was dried under vacuum for 120 h at 420 K and further purified by passing chlorine gas for 30 min at 773 K. UCl_3-LiCl-KCl electrolyte was prepared by adding stoichiometric amounts of $CdCl_2$ and excess U metal in purified LiCl-KCl melt and equilibrated for about 30-40 h in argon atmosphere glove box maintained at positive pressure. A similar procedure was adopted for the preparation of $PuCl_3$-LiCl-KCl, where plutonium metal was equilibrated with $CdCl_2$ at 773 K in an inert atmosphere glove box, where the pressure was maintained at 20 mm to 40 mm of water column with respect to ambient pressure. The oxygen and moisture levels controlled within 10 ppm. UO_2Cl_2-NaCl-CsCl prepared by initially purifying NaCl-CsCl eutectic mixture with chlorine gas at 923 K followed by dissolving UO_2 by bubbling a mixture of chlorine and oxygen gas into the melt at 923 K for about 30 min. UCl_3-LiCl-KCl, $PuCl_3$-LiCl-KCl and UO_2Cl_2-NaCl-CsCl pyrochemical salts were prepared with concentration of U and Pu ranging from 0.1 – 5 wt%.

2.1.1.4 Synthesis of trialkyl phosphates

All trialkyl phosphates (tri-*sec*-butyl phosphate (TsBP), triamyl phosphate (TAP), tri-*iso*-amyl phosphate (TiAP) and trihexyl phosphate (THP)) were synthesized by the condensation reaction between phosphoryl chloride ($POCl_3$) and stoichiometric equivalent of corresponding alcohol in the presence of pyridine using *n*-heptane as a solvent as reported earlier from our laboratory [155, 156].

TAP was synthesised by reacting amyl alcohol (1.1 moles) and pyridine (1 mol) in a three necked flask containing 0.5 L of n-heptane as a solvent. The flask containing the reactant was kept in ice bath to maintain low temperature (~ 273 K). The reaction mixture was stirred for a few minutes to ensure the attainment of low temperature inside the flask before starting the reaction. About 0.33 moles of $POCl_3$ (in 100 mL of heptane) was added drop-wise into the reaction mixture at a constant rate of 50-60 drops per minute with continuous stirring using a mechanical operated stirrer. After the complete addition of $POCl_3$, the slurry was stirred for 24 h to ensure the complete conversion of reactant to TAP.

$$\underset{\text{Amyl alchohol}}{3C_5H_{11}OH} + POCl_3 + 3C_5H_5N \longrightarrow \underset{\text{Triamyl phosphate}}{(C_5H_{11}O)_3(PO)} + 3C_5H_5NH^+Cl^- \quad (2.1)$$

The product mixture was washed with distilled water to remove pyridinium hydrochloride. The acidic impurities in TAP were removed by washing with concentrated NaOH followed by water. TAP was further purified by vacuum distillation. Similar procedure was adopted for the synthesis of other trialkyl phosphates. The synthesized trialkyl phosphates were characterized by ^1H, ^{31}P-NMR, IR and GC-MS techniques, wherever applicable. The purity of these trialkyl phosphates was estimated using gas chromatography (GC) with flame ionization detector (FID). The characterization and purity details are provided in **Appendix-1**.

2.1.1.5 Synthesis of dialkylalkyl phosphonates

The dialkylalkyl phosphonates were synthesized by Michaelis-Becker reaction as reported earlier from our laboratory [164, 165, 179]. The precursor for the synthesis of dialkylalkyl phosphonate is dialkylhydrogen phosphonate and it was prepared by the reaction between phosphorus trichloride (PCl_3) and corresponding alcohol. Subsequently, the precursor dialkylhydrogen phosphonate was treated with sodium in *n*-hexane to yield sodium salt of dialkylhydrogen phosphonate. Sodium salt of dialkylhydrogen phosphonate was reacted with corresponding bromoalkane to yield dialkylalkyl phosphonates.

Diamylamyl phosphonate (DAAP) was synthesised by reacting PCl_3 (0.33 mol) with *n*-pentanol (1 mol) under a purge of argon over a period of 30 min at 273 K with continuous stirring. The stirring was continued for an hour to remove the liberated HCl. Ice water was added to the above reaction mixture and the remaining HCl was neutralized with the addition of potassium carbonate. The product was separated and vacuum distilled at 393 K and 0.1 torr to obtain diamylhydrogen phosphonate [180].

$$\underset{\text{n-pentanol}}{3C_5H_{11}OH} + PCl_3 \longrightarrow \underset{\text{diamylhydrogen phosphonate}}{(C_5H_{11}O)_2(PO)H} + C_5H_{11}Cl + 2HCl \qquad (2.2)$$

In the subsequent step, sodium (1.15 g) in *n*-hexane was (100 mL) placed in a three necked flask and diamylhydrogen phosphonate was added drop-wise over a period of 30 min under reflux condition. The addition continued until the sodium was completely dissolved. *n*-bromoalkane was then added over a period of half-an-hour and the mixture was stirred continuously by means of a magnetic stirrer at reflux conditions for 4 h. The whole reaction mixture was washed with the distilled water. Subsequently the product was separated and distilled at 373 K and 0.1 torr. The acidic impurities present in the final product were removed by washing with 0.25 M sodium carbonate followed by dilute nitric acid and water.

$$2(C_5H_{11}O)_2(PO)H + 2Na \longrightarrow 2(C_5H_{11}O)_2(PO)Na + H_2 \qquad (2.3)$$

diamylhydrogen phosphonate diamylsodium phosphonate

$$(C_5H_{11}O)_2(PO)Na + C_5H_{11}Br \longrightarrow (C_5H_{11}O)_2(PO)C_5H_{11} + NaBr \qquad (2.4)$$

diamylsodium phosphonate diamylamyl phosphonate

Similar procedure was adopted for the synthesis of dibutylbutyl phosphonate (DBBP). The synthesized dialkylalkyl phosphonates were characterized by ^{1}H, ^{31}P-NMR, IR and GC-MS techniques wherever applicable. The purity of these trialkyl phosphates was estimated using gas chromatography (GC) with flame ionization detector (FID). The characterization and purity details are provided in **Appendix-1**.

2.1.2 Solubility measurements in supercritical fluids

The determination of solubilities of compounds in supercritical fluids has been well reviewed by Aim and Fermeglia [181], Dohrn and Brunner [71], McHugh and Krukonis [7] and Knox [182]. There are different techniques reported in the literature for the measurement of solubility of solutes in supercritical fluids. These methods mainly classified as static methods and dynamic methods.

2.1.2.1 Static methods

In this method, the compound to be investigated is loaded into a high pressure equilibration cell which is placed in a thermostat to maintain the constant temperature [181]. Then the equilibration cell (pre-loaded with the solute) was filled with $SCCO_2$ until it reaches to desired pressure. The contents of the equilibration cell are mixed thoroughly using a stirrer to achieve the faster equilibrium. Determination of the equilibrium composition of the phase yields the solubility data. Depending on the sampling procedure and type of high pressure cells used, static methods can be sub divided into (a) analytical methods [183, 184]; (b) synthetic methods [65] and (c) gravimetric methods [65, 185-187]

2.1.2.2 Dynamic method

Dynamic methods are the most frequently used for determining the solubility of compounds in supercritical fluids. The dynamic method can be modified according to the needs. The experimental set-up and procedure adopted in the dynamic method was studied by several researchers with different modifications [107, 184, 188-190]. In this method, the solute was loaded in to a series of high pressure equilibrium cells and supercritical fluid is continuously passed through the equilibrium cell. The flow rate of CO_2 is optimized so that the outgoing CO_2 stream is assumed to reach equilibrium. The exiting CO_2 stream is analyzed for the solute concentration by chromatographic, gravimetric, spectroscopic methods etc. Dynamic methods are further classified as (a) recirculation methods [65, 181, 182] (b) flow methods [181] and (c) transpiration or saturation methods [65, 181]

The saturation methods are the simplest and most widely used method for the measurement of solubility of compounds in supercritical fluids. Recently, several research groups have employed the saturation method for measurement of solubility of wide variety of compounds in $SCCO_2$ [97, 190-192]. The advantage of saturation methods can be summarized as follows [7, 65]

- The experimental set-up can be assembled from easily available parts
- Simple and straightforward sampling procedure
- Solubility of extremely low volatile compounds can be measured
- Fast process and large amount of solubility data can be obtained in a short interval of time
- In addition to solubility measurements, this technique can be employed for extraction and fractionation of different compounds

In the present work, saturation or transpiration method was employed for the measurement solubility of liquids solutes in $SCCO_2$ medium.

2.1.3 Supercritical fluid extraction experimental set-up

The schematic of the experimental set-up employed in the present study for measuring the solubility of compounds in $SCCO_2$ and supercritical fluid extraction studies is shown in **Figure 2.1 and 2.2** respectively. The experimental set-up consisted of a carbon dioxide cylinder, a high pressure reciprocating CO_2 pump (JASCO-PU-2080-CO_2-PLUS), co-solvent / modifier pump (JASCO-PU-2080-PLUS) 10 mL CO_2 heat exchanger (JASCO), high pressure equilibrium/extraction vessels (JASCO), thermostat (JASCO-CO-1560), an automatic back pressure regulator (JASCO-BP-2080-PLUS) and collection vessel. The individual units of the system is described briefly as shown below

(a) Carbon dioxide cylinder

Carbon dioxide gas used in the present study has a purity of 99.9% with moisture content less than 10 ppm. At room temperature, the cylinder pressure is about 6 MPa and is connected with a dip tube. CO_2 is drawn from cylinder using the dip tube and fed to CO_2 pump.

(b) High pressure reciprocating CO_2 pump

In the present study, reciprocating pump was employed to deliver the CO_2 for solubility and SFE experiments, at a fixed flow rate against the back pressure. It is a dual headed reciprocating pump with in-built cooling system (Peltier element) which cools CO_2 to 263 K. The pump provides a uniform flow rate of CO_2 via slow suction and quick delivery (SSQD). These pumps also offer the advantage of choosing the mode of pumping either by constant flow rate or constant pressure. The operating flow rates are ranging from 0.001-10 mL/min with an increment of 0.001 mL/min. The pump operates up to a maximum pressure of 50 MPa and has safety in-built system in case of over pressurization.

(c) Co-solvent or modifier pump

In the present study the purpose of co-solvent pump is twofold: (i) In case of solubility experiments, co-solvent pump is used to add desired percentage of co-solvent (e.g. methanol, propanol, *n*-hexane) to the CO_2 stream and (ii) In case of SFE of metal ions, the co-solvent pump is used for controlled deliver of ligands in to the CO_2 stream. The co-solvent pump is a double headed reciprocating pump. The SSQD ensures the accurate and stable solvent delivery of co-solvents with a precision of 0.1%. The pump is provided with inbuilt safety features and also a purge valve at the pump head for venting and replacing the solvents.

(d) High pressure extraction vessels

High pressure vessels of 10 and 50 mL capacity were employed for the solubility measurements. Extraction vessels of 1 and 10 mL capacity were used for the supercritical fluid extraction of actinides. These vessels are made up of high quality stainless steel (SS 304) and designed to withstand higher pressures up to 50 MPa.

(e) Thermostat

A column oven (JASCO, CO-1560) was used in the present study to maintain constant temperature of high pressure equilibrium cell for solubility and SFE experiments. The temperature of the oven was maintained by circulating air and the oven has the temperature control range from 288 to 353 K with a precision of ±0.1 K. The thermostat has inbuilt safety features such as heating/cooling power shut off when unusually high temperatures or flammable solvent leaks are detected.

(f) Back pressure regulator

Back pressure regulator (BPR) pressurizes the system from delivery pump to the detector and regulates the pressure according to a set value. In the present work, an automatic BPR (precision: ± 0.1 MPa) was used to control the pressure of the system and is a complex regulator, which consists of pressure sensing device and a needle valve. It controls the system back pressure irrespective of the flow rate of the SCF. The regulator consists of a needle valve, which is driven by a solenoid. For regulating the pressure at a desired value, the valve is used in combination with pressure sensor and a control circuit. A pressure signal from the sensor is amplified and compared with the set pressure. The output of the comparator regulates the solenoid movement to open and close the valve. The pressure is controlled by high speed switching of the fluid flow with continuously opening and closing of the flow path. This configuration is very much suitable for eliminating the blockage of valve flow path.

2.1.4 Procedure employed in the present study for solubility measurements

A dynamic flow saturation type apparatus was used to measure the solubility of solutes in $SCCO_2$ with and without a co-solvent (**Figure 2.1**). The experimental set-up consisted of a carbon dioxide cylinder, a high pressure reciprocating CO_2 pump (JASCO-PU-2080-CO_2-PLUS), HPLC pump (JASCO-PU-2080-PLUS), 10 mL heat exchanger, 50 mL/10 mL twin high pressure equilibrium cells, 10 mL entrainer column, thermostat (JASCO-CO-1560 and inbuilt oven), and a back pressure regulator (JASCO-BP-2080-PLUS). Initially $SCCO_2$ was continuously passed through the equilibrium cells pre-loaded with the solute for a known period of time (20 min for solutes with high solubility, e.g. TBP and 48 hours for solutes with low solubility, e.g. TOMAC) to remove the presence of any volatile impurities.

Carbon dioxide from gas cylinder (1) was passed through a silica gel column (2) to remove traces of water and then fed into a CO_2 pump (3) where it was liquefied using a Peltier element. Liquid carbon dioxide was pressurized and sent to the heat exchanger (6) placed inside the thermostat to attain the desired temperature, after which it flows into the equilibrium cells containing the solute (7&8). At a fixed experimental temperature, the equilibrium cells (pre-loaded with the solute) were pressurized with $SCCO_2$ until the desired pressure was reached. The system was kept at the desired temperature and pressure for an hour to reach the equilibrium. After equilibration, $SCCO_2$ was allowed continuously to flow through the system at a constant flow rate. The exiting CO_2 stream from equilibrium cells was introduced into a collection vessel (12), where the pressure was reduced to atmospheric pressure. The concentrate of the solute in the $SCCO_2$ stream was monitored continuously. Saturation solubility was observed by periodically collecting the solute and quantifying the same.

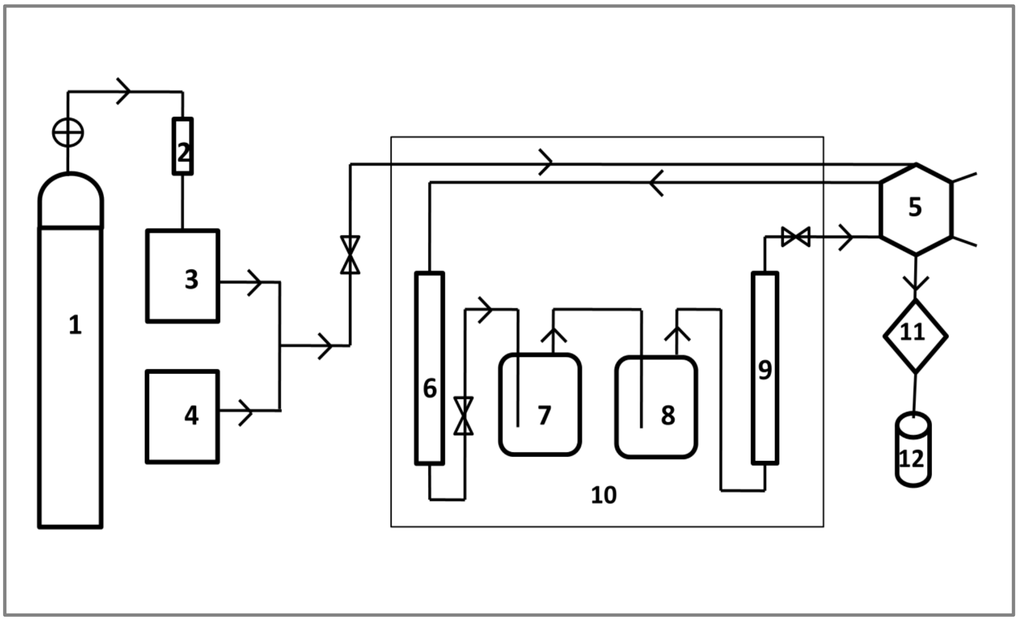

Figure 2.1 Schematic diagram of experimental set-up used for the solubility measurements; (1) Carbon dioxide cylinder, (2) molecular sieve filter, (3) carbon dioxide pump, (4) co-solvent pump, (5) six way valve, (6) heat exchanger, (7&8) equilibrium vessels, (9) entrainer column, (10) oven, (11) back pressure regulator, (12) collection vessel.

The primary criterion for the accurate measurement of solubilities in $SCCO_2$ is that the exiting stream has to be saturated with the solute. Repeated measurements were carried out at different flow rates of CO_2 between 0.1 to 1 mL/min, to identify the suitable flow rate for achieving the saturation solubility. The flow rate of $SCCO_2$ was optimized (0.1 - 0.3 mL/min) to ensure complete saturation of exiting stream of $SCCO_2$. The exiting stream was trapped and collected in a collection vessel containing *n*-hexane, at regular intervals of time. Subsequently, *n*-hexane was evaporated and the amount of solute collected was determined gravimetrically using an analytical balance (Shimadzu, AUW220D). In some experiments, the solute was trapped in a collection vessels containing quartz wool. The collection efficiency of quartz wool methods was found to be similar to that of *n*-hexane.

In case of use of experiments involving co-solvent, it was delivered using a liquid chromatography (HPLC) pump and passed through a T-joint to get it mixed into the CO_2 stream. The resultant CO_2 and the co-solvent stream was fed in to a 10 mL heat exchanger to ensure the desired temperature and a thorough mixing of CO_2 and co-solvent, before entering into high pressure twin equilibrium cells. At a fixed experimental temperature, equilibrium cells pre-loaded with solute, pressurized until the desired pressure has been reached. CO_2 and co-solvent mixed stream was allowed continuously flow through the system at a constant flow rate and the concentration of solute in the $SCCO_2$ stream was monitored continuously. The flow rate of co-solvent was varied from 0.001 – 0.005 mL/min, for the desired mol % of the co-solvent in a particular binary mixture of CO_2 and co-solvent.

In each experiment, a minimum of 30 mg of solute was collected by varying the collection periods. In general, an average about 250 mg of solute was collected for the gravimetric determination. The uncertainty in the gravimetric determination was < 0.5 %. On the basis of total flow of $SCCO_2$ and amount of solute collected for unit time, the solubility of solute was determined. All the experiments were repeated in triplicate and the uncertainty in the experimental solubilities was generally found to be ± 5%. The reliability of the experimental set-up and procedures were tested by measuring the solubility of tributyl phosphate and trioctyl amine in $SCCO_2$ medium. The solubility is expressed in terms of mole fraction (y_2) using the formula

$$y_2 = \frac{n_a}{\left(\left[f * t * \left(\frac{\rho_a}{M}\right)\right] + n_a\right)} \tag{2.5}$$

$$S = \frac{W * 1000}{\left(\left[f * t * \left(\frac{\rho_a}{\rho_b}\right)\right] + \left(\frac{W}{\rho_c}\right)\right)} \tag{2.6}$$

In Eq. (2.5) and (2.6), n_a represents the number of moles of solute collected, f is the flow rate of CO_2 in mL/min at CO_2 pump, t is the sample collection time in min and ρ_a gives the density of CO_2 at pump head, ρ_b represents the density of CO_2 at experimental temperature and pressure, ρ_c is density of the compound at experimental temperature and pressure, M is the molecular weight of CO_2 and W is amount of compound collected in grams.

2.1.5 Solubility measurements

There are certain issues which experimentalist has to take care before starting the experiments. These are as follows

- There is always a possibility that the exiting CO_2 stream has not reached saturation with the solute. To ensure the complete saturation, the equilibrium cell has to be properly designed and often two or more equilibrium cells have to be connected in series. The flow rate of CO_2 has to be optimized to ensure the saturation solubility.
- Entrainment of solute droplets with the CO_2 stream has to be avoided.
- At high pressures, if the density of supercritical fluid is higher than that of the solute, solute can float and pushed out of the equilibrium cells leading to erroneous results.

The above three issues have been taken care during the solubility measurements as explained below.

2.1.5.1 Saturation of $SCCO_2$ stream with the solute

The primary criterion for the measurement of solubility of compounds in $SCCO_2$ is that the exiting stream of CO_2 has to be saturated with the analyte, e.g., trialkyl phosphate. The saturation of $SCCO_2$ with solute depends on residence of time of CO_2 (equilibration period) and flow rate of carbon dioxide. The effect of equilibration period and flow rate of CO_2 on the solubility measurements was studied and conditions are optimized for the solubility measurements. Initial experiments were carried out with one equilibrium cell. In all these experiments it was observed that, the outlet $SCCO_2$ stream has not reached the saturation. Moreover, the concentrations of solute in $SCCO_2$ stream are not constant and decrease with the time. Our experimental results indicated that a minimum of two equilibrium cells have to be connected in series to achieve the saturation solubility. Hence all the experiments were carried out with minimum of two equilibrium vessels to get the equilibrium solubility data.

Equilibration period:

The optimization of static equilibration period was carried out by trial experiments. At a fixed experimental temperature, the equilibrium cells (pre-loaded with trialkyl phosphate) were pressurized with $SCCO_2$ until the desired pressure was reached. The system was kept at the desired temperature and pressure for a known amount of time to reach the equilibrium. After equilibration, the CO_2 was allowed to flow through the system at constant flow rate and concentration of solute in the CO_2 stream was monitored continuously. This was done by collecting sample at regular intervals of time and measuring the solubility through gravimetry. Our results indicated that a minimum of 60 min static equilibration is required to achieve the complete saturation of $SCCO_2$ with the trialkyl phosphate.

In a typical solubility measurement, the trialkyl phosphate sample was allowed to equilibrate for 1 hour and subsequently, $SCCCO_2$ was allowed to pass through the vessels containing trialkyl phosphate at 0.2 mL/min. Saturation solubility was ensured by periodically collecting the analyte and quantifying the same. **Figure 2.2** represents a typical sampling procedure adopted for quantifying solubility of trialkyl phosphates. The procedure was also validated by measuring solubility of tributyl phosphate and tri-*n*-octyl amine which were reported in literature.

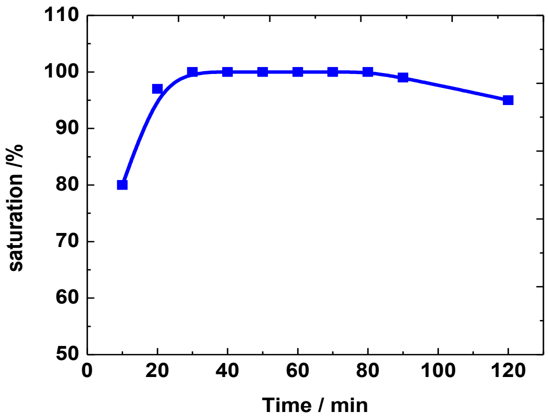

Figure 2.2 Effect of equilibration period on the saturation of TiAP with $SCCO_2$
Experimental conditions: Pressure: 15 MPa; temperature: 323 K; CO_2 flow rate: 0.2 mL/min, Equilibrium cell volume: 50 mL, No. of equilibrium cells connected in series: 2; sample loaded in equilibrium cells: 1st cell-35 mL and 2nd cell: 25 mL; heat exchanger: 10 mL; entrainer column: 10 mL;

Optimization of flow rate:

The primary criterion for the measurement of solubility of compounds in $SCCO_2$ is that the exiting stream of CO_2 has to be saturated with the analyte, trialkyl phosphate. Experiments were performed at various flow rates of CO_2 ranging from 0.1 to 1 mL/min, keeping temperature and pressure constant, to ensure saturation of the solute with the exiting CO_2 stream. No changes in the solubilities were observed when the CO_2 flow rate was less than 0.3 mL/min (**Figure 2.3).** However, when the flow rate was increased beyond 0.3 mL/min, the concentration of solute in the exiting CO_2 stream decreased with the time indicating that the stream is not saturated. Hence, a typical CO_2 flow rate of 0.1 mL/min was employed to ensure that the exiting CO_2 stream was saturated with the trialkyl phosphate.

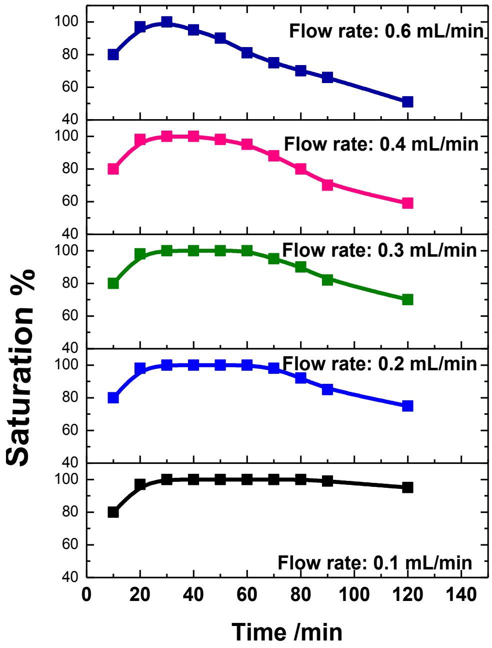

Figure 2.3 Effect of flow rate on the solubility of TiAP in $SCCO_2$

Experimental conditions: Pressure: 15 MPa; temperature: 323 K; equilibrium cell volume: 50 mL, No. of equilibrium cells connected in series: 2; sample loaded in equilibrium cells: 1st cell-35 mL & 2nd cell: 25 mL; heat exchanger: 10 mL; entrainer column: 10 mL;

2.1.5.2 Prevention of entrainment of solute with $SCCO_2$ stream

Entrainment of solute drops or particles with $SCCO_2$ stream leads to collection of higher amount of solutes in the trap than the equilibrium amount, resulting in an erroneous data. Therefore it is necessary to avoid entrainment of particles along with the $SCCO_2$ stream. In the present work, entrainment of liquid solute is controlled using following methodologies.

(a) In solubility measurements, two equilibrium cells are connected in series and are placed vertically. About 70% volume of the first equilibrium cell is filled with the solute and 50% of volume of the second equilibrium cell is filled with solute. The $SCCO_2$ is always allowed to enter through the bottom of the equilibrium cells and is exited at top of the cell to minimize the entrainment of liquid solute.

(b) An entrainer-column was used to avoid the entrainment of the liquid solute. The entrainer column is filled with alternative layers of fine teflon particles and glass wool /

quartz wool. The entrainer column is connected to outlet of second equilibrium cell. The $SCCO_2$ stream saturated with the solute enters into the entrainer column; entrained liquid solute is trapped here (if any) and then directed to BPR for collection.

2.1.5.3 Density inversion leading pushing out of phases

If the density of $SCCO_2$ is higher than the solute, the solute can be pushed out of equilibrium cells, resulting in collection of higher amounts of solutes than that of equilibrium amount. In the present work, all experiments were carried out at $SCCO_2$ density, which is always lower than that of solute density, to prevent density inversion. However, in one of the experiments involving measurement of solubility of TOMAC in $SCCO_2$ at 313 K and 30MPa, there is possibility for density inversion. The density of $SCCO_2$ at these conditions (~910 $kg.m^{-3}$) is higher than that of the solute density of the ligand, TOMAC (~884 $kg.m^{-3}$). The experiment was intentionally carried out to examine the influence of density inversion. The experimental solubility data obtained at this point is consistent with the data obtained at different temperatures and pressures (where there was no density inversion). Hence, it is assumed that at this particular experimental condition, density inversion did not significantly affect the solubility measurements. This can be possibly due to (i) density difference being not significantly different (ii) TOMAC is a highly viscous compound and it cannot be easily pushed out with $SCCO_2$.

2.1.5.4 Validation of experimental set-up and procedure

A dynamic flow method was employed in the present study to measure the solubility of trialkyl phosphate in $SCCO_2$ medium. The experimental method was validated by measuring the solubility of TBP and trioctyl TOA in $SCCO_2$ medium.

(a) Solubility of TBP in $SCCO_2$

The solubility of TBP in $SCCO_2$ was determined at 313-333 K with pressure from 10-25 MPa. These results are compared with Meguro *et al.* [79] and are in good agreement with the literature data with an average deviation of < 10% (**Figure 2.4**).

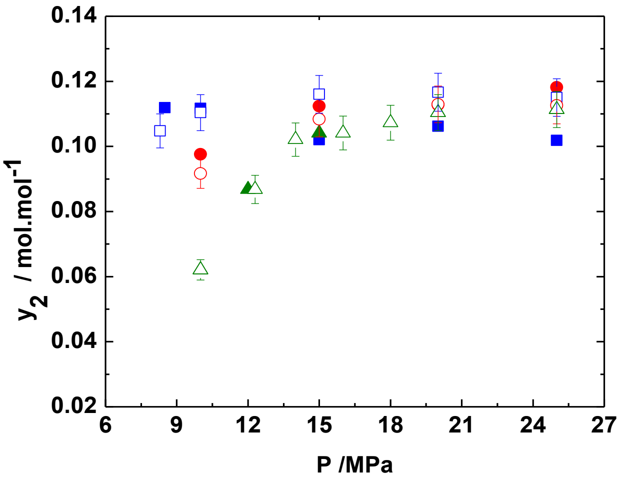

Figure 2.4 Solubility of tributyl phosphate in supercritical carbon dioxide at different temperatures; ■, 313 K; ●, 323 K; ▲, 333 K;
Open symbols represents present work; Solid symbol represent *Meguro *et al.* data [79]

(b) Solubility of TOA in SCCO$_2$

The solubility of TOA in SCCO$_2$ was determined at 308-328 K with pressure ranging from 10-20 MPa. These results are compared with Ghaziaskar *et al.* [193] and are in good agreement with literature data with an average deviation < 7% (**Figure 2.5**).

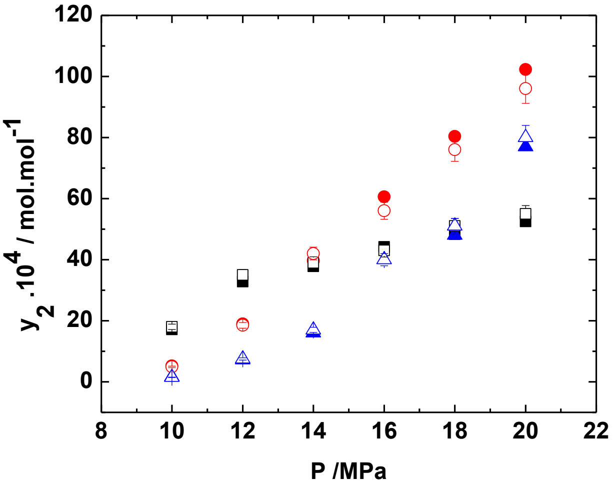

Figure 2.5 Solubility of trioctyl amine in supercritical carbon dioxide at different temperatures; ■, 308 K; ●, 318 K; ▲, 328 K;
Open symbols represents present work; Solid symbol represent Ghaziaskar *et al.* [193]

2.1.6 Supercritical fluid extraction studies

The schematic of the SFE apparatus for "extraction studies" used in the present work is slightly different from the one used for the solubility measurements (**Figure 2.6)**. High pressure extraction vessels of 1 mL and 10 mL capacity were used in this study. In case of the extraction studies, the twin high pressure equilibrium cells and entrainer column were replaced with 1 or 10 mL extraction vessel.

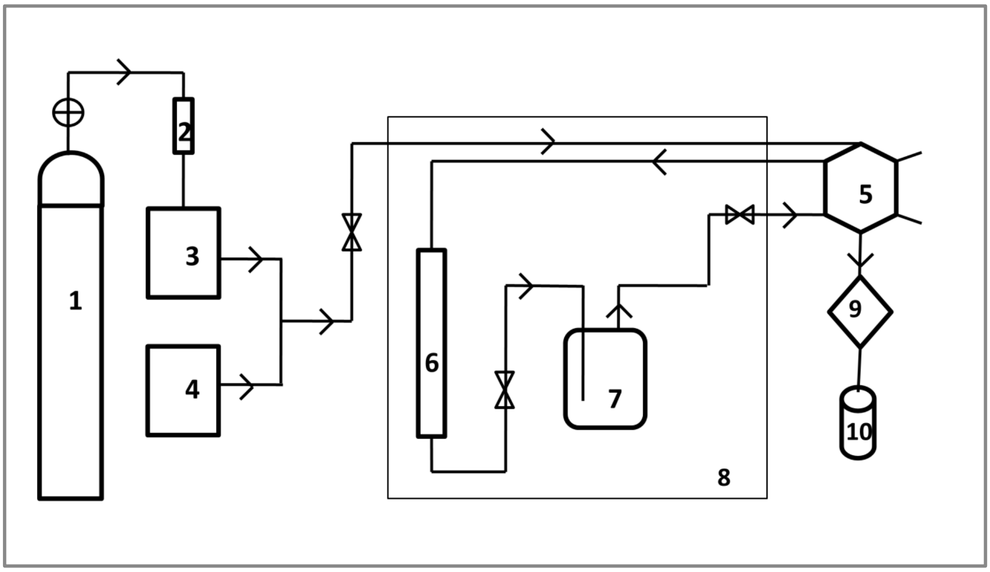

Figure 2.6 Schematic diagram of experimental set-up for the supercritical fluid extraction studies; (1) Carbon dioxide cylinder, (2) molecular sieve filter, (3) carbon dioxide pump, (4) co-solvent pump, (5) six way valve, (6) heat exchanger, (7) High pressure extraction vessel (8) oven, (9) back pressure regulator, (10) collection vessel.

In a typical SFE experiment, the compound of interest was loaded in to a high pressure extraction vessel. CO_2 is delivered to the extraction vessel at a desired flow rate. The modifier (co-solvent) pump is employed to mix the desired percentage of the co-solvent (in case of polar analytes) or ligand (in case of metal ions extraction) to the CO_2 stream. The CO_2 and co-solvent streams are mixed using T-joint and the stream is allowed to pass through a 5 meter long spiral coil or 10 mL heat exchanger for acquiring homogeneity and desired temperature. At a fixed experimental temperature, the system was pressurized until desired pressure is reached. The CO_2 stream is continuously allowed to pass through the extraction vessel (pre-loaded with the analyte) at a constant flow rate. The $SCCO_2$ containing the analyte is continuously depressurized to atmospheric pressure using the back pressure regulator. The $SCCO_2$ stream with the analyte is directly bubbled into a collection vessels containing suitable solvent, where the analytes is stripped into the solvent and CO_2 escapes as a gas. In the case of experiments involving extraction of radioisotopes e.g. ^{239}Pu, the SFE system is housed in a special glove box with all safety features for handling radioactive materials [194]. SFE of metal ions is carried out in two different modes: (i) static mode and (ii) dynamic mode

(i) Static extraction

In static mode of extraction, known amount of analyte (e.g. metal ions) and sufficient amount of ligand/complexing agent were loaded into a high pressure extraction vessel. The extraction vessel was kept inside a thermostat and pressurized with $SCCO_2$ until desired pressure is achieved. After achieving the desired temperature and pressure, the extraction vessels were closed under supercritical conditions for static equilibration for a known time period (e.g. 30 min. to 120 min.). During the equilibration, metal ion reacts with the ligand and forms a metal-ligand complex which is soluble in $SCCO_2$ medium. Subsequent to the static equilibration, neat $SCCO_2$ was continuously allowed to pass through the extraction vessel (e.g. 30 min.) and the extracts were collected in a collection vessel.

(ii) Dynamic extraction

In dynamic mode of extraction, known amount of analyte (e.g. metal ions) was loaded onto a high pressure extraction vessel. Ligand is continuously mixed with the $SCCO_2$ stream and the resultant mixture is continuously allowed to pass through the extraction vessel at a constant flow rate. During the process, metal ions forms a complex with the ligand and the metal-ligand complex is transported by the $SCCO_2$ to the collection vessel.

Depending on the chemical nature of the metal ions and nature of the matrix, (a) static or (b) dynamic or (c) static + dynamic extraction modes are employed for the efficient extraction of metal ions. Metal ions present in the extracts were back stripped into 0.01 N HNO_3 and the analysis was carried out using suitable analytical techniques. The remains of the extraction vessels (un-extracted sample in the vessel) was washed with 1 N HNO_3, evaporated to near dryness and re-dissolved in 0.01 N HNO_3 for their estimation. The extraction efficiency, E (%) is defined by the following equation

$$E(\%)=\left(\frac{Amount\,of\ metal\,extracted}{Amount\,of\ metal\,loaded}\right)*100 \qquad (2.7)$$

Each experiment was repeated thrice and the uncertainty in the extraction efficiency was found to be within ± 5%.

2.1.7 Analysis of metal ions using high pressure liquid chromatography

The SFE extracts were collected into a mixture of 0.01 N HNO_3 and chloroform mixture; the end of flow restrictor was directly placed on to a HNO_3-chloroform mixture and the metal solvate dissolved in $SCCO_2$ stream was directly bubbled into this. In this process, metal solvates were first dissolved in chloroform and then back stripped into 0.01 N HNO_3 medium. The back stripping efficiency of metal ions was found to be > 97 % in these experiments. The remains (un-extracted) of the uranium and thorium in the extraction vessel were washed and collected in 0.01 N HNO_3 medium and analyzed for uranium and thorium contents. However in the case of SFE experiments involving HDEHP, H-phosphonates and CMPO as ligands, the extracts were collected in chloroform followed by back stripping with sodium carbonate. The extracts containing metal ions were acidified with dil. HNO_3 and subsequently analyzed by HPLC technique.

The assay of uranium, thorium and lanthanides were carried out using HPLC technique. The HPLC system (JASCO, Japan) employed in the present study consisted of solvent delivery pump (JASCO-PU-1580), gradient mixer, sample injector (Rheodyne-7725), reverse phase C_{18} column (Hypersil -250x4.6mmx5μ; made up of octadecyl silane), post-column delivery pump and UV-VIS spectrophotometric detector (UV-1570).

α-hydroxy-*iso*-butyric acid (pH: 3.0-3.4) was used as a mobile phase for the separation and estimation of uranium and thorium. A mixture of 0.1 M α-HIBA and 0.01 M (1S)-(+)-camphor-10-sulfonic acid with a pH 3.5 was employed as the mobile phase for the separation of lanthanides, uranium and thorium [195]. Metal ions are injected into the HPLC system through a 20 μL sample loop injector. The metal ions are separated on the column and the effluent from the column was mixed with the chromogenic reagent, Arsenazo (III) (2,2'-(l,8-dihydroxy-3,6-disulfonapthalene-2,7-bisazo)bis(benzene-arsenic acid)) (1.5×10^{-4} M) using a "T" connector and the complexes were monitored using a UV-Vis detector. Uranium, thorium and lanthanide complexes were detected at 655 nm. The concentration of uranium, thorium and lanthanides was determined using a calibration plot, obtained with standard solutions and is briefly described in **Appendix-3.**

2.1.8 Analysis of plutonium

Plutonium assay was carried out using liquid scintillation counting (LSC) technique (300SL TDCR liquid scintillation analyzer, Hidex, Finland). LSC is an analytical technique to quantify the radioactivity of the sample (mostly beta/alpha emitting radioisotopes) using a liquid scintillation cocktail. Liquid scintillation cocktail absorbs the energy emitted by the radioisotopes and convert it into photons in the visible region which in turn are converted into photoelectrons by photomultiplier tube and subsequently measured as an electronic pulse [196]. LSC cocktail solution was used for counting radionuclide in both aqueous and organic media. An aliquot of Pu containing solution was added to the cocktail solution and the plutonium content was assayed by LSC.

Chapter 2 (b)

Semi-empirical models for solubility correlations

The following semi-empirical models were employed in the present work for correlating the solubility of different ligands in $SCCO_2$.

2.2.1 Chrastil model

Chrastil model [101] is one of the first density-based models employed for correlating the solubility of compounds in supercritical fluids. It assumes the formation of an equilibrium solvato-complex between solute and $SCCO_2$ molecules. Chrastil model relates the solubility of solute and density of pure $SCCO_2$ as follows:

$$\ln S = k \ln \rho + \frac{A_1}{T} + B_1 \qquad (2.8)$$

In Eq. (2.8), S is the solubility of solute in $SCCO_2$ in g/L; ρ is the density of the $SCCO_2$ in g/L; *k* is the association number which describes the average number of $SCCO_2$ molecules associated with the solvato-complex; A_1 is a function of enthalpy of vaporization and enthalpy of solvation; T is the temperature in K; B_1 depends on the association number and molecular weight of solute and $SCCO_2$.

2.2.2 Adachi and Lu model

Chrastil model has limitation to compounds with higher solubility and wide range of temperatures [95, 197]. Therefore the model underwent several modifications. Adachi and Lu [198] proposed a modification for the Chrastil equation by treating association number (*k*) as density dependent and changed it to a second order polynomial of $SCCO_2$ density to minimize the errors in the solubility predictions. Adachi and Lu equation can be expressed as

$$\ln S = (A_2 + B_2\rho + C_2\rho^2)\ln \rho + \frac{D_2}{T} + E_2 \qquad (2.9)$$

In Eq. (2.9), S represents the solubility of solute in SCF (g/L), ρ is density of SCF (g/L), T is temperature (K) and A_2, B_2, C_2, D_2 and E_2 are model parameters which can be obtained by the regression analysis of the experimental data.

2.2.3 Chrastil model for solubility of solutes in presence of co-solvents

Chrastil equation correlates the solubilities of solutes in pure $SCCO_2$. Gonzalez *et al.*[116] modified the Chrastil equation to correlate the solubilities of solutes in $SCCO_2$ in the presence of a co-solvent by considering the solute-co-solvent-solvent complex formation. The modified form of Chrastil equation is given by

$$\ln S = k \ln \rho + \gamma \ln m + \frac{A_3}{T} + B_3 \qquad (2.10)$$

In Eq. (2.10), S is the solubility of solute in $SCCO_2$ + co-solvent mixture ($kg.m^{-3}$), k denotes the number of solvent molecules associated in the solvato complex, ρ is the density of SCF ($kg.m^{-3}$), γ represent the association number of co-solvent, m is the concentration of co-solvent ($kg.m^{-3}$). A_3 is a constant and defined as $\Delta H/R$, where ΔH is the sum of enthalpy of vaporization and solvation and R is the gas constant, B_3 is a constant and is a function of k, γ and molecular weights of solute, solvent and co-solvent.

2.2.4 Mendez - Santiago and Teja (MT) model

Mendez - Santiago and Teja [103] derived a model for the solubility of solutes in supercritical fluids using a classical expansion of Helmholtz energy around the critical point of solvent to represent mixture properties at infinite dilution. The derived model expresses the solubility of a solute as a function of temperature, pressure and the density of $SCCO_2$ as follows

$$T \ln(Py_2) = A_4 + B_4\rho + C_4 T \qquad (2.11)$$

In Eq. (2.11), y_2 is the mole fraction solubility (moles of compound per mole of $SCCO_2$, $mol.mol^{-1}$), T is temperature in K, P represents pressure in MPa and ρ is density of supercritical fluid in kg.m^{-3}. A_4, B_4, C_4 are temperature independent constants that can be obtained by regression. Rearranging Eq. (2.11) gives

$$T\ln(Py_2) - C_4 T = B_4\,\rho + A_4 \qquad (2.12)$$

From Eq. (2.12), the plot between $T\ln(Py_2)-C_4T$ with ρ gives a single straight line at all isotherms. The consistency of the experimental data can be checked by the convergence of all solubility isotherms into a single straight line.

2.2.5 Solution model based on Wilson activity co-efficient model

Empirical/semi-empirical models that correlate the “liquid solubilities” in SCFs are limited. A semi-empirical equation with three parameters was developed for correlating solubilities of liquid solutes using solution theory coupled with Wilson activity coefficient model [199]. This model was derived by treating the fugacity of the solute similar in both liquid and SCF phases, at equilibrium. Further, the activity coefficient of the solute in SCF phase was determined using Wilson activity coefficient model. The simplified form of the equation is

$$\ln\left(\phi y_2\right) = A_5\phi + \frac{B_5}{T} + C_5 \qquad (2.13)$$

In Eq. (2.13), ϕ is pure component molar volume ratio liquid solute to supercritical solvent, y_2 is mole fraction solubility, T is temperature (K) and A_5, B_5 and C_5 are temperature independent constants.

2.2.6 Association theory based on van Laar activity coefficient model

This model was derived using association theory, where a molecule of solute *A* (liquid) associates with *k* molecules of solvent *B* ($SCCO_2$) to form a solvate complex, which is in equilibrium with the supercritical phase [191]. An expression in terms of densities of both phases, fugacities, activity coefficients, pressure and temperature is obtained as

$$\ln y_2 = (k-1)\ln\left(\frac{P}{P*}\right) + \frac{\Delta H_s}{RT} - q_s - [2(B_{AB_kB} - kB_{BB}) + (k-1)B]\rho_B - \ln\left(\frac{\phi_B^{*k}}{\phi_{AB_k}^{*}}\frac{\phi_A^{*}}{\phi_{sat}}\frac{P^{*}}{x_A}\right) + A_v - \frac{B_v}{T} + \ln\gamma_A + \frac{\rho_B}{\rho_A} \quad (2.14)$$

The above expression was simplified and the activity coefficient was modeled using a van Laar activity coefficient model and can be expressed as [191],

$$y_2 = \left(\frac{P}{P^*}\right)^{K_{VL}-1} \exp\left[\left(\frac{1}{T}\right)\left\{A_{VL} + C_{VL}\left(\frac{\rho_B}{\rho_A}\right) + D_{VL}\left(\frac{\rho_B}{\rho_A}\right)^2\right\} + E_{VL}\left(\frac{\rho_B}{\rho_A}\right) + F_{VL}\right] \quad (2.15)$$

In Eq. (2.15), y is solubility, P is pressure in MPa, $P*$ is reference pressure, T is temperature in K, k_{VL} represents association number, A_{VL}, C_{VL}, D_{VL}, $E_{VL}$and F_{VL} are temperature independent constants. Eq. (2.15) was used for correlating the solubilities of liquid solutes in SCCO$_2$.

The above models were employed in the present work to correlate the solubility of various ligands in SCCO$_2$ medium. Multiple linear regression and non-liner curve fitting methods are used to evaluate the model parameters. The experimental solubilities are compared with the correlated solubilities using the above models. The deviation of experimental solubilities from the solubilities obtained from the semi-empirical models was quantified using an objective function average absolute relative deviation (AARD %) and is given by Eq. (2.16)

$$AARD\% = \frac{100}{N}\sum_{i=1}^{N}\left(\frac{\left|y_{2,cal} - y_{2,\exp}\right|}{y_{2,\exp}}\right) \qquad (2.16)$$

In Eq. (2.16), y_{2cal} is the solubility derived from the model, $y_{2,exp}$ represents experimental solubility and N is number of data points.

Chapter 3

Experimental determination and correlation of solubility of trialkyl phosphates in supercritical carbon dioxide

---

Chapter 3(a)

Solubility of trialkyl phosphates in supercritical carbon dioxide

---

3.1.1 Introduction

The determination of solubility of trialkyl phosphates in $SCCO_2$ is crucial step towards designing a SFE method for recovery of actinides from aqueous medium, e.g. recovery of actinides from nitric acid medium. However, the literature data on solubilities of organophosphorus compounds in $SCCO_2$ is scarce. Among the trialkyl phosphates, the solubility of only TBP was reported and the solubility behavior of other trialkyl phosphates has not been studied. Other trialkyl phosphates e.g. THP is an alternate candidate material for fast reactor fuel reprocessing. Hence, the solubilities of series of trialkyl phosphates in $SCCO_2$ medium were investigated at different temperatures and pressures.

3.1.2 Solubility of trialkyl phosphates in supercritical carbon dioxide

The solubilities of various trialkyl phosphates: TMP, TEP, TBP, TAP and THP were measured at temperatures of 313, 323 and 333 K in the pressure range of 10 to 25 MPa. The solubilities were measured three times at each experimental condition. The uncertainty of experimental measurements was found to be ± 5%.

In general, solubilities of trialkyl phosphates were found to be high in the investigated region (**Table 3.1)**. The variation of solubilities of trialkyl phosphates with temperature and pressure is shown in **Figure 3.1**. Across all the isotherms, (313, 323 & 333 K) the solubilities of trialkyl phosphates increases with the pressure. Increasing the pressure at isothermal conditions increases the density of $SCCO_2$, improving the specific interactions between CO_2 and solute molecules, enhancing the solvating power, leading to higher solubility. The retrograde behavior was observed with temperature and the solubilities of trialkyl phosphates decrease with raise in temperature in the entire pressure region. The effect of temperature on the solubility is not straight forward and there are two competing factors that can influence the solubility. The vapor pressure of the solute generally increases with the temperature whereas density of $SCCO_2$ decreases with increase in temperature. However, the vapor pressure of the trialkyl phosphates in the investigated temperature region of 313 to 333 K is very low, thus making density as the dominating factor. The decrease of $SCCO_2$ density with temperature results in reduced solubility at 333 K compared to that obtained at 313 K (**Figure 3.1)**.

From the solubility data, it is observed that TMP has highest solubility among its homologous series investigated in the present study. The solubilities of TMP ranged from 0.122 to 0.194 moles per mole of $SCCO_2$ (mol/mol). THP has relatively lower solubilities, ranging from 0.005 to 0.085 mol/mol. All other trialkyl phosphates show intermediate solubility in comparison to TMP and THP. It was found that the solubility is inversely related to the number of carbon atoms present in the trialkyl phosphate. The vapor pressure is a parameter influencing the solubility behavior and is directly dependent on the molecular weight of the compound. For a homologous series, the solubility of a solute generally decreases with increase in carbon number (vapor pressure decrease with increase in carbon chain) [200, 201]. Experimental solubilities of trialkyl phosphates were plotted against their carbon number at 20 MPa with temperature ranging from 313 to 333 K (**Figure 3.2**). It was found that, in the homologous series of trialkyl phosphates, the solubility decreases with carbon number at all isotherms; solubility of trialkyl phosphates decreases with increase in the temperature. Thus density term mainly influence solubility of phosphates rather than changes in vapor pressure (trialkyl phosphates have negligible vapor pressure in the temperature range of study).

Table 3.1 Experimental solubilities of trialkyl phosphates in SCCO$_2$ medium as a function of temperature and pressure

T (K)	*P* (MPa)	Density* (kg/m^3)	Solubility, y_2 (mol/mol)				
			TMP	**TEP**	**TBP**	**TAP**	**THP**
313.0	8.3	320.54	0.188	0.160	0.105	0.097	0.075
313.0	10.3	651.49	0.191	0.162	0.110	0.099	0.081
313.0	12.3	727.57	0.191	0.163	0.113	0.099	0.082
313.0	15.0	781.32	0.192	0.163	0.116	0.101	0.083
313.0	20.0	840.61	0.193	0.163	0.117	0.102	0.084
313.0	25.0	880.15	0.194	0.163	0.115	0.103	0.085
323.0	10.3	423.74	0.180	0.145	0.092	0.091	0.065
323.0	12.3	604.62	0.189	0.152	0.103	0.098	0.074
323.0	15.0	701.08	0.190	0.156	0.108	0.098	0.079
323.0	20.0	785.16	0.191	0.158	0.113	0.099	0.080
323.0	25.0	834.89	0.192	0.160	0.113	0.100	0.081
333.0	10.3	309.89	0.122	0.090	0.062	0.014	0.005
333.0	12.3	458.89	0.153	0.116	0.087	0.054	0.024
333.0	14.0	563.09	0.165	0.144	0.102	0.092	0.046
333.0	16.0	638.84	0.177	0.150	0.104	0.096	0.064
333.0	18.0	688.34	0.182	0.153	0.107	0.096	0.070
333.0	20.0	724.63	0.185	0.154	0.110	0.097	0.074
333.0	25.0	787.28	0.186	0.155	0.111	0.098	0.077

* Density values taken from http://webbook.nist.gov/chemistry/fluid/

Experimental conditions: CO$_2$ flow rate: 0.1 mL/min, Equilibrium cell volume: 50 mL, No. of equilibrium cells connected in series: 2; sample loaded in equilibrium cells: 1st cell-35 mL and 2nd cell: 25 mL; heat exchanger: 10 mL; entrainer column: 10 mL;

Standard uncertainties (u) are u(T) = 0.1 K, u(P) = 0.1 MPa and relative uncertainty (u$_r$), u$_r$(y_2) = 0.05

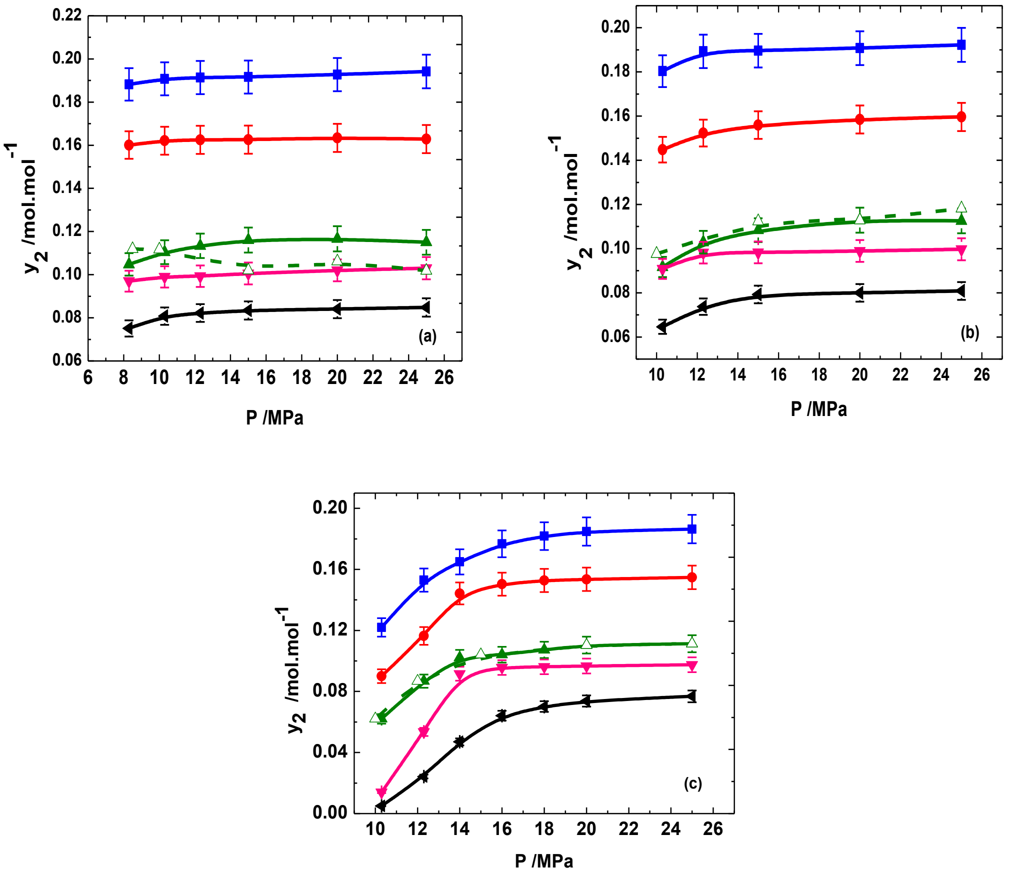

Figure 3.1 Variation of solubility of trialkyl phosphates with pressure at different temperatures of (a) 313 K; (b) 323 K; (c) 333 K; (■, trimethyl phosphate; ●, triethyl phosphate; ▲, tributyl phosphate ; ▼, triamyl phosphate; ◀, trihexyl phosphate); Solid symbols and solid lines represent the present work; Open symbols and dash line represent the tributyl phosphate (TBP) data by Meguro *et al.* [79]

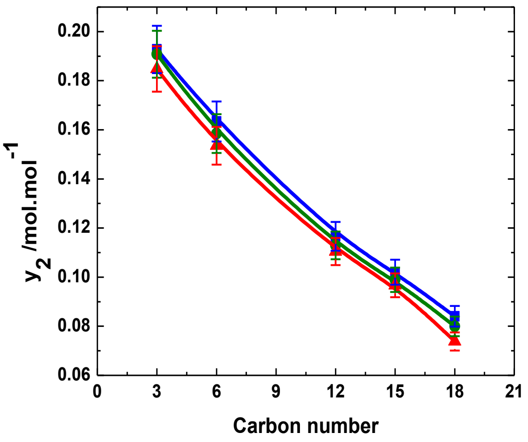

Figure 3.2 Variation of solubility of trialkyl phosphates with their carbon number at 20 MPa, with temperatures ■, 313 K; ●, 323 K; ▲, 333 K

The interaction and solubility of trialkyl phosphates in $SCCO_2$ is mainly due to Lewis acid (LA)- Lewis-base (LB) interactions and weak C-H--O hydrogen bonding [202]. Because of CO_2 quadrupole moment, there will be a charge separation between carbon and oxygen atoms and electron density moves towards oxygen. Therefore, the carbon atom has partial positive charge, acting as a LA and oxygen atoms having negative charge act as a LB. The phosphoryl group of the trialkyl phosphate acts as LB and interacts with the CO_2 through LA-LB interactions [202]. The partial negative charge on oxygen atom induce the electrostatic interaction with –C-H group present in the trialkyl phosphate to form a weak H- bonding. Kim *et al*. performed quantum mechanical calculations for the CO_2-TMP complex and found that the LA-LB interaction energy was much higher than the weak H- bonding and it could be the main driving force for the higher solubility in CO_2[202]. The higher solubilities in the investigated pressure and temperature range may be due to the complete miscibility of the trialkyl phosphates with $SCCO_2$. Meguro *et al*. reported high solubility behavior of TBP in $SCCO_2$ due to the formation of single phase TBP - $SCCO_2$ [79]. The phase behavior of TBP/CO_2 system is studied by Page et al., [80] and P-T-*X* diagrams revealed that up to 15.5 mol% of TBP, TBP/CO_2system is in a single phase with corresponding temperature and pressure.

3.1.3 Model correlations

(a) Mendez-Teja model

Mendez-Teja (MT) (Eq. (2.11)) model was employed in the present study to check self-consistency of the experimental solubility data. The model parameters of the MT model were obtained by the regression of the experimental data and represented in **Table 3.2**. The consistency of the solubility data was checked by plotting the density with $T \ln (Py_2)-C_4T$ at different isotherms. The plot of $T \ln (Py_2)-C_4T$ and □□□was linear with all experimental data collapsing on to single straight line (**Figure 3.3**) and this indicates that the data is self-consistent. MT model was also employed to correlate and predict the solubility of trialkyl phosphates in the investigated regions. MT model successfully correlated the solubility data with an average deviation of less than 10%.

(b) Chrastil model

Chrastil equation has been employed to correlate the solubility data of trialkyl phosphates in $SCCO_2$. The experimental solubilities were regressed with Eq. (2.8) to obtain the model parameters *k*, A_1 and B_1 and are reported in **Table 3.2**. The logarithm of solubility (g/L) data was plotted against the logarithm of density (g/L) of $SCCO_2$. These plots represent straight lines for different isotherms and are shown in **Figure 3.4**. The association number (*k*) for trialkyl phosphates was determined from the slopes of the lines and found to be about 1 in the investigated pressure and temperature region. The slope of the isotherms is close; however, the slope shows a small increase at higher temperature, revealing lower vapor pressures of trialkyl phosphates; thus density is the dominating factor that influences the solubility.

(c) Association theory based on van Laar activity coefficient model

An association model was developed for the correlation of solubilities of liquid solutes in $SCCO_2$ medium [106]. The simplified form of the equation is represented by

$$y_2 = \left(\frac{P}{P^*}\right)^{K_{VL}-1} \exp\left[\left(\frac{1}{T}\right)\left\{A_{VL} + C_{VL}\left(\frac{\rho_B}{\rho_A}\right) + D_{VL}\left(\frac{\rho_B}{\rho_A}\right)^2\right\} + E_{VL}\left(\frac{\rho_B}{\rho_A}\right) + F_{VL}\right] \qquad (3.1)$$

From Chrastil model correlations, the association number (k_{VL},) was close to unity. Assuming k_{VL} to be unity in Eq. (3.1), and the equation can be rewritten as,

$$y_2 = \exp\left[\left(\frac{1}{T}\right)\left\{A_{VL} + C_{VL}\left(\frac{\rho_B}{\rho_A}\right) + D_{VL}\left(\frac{\rho_B}{\rho_A}\right)^2\right\} + E_{VL}\left(\frac{\rho_B}{\rho_A}\right) + F_{VL}\right] \qquad (3.2)$$

The model parameters in Eq. (3.2) were obtained by non-linear curve fitting and represented in **Table 3.2**. The solubilities correlated by the model are depicted by **Figure 3.5**. Among the models employed in the present work, van Laar activity coefficient model resulted in better solubility correlations with an AARD < 7%.

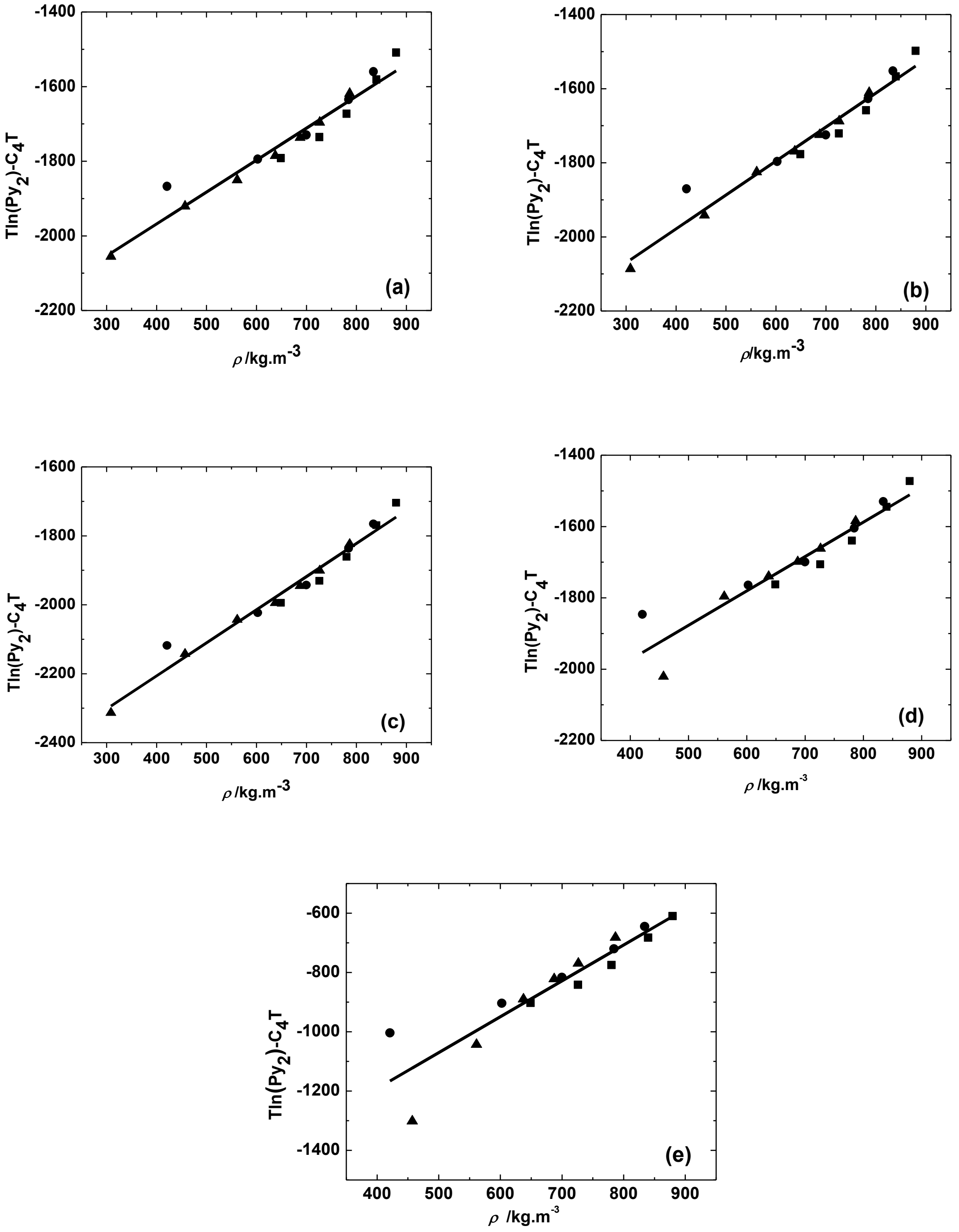

Figure 3.3 Solubility of (a) trimethyl phosphate, (b) triethyl phosphate, (c) tributyl phosphate, (d) triamyl phosphate, (e) trihexyl phosphate at different temperatures, ■, 313 K; •, 323 K; ▲, 333 K. Solid line represents the MT model fit (Eq. (2.11)).

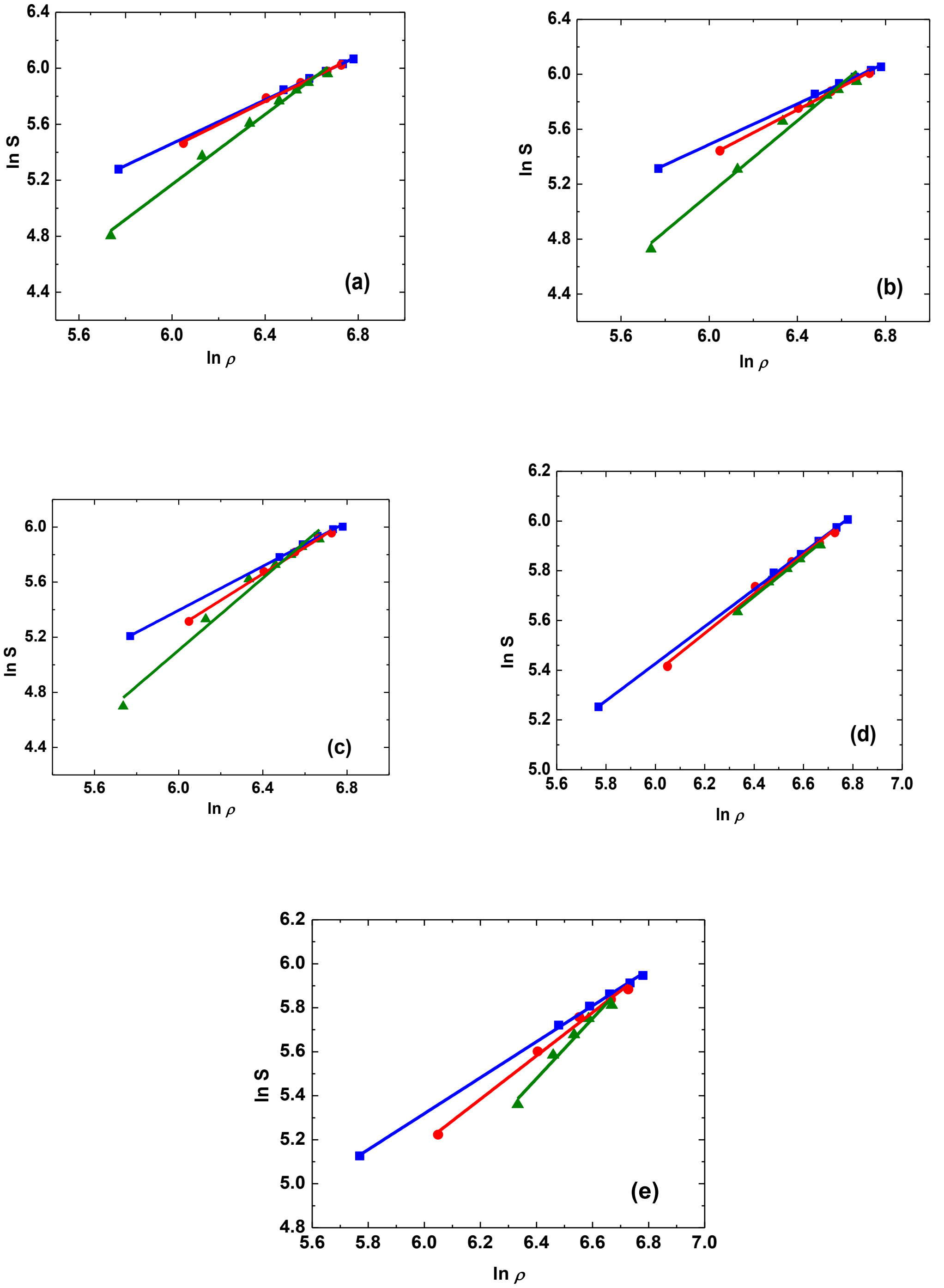

Figure 3.4 Correlation plots of ln S vs. ln ρ (Eq. (2.8)) for trialkyl phosphates in the pressure range of 10 to 25 MPa, and the temperature of ■, 313 K; ●, 323 K; ▲, 333 K; (a) trimethyl phosphate, (b) triethyl phosphate, (c) tributyl phosphate, (d) triamyl phosphate, (e) trihexyl phosphate

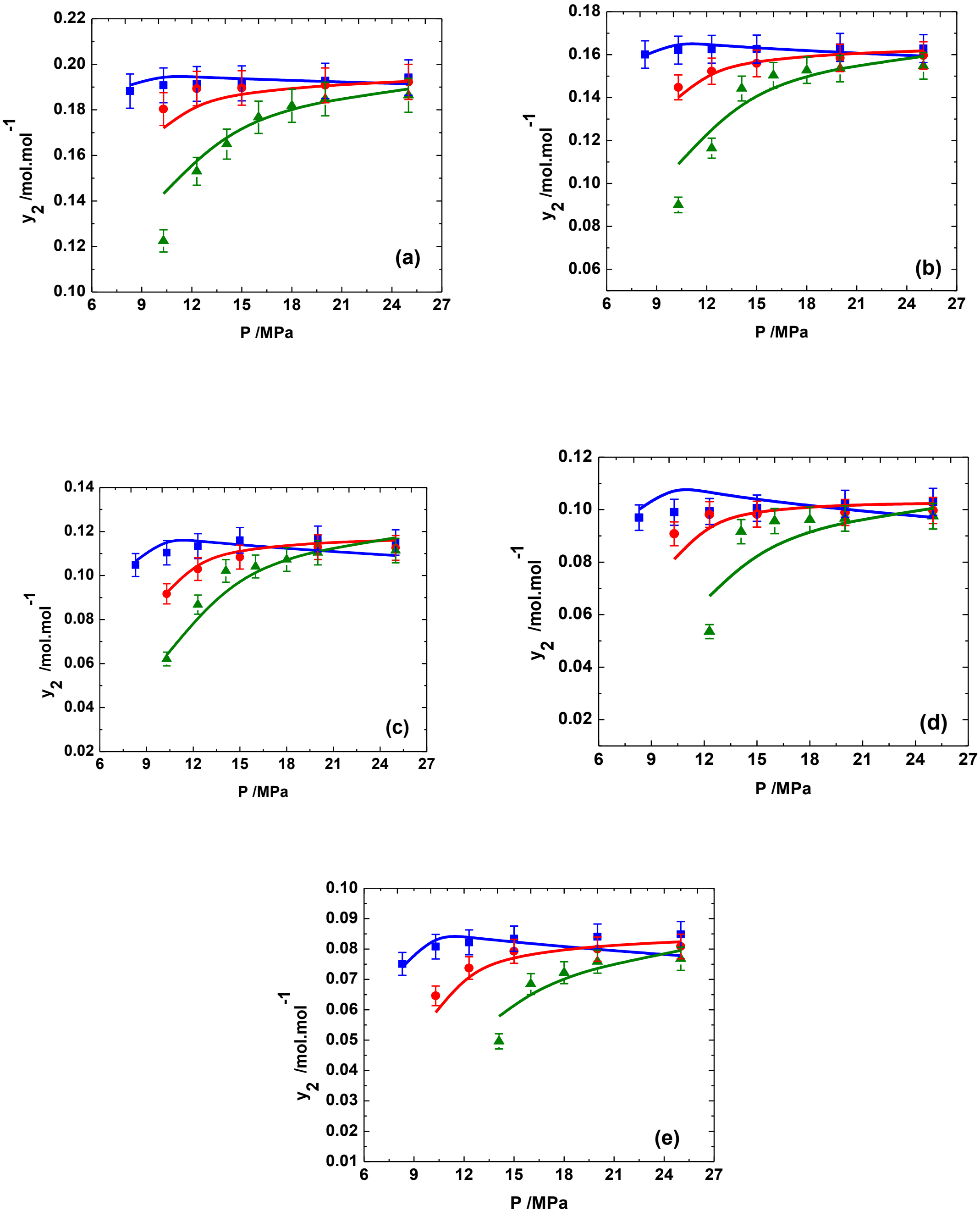

Figure 3.5 Variation of solubility of trialkyl phosphates with pressure at different temperatures; ■, 313 K; ●, 323 K; ▲, 333 K; in supercritical carbon dioxide. (a) trimethyl phosphate, (b) triethyl phosphate, (c) tributyl phosphate, (d) triamyl phosphate, (e) trihexyl phosphate; The solid line represents the association model based on van Laar activity coefficient model (Eq. (3.2))

Table 3.2 Regression analysis and model parameters for the correlation of solubilities of trialkyl phosphates using different models

Model	Model Parameters	TMP	TEP	TBP	TAP	THP
MT model Eq. (2.11)	A_4	-2313±36	-2358±35	-2593±30	-2363±60	-2052±60
	B_4	0.85±0.05	0.92±0.05	0.96±0.04	0.97±0.08	0.94±0.08
	C_4	6.4±0.5	6.26±0.5	6.54±0.54	5.7±0.5	4.54±0.4
	R^2	0.942	0.954	0.967	0.885	0.913
	AARD (%)	7	7	6	9	10
Chrastil model Eq. (2.8)	A_1	514±4	433±4	392±4	106±1	546±3
	B_1	-1.56±0.01	-1.75±0.02	-1.50±0.01	0.53±0.02	-1.84±0.01
	k	0.890±0.03	0.957±0.04	0.929±0.01	0.758±0.01	0.896±0.01
	R^2	0.937	0.954	0.968	0.997	0.973
	AARD (%)	6	7	5	3	4
Association model based on van Laar activity coefficient model Eq. (3.2)	k_{VL}	1	1	1	1	1
	A_{VL}	2369 ±27	3169 ±40	4400 ±150	5520 ±105	6250 ±150
	C_{VL}	-3295±18	-3885±23	-5192±27	-6110±61	-6980±48
	D_{VL}	-118±5	-176±5	-289±6	-376±12	-390±20
	E_{VL}	10.9±0.4	13±0.1	17.8±0.6	21±1.2	24±0.8
	F_{VL}	-9.3±0.1	-12.1±0.12	-16.6±0.13	-20.3±0.4	-23±0.5
	R^2	0.90	0.87	0.92	0.70	0.84
	AARD (%)	3	3	3	7	5

While correlating the solubilities of alkanes in supercritical carbon dioxide, it was observed that the adjustable binary interaction parameters in the model vary linearly with the chain length of the *n*-alkanes [203]. Other studies have indicated that the vapor pressure is an important physicochemical parameter influencing the solubility behavior and gives a direct correlation on the solubilities in supercritical fluids [200]. Based on the above observations, the boiling points of the trialkyl phosphates [204, 205] were correlated with the carbon number of the trialkyl phosphates. This relationship is linear as observed in the inset of **Figure 3.6(c)**. Therefore, the model parameters of the all three models used in the present study were correlated with the carbon number of the trialkyl phosphates. The model parameters of the MT and Chrastil model did not show any particular trend with the carbon number, as shown in **Figure 3.6(a)** and **Figure 3.6(b)**. However, the five model parameters of the association model based on van Laar activity coefficient model successfully correlated with the carbon number of the trialkyl phosphates. A linear relationship was observed, as shown in **Figure 3.6(c)**. These equations reveal the anticipated trend of solubility with the molecular weight of the trialkyl phosphates. All the three models discussed in the study gave average AARD values ranging from 4% to 8%. However, the association model gave a linear relationship between the model parameters and the carbon number of the trialkyl phosphates. This provides an easy method to calculate the unknown solubilities of other members of the trialkyl phosphate series as well as predict the solubilities of these compounds at different temperatures and pressures.

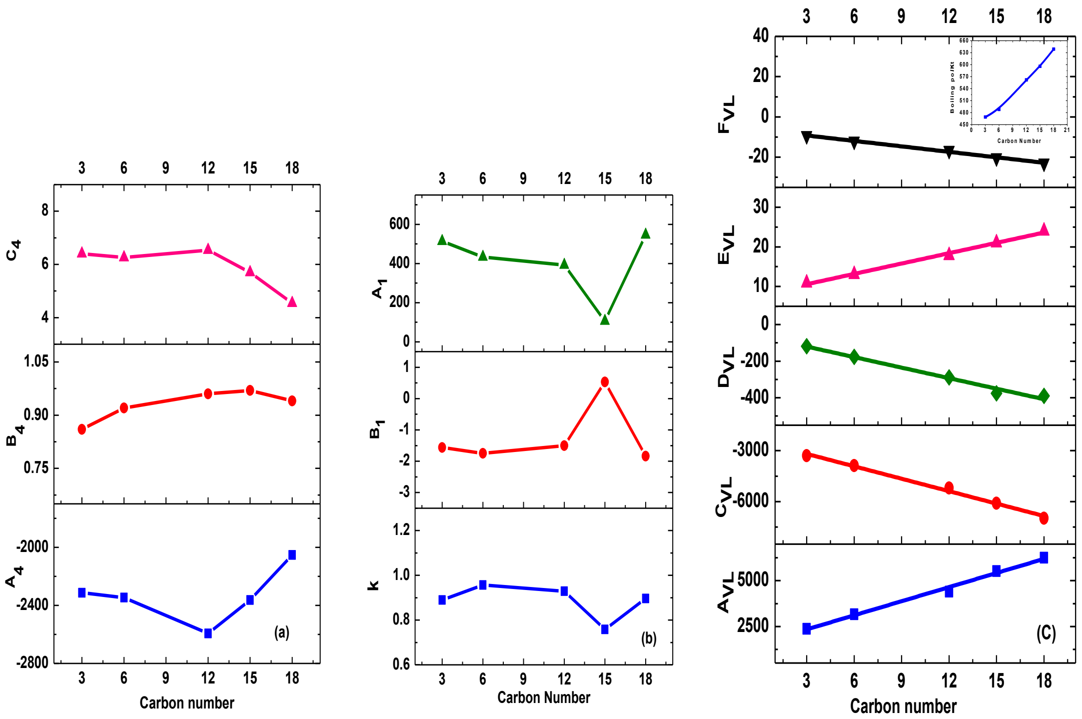

Figure 3.6 Correlation of model parameters with carbon number of trialkyl phosphates;

(a) MT model (Eq.(2.11)); Model parameters are represented by the symbols, ■, A_4; ●, B_4; ▲, C_4;

(b) Chrastil model (Eq.(2.8)); Model parameters are represented by the symbols, ■, *k*; ●, A_1; ▲, B_1;

(c) Association model based on van Laar activity coefficient model (Eq. (3.2)); Model parameters are represented by the symbols, ■, A_{VL}; ●, C_{VL}; ◆, D_{VL}; ▲, E_{VL}; ▼, F_{VL}. The inset of this figure represents the relation between carbon number and normal boiling point of the trialkyl phosphates.

3.1.4. Conclusions

The solubilities of a series of trialkyl phosphates were measured in $SCCO_2$ medium. The solubility of trialkyl phosphates increases with the pressure at constant temperature and it decreases with the temperature in the investigated pressure range. At constant temperature and pressure, solubility of trialkyl phosphates decreases with increase in molecular weight. The experimental results were successfully correlated using MT model, Chrastil and an association model based on van Laar activity coefficient model. The least AARD of 4% was obtained for the association model based on van Laar activity coefficient model. The model parameters of the association model followed a linear relationship with the carbon number (and boiling point) of the trialkyl phosphates and thus can be used to predict the solubilities of a homologous series of trialkyl phosphates. The trialkyl phosphates examined in the present study are highly soluble in $SCCO_2$ and can be employed as ligands in the SFE of actinides.

Chapter 3(b)

Solubility of tri-*iso*-amyl phosphate in supercritical carbon dioxide

---

3.2.1 Introduction

Tributyl phosphate (TBP) has some limitations such as relatively higher aqueous solubility (400 ppm), third phase formation under high metal loading conditions, chemical and radiolytic degradation [206]. Earlier solvent extraction studies from our laboratory have shown that tri-*iso*-amyl phosphate (TiAP, aqu.solubility <100 ppm), as a potential alternate ligand to TBP for spent nuclear fuel reprocessing [207]. In this context, solubility behavior of TiAP in $SCCO_2$ medium was studied with an overall objective of employing the ligand in supercritical medium for recovery of actinides.

3.2.2 Solubility of TiAP in $SCCO_2$

The solubility of TiAP in $SCCO_2$ was measured at three isotherms 313, 323 and 333 K through a pressure range of 10-25 MPa. Solubilities are expressed in terms of mole fraction (y_2) (**Table 3.3)** and data point reported is the average of least three experimental measurements with a relative standard deviation of less than 5%. The solubility of TiAP was found to be high in the investigated region and ranged from 0.014 to 0.091 mol/mol. Similarly high solubility behavior was observed in other straight-chain homologues of TiAP [79]. The high solubility of trialkyl phosphates is mainly due to the Lewis-Acid and Lewis-Base interaction between CO_2 and trialkyl phosphate respectively [202]. It has been observed that C-H…O hydrogen bonding also plays a major role in higher solubility of trialkyl phosphates [202].

The solubility data of TiAP was compared with the solubilities of TMP, TEP, TBP, TAP and THP (reported from present work; **Chapter 3(a)**) under similar experimental conditions. The solubility of TiAP was found to fall in between TBP and THP. TiAP shows a higher solubility than THP and lower solubility than TBP. This indicates that in a homologous series solubility decreases with an increase in the carbon number [200, 203]. TiAP shows a marginal decrease in the solubility than that of its corresponding straight-chain isomer TAP. In general, compounds having a branched chain are comparatively more soluble than their straight chain isomer in $SCCO_2$ [208]. The solubility difference between the isomers can be attributed to the differences in their boiling point, vapor pressure, dipole moment and molecular interactions. The boiling point and dipole moment of TiAP is lower than that of its straight chain isomer, TAP [205, 209]. Despite its (TiAP) marginal increase in vapor pressure and smaller dipole moment compared to TAP, TiAP shows marginally lower solubility than TAP.

Table 3.3 Experimental solubilities of TiAP in $SCCO_2$ medium

T (K)	P (MPa)	Density* (kg/m^3)	Solubility y_2 (mol/mol)
313.0	8.3	320.54	0.083
313.0	10.3	651.49	0.086
313.0	12.3	727.57	0.088
313.0	15.0	781.32	0.089
313.0	20.0	840.61	0.090
313.0	25.0	880.15	0.091
323.0	10.3	423.74	0.079
323.0	12.3	604.62	0.088
323.0	15.0	701.08	0.088
323.0	20.0	785.16	0.089
323.0	25.0	834.89	0.089
333.0	10.3	309.89	0.014
333.0	12.3	458.89	0.064
333.0	14.0	563.09	0.080
333.0	16.0	638.84	0.083
333.0	18.0	688.34	0.084
333.0	20.0	724.63	0.084
333.0	25.0	787.28	0.085

* Densities of carbon dioxide are taken from http://webbook.nist.gov/chemistry/fluid/

Experimental conditions: CO_2 flow rate: 0.1 mL/min, Equilibrium cell volume: 50 mL, No. of equilibrium cells connected in series: 2; sample loaded in equilibrium cells: 1st cell-35 mL and 2nd cell: 25 mL; heat exchanger: 10 mL; entrainer column: 10 mL.

Standard uncertainties (u) are u(T) = 0.1 K, u(P) = 0.1 MPa and relative uncertainty (u_r), $u_r(y_2) = 0.05$

The variation of solubility of TiAP with pressure at different temperatures is shown in **Figure 3.7**. The solubility of TiAP increases with pressure at all isotherms due to enhancement of $SCCO_2$ density. With increasing $SCCO_2$ density, the intermolecular distance between $SCCO_2$ and TiAP decrease there by increasing the specific interactions. The increase in the specific interactions between $SCCO_2$ and TiAP provides higher solubility at higher pressures. The effect of temperature on the solubility is more complex because of its simultaneous effect on the vapor pressure of solute and density of $SCCO_2$. An increase in temperature leads to a concomitant increase in the vapor pressure of the solute (for solute molecules having significant vapor pressure), thereby enhancing the solubility of the solute in supercritical fluid phase. For an isobaric system, an increase in temperature increases the solubility of solute over a certain pressure range and decreases the solubility in other pressure ranges. The region of pressure where the solubility decrease with temperature is called retrograde region [210, 211]. However, TiAP shows retrograde solubility behavior, indicating density as the decisive factor in influencing the solubility of TiAP, whose vapor pressure is low at 313-333 K.

3.2.3 Solubility correlations

The experimental solubility data of TiAP was correlated with various fundamental properties using MT, Chrastil, Adachi-Lu and solution theory based on Wilson activity coefficients. The consistency of experimental solubility data of TiAP was tested by using MT equation. The model parameters were obtained by multiple linear regression and non-linear curve fitting (**Table 3.4**). The consistency of experimental solubilities was verified by plotting $T \ln (Py_2) - C_4 T$ against the density of $SCCO_2$ (ρ) (**Figure 3.8)**. It can be observed that the experimental data at different temperatures collapse onto a straight line, indicating the self-consistency of experimental solubilities of TiAP. The experimental solubility data was compared with the calculated solubility using MT model. MT model successfully correlated the solubility of TiAP with an AARD of 10%.

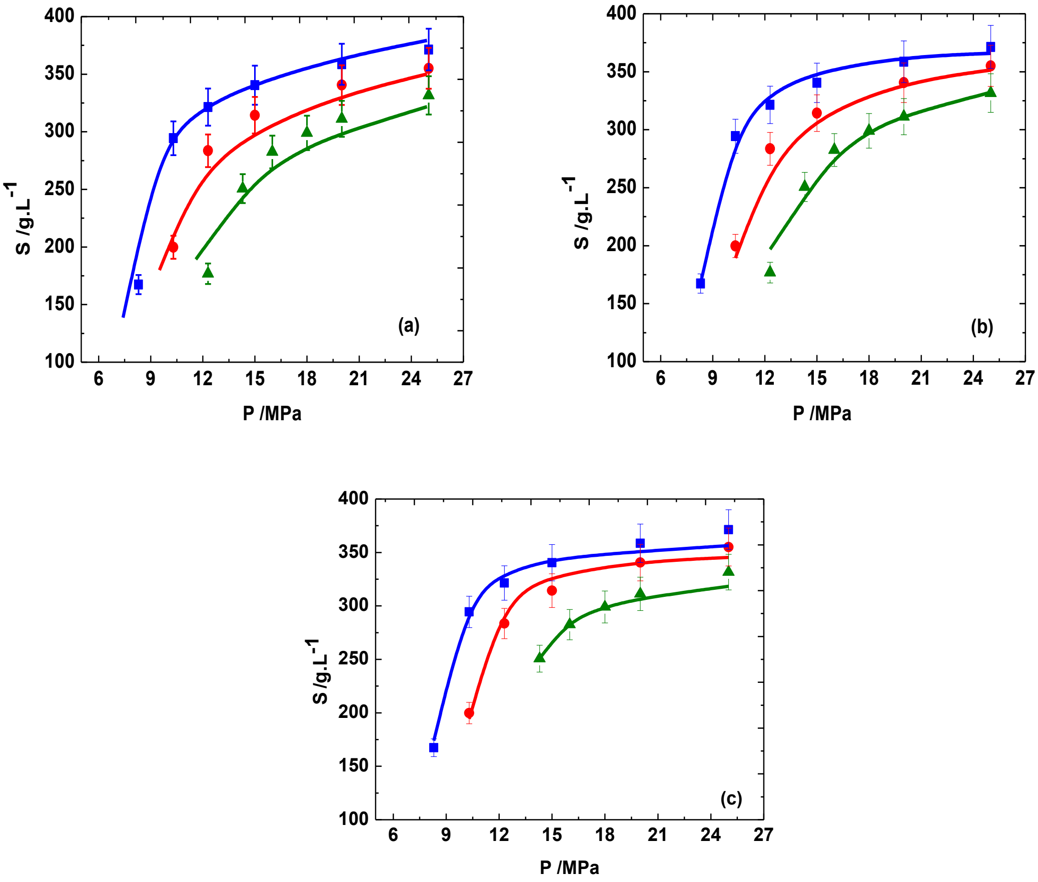

Figure 3.7 Variation of solubility of TiAP against pressure at different temperatures; ■, 313 K; ●, 323 K; ▲, 333 K; The solid lines are model predictions based on (a). Chrastil model (Eq. (2.8)), (b). Adachi and Lu model (Eq. (2.9)), (c). Solution theory coupled with Wilson activity coefficient model (Eq. (2.13))

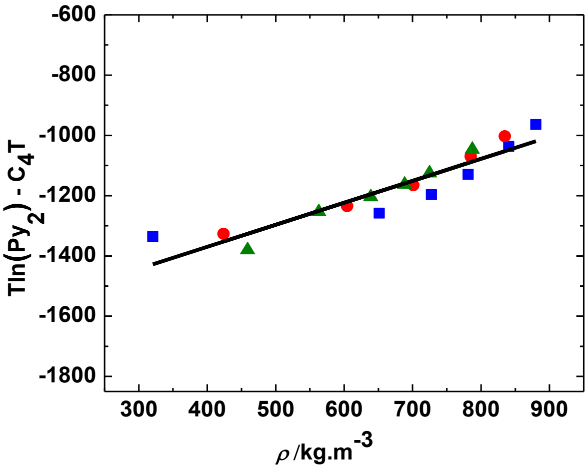

Figure 3.8 Solubility of TiAP in $SCCO_2$ medium with pressure ranging from 10.3 to 25 MPa at different temperatures, ■, 313 K; ●, 323 K; ▲, 333 K. The solid line represents model predictions based on MT model (Eq. (2.11))

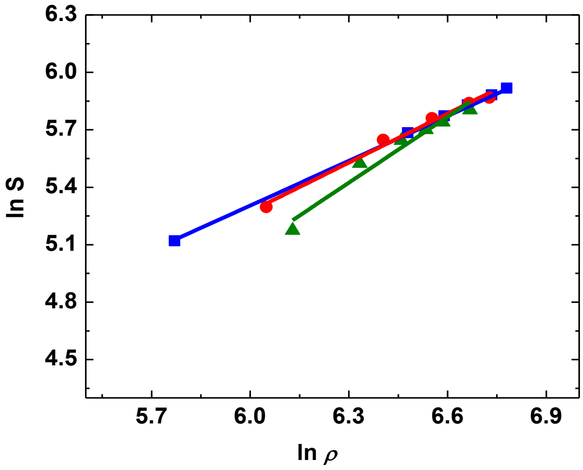

Figure 3.9 Correlation plots of ln S vs. ln ρ using Chrastil model (Eq. (2.8)) for the solubilities of TiAP in SCCO$_2$ at ■, 313 K; ●, 323 K; ▲, 333 K with pressure ranging from 10.3 to 25 MPa

Table 3.4 Regression analysis and model parameters for solubility of TiAP in SCCO$_2$ using different models

Model	**Model parameters**	
	Model parameter	**Values**
MT model (Eq. (2.11))	A_4	-1667 ± 10
	B_4	0.73 ± 0.02
	C_4	3.9 ± 0.03
	R^2	0.897
	AARD %	10
Chrastil model (Eq. (2.8))	k	0.86 ± 0.04
	A_1	278 ± 3.7
	B_1	-0.75 ± 0.05
	R^2	0.961
	AARD %	4
Adachi-Lu model (Eq. (2.9))	A_2	-2.17 ± 0.1
	B_2	1.6E-03 ±07E-06
	C_2	-7.7E-07 ± 7.5E-09
	D_2	298 ±12.2
	E_2	14.2 ± 0.37
	R^2	0.975
	AARD %	3
Solution theory + Wilson activity coefficient model (Eq. (2.13))	A_5	6.2E-03 ±6.5E-05
	B_5	200 ± 5
	C_5	0.89 ± 0.02
	R^2	0.965
	AARD %	5

The Chrastil model was employed in the present work to correlate the solubility of TiAP in $SCCO_2$. The logarithm of solubility (g/L) data was plotted against the logarithm of density (g/L) of $SCCO_2$. It was observed that log-log plot of solubility vs density is linear for all isotherms (**Figure 3.9**). The association number (*k*) for TiAP was determined from slopes and was ~ 1 in the investigated pressure and temperature region. The association number for the straight-chain isomer of TiAP, TBP was reported and is also close to unity under similar experimental conditions [79]. The slopes of the isotherms are quite close; however, the slope values show a small increase with temperature. This indicates that the lower vapor pressure of TiAP makes the solubility as density dependent in the investigated pressure and temperature region.

Chrastil (Eq. (2.8)) Adachi and Lu model (Eq. (2.9)) and solution theory based on Wilson activity coefficient model (Eq. (2.13) have also been employed to correlate the solubilities of TiAP in $SCCO_2$ and the model parameters are represented in **Table 3.4**. The experimental solubilities are compared with the calculated solubilities using the above models (**Figure 3.7)**. All three models successfully correlated the solubility of TiAP. The average AARD% for Chrastil model, Adachi and Lu model and solution model based on Wilson activity coefficient is 4, 3 and 5% respectively. These results demonstrate that the above models can be used to predict the solubilities of TiAP at any desired temperature and pressure in the investigated region.

3.2.4. Conclusions

The solubility TiAP in $SCCO_2$ medium was measured using a dynamic method. The solubility of TiAP was found to increase with increasing pressure, while a decreasing trend was seen with increasing temperature in the investigate regions. The experimental solubilities were successfully correlated using MT model, Chrastil model, Adachi and Lu model and a solution model with Wilson activity coefficient model and average AARD % was found to be 9, 4, 3 and 5% respectively.

Chapter 4

Solubility of dialkylalkyl phosphonates in supercritical carbon dioxide medium

---

4.1 Introduction

Dialkylalkyl phosphonates have higher basicity on phosphoryl oxygen atom (P=O) compared to their corresponding trialkyl phosphates, e.g. TBP. Dialkylalkyl phosphonates have strong and superior extracting properties than the corresponding phosphates [162]. The same is required for selective extraction of actinides from a mixture of metal ions. The solubility behavior of phosphonates in $SCCO_2$ medium has not been studied in literature. Hence, solubility of dialkylalkyl phosphonates in $SCCO_2$ medium was measured to examine their utility as ligands for the actinide recovery.

4.2 Solubility of dialkylalkyl phosphonates in supercritical carbon dioxide

The solubilities of DBBP and DAAP (structures are shown in **Figure 4.1**) were determined at three isotherms 313, 323 and 333 K with pressure ranging from 10.3 to 25 MPa. The measured solubilities are expressed in terms of mole fraction (y_2) (**Table 4.1**) and data reported is the average of three independent measurements with a relative standard deviation of less than 5%.

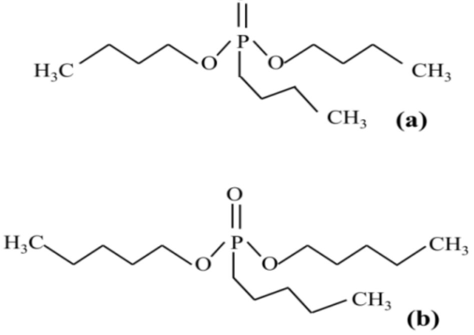

Figure 4.1 Structures of dialkylalkyl phosphonates employed in the present study; (a) Dibutylbutyl phosphonate (b) Diamylamyl phosphonate

The solubilities ranged from 0.088 to 0.118 mole/mole and 0.067 to 0.099 mole/mole of CO_2 for DBBP and DAAP respectively, in the investigated region. Similar solubility behavior was observed for other members of the organophosphorus compounds such as trialkyl phosphates and trialkyl phosphine oxides in $SCCO_2$. The higher solubility of trialkyl phosphates in $SCCO_2$ is mainly due to the Lewis-Acid and Lewis-Base interaction between CO_2 and trialkyl phosphate molecule [202]. The difference between trialkyl phosphates and dialkylalkyl phosphonates is the nature of substituents attached to the phosphorous atom. Replacement of one alkoxy group (-OR) present in trialkyl phosphates with alkyl group (-R) results in dialkylalkyl phosphonate with enhanced basicity on the phosphoryl oxygen. Therefore, we can expect similar Lewis-Acid and Lewis-Base interactions between carbon dioxide and dialkylalkyl phosphonates, similar to trialkyl phosphates. The solubilities of DBBP and DAAP are almost comparable to their corresponding trialkyl phosphates, tributyl phosphate (TBP) and triamyl phosphate (TAP) respectively. The solubility of DBBP at 323 K and 20 MPa is 0.111 (mole/mole) and the corresponding trialkyl phosphate, TBP solubility is 0.113 (mole/mole). Similarly, the solubility of DAAP at 323 K and 20 MPa is 0.099 (mole/mole) and the corresponding trialkyl phosphate, TAP is 0.099 (mole/mole).

The variation of solubility of DBBP and DAAP with pressure at three different temperatures 313, 323 and 333 K are shown in **Figure 4.6**. The solubility of DBBP is higher than that of DAAP at a given temperature and pressure. This can be attributed to high molecular weight and low vapor pressure of DAAP in comparison with DBBP. In general, the solubility decreases with the carbon number and unsaturation in the molecules. This is observed in the other homologues series, trialkyl phosphates, mono esters, fatty acids etc., where the solubility decreases with the alkyl chain length [106, 200, 201, 212]. It is observed that for a homologous series, the solubility of a solute decreases with increase in carbon number generally because the lowering vapor pressure with increase in carbon chain.

Table 4.1 Experimental solubilities of dibutylbutyl phosphonate and diamylamyl phosphonate in $SCCO_2$ medium

T (K)	***P*** (MPa)	**Density**[#] (kg/m^3)	**Solubility, y_2 (mol/mol)**[*]	
			Dibutylbutyl phosphonate	**Diamylamyl phosphonate**
313.0	10.3	651.49	0.097	0.082
313.0	12.3	727.57	0.100	0.087
313.0	15.0	781.32	0.102	0.089
313.0	20.0	840.61	0.103	0.090
313.0	25.0	880.15	0.104	0.091
323.0	10.3	423.74	0.093	0.073
323.0	12.3	604.62	0.106	0.089
323.0	15.0	701.08	0.110	0.094
323.0	20.0	785.16	0.111	0.094
323.0	25.0	834.89	0.112	0.095
333.0	10.3	309.89	0.088	0.067
333.0	12.3	458.89	0.109	0.089
333.0	15.0	605.60	0.115	0.095
333.0	20.0	724.63	0.117	0.098
333.0	25.0	787.28	0.118	0.099

Experimental conditions: CO_2 flow rate: 0.1 mL/min, Equilibrium cell volume: 50 mL, No. of equilibrium cells connected in series: 2; sample loaded in equilibrium cells: 1st cell-35 mL and 2nd cell: 25 mL; heat exchanger: 10 mL; entrainer column: 10 mL.

[*] Standard uncertainties in u are u(T) = 0.1 K, u(P) = 0.1 MPa and $u_r(y_2) = 0.05$

[#] Densities values are taken from http://webbook.nist.gov/chemistry/fluid/

The solubility of DBBP and DAAP increases with the pressure along all isotherms. This is due to an increase in the density of $SCCO_2$ with pressure for a given temperature where the vapor pressure is constant [213]. Increase in the density of $SCCO_2$ leads to enhanced interaction between carbon dioxide and dialkylalkyl phosphonate, providing better solubility at higher pressures. The solubility of DBBP and DAAP increases with temperature at certain pressure regions. However, the effect of temperature on solubility is not straightforward. As the temperature increases, density of $SCCO_2$

decreases, consequently, the solubility of solute decreases. At the same time, an increase in temperature can increase the vapor pressure of solute, which enhances the solubility of solute in $SCCO_2$. The net effect of these two competing factors determines the solubility behavior with temperature. Below 12 MPa, the solubility decreases with temperature at constant pressure (**Figure 4.6**). Above 12 MPa, the solubility increases with temperature resulting in crossover phenomenon. From these studies, it can be concluded that crossover pressure region was about 12 MPa. At high pressures, density of $SCCO_2$ is not sensitive to pressures as it does in the case of lower pressures. Therefore, the volatility effect becomes dominating factor at higher pressures and the solubility increases with the temperature. Below the crossover pressure, the solubility of dialkylalkyl phosphonates decreases with temperature and is known as retrograde behavior.

4.3 Solubility correlations

(a) Mendez-Teja model

The consistency of the experimental solubility data of dialkylalkyl phosphonates was tested by using MT model (Eq. (2.11)). The model parameter values derived from regression analysis are reported in **Table 4.2**. A plot of $T \ln (Py_2)-C_4T$ against the density of $SCCO_2$ (ρ) is shown in **Figure 4.2**. The experimental solubility data at different isotherms collapse onto a single straight line indicating the self-consistency of the experimental data. MT model is also employed to correlate the experimental solubilities. MT model successfully correlated the solubility of DAAP and DBBP with an AARD of 8%.

(b) Chrastil model

The experimental solubilities of two dialkylalkyl phosphonates employed in the present work were correlated using Chrastil model. Model parameters were evaluated using regression analysis (**Table 4.2)**. The correlations based on Chrastil model are shown in **Figure 4.3** and **Figure 4.4**. Logarithmic relationship between the solubility (kg/m^3) and density of supercritical fluid (kg/m^3) is a straight line, satisfying the Chrastil equation (**Figure 4.3**). The slope of each straight line in **Figure 4.3**, gives the association number (k) at a particular temperature. The association numbers for both DBBP and DAAP are found to be close to unity in the investigated region. Chrastil model successfully correlated the solubility of dialkylalkyl phosphonates with an AARD of 4%.

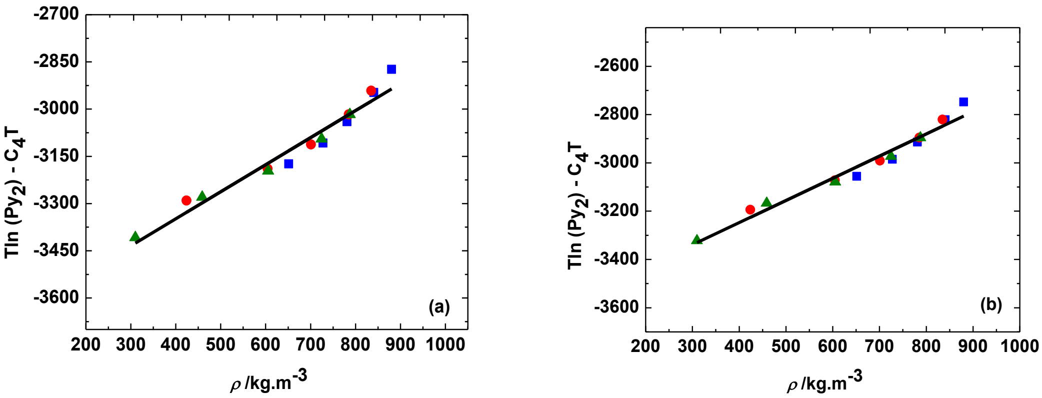

Figure 4.2 Solubilities of (a) dibutylbutyl phosphonate and (b) diamylamyl phosphonate in SCCO$_2$ at different temperatures ■, 313 K; •, 323 K; ▲, 333 K with pressure ranging from 10.3 to 25 MPa. Solid line represents the model predictions based on MT model

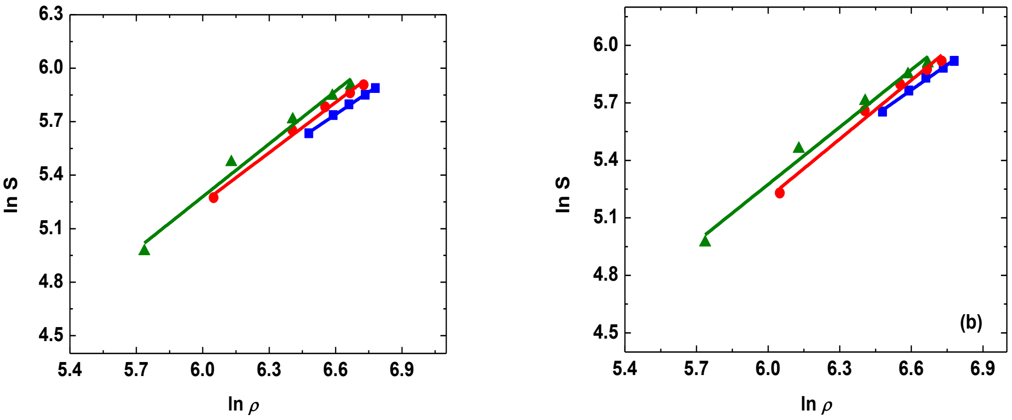

Figure 4.3 Correlation plots of ln S vs. ln ρ using Chrastil equation for (a) dibutylbutyl phosphonate, (b) diamylamyl phosphonate in the pressure range of 10.3 to 25 MPa, and temperature of ■, 313 K; •, 323 K; ▲, 333 K;

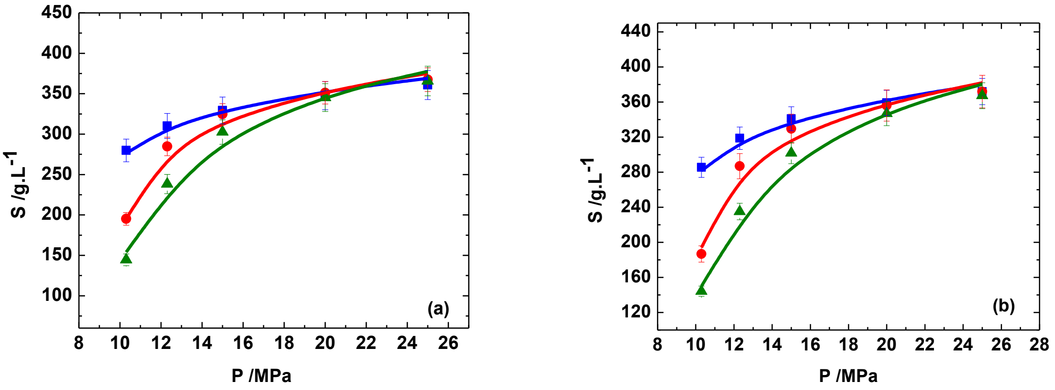

Figure 4.4 Variation of solubility of (a) dibutylbutyl phosphonate and (b) diamylamyl phosphonate in $SCCO_2$ with pressure at different temperatures; ■, 313 K; ●, 323 K; ▲, 333 K. The solid lines represent the model prediction by the Chrastil model

(c) Solution theory based on Wilson activity coefficient model

A solution theory model was developed using Wilson activity coefficients (Eq. (2.13)) for correlating the liquid solubilities in supercritical fluids[199]. The molar volume of DBBP was determined at temperatures, 313, 323 and 333K and found to be 267, 271 and 272 cm^3/mol respectively. Similarly, the molar volume of DAAP was determined and found to be 316, 319 and 321 cm^3/mol at 313, 323 and 333 K respectively. The uncertainty in the determination of molar volume is less than 1%. The correlation parameters are presented in **Table 4.2**. The experimental solubility data was compared with the model predictions and represented by **Figure 4.5**. Solution theory model successfully correlated the solubility of dialkylalkyl phosphonates with an average deviation of 4%. However, the cross-over phenomenon in the solubility is not captured by Wilson activity coefficient model.

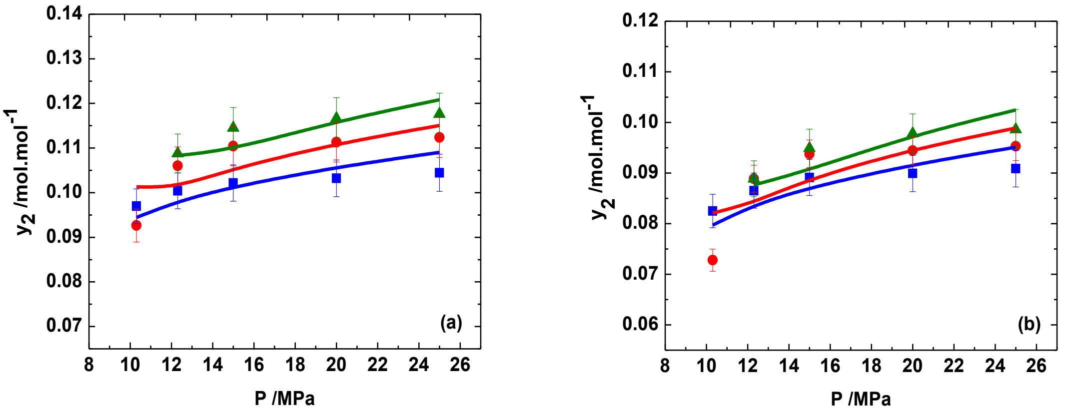

Figure 4.5 Variation of solubility of (a) dibutylbutyl phosphonate and (b) diamylamyl phosphonate in $SCCO_2$ with pressure at different temperatures; ■, 313 K; ●, 323 K; ▲, 333 K. The solid lines represent the model prediction based on solution model coupled with Wilson activity coefficient model

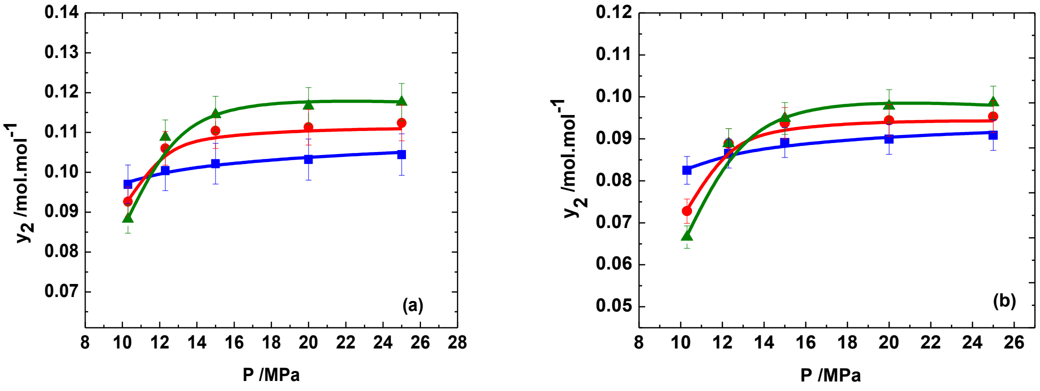

Figure 4.6 Variation of solubility of (a) dibutylbutyl phosphonate and (b) diamylamyl phosphonate in $SCCO_2$ with pressure at different temperatures; ■, 313 K; ●, 323 K; ▲, 333 K. The solid lines represent the model prediction based on association model based on van Laar activity coefficient model

(d) Association theory based on van Laar activity coefficient model

In this study, association model based on van Laar activity coefficient model Eq. (2.15) was used to correlate the solubilities of DBBP and DAAP in supercritical fluid at different temperatures and pressures. The solubility correlations were depicted in **Figure 4.6**. The model parameters are evaluated using regression analysis and represented in

Table 4.2. Association theory based on van Laar activity coefficient model successfully correlated the solubility of dialkylalkyl phosphonates with an average deviation of 2%.

The experimental solubilities are correlated using MT model, Chrastil equation, a solution model coupled with Wilson activity coefficient and an association model based on van Laar activity coefficient model. All the models employed in the present study successfully correlated the solubilities of dialkylalkyl phosphonates with an average deviation of less than 8%. The solubility of DBBP and DAAP increases with temperature at certain pressure regions and the temperature inversion is captured by van Laar activity coefficient model **(Figure 4.6)**. Among the four models employed in the present study the cross-over phenomenon in the solubility (temperature inversion) is only captured by MT and van Laar activity coefficient models. Further, the association model based on van Laar activity coefficients resulted in lower AARD% for dialkylalkyl phosphonates compared to other models employed in the present work. Therefore, it is possible to predict the solubility of dialkylalkyl phosphonates at any desired temperature and pressure in the investigated regions using the correlation parameters.

4.4 Conclusions

Dibutylbutyl phosphonate (DBBP) and diamylamyl phosphonate (DAAP) were synthesised and their solubility in supercritical carbon dioxide medium ($SCCO_2$) medium was measured using a dynamic flow technique. The solubilities of DBBP and DAAP were investigated in the pressure range of 10 to 25 MPa and temperature, varying from 313 to 333 K. The solubilities of these phosphonates were found to be high in the investigated temperature pressure regions. Chrastil model, MT model, solution model coupled with Wilson activity coefficient and association model based on van Laar activity coefficient models were employed to correlate the experimental solubilities of dialkylalkyl phosphonates. The results showed that these models can be applied for satisfactory solubility predictions at different pressures and temperatures with an average deviation of less than 10%. Among the models employed in the present study, association model based on the van Laar activity coefficient model resulted in much better correlation of solubilities with an average deviation of 3%.

Table 4.2 Regression analysis and model parameters for the solubilities of dialkylalkyl phosphonates using different models

Model	Model Parameters	Dibutylbutyl phosphonate	Diamylamyl phosphonate
MT model Eq. (2.11)	A_4	-3693±35	-3615±30
	B_4	0.86±0.05	0.92±0.05
	C_4	10.1±0.1	9.6±0.1
	R^2	0.941	0.956
	AARD (%)	8	8
Chrastil model Eq. (2.8)	A_1	-678.6±30	-581.6±20
	B_1	1.55±0.01	1.03±0.01
	k	0.963±0.02	0.998±0.02
	R^2	0.986	0.988
	AARD (%)	5	5
Solution theory with Wilson activity coefficient Eq. (2.13)	A_5	1.83±0.1	1.95±0.1
	B_5	-846±20	-766±10
	C_5	-1.3±0.1	-1.8±0.1
	R^2	0.975	0.968
	AARD (%)	4	4
Association model based on van Laar activity coefficient model Eq. (2.15)	k_{VL}	1.25±0.1	1.29±0.1
	A_{VL}	-1727±40	-2419 ±30
	C_{VL}	2488±40	3842±56
	D_{VL}	-749±25	-975±45
	E_{VL}	-4.7±0.1	-7.8±0.2
	F_{VL}	1.48±0.1	2.96±0.1
	R^2	0.988	0.988
	AARD (%)	2	2

Chapter 5

Solubility of trioctylmethylammonium chloride in supercritical carbon dioxide with co-solvent and development of new models for ternary solubilities

---

Chapter 5(a)

Solubility of trioctylmethylammonium chloride in supercritical carbon dioxide

---

5.1.1 Introduction

In chloride salt matrices of LiCl-KCl, actinides are present, possibly in anionic form, because of higher chloride contents and strong complexing ability of chloride ions with actinides. Therefore, the recovery of actinides from chloride salt matrix demands use of basic extractants (basic extractants extract metal ions by ion association resulting from the physical attractive forces between oppositely charged species) such as quaternary ammonium salts. Hence, ion-pair extractants such as ionic liquids (e.g. TOMAC) have to be considered for the recovery of actinides from such matrices. In this connection, the solubility behavior of TOMAC in $SCCO_2$ medium was investigated at various experimental conditions. The influence of co-solvent on the solubility of TOMAC has also been studied.

5.1.2 Preparation of $SCCO_2$ + co-solvent binary mixture

Addition of co-solvent to the $SCCO_2$ increases both the critical temperature and critical pressure of the resultant mixture. The operating temperature and pressure has to be chosen such that the resultant $SCCO_2$ stream should be in supercritical region. The critical loci of CO_2 + methanol, CO_2 + *n*-propanol and CO_2 + *n*-hexane were reported in the literature [214-216]. All the experiments involving CO_2 + co-solvent mixtures were conducted above the critical temperature and pressure of the mixtures. The binary mixtures of CO_2 + co-solvents were prepared by adjusting the flow rates of CO_2 and co-solvent. During the solubility measurements, the composition of CO_2+co-solvent mixture was assumed to be constant; therefore the composition at the outlet was not monitored. However, complete study on the dissolution of co-solvent in liquid solute has to carried out to understand to composition change (if any) during the solubility experiments.

X mol % of the co-solvent in a binary mixture of CO_2 + co-solvent can be obtained using the formula

$$X(mol\%) = \left[1 + \left(\frac{f_{CO_2} * \rho_{CO_2} * MW_C}{f_C * \rho_C * MW_{CO_2}} \right) \right]^{-1} * 100 \tag{5.1}$$

where, f_{CO_2} and f_C denotes the flow rates, MW_{CO_2} and MW_C represents the molecular weight and ρ_{CO2} and ρ_C stands for the densities of CO_2 and co-solvent, respectively.

5.1.3 Results and Discussions

5.1.3.1 Solubility of TOMAC in neat $SCCO_2$

The solubility of TOMAC in neat $SCCO_2$ was determined at 313, 323 and 333 K with pressure ranging from 10 to 30 MPa. The solubilities varied from 0.5×10^{-5} to 12.7×10^{-5} in the investigated region (**Table 5.1).** The effect of temperature and pressure on the solubility of TOMAC in $SCCO_2$ is depicted by **Figure 5.1(b) and 5.2(b).** The solubility of TOMAC was found to increase with pressure across all isotherms. At a constant temperature, the density of $SCCO_2$ increases with pressure that improves the specific interactions between $SCCO_2$ and TOMAC, enhancing the solvating power and thus leading to higher solubility. It can be observed from **Figure 5.1(b) and 5.2(b)** that the solubility decreased with increase in temperature at isobaric conditions. Temperature simultaneously affects the solute vapor pressure, $SCCO_2$ density and intermolecular interactions. There are two competing factors which influences the solubilities of TOMAC: (a) vapor pressure of TOMAC and (b) $SCCO_2$ density. TOMAC is a high molecular weight compound and thus has a significantly lower vapor pressure due to the presence of large hydrocarbon backbone in its molecular structure. Therefore, the vapor pressure of the TOMAC in the temperature region of 313 to 333 K is insignificant, thus making the density term of $SCCO_2$ as the dominating factor. The decrease of $SCCO_2$ density with temperature reflected in the decrease of solubility with temperature. Thus, the retrograde behavior of the solubility was observed in the present study.

Table 5.1 Experimental solubilities of TOMAC in $SCCO_2$ medium

T (K)	*P* (MPa)	Density* (kg/m^3)	Solubility (mol/mol) y_2 x 10^5
313.0	8.3	320.54	1.4
313.0	10.3	651.49	6.1
313.0	15.0	781.32	8.9
313.0	20.0	840.61	10.5
313.0	25.0	880.15	12.1
313.0	30.0	910.47	12.7
323.0	10.3	423.74	1.8
323.0	15.0	701.08	5.3
323.0	20.0	785.16	7.9
323.0	25.0	834.89	9.5
323.0	30.0	871.03	10.2
333.0	10.3	309.89	0.6
333.0	15.0	605.6	3.6
333.0	20.0	724.63	5.2
333.0	25.0	787.28	6.6
333.0	30.0	830.33	7.6

* Density values taken from http://webbook.nist.gov/chemistry/fluid/

Experimental conditions: CO_2 flow rate: 0.2 mL/min, Equilibrium cell volume: 50 mL, No. of equilibrium cells connected in series: 2; sample loaded in equilibrium cells: 1st cell-30 mL and 2nd cell: 25 mL; heat exchanger: 10 mL; entrainer column: 10 mL.

Standard uncertainties (u) are u(T) = 0.1 K, u(P) = 0.1 MPa and relative uncertainty (u_r), $u_r(y_2) = 0.1$

5.1.3.2 Solubility correlations

The self-consistency of the experimental solubilities of TOMAC in neat $SCCO_2$ was tested by using MT model (Eq. (2.11)). The plot of $T \ln (Py_2)-C_4T$ with ρ is linear with all data points falling onto a single straight line (**Figure 5.1(a))**. The solubilities of TOMAC in neat $SCCO_2$ were successfully correlated using the MT model with an AARD of 8% (**Figure 5.1(b)**. The experimental solubilities were also fitted using the Chrastil model (**Figure 5.2(b))** with an AARD of 6%. The logarithm of solubility (kg/m^3) was also plotted against the logarithm of density (kg/m^3) of $SCCO_2$ (**Figure 5.2(a))**. It was observed that the log-log plot of solubility with density is linear for all the isotherms. The association number (*k*) for TOMAC can be obtained from slope of these lines and it was found to be about 3 in the investigated range of temperature and pressure. The slopes of all isotherms were similar. However, the slope showed a small increase at higher temperatures indicating that the lower vapor pressure of TOMAC making “density term” as deciding factor in influencing solubility.

Solution theory based Wilson activity coefficient models (Eq. (2.13)) and association model with van Laar activity coefficient model (Eq. (2.15)) were also examined in the present work to correlate the solubility of TOMAC in $SCCO_2$ medium. The correlation parameters are shown in **Table 5.2**. The experimental solubilities are compared with the model predictions and are shown in **Figure 5.3**. Solution theory based on Wilson activity coefficient model resulted in an AARD of 10%. Association theory based on van Laar activity coefficient model successfully correlate the solubility of TOMAC in $SCCO_2$ with an AARD of 2%.

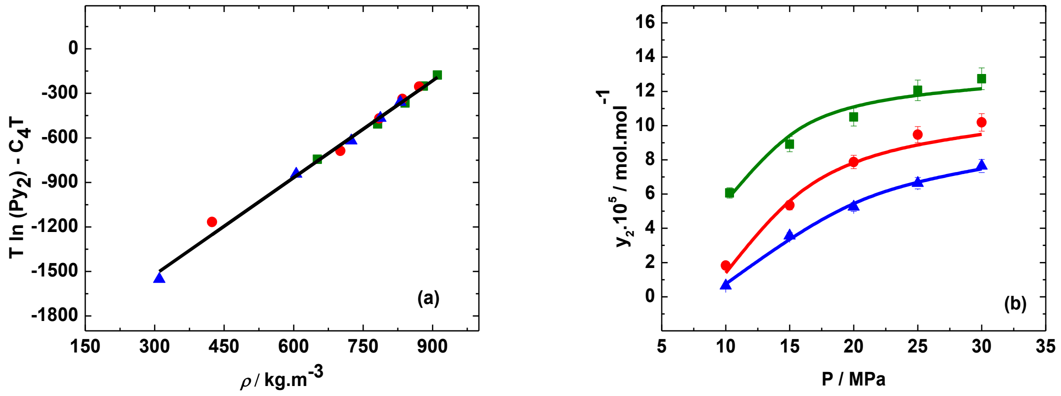

Figure 5.1 (a) variation of solubility of TOMAC in neat SCCO$_2$ with density at different temperatures; ■, 313 K; ●, 323 K; ▲, 333 K as represented by Eq. (2.11)); (b) Variation of solubilities of TOMAC in neat SCCO$_2$ with pressure at different temperatures; ■, 313 K; ●, 323 K; ▲, 333 K; Solid lines represent the model predictions based on the MT model (Eq. (2.11))

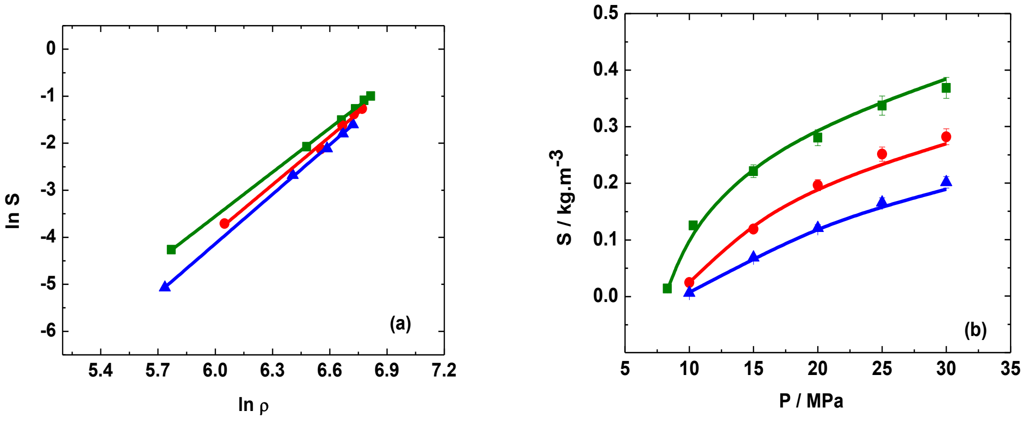

Figure 5.2 (a) Variation of solubilities of TOMAC in neat SCCO$_2$ with pressure at different temperatures; ■, 313 K; ●, 323 K; ▲, 333 K; (b) variation of solubility of TOMAC in neat SCCO$_2$ with density as represented by Eq. (2.8). Solid lines represent the model predictions based on the Chrastil model (Eq. (2.8))

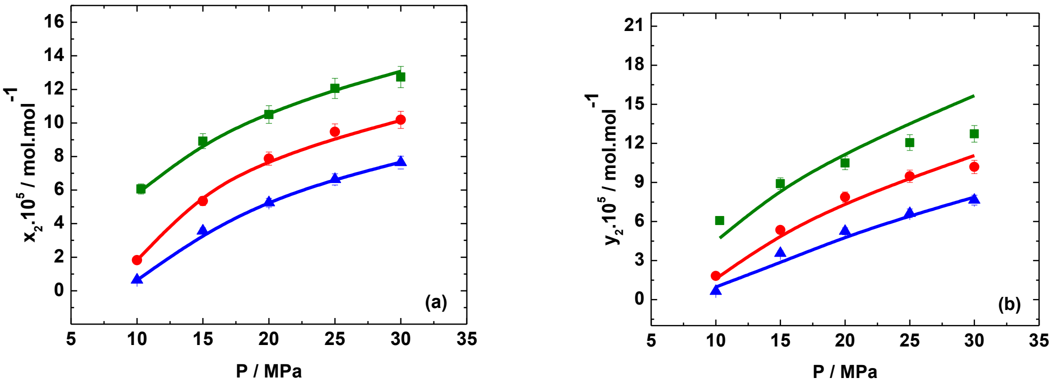

Figure 5.3 Variation of solubilities of TOMAC in neat SCCO$_2$ with pressure at different temperatures; ■, 313 K; ●, 323 K; ▲, 333 K; solid line represents the model predictions based on (a) association theory based on van Laar activity coefficient (Eq.(2.15)) and (b) solution theory based on Wilson activity coefficient model(Eq.(2.13))

Table 5.2 Regression analysis and model parameters from different correlations for solubilities of TOMAC in neat SCCO$_2$

Model	Model Parameter	Values
MT model (Eq. (2.11))	A_4	-2173 ± 40
	B_4	2.2 ± 0.1
	C_4	-5 ± 0.1
	R^2	0.992
	AARD (%)	8.0
Chrastil model (Eq. (2.8))	*k*	3.3 ± 0.1
	A_1	2069 ± 10
	B_1	-29 ± 1
	R^2	0.996
	AARD (%)	6.0
Solution theory coupled with Wilson activity coefficient Eq. (2.13)	A_5	-14.7 ± 0.1
	B_5	0.057 ± 0.002
	C_5	1595 ± 20
	R^2	0.981
	AARD (%)	10
Association model based on van Laar activity coefficient model Eq. (2.15)	k_{VL}	1.8 ± 0.1
	A_{VL}	4480 ± 200
	C_{VL}	331 ± 10
	D_{VL}	-1670 ± 40
	E_{VL}	8.3 ± 0.2
	F_{VL}	-29.8 ± 1.6
	R^2	0.998
	AARD (%)	2

5.1.3.3 Solubility of TOMAC in $SCCO_2$ in the presence of co-solvents

In the present work, the solubility of TOMAC in the presence of co-solvents is represented as x_2 (mole per mole of $SCCO_2$ + co-solvent). The solubility of TOMAC in neat $SCCO_2$ was found to be low, varying from 0.5×10^{-5} to 12.7×10^{-5} mole/mole in the investigated region. The weak solvating power of $SCCO_2$ for strongly polar compounds and metal ions is a limitation for its applications to many SCF based techniques. Presence of small amount of co-solvents (generally polar compounds) considerably increases the solubility of compounds in $SCCO_2$ [217, 218]. Thus, in the present study, one non-polar solvent, *n*-hexane and two polar solvents, methanol and *n*-propanol were employed along with the $SCCO_2$ to study the solubility of TOMAC in $SCCO_2$. The influence of co-solvents on the solubility of TOMAC in $SCCO_2$ was examined at 313 & 323 K with pressure ranging from 10-30 MPa. The experiments were carried out with $SCCO_2$ + co-solvent mixtures with the co-solvent composition ranging from 1.05 to 4.2 mol %.

The experimental solubilities of TOMAC in the presence of co-solvents are shown in **Tables 5.3, 5.4 & 5.5,** respectively and **Figure 5.4, 5.5 & 5.6,** respectively. It can be observed that the solubility of TOMAC increases with the pressure at a constant temperature irrespective of the nature of co-solvent. The effect of *n*-hexane on the solubility of TOMAC in $SCCO_2$ is not appreciable **(Figure 5.4**). The solubility of TOMAC in $SCCO_2$ + *n*-hexane mixture was found to be similar to that observed with neat $SCCO_2$. Similar results were obtained by W Wu *et al.* for the solubility of [bmim] [PF_6]. The effect of *n*-hexane on the solubility [bmim] [PF_6] was studied and the solubility enhancement was only marginal even at 29 mol % of *n*-hexane in $SCCO_2$ [85, 86]. *n*-hexane is a no*n*-polar solvent and it has weak interactions with the TOMAC. The solvating power of *n*-hexane is nearly similar to that of the $SCCO_2$. Therefore, the presence of *n*-hexane in $SCCO_2$ did not reflect any major changes in the solubility behavior.

Table 5.3 Solubilities of TOMAC in SCCO$_2$ medium in the presence of *n*-hexane

T **(K)**	***P*** **(MPa)**	**Solubility, x_2 x 10^5 (mol/mol)**			
		Neat SCCO$_2$	**1.05 mol % *n*-hexane**	**2.10 mol % *n*-hexane**	**4.20 mol % *n*-hexane**
313.0	10.0	6.1	5.8	7.8	9.5
313.0	15.0	8.9	8.9	11.4	12.5
313.0	20.0	10.5	10.5	13.5	14.0
313.0	25.0	12.1	11.2	14.6	14.6
313.0	30.0	12.7	11.9	15.3	15.3
323.0	10.0	1.8	1.8	2.7	4.4
323.0	15.0	5.3	4.9	7.1	8.0
323.0	20.0	7.9	7.0	9.6	10.5
323.0	25.0	9.5	8.6	12.1	12.9
323.0	30.0	10.2	10.2	13.6	13.6

Experimental conditions: CO$_2$ flow rate: 0.1 mL/min; co-solvent flow rate: 0.001-0.02 mL/min, Equilibrium cell volume: 50 mL; No. of equilibrium cells: 2; sample loaded: 1st cell-30 mL and 2nd cell: 25 mL; heat exchanger: 10 mL; entrainer column: 10 mL;

Standard uncertainties (u) are u(T) = 0.1 K, u(P) = 0.1 MPa and relative uncertainty (u_r), $u_r(x_2)$ = 0.1

Table 5.4 Solubilities of TOMAC in SCCO$_2$ medium in the presence of *n*-propanol

T **(K)**	***P*** **(MPa)**	**Solubility, x_2 x 10^5 (mol/mol)**			
		Neat SCCO$_2$	**1.05 mol % *n*-propanol**	**2.10 mol % *n*-propanol**	**4.20 mol % *n*-propanol**
313.0	10.0	6.1	8.7	23	109
313.0	15.0	8.9	19	53	231
313.0	20.0	10	26	87	331
313.0	25.0	12	37	111	429
313.0	30.0	13	43	127	490
323.0	10.0	1.8	2.0	5.5	15
323.0	15.0	5.3	11	31	116
323.0	20.0	7.9	21	61	227
323.0	25.0	9.5	28	95	360
323.0	30.0	10	34	119	440

Experimental conditions: CO$_2$ flow rate: 0.1 mL/min; co-solvent flow rate: 0.001-0.02 mL/min, Equilibrium cell volume: 50 mL; No. of equilibrium cells: 2; sample loaded: 1st cell-30 mL and 2nd cell: 25 mL; heat exchanger: 10 mL; entrainer column: 10 mL;

Standard uncertainties (u) are u(T) = 0.1 K, u(P) = 0.1 MPa and relative uncertainty (u_r), $u_r(x_2)$ = 0.1

Table 5.5 Solubilities of TOMAC in $SCCO_2$ in the presence of methanol

T (K)	P (MPa)	Solubility, $x_2 \times 10^5$ (mol/mol)			
		Neat $SCCO_2$	1.05 mol % methanol	2.10 mol % methanol	4.20 mol % methanol
313.0	10.0	6.1	10.5	27	100
313.0	15.0	8.9	25	71	311
313.0	20.0	10.5	33	105	436
313.0	25.0	12	43	146	557
313.0	30.0	13	49	169	633
323.0	10.0	1.8	2.6	6.4	18
323.0	15.0	5.3	13	36	142
323.0	20.0	7.9	23	70	279
323.0	25.0	9.5	33	103	420
323.0	30.0	10.2	41	127	515

Experimental conditions: CO_2 flow rate: 0.1 mL/min; co-solvent flow rate: 0.001-0.02 mL/min, Equilibrium cell volume: 50 mL; No. of equilibrium cells: 2; sample loaded: 1st cell-30 mL and 2nd cell: 25 mL; heat exchanger: 10 mL; entrainer column: 10 mL;

Standard uncertainties (u) are u(T) = 0.1 K, u(P) = 0.1 MPa and relative uncertainty (u_r), $u_r(x_2) = 0.1$

Figures 5.5 and **5.6** represent the solubilities of TOMAC in $SCCO_2$ in the presence of *n*-propanol and methanol, respectively. The solubility of TOMAC increases drastically in the presence of *n*-propanol and methanol. At 313 K, 30 MPa and 4.2 mol% of co-solvent, the solubilities of TOMAC in presence of *n*-propanol and methanol were found to be 490×10^{-5} and 633×10^{-5} mole/mole, respectively. Under similar experimental conditions, the corresponding solubility in the absence of co-solvent was only 12.7×10^{-5} mole/mole. In case of methanol as a co-solvent, the solubility increased by 50 times. The effect of polar co-solvent on the solubility of ionic liquids such as [bmim] [PF_6] was studied by Wu *et al.* and the solubility of ionic liquids in $SCCO_2$ was found to be increased by 10^3 times in the presence of polar co-solvents [85, 86].

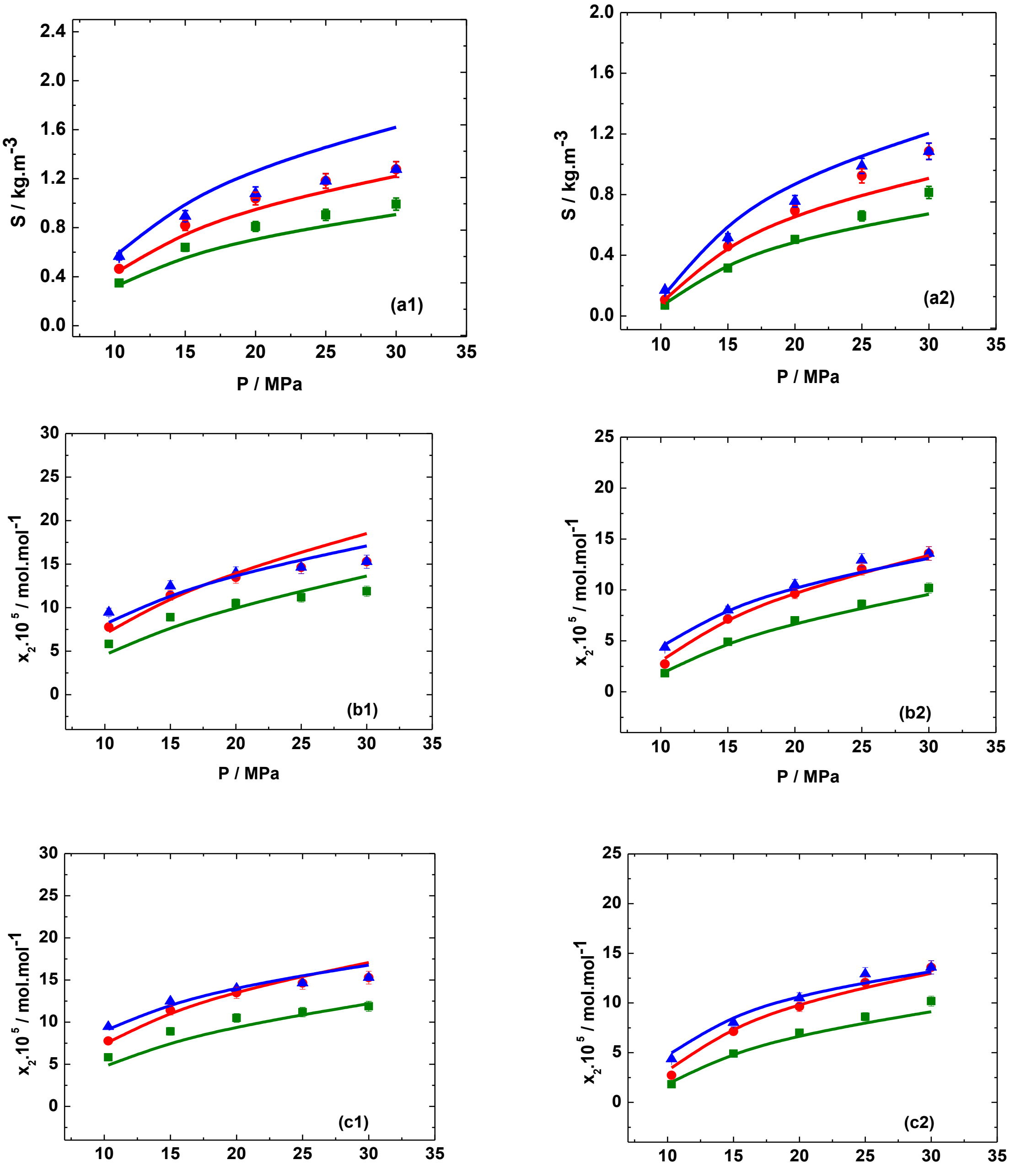

Figure 5.4 Solubilities of TOMAC at (a1, b1, c1) 313 K and (a2, b2, c2) 323 K in the presence of *n*-hexane as a co-solvent; ■, 1.05 mol % *n*-hexane; ●, 2.10 mol % *n*-hexane; ▲, 4.20 mol % *n*-hexane. The solid lines are model predictions based of (a1, a2) modified Chrastil equation (Eq. (2.10)); (b1, b2) association theory based Wilson activity coefficient model (Eq. (5.9)); (c1, c2) association theory based van Laar activity coefficient model (Eq. (5.8))

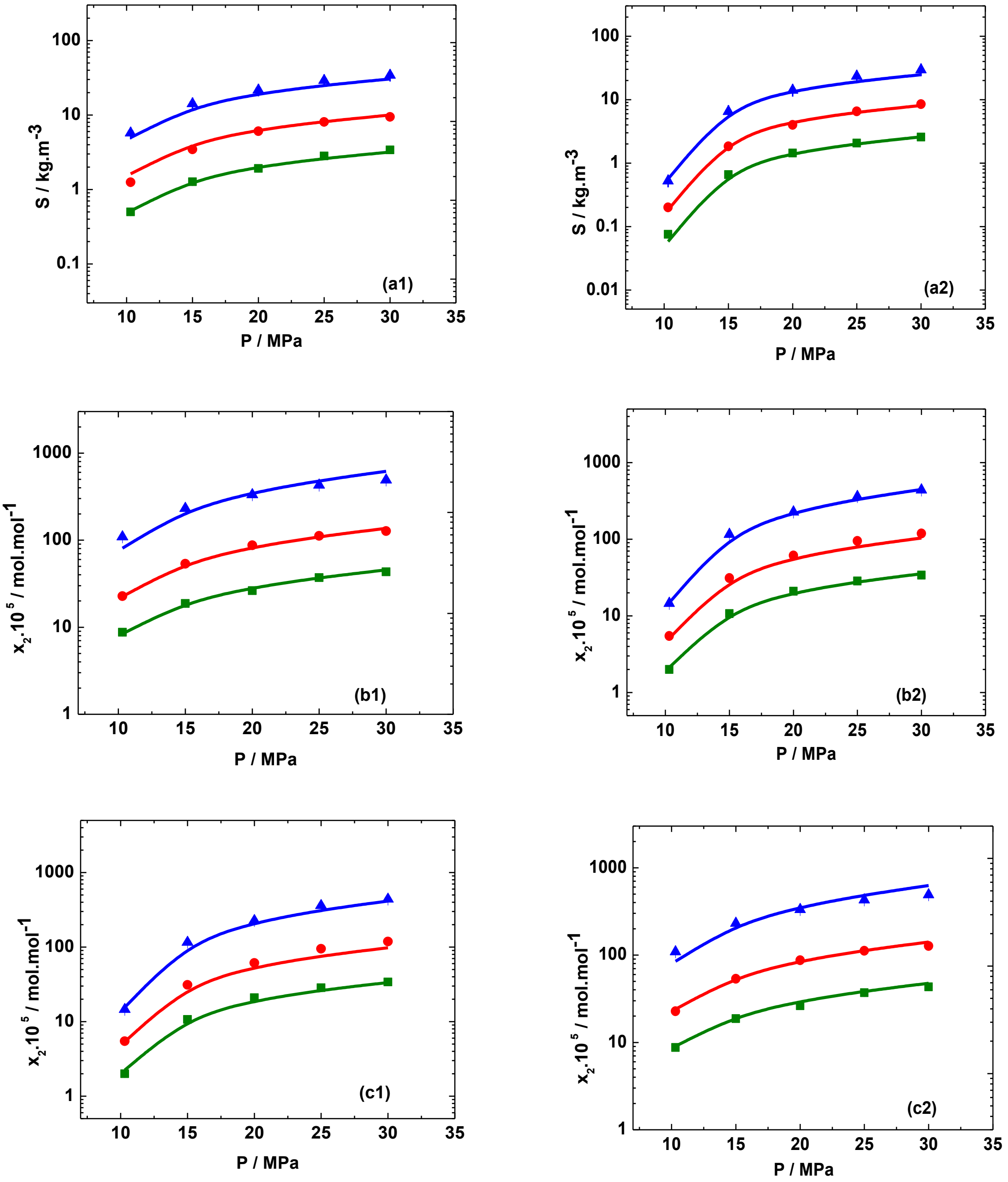

Figure 5.5 Solubilities of TOMAC at (a1, b1, c1) 313 K and (a2, b2, c2) 323 K in the presence of *n*-propanol as a co-solvent; ■, 1.05 mol % *n*- propanol; ●, 2.10 mol % *n*-propanol; ▲, 4.20 mol % *n*-propanol. The solid lines are model predictions of (a1, a2) modified Chrastil equation (Eq. (2.10)); (b1, b2) association theory based Wilson activity coefficient model (Eq. (5.9)); (c1, c2) association theory based van Laar activity coefficient model (Eq. (5.8))

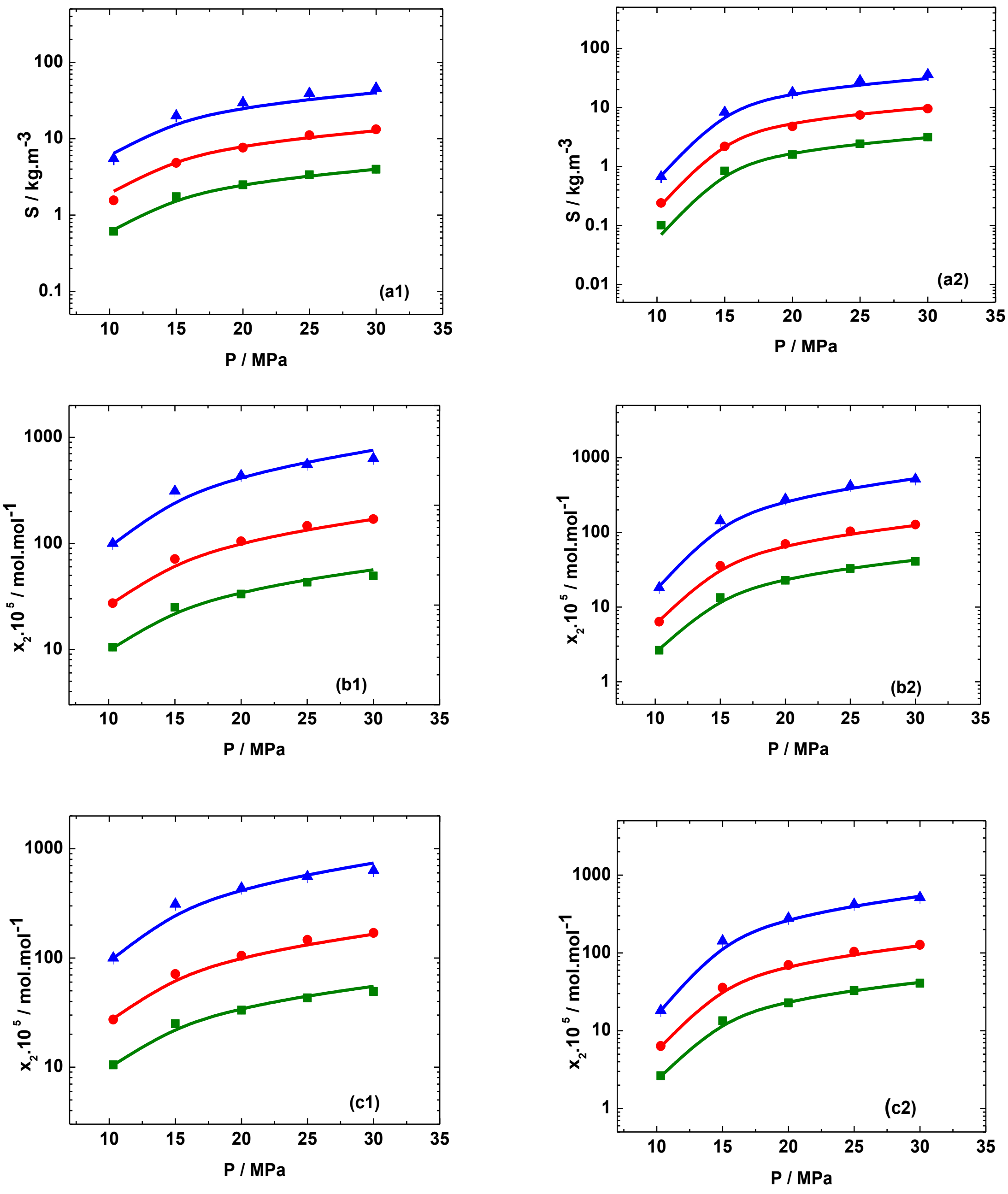

Figure 5.6 Solubility of TOMAC at (a1, b1, c1) 313 K and (a2, b2, c2) 323 K in the presence of methanol as a co-solvent; ■, 1.05 mol % methanol; ●, 2.10 mol % methanol; ▲, 4.20 mol % methanol. The solid lines are model predictions of (a1, a2) modified Chrastil equation (Eq. (2.10)); (b1, b2) association theory based Wilson activity coefficient model (Eq. (5.9)); (c1, c2) association theory based van Laar activity coefficient model (Eq. (5.8))

TOMAC is a quarternary ammonium compound with an ionisable moiety [219]. The solubility enhancement is mainly due to the strong interactions of the TOMAC with the polar co-solvent. Polar co-solvents such as methanol and *n*-propanol are both hydrogen bond donors and acceptors and thus can associate through hydrogen bonding. Methanol and *n*-propanol can interact with TOMAC by forming a hydrogen bond with "N" present in the TOMAC molecule. Therefore, addition of polar compounds to the $SCCO_2$ can enhance the interactions with TOMAC, leading to higher solubilities. The solubilities of TOMAC in $SCCO_2$ in the presence of three co-solvents at a 313 K and 30 MPa are depicted in **Figure 5.7**. It can be observed that the effect of co-solvent on solubility behavior is as follows, *n*-hexane < *n*-propanol < methanol, in line with their polarities. The dipole-moment increases in the order of *n*-hexane < *n*-propanol < methanol. As the dipole-moment of the co-solvent increases, the tendency of neutralization of the charge in the ionic liquid increase, leading to increased solubility in $SCCO_2$. Therefore, polarity of the co-solvent is one of the main factors that decide the solubility of TOMAC in modified $SCCO_2$ medium.

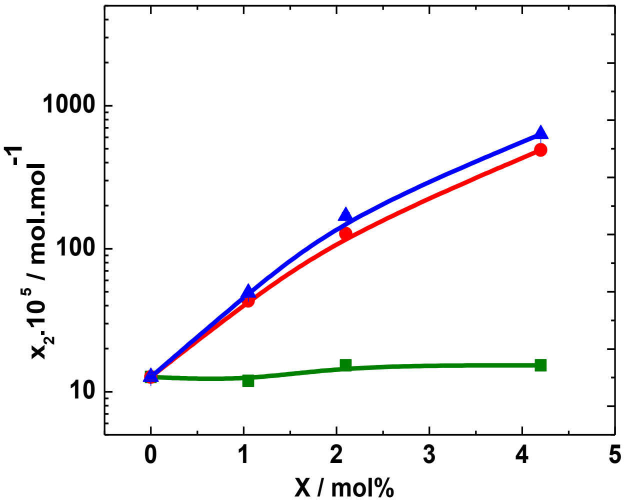

Figure 5.7 Influence of co-solvent concentration on the solubilities of TOMAC in $SCCO_2$ at T = 313 K and P = 30 MPa; ■, *n*-hexane; ●, *n*-propanol; ▲, methanol

In order to quantify the effect of co-solvent on the solubility of TOMAC in $SCCO_2$, solubility enhancement factor, I_2, is introduced and is as follows [220]

$$I_2 = \frac{x_{2,ternary}}{x_{2,binary}} \qquad (5.2)$$

In eq. (5.2) $x_{2,\mathrm{ternary}}$ denotes the solubility of TOMAC in $SCCO_2$ with co-solvents and $x_{2,\mathrm{binary}}$ denotes the solubility of TOMAC in neat $SCCO_2$. The solubility enhancement factor, I_2 is always greater than unity, irrespective of temperature and pressure employed. The solubility enhancement factor is dependent on the co-solvent composition and nature of the co-solvent employed. The magnitudes of the solubility enhancement factor follows an order of, *n*-hexane < *n*-propanol < methanol. i.e methanol is more effective in increasing the solubility of TOMAC in $SCCO_2$ compared to *n*-hexane and *n*-propanol (**Figure 5.7)**. The solubility enhancement factor varied close to unity for *n*-hexane regardless of temperature, pressure and co-solvent composition. In the case of methanol and *n*-propanol, the solubility enhancement factor increased with pressure and composition of the co-solvent. The solubility enhancement factor for *n*-propanol varied from 3.4 to 38 with co-solvent composition ranging from 1.05 to 4.2 mol% at 313 K and 30 MPa. Under similar experimental conditions, the solubility enhancement factor for methanol varied from 3.8 to 50.

The solubility data of TOMAC in $SCCO_2$ with co-solvents: *n*-hexane, *n*-propanol and methanol at 313 K and 323 K were correlated using the modified Chrastil equation, Eq. (2.10) as depicted in **Figure 5.4(a1, a2), 5.5(a1, a2)** and **5.6(a1, a2),** respectively. An AARD of 12% was obtained between the experimental and calculated solubilities using the modified Chrastil equation (**Table 5.6**).

Chapter 5(b)

Development of new models to correlate the solubility of liquid solutes in supercritical carbon dioxide in the presence of co-solvent

---

5.2.1 New models

In the present work, two new models have been developed for the first time for ternary system (SCCO$_2$ + co-solvent + solute) to correlate solubilities of liquid solutes in SCCO$_2$ in the presence of co-solvents using association theory based on Wilson and van Laar activity coefficient models. Subsequently, these models were employed to correlate the solubility of TOMAC in SCCO$_2$ in the presence of co-solvents.

The solubility of solutes in SCCO$_2$ with co-solvent depends on the pressure, temperature, density and co-solvent composition. Semi-empirical models have been developed in the literature for the solubility of solid solutes in SCCO$_2$ modified with a co-solvent using association theory [112, 113]. These equations were developed by assuming each solute molecule is being associated with some molecules of SCCO$_2$ and co-solvent to form a solvato complex. Same concept was adopted for deriving the equations for the solubility of liquid solutes in SCCO$_2$ modified with a co-solvent.

The final expression for the solubility of liquids in supercritical fluids in the present of co-solvents in terms of activity coefficient of solute and co-solvent is represented by Eq. (5.3). The detailed derivation is presented in **Appendix-2**.

$$\ln x_2 = \ln x_3 + (k-1)\ln\left(\frac{P}{P*}\right) + \frac{\Delta H_s}{RT} - q_s + k\rho_1(2x_1B_{11} - B) + (A_2 + A_3) - \frac{(B_2 + B_3)}{T}$$
$$- \left(\frac{\phi_{231_k}\phi_1^{*k}}{\phi_{231_k}^*}\frac{\phi_2^*\phi_3^*}{\phi_{sat}^2}\frac{\left(P^*\right)^2}{x_2^l\gamma_2^l}\right) + \rho_1\left(\frac{1}{\rho_2} + \frac{1}{\rho_3}\right) + \ln\frac{\gamma_3}{\gamma_2^\infty} \tag{5.3}$$

In Eq. (5.3), x_2 is the mole fraction solubility of solute in SCCO$_2$+ co-solvent, x_3 represents the co-solvent mole fraction, P^* is assumed to be 1 atm. ρ_1, ρ_2 and ρ_3 are the molar densities of solvent, solute and co-solvent, respectively. γ_2^∞ and γ_3 can be expressed using different activity coefficient models. In this work, γ_2^∞ and γ_3 are expressed using Wilson (Case 1) and van Laar activity coefficient models (Case 2).

Case 1: New model based on Wilson activity coefficient model

The activity coefficient of any component 'k' in a multi component mixture is given by the following expression using the Wilson activity coefficient model [221]

$$\ln \gamma_k = -\ln\left(\sum_{j=1}^{m} x_j \Lambda_{kj}\right) + 1 - \sum_{j=1}^{m} \frac{x_i \Lambda_{ik}}{\sum_{j=1}^{m} x_j \Lambda_{ij}} \tag{5.4}$$

$$\text{Where, } \Lambda_{ij} = \frac{V_j}{V_i} \exp\left(\frac{-\lambda_{ij} - \lambda_{ii}}{RT}\right) \tag{5.5}$$

Using the above formulation for activity coefficients along with the Eq. (5.3), a model with seven was obtained for correlating the solubilities in SCCO$_2$ in the presence of a co-solvent as mentioned below Eq. (5.6). The detailed derivation is presented in the **appendix-2**.

$$\begin{aligned} \ln x_2 = \ln x_3 + (k-1)\ln\left(\frac{P}{P*}\right) + \frac{W_1}{T} + \left(\frac{\rho_1}{\rho_2} + \frac{\rho_1}{\rho_3} + x_3\left(\frac{\rho_1}{\rho_2} - \frac{\rho_1}{\rho_3}\right) + kW_2\rho_1\right) \\ + \frac{\rho_1}{RT\rho_3}\left(W_3 - x_3W_4\right) + \left(\frac{\rho_2}{\rho_1} - \frac{\rho_2}{\rho_1 TR} W_5\right) + W_6 \end{aligned} \tag{5.6}$$

Where,

$$W_1 = \frac{\Delta H_s}{R} - (B_2 + B_3) + \frac{\lambda_2'' - \lambda_2}{R} \tag{5.6a}$$

$$W_2 = 2B_{11} - B \tag{5.6b}$$

$$W_3 = -\lambda_{13} - \lambda_{11} \tag{5.6c}$$

$$W_4 = -\lambda_{13} - \lambda_{33} \tag{5.6d}$$

$$W_5 = -\lambda_{12} - \lambda_{22} \tag{5.6e}$$

$$W_6 = A_2 + A_3 - q_s - \left(\frac{\phi_{231_k} \phi_1^{*k}}{\phi^*_{231_k}} \frac{\phi_2^* \phi_3^*}{\phi^2_{sat}} \frac{\left(P^*\right)^2}{x_2^l \gamma_2^l} \right) \tag{5.6f}$$

Eq. (5.6) correlates the solubility of liquid solute in SCCO$_2$ + co-solvent system in terms of co-solvent composition, temperature, pressure and density of supercritical fluid. *k* is the association number for SCF, W$_1$ to W$_6$ are the temperature independent parameters and ρ_1, ρ_2 and ρ_3 are the molar densities of solvent, solute and co-solvent, respectively.

Case 2: New model based on van Laar activity coefficient model

The activity coefficient for a solute (γ_2) in a ternary mixture using van Laar activity coefficient model can be written as [221],

$$\ln \gamma_2 = \frac{x_3^2 A_{23} \left(\frac{A_{32}}{A_{23}} \right)^2 + x_1^2 A_{21} \left(\frac{A_{12}}{A_{21}} \right)^2 + x_3 x_1 \left(\frac{A_{32}}{A_{23}} \right) \left(\frac{A_{12}}{A_{21}} \right) \left(A_{23} + A_{21} - A_{13} \left(\frac{A_{21}}{A_{12}} \right) \right)}{\left(x_2 + x_3 \frac{A_{32}}{A_{23}} + x_1 \frac{A_{12}}{A_{21}} \right)^2} \tag{5.7}$$

The expression for the solubility of liquid solute (x_2) in SCCO$_2$ in presence of a co-solvent can now be obtained using the above activity coefficient model and Eq. (5.3),

$$\ln x_2 = \ln x_3 + (k-1) \ln \left(\frac{P}{P*} \right) + \frac{L_1}{T} + \left(\frac{\rho_1}{\rho_2} + \frac{\rho_1}{\rho_3} - \frac{\rho_1 x_3 L_2}{\rho_3} + k \rho_1 L_3 \right) + L_4 \tag{5.8}$$

Where,

$$L_1 = \frac{\Delta H_s}{R} - (B_2 + B_3) \tag{5.8a}$$

$$L_2 = 4q_3a_{13} - 2q_3\left(a_{23} - a_{12} - a_{13}\right) \tag{5.8b}$$

$$L_3 = 2B_{11} - B \tag{5.8c}$$

$$L_4 = A_2 + A_3 - q_s - \left(\frac{\phi_{231_k}\phi_1^{*k}}{\phi_{231_k}^{*}} \frac{\phi_2^{*}\phi_3^{*}}{\phi_{sat}^{2}} \frac{\left(P^{*}\right)^2}{x_2^l\gamma_2^l} \right) \tag{5.8d}$$

Eq. (5.8) represents the new five parameter model for the solubility of liquid solute in $SCCO_2$ in presence of co-solvents developed using association theory based on the van Laar activity coefficient model. The detailed derivation is presented in **appendix-2**.

5.2.2 Solubility correlations

Two new model equations (Eq. (5.6) and (5.8)) were developed in the present study to correlate the solubility of liquid solute, TOMAC in $SCCO_2$ in the presence of co-solvents using association theory with Wilson and van Laar activity coefficient models, respectively. The new correlation, Eq. (5.6) was obtained using the association theory coupled with the Wilson activity coefficient model and it is comprised of seven adjustable parameters. These parameters were obtained from the non-linear regressions performed using the experimental data by applying some constraints on the model parameters. For example, *k* is the association number and it should be always positive. In (Eq. (5.6)), W_1 values can be either positive or negative, this value depends on the heat of solvation, virial coefficients and interaction parameters for solute, solvent and co-solvent interactions. The value of W_1 is always found to be positive from the regression implying $\Delta H_s > ((B_2 + B_3)R + \lambda_2'' - \lambda_2)$. Unlike W_1, W_2 are always found to be negative through regression. The value of W_3 depends on the interaction parameters for solvent/co-solvent and solvent/solvent interactions. W_4 accounts for the interactions between solvent/co-solvent and co-solvent/co-solvent systems, respectively. Similarly, W_5 takes into account the interactions between solvent/solute and solute/solute interactions. The value of these three parameters: W_3, W_4 and W_5 were always found to be positive for a no*n*-polar co-solvent, *n*-hexane and these were negative for polar co-solvents, methanol and *n*-propanol (which aids solubility of solute in $SCCO_2$). This indicates that the interaction between solvent/co-solvent (λ_{13}) also plays a major role in enhancing the solubility of solutes in $SCCO_2$ in the presence of co-solvent. Further, the value of W_6 can be positive or negative depending on the value of $(A_2 + A_3)$ is greater or less than the value of $q_s + \left(\frac{\phi_{231_k} \phi_1^{*k}}{\phi_{231_k}^*} \frac{\phi_2^* \phi_3^*}{\phi_{sat}^2} \frac{\left(P^*\right)^2}{x_2^l \gamma_2^l} \right)$. W_6 was always found to be negative from the regressions.

It was also observed that the contribution from the W_5 term ($-\lambda_{12}-\lambda_{22}$) in Eq. (5.6) is negligible and hence, it can be neglected. Thus, Eq. (5.6), the association model based on Wilson activity coefficient model reduces to a simplified six parameter model,

$$\begin{aligned} \ln x_2 = \ln x_3 + (k-1)\ln\left(\frac{P}{P*}\right) + \frac{W_1}{T} + \left(\frac{\rho_1}{\rho_2} + \frac{\rho_1}{\rho_3} + \frac{\rho_2}{\rho_1} + x_3\left(\frac{\rho_1}{\rho_2} - \frac{\rho_1}{\rho_3}\right) + kW_2\rho_1\right) \\ + \frac{\rho_1}{RT\rho_3}\left(W_3 - x_3W_4\right) + W_6 \end{aligned} \tag{5.9}$$

Eq. (5.9) was employed to correlate the solubility of TOMAC in $SCCO_2$ at 313 K and 323 K in the presence of different co-solvents as shown in **Figure 5.3(b1, b2), 5.5(b1, b2)** and **5.6(b1, b2),** respectively. The model parameters along with the AARD values are reported in **Table 5.6**.

The second model equation (Eq. (5.8)), developed using the association theory with van Laar activity coefficient model is comprised of five adjustable parameters to correlate the solubility of liquid solutes in $SCCO_2$ in the presence of co-solvents.

$$\ln x_2 = \ln x_3 + (k-1)\ln\left(\frac{P}{P*}\right) + \frac{L_1}{T} + \left(\frac{\rho_1}{\rho_2} + \frac{\rho_1}{\rho_3} - \frac{\rho_1 x_3 L_2}{\rho_3} + k\rho_1 L_3\right) + L_4 \qquad (5.8)$$

Where *k*, L_1 to L_4 are temperature independent parameters and were obtained using the no*n*-linear curve fitting with a constraint on value of *k* being always positive. In (Eq. (5.8)), L_1 values can be positive or negative depending on the values of heat of solvation and virial coefficients. L_1 was always found to be positive from the regression, implying $\Delta H_s > (B_2 + B_3)R$. The parameter, L_2 values account for the interaction between solvent/co-solvent, solute/co-solvent and solvent/solute. It can be positive or negative depending on the value of $3a_{13}$. In case of methanol and *n*-propanol, the value of L_2 was found to be negative, suggesting that $(a_{23}-a_{12}) > 3a_{13}$. L_3 term in Eq. (5.8) that comprises of the virial coefficients is same as that of W_2 in Eq. (5.6) and its value is also found to be negative. In Eq. (5.8), the term L_4 is equivalent to term W_6 in Eq. (5.9) and the value of L_4 is always found to be negative. The values of L_4 and W_6 were also found to be comparable for all three co-solvents. L_4 can be positive or negative depending on the whether the value of $(A_2 + A_3)$ is greater or less than the value of $q_s + \left(\frac{\phi_{231_k}\phi_1^{*k}}{\phi_{231_k}^{*}} \frac{\phi_2^{*}\phi_3^{*}}{\phi_{sat}^{2}} \frac{\left(P^{*}\right)^2}{x_2^l \gamma_2^l}\right)$. Eq. (5.8) was employed to correlate the solubilities of TOMAC in $SCCO_2$ in presence of different co-solvents. Experimental solubilities are compared with the calculated solubilities and shown in the **Figure 5.3(c1, c2), 5.5(c1, c2)** and **5.6(c1, c2),** respectively. The model parameters along with the AARD values are reported in **Table 5.6**.

The results based on the four parameters modified Chrastil model (Eq. (2.10)), five parameters association theory based van Laar activity coefficient model (Eq. (5.8)) and six parameters association theory based Wilson activity coefficient model (Eq. (5.9)) are shown in **Table 5.6** along with their respective AARD %. Modified Chrastil equation (Eq. (2.10)) correlated the solubilities with an AARD of around 12%. It was observed that the newly derived models (Eq. (5.8) and Eq. (5.8)) have successfully correlated the solubility of TOMAC in SCCO$_2$ in the presence of co-solvents with an AARD of within 8%, lesser than the modified Chrastil model. The parameters in the Eq. (5.8) and Eq. (5.9) also provide some preliminary physical interpretation of interactions between solute, solvent and co-solvent molecules. Thus, the current models are first of its kind to correlate the liquid solute solubilities in SCCO$_2$ in the presence of different co-solvents. However, it is important to note that the three models used for correlating the solubilities in SCCO$_2$ in the presence of co-solvents consist of different number of parameters (4, 5 and 6). Thus, it is crucial to account the effect of different number of parameters to comment on the superiority of a model. This effect of different relative deviations and the number of parameters from different models can be accounted by using the Akaike information criteria (AIC) to obtain the best model for correlating the solubilities.

AIC penalizes for the addition of parameters and provides a bridge between the goodness of the fit and the model complexity. It is given by,

$$AIC = n \ln\left(\frac{ESS}{n}\right) + 2p \tag{5.10}$$

In Eq. (5.10), n and p denotes the number of data points and the number of parameters in model, respectively. ESS is the error sum of squares or the residual sum of squares obtained after regressing the experimental data using a particular model. However, the AIC is used for a large sample size when (n / p > 40) and thus is not accurate for the small sample size. Hence, the Eq. (5.10) was corrected for the small sample size and is named as corrected Akaike information criterion (AIC_C) **[191, 222]**,

$$AICc = AIC + \frac{2p\ (p+1)}{n-p-1} \tag{5.11}$$

The model providing the minimum value of AICc among the compared models is the best model. Thus, Eq. (5.11) was used to compare the three models used in the present study to correlate the solubilities of TOMAC in $SCCO_2$ with different co-solvents. The AICc values obtained for each model for different compositions of co-solvents have been provided in **Table 5.6**. AICc results (**Table 5.6)** indicates that the four parameter modified Chrastil model (Eq. (2.10)) is always better than the other two models (Eq. (5.8) and Eq. (5.9)) for correlating the solubilities in $SCCO_2$ with co-solvents for lower concentration of co-solvents (1.05 mol %). Similarly, the newly developed five parameters association theory based van Laar activity coefficient model (Eq. (5.8)) is always better than the other two models (Eq. (2.10) and Eq. (5.9)) for correlating the solubilities in $SCCO_2$ with co-solvents for higher concentration of co-solvents (4.20 mol %). However, for the intermediate concentration of co-solvents (2.10 mol %), both of these models (Eq. (2.10) and Eq. (5.8)) can be used to correlate the experimental solubility data.

Table 5.6 Regression analysis and model comparison for solubilities of TOMAC in $SCCO_2$ with different co-solvents

Model	**Model Parameters**	**Parameter Values**								
		***n*-hexane as a co-solvent**			***n*-propanol as a co-solvent**			**methanol as a co-solvent**		
Modified Chrastil model (Eq. (2.10))	*k*	2.9 ± 0.1			5.1 ± 0.1			5.1 ± 0.1		
	γ	0.45 ± 0.01			1.7 ± 0.1			1.7 ± 0.04		
	A_3	1703 ± 40			-145 ± 10			255 ± 10		
	B_3	-20 ± 1			-26± 2			-26 ± 2		
	R^2	0.968			0.992			0.991		
	AARD (%)	12.0			12.0			12.0		
	Co-solvent (mol %)	**1.05**	**2.10**	**4.20**	**1.05**	**2.10**	**4.20**	**1.05**	**2.10**	**4.20**
	AICc	-215.1	-213.1	-198.7	-196.5	-171.3	-125.9	-206.8	-169.9	-123.0
Association model based on Wilson activity coefficient model (Eq. (5.9))	*k*	1.2			1.2			1.2		
	W_1	1713 ± 6			127 ± 6			598 ± 22		
	W_2	$-4.5\ x\ 10^{-4} \pm 5\ x\ 10^{-6}$			$-2.2\ x\ 10^{-4} \pm 5\ x\ 10^{-6}$			$-2\ x\ 10^{-4} \pm 1\ x\ 10^{-6}$		
	W_3	2188 ± 100			-1251 ± 100			-1130 ± 45		
	W_4	40114 ± 1474			-51154 ± 3000			-90426 ± 3600		
	W_6	-13.7 ± 0.2			-9.7 ± 0.1			-11 ± 0.1		
	R^2	0.996			0.995			0.997		
	AARD (%)	8.0			7.0			6.0		
	Co-solvent (mol %)	**1.05**	**2.10**	**4.20**	**1.05**	**2.10**	**4.20**	**1.05**	**2.10**	**4.20**
	AICc	-207.2	-199.4	-199.1	-186.5	-150.2	-113.6	-170.7	-157.7	-114.3

Model	**Model Parameters**	**Parameter Values**								
		***n*-hexane as a co-solvent**			***n*-propanol as a co-solvent**			**methanol as a co-solvent**		
Association model based on van Laar activity coefficient model (Eq. (5.8))	*k*	1.1			1.2			1.1		
	L_1	1684 ± 50			1298 ± 20			385 ± 10		
	L_2	12 ± 0.5			-24 ± 1			-45 ± 2		
	L_3	$-4 \; x \; 10^{-4} \pm 5 \; x \; 10^{-6}$			$-2.5 \; x \; 10^{-4} \pm 5 \; x \; 10^{-6}$			$-2.3 \; x \; 10^{-4} \pm 2 \; x \; 10^{-6}$		
	L_4	-13 ± 0.2			-13 ± 0.2			-10 ± 0.2		
	R^2	0.966			0.993			0.997		
	AARD (%)	7.0			8.0			5.0		
	Co-solvent (mol %)	**1.05**	**2.10**	**4.20**	**1.05**	**2.10**	**4.20**	**1.05**	**2.10**	**4.20**
	AICc	-211.2	-211.4	-211.7	-190.8	-158.8	-126.7	-190.0	-171.0	-132.1

5.2.3 Conclusions

Two new models were developed for correlating the ternary solubilities ($SCCO_2$+co-solvent+liquid solute) based on association theory along with the Wilson and van Laar activity coefficient models. These two equations (with 5 and 6 parameters) are employed to correlate the solubilities of TOMAC in $SCCO_2$ in the presence of different co-solvents. The correlation results are compared with modified Chrastil model (4 parameter model). A lower AARD of less than 8% was obtained using the new models having 5 and 6 parameters in comparison to the existing 4 parameters model. The penalty for the increased number of parameters in a model was accounted by the AICc values for the best model to be used. It was observed that AICc value was minimum for modified Chrastil model for lower concentrations (1.05 mol %) of co-solvents whereas, it was found to be minimum for association theory based van Laar activity coefficient model for higher concentrations (4.20 mol %). Thus, both these models can be used appropriately for correlating the solubilities of polar RTILs in $SCCO_2$ with co-solvents.

Chapter 6

Solubility of *N*,*N*-dialkylamides in supercritical carbon dioxide: experimental and modeling approach

---

6.1 Introduction

N,*N*-dialkyl amides are proposed as potential alternative extractants to trialkyl phosphates (e.g. TBP) and dialkylalkyl phosphonates (e.g. DAAP) for the extraction and recovery of actinides. Dialkylalkyl amides are resistant to hydrolysis and radiolysis, innocuous nature of their degradation products and possibility of complete incineration leading to reduction in the liquid secondary waste [169]. There is enough literature data available for the solvent extraction of actinides using *N*,*N*-dialkylamides. However, there is no solubility data on dialkylamides in supercritical medium and these compounds have not been explored in SFE mode for actinide recovery. Hence, a series of linear and branched *N*,*N*-dialkyl amides were taken-up and their solubility in $SCCO_2$ medium have been measured for the first time to assess their utility as ligands in supercritical fluid extraction of actinides.

6.2 Results and discussions

6.2.1 Solubility of *N*,*N*-dialkyl amides in supercritical carbon dioxide

A series of linear chain *N*,*N*-dialkylamides (*N*,*N*-dihexylhexanamide, *N*,*N*-dihexyloctanamide and *N*,*N*-dihexyldecanamide) and branched *N*,*N*-dialkylamides (*N*,*N*-di-2-ethylhexylacetamide, *N*,*N*-di-2-ethylhexyl-*iso*-butyramide and *N*,*N*-di-2-ethylhexylpivalamide) are synthesised as reported in literature [177]. The structures of these amides are shown in **Figure 6.1.** The solubilities of these *N*,*N*-dialkyl amides are measured at temperatures, 313 to 333 K with pressure ranging from 10 to 20 MPa. The mole fraction solubilities (mole per mole of CO_2) of these amides are shown in **Table 6.1**.

The values reported in **Table 6.1** are average of three replicate measurements with a relative standard deviation less than 5%.

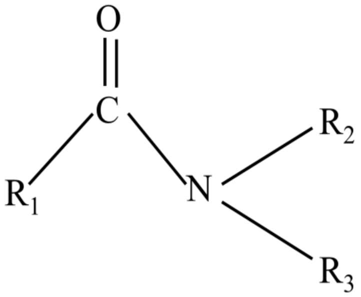

Name	Abbreviation	R_1	$R_2 = R_3$
N,N-dihexylhexanamide	DHHA	C_5H_{11}	C_6H_{13}
N,N-dihexyloctanamide	DHOA	C_7H_{15}	C_6H_{13}
N,N-dihexyldecanamide	DHDA	C_9H_{19}	C_6H_{13}
N,N-di-2-ethylhexylacetamide	D2EHAA	CH_3	$CH_2\,CH(C_2H_5)(CH_2)_3CH_3$
N,N-di-2-ethylhexyl-*iso*-butyramide	D2EHiBA	$(CH_3)_2CH$	$CH_2\,CH(C_2H_5)(CH_2)_3CH_3$
N,N-di-2-ethylhexylpivalamide	D2EHPVA	$(CH_3)_2C$	$CH_2\,CH(C_2H_5)(CH_2)_3CH_3$

Figure 6.1 General formula for *N,N*-dialkylamides employed in the present study

The solubilities of *N*,*N*-dialkylamides are ranging from 0.005 x 10^{-3} t 102 x 10^{-3} mole/mole in the investigated region. The effect of temperature and pressure on the solubility of amides is depicted (**Figure 6.2)**. The experimental data presented in **Table 6.1** and **Figure 6.2** illustrate that an isothermal increase in pressure leads to an increase in solubility. At constant pressure, the solubility decreases with increasing in temperature, indicating retrograde solubility behavior in the investigated regions. *N,N*-dialkylamides have negligible vapor pressure in the experimental temperature regions; therefore density of $SCCO_2$ is the prevailing factor in deciding the solubility.

The solubilities of primary amides and phenylacetamides are reported and are in the order of 10^{-4} mole/mole [87, 88, 223]. The solubilities of *N*,*N*-dialkylamides are found to be higher than various primary amides. Primary amides possess considerable polarity and are reflected by their high boiling points and water solubility. Primary amides show strong intermolecular interactions owing to the high electron density on the hydrogen atom attached to the “N”. The presence of N-H dipole allows amides to act as hydrogen bond donor. As a result, the water solubility of amides is greater than that of corresponding hydrocarbons [224]. The solubility of these primary amides in non-polar solvents is less. For e.g. acetamide is soluble in water and has poor solubility in non-polar solvents. As the substitution on “N” atom increases, the boiling point and water solubility decreases and hydrophobicity and solubility in non-polar solvents increases. Therefore, we can expect that *N*,*N*-disubstitued amides can show higher solubility in $SCCO_2$ medium compared to that of primary amides.

At the same temperature and pressure, solubilities of *N*,*N*-dialkylamides decreases with increase in the carbon number or molecular weight (DHHA > DHOA > DHDA and D2EHAA > D2EHiBA > D2EHPVA). The variation of solubility of linear and branched *N*,*N*-dialkylamides are shown in **Figure 6.3**. This indicates that in a homologous series, solubility decreases with an increase in the carbon number [200, 203]. The solubility of two linear *N*,*N*-dialkylamides, DHHA and DHOA are compared with their branched isomers, D2EHAA and D2EHiBA (**Figure 6.3**). In general, compounds with branching are relatively more soluble than their straight chain isomer in $SCCO_2$ [208] and same trend is observed in the present study. The amides, D2EHAA and D2EHiBA show an increase in the solubility than that of their corresponding straight-chain isomers, DHHA and DHOA.

Table 6.1 Solubility of *N*,*N*-dialkylamides in $SCCO_2$ medium

T (K)	*P* (MPa)	Density* (kg/m^3)	Solubility (mol/mol) $y_2 \times 10^3$					
			Straight chain *N*,*N*-dialkyl amides			Branched *N*,*N*-dialkyl amides		
			DHHA	DHOA	DHDA	D2EHAA	D2EHiBA	D2EHPVA
313.0	8.0	277.90	0.05	0.05	0.01	0.16	0.06	0.03
313.0	10.0	628.61	12.3	8.4	1.8	23	11.2	8.7
313.0	12.0	717.76	33	19	4.5	51	31	26
313.0	14.0	763.27	58	32	7.6	71	46	38
313.0	16.0	794.90	73	40	12.5	83	58	48
313.0	18.0	819.51	92	47	19.7	90	65	56
313.0	20.0	839.81	102	52	28	95	71	61
323.0	10.0	384.33	0.37	0.26	0.05	0.62	0.35	0.27
323.0	12.0	584.71	6.1	4.2	1.1	9.2	7.0	4.7
323.0	14.0	672.17	18.0	12.4	3.2	30	18	14.4
323.0	16.0	722.09	32	22	5.9	52	31	26
323.0	18.0	757.12	49	27	9.9	65	44	35
323.0	20.0	784.29	62	32	13.6	75	58	45
333.0	10.0	289.95	0.06	0.04	0.005	0.10	0.06	0.03
333.0	12.0	434.43	0.69	0.53	0.09	1.5	0.84	0.56
333.0	14.0	561.37	4.6	2.8	0.68	9.1	4.2	3.2
333.0	16.0	637.50	10.5	8.2	2.2	19.3	10.9	8.5
333.0	18.0	687.25	20	13.5	4.1	36	20	15.5
333.0	20.0	723.68	29	18.7	6.6	51	29	25

* Density values taken from http://webbook.nist.gov/chemistry/fluid/

Experimental conditions: CO_2 flow rate: 0.1 mL/min;, Equilibrium cell volume: 10 mL; No. of equilibrium cells connected in series: 2; sample loaded in equilibrium cells: 1st cell-8 mL and 2nd cell: 6 mL; heat exchanger: 10 mL; entrainer column: 10 mL.

Standard uncertainties (u) are u(T) = 0.1 K, u(P) = 0.1 MPa and relative uncertainty (u_r), $u_r(y_2)$ = 0.05

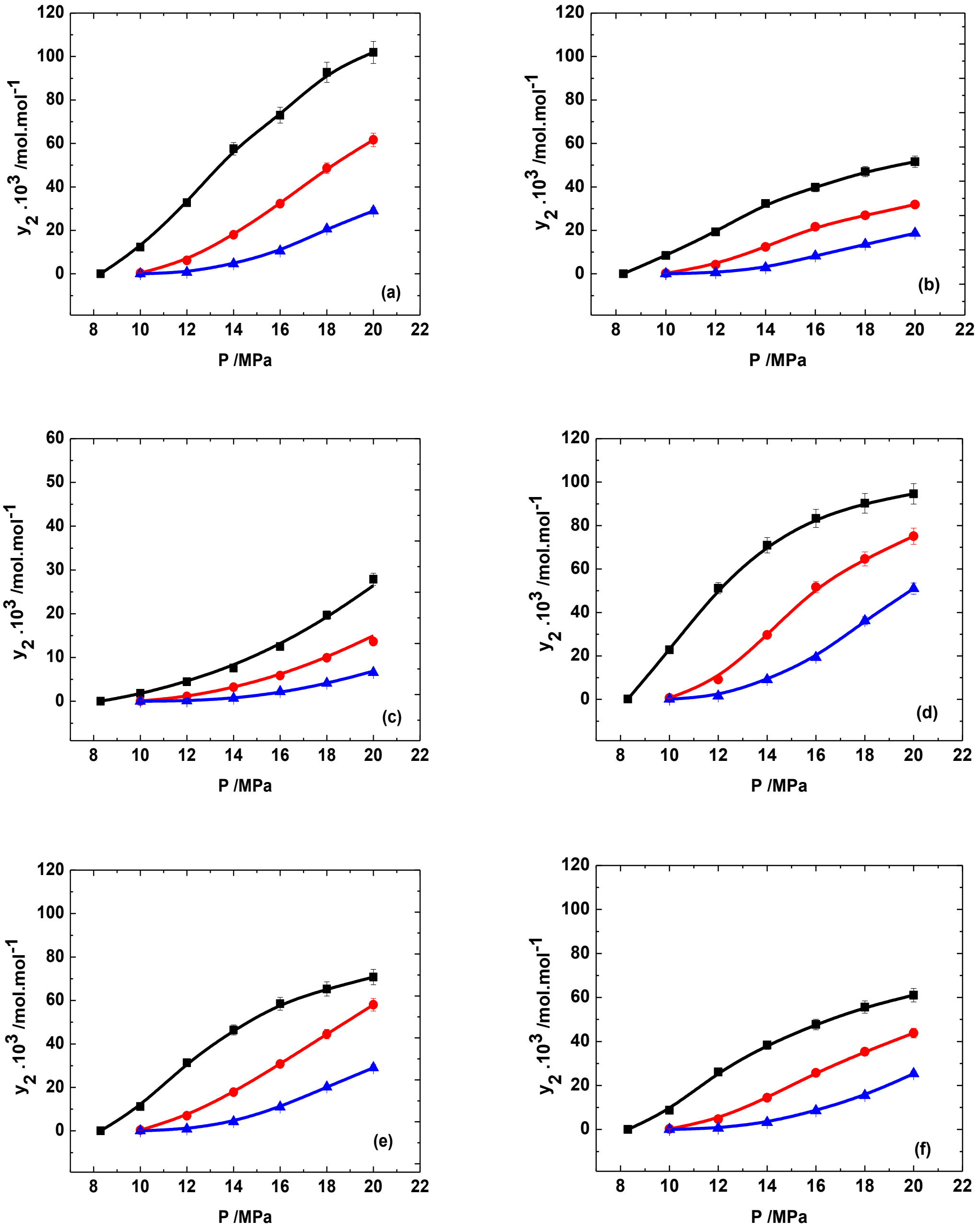

Figure 6.2 Variation of solubility of *N,N*-dialkylamides with pressure at different temperatures, (■) 313 K; (●) 323 K; (▲) 333 K in supercritical carbon dioxide (a) dihexylhexanamide, (b) dihexyloctanamide, (c) dihexyldecanamide, (d) di-2-ethylhexylacetamide (e) di-2-ethylhexyl-*iso*-butyramide, (f) di-2-ethylhexylpivalamide

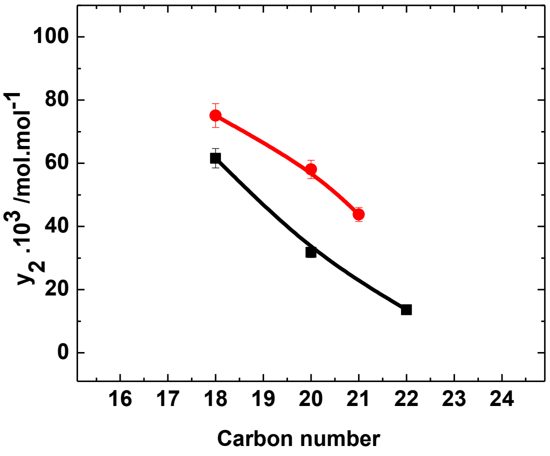

Figure 6.3 Typical trend of variation of solubility of *N,N*-dialkylamides with their carbon number at 333 K and 20 MPa; (■) straight chain *N,N*-dialkylamides ; (●) branched *N,N*-dialkylamides

6.2.2 Model correlations

(a) Mendez-Teja (MT) model

The consistency of the experimental solubility data has been verified with MT equation (Eq. (2.11)) by plotting $T\ ln\ (Py_2)\text{-}C_4T$ with the density of $SCCO_2$. This is represented by **Figure 6.4**, wherein all data points at different isotherms falls onto a single straight line, indicating the self-consistency of the experimental data. MT model was also employed to correlate experimental solubilities (**Table 6.2).** Experimental solubilities are compared with the solubilities calculated by MT model. The model correlated solubilities of *N,N*-dialkylamides with an AARD of less than 20%. Minimum AAARD of 14% is observed for DHHA whereas maximum AARD of 19% is obtained for branched *N,N*-dialkylamides, D2EHAA and D2EHPVA.

(b) Chrastil model

Chrastil model (Eq. (2.8)) has been employed in the present work to correlate the solubility of *N,N*-dialkylamides in $SCCO_2$. The plots of $ln\ S$ vs $ln\ \rho$ represent straight lines for different isotherms with slope indicating association number, *k*. The experimental solubilities were regressed with Eq. (2.8) to obtain the model parameters

(**Table 6.2**). The association number for the linear as well as for branched *N,N*-dialkylamides varies from 7 to 9. The solubility correlations by Chrastil equation for all six amides, DHHA, DHOA, DHDA, D2EHAA, D2EHiBA and D2EHPVA are shown in **Figure 6.5(a), 6.6(a), 6.7(a), 6.8(a), 6.9(a),** and **6.10(a)** respectively. Chrastil equation correlated the solubilities with an AARD of ~ 13%.

(c) Solution theory based on Wilson activity coefficients

The solubilities of *N,N*-dialkylamides in $SCCO_2$ medium are correlated using a solution theory model based on Wilson activity coefficients (Eq. (2.13)). The correlation parameters are shown in **Table 6.2**. The experimental solubilities of *N,N*-dialkylamides are compared with the model predictions based on the solution model. The solubility correlations by solution theory model for all six amides, DHHA, DHOA, DHDA, D2EHAA, D2EHiBA and D2EHPVA are shown in **Figure 6.5(b), 6.6(b), 6.7(b), 6.8(b), 6.9(b),** and **6.10(b)** respectively.

(d) Association theory with van Laar activity coefficients

The experimental solubility data for all the six amides are fitted using an association theory with van Laar activity coefficient model (Eq. (2.15)). The solubility correlations using association theory for all six amides, DHHA, DHOA, DHDA, D2EHAA, D2EHiBA and D2EHPVA are shown in **Figure 6.5(c), 6.6(c), 6.7(c), 6.8(c), 6.9(c),** and **6.10(c)** respectively. The relative deviation between the experimental and predicted solubility data is evaluated using AARD and the values are reported in **Table 6.2**. The correlation results demonstrated that the association theory based on van Laar activity coefficient model was better to predict the solubility data with an AARD of less than 8%.

Table 6.2 Correlation results and model parameters for the solubility of *N,N*-dialkylamides in $SCCO_2$ using four different models

Model	Model Parameter	Straight chain *N,N*-dialkyl amide			Branched *N,N*-dialkyl amide		
		DHHA	**DHOA**	**DHDA**	**D2EHAA**	**D2EHiBA**	**D2EHPVA**
MT model Eq. (2.11)	A_4	-4961±50	-5326±50	-7704±50	-5560±100	-5756±90	-6009±50
	B_4	4.8±0.1	4.7±0.1	5.56±0.1	4.53±0.2	4.76±0.1	4.96±0.3
	C_4	3.89±0.1	4.49±0.2	9.09±0.2	6.74±0.2	6.36±0.1	6.50±0.1
	R^2	0.994	0.991	0.993	0.982	0.990	0.990
	AARD (%)	14	18	18	19	15	19
Chrastil model Eq.(2.8)	A_1	899±10	565±10	-147±50	66±5	399.9±30	277.7±20
	B_1	-48±2	-46±3	-54±2	-41.7±3	-48±2	-45.4±3
	k	7.6±0.3	7.4±0.1	8.8±0.2	7.1±0.2	7.8±0.3	7.5±0.3
	R^2	0.998	0.998	0.996	0.993	0.998	0.997
	AARD (%)	7	10	11	13	10	9

	Model	**Straight chain *N*,*N*-dialkyl amide**			**Branched *N*,*N*-dialkyl amide**		
Model	**Parameter**	**DHHA**	**DHOA**	**DHDA**	**D2EHAA**	**D2EHiBA**	**D2EHPVA**
Solution theory model Eq.(2.13)	A_5	-10.7±0.5	-9.77±0.5	-13.3±0.2	-7.2±0.3	-7.9±0.5	-8.2±0.5
	B_5	2.2±0.1	1.92±0.1	1.91±0.1	2±0.05	1.9±0.1	1.93±0.1
	C_5	-773±30	-1055±45	-602±40	-1466±40	-1530.7±50	-1698.3±30
	R^2	0.990	0.986	0.988	0.978	0.984	0.985
	AARD (%)	20	23	20	25	23	25
Association model Eq. (2.15)	k_{VL}	1.4±0.1	1.92±0.1	4.27±0.2	1.39±0.1	1.99±0.1	2.44±0.1
	A_{VL}	91±8	2035±50	11166±20	4228±100	1610±50	1963±100
	C_{VL}	715±31	605±40	-293.5±30	-208.7±10	643±50	835±60
	D_{VL}	-66±5	-75±5	-72±4	-84.6±10	-79±4	-83±4
	E_{VL}	1.2±0.05	1.58±0.05	4.1±0.2	4.37±0.2	1.6±0.1	1.13±0.05
	F_{VL}	-16.95±0.1	-24.85±0.1	-60±2	-29.4±1	-23.7±2	-26.84±1
	R^2	0.999	0.999	0.999	0.999	0.998	0.998
	AARD (%)	4	5	5	8	6	7

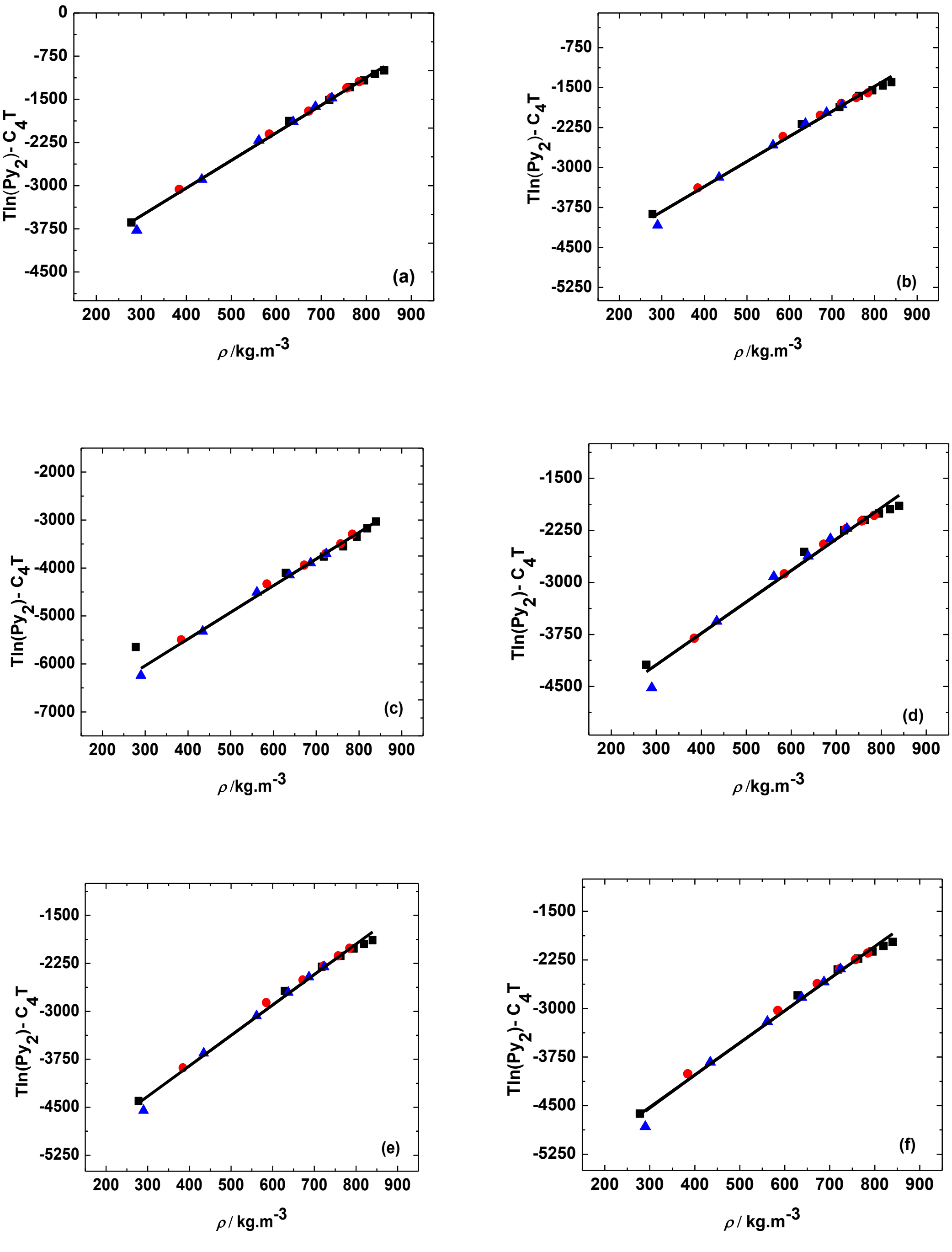

Figure 6.4 Solubility of *N,N*-dialkylamides in supercritical carbon dioxide at different temperatures, (■) 313 K; (●) 323 K; (▲) 333 K. (a) *N,N*-dihexylhexanamide, (b) *N,N*-dihexyloctanamide, (c) *N,N*-dihexyldecanamide, (d) *N,N*-di-2-ethylhexylacetamide, (e) *N,N*-di-2-ethylhexyl-*iso*-butyramide, (f) *N,N*-di-2-ethylhexylpivalamide; Solid line represents the correlations with MT model (Eq. (2.11))

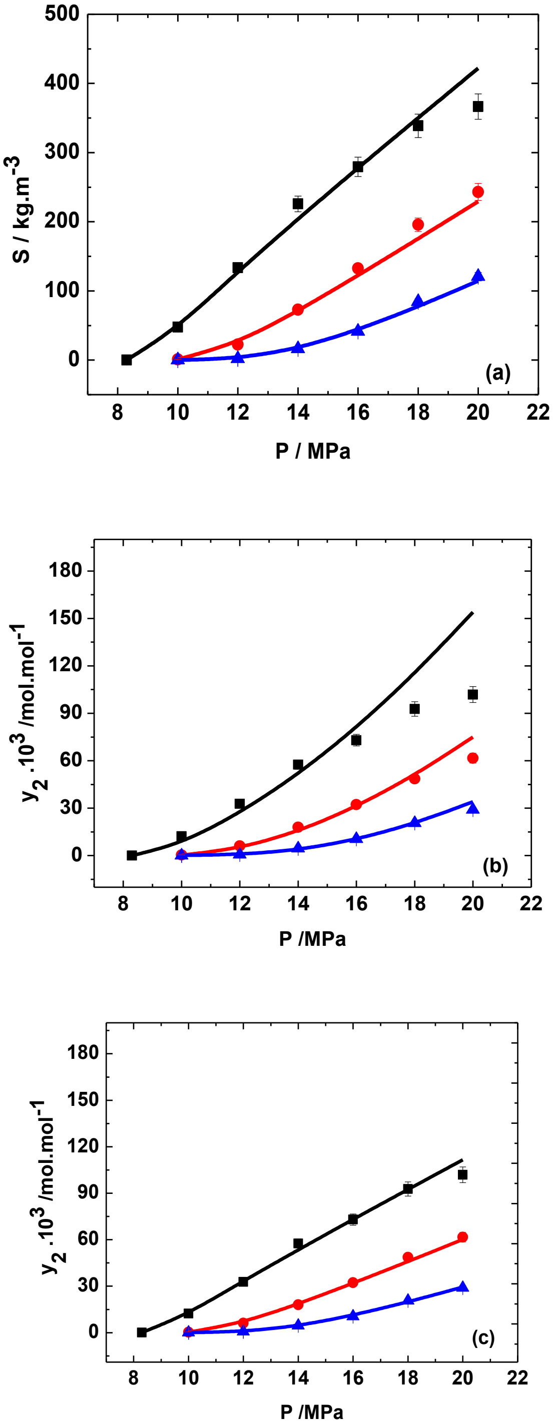

Figure 6.5 Experimental solubility of *N*,*N*-dihexylhexanamide in supercritical carbon dioxide at different temperatures, (■) 313 K; (●) 323 K; (▲) 333 K; The solid lines represents the model correlations based on (a) Chrastil model (Eq. (2.8)), (b) solution theory based on Wilson activity coefficient model (Eq. (2.13)), (c) association model based on van Laar equation for activity coefficient (Eq. (2.15))

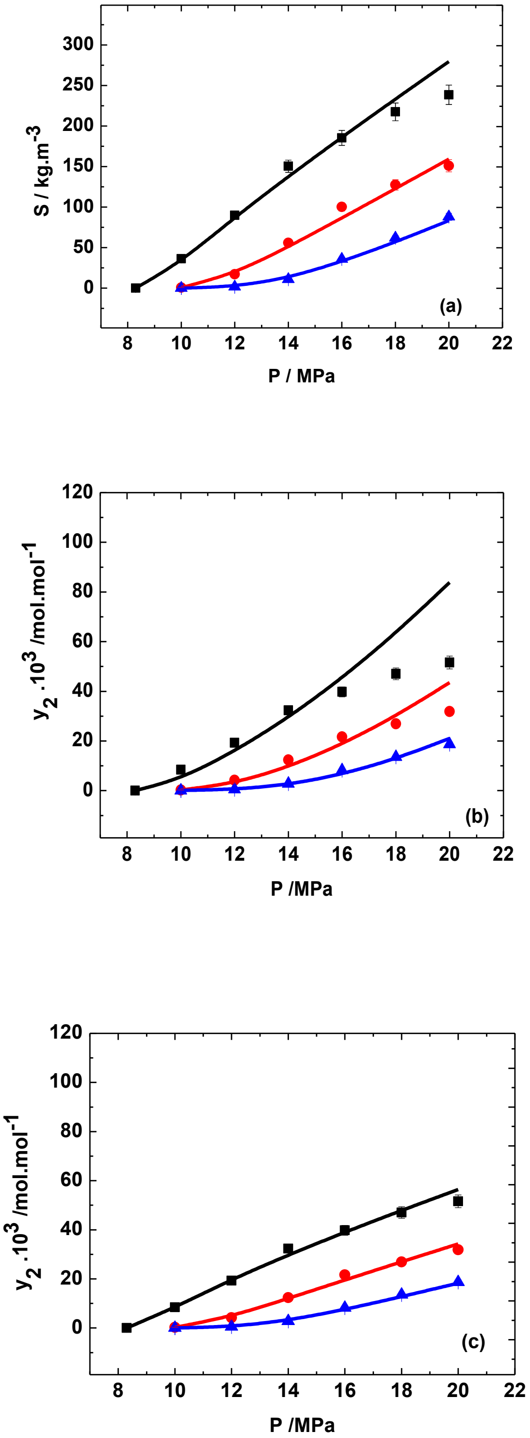

Figure 6.6 Experimental solubility of *N*,*N*-dihexyloctanamide in supercritical carbon dioxide at different temperatures, (■) 313 K; (●) 323 K; (▲) 333 K; The solid lines represents the model correlations based on (a) Chrastil model (Eq. (2.8)), (b) solution theory based on Wilson activity coefficient model (Eq. (2.13)), (c) association model based on van Laar equation for activity coefficient (Eq. (2.15))

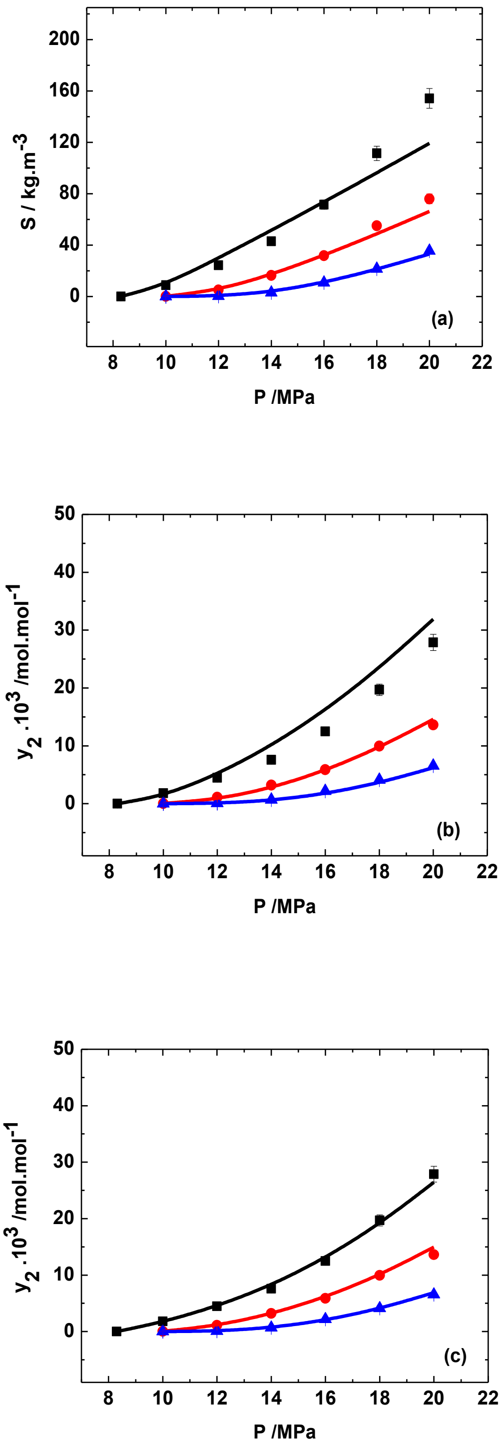

Figure 6.7 Experimental solubility of *N,N*-dihexyldecanamide in supercritical carbon dioxide at different temperatures, (■) 313 K; (●) 323 K; (▲) 333 K; The solid lines represents the model correlations based on (a) Chrastil model (Eq. (2.8)), (b) solution theory based on Wilson activity coefficient model (Eq. (2.13)), (c) association model based on van Laar equation for activity coefficient (Eq. (2.15))

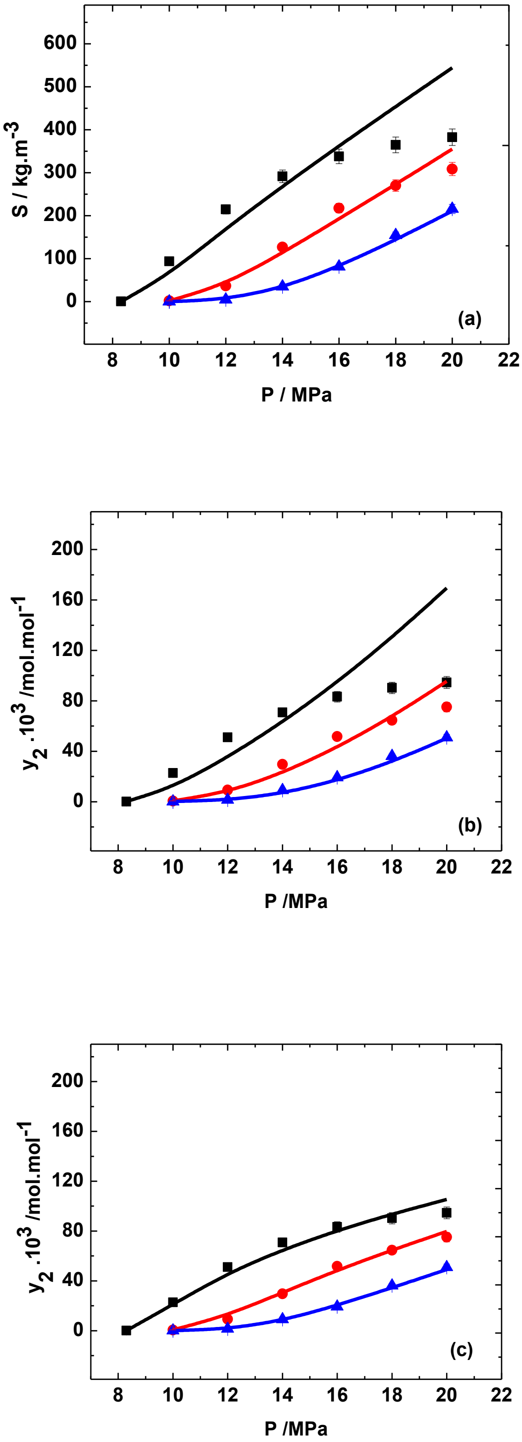

Figure 6.8 Experimental solubility of *N,N*-di-2-ethylhexylacetamide in supercritical carbon dioxide at different temperatures, (■) 313 K; (●) 323 K; (▲) 333 K; The solid lines represents the model correlations based on (a) Chrastil model (Eq. (2.8)), (b) solution theory based on Wilson activity coefficient model (Eq. (2.13)), (c) association model based on van Laar equation for activity coefficient (Eq. (2.15))

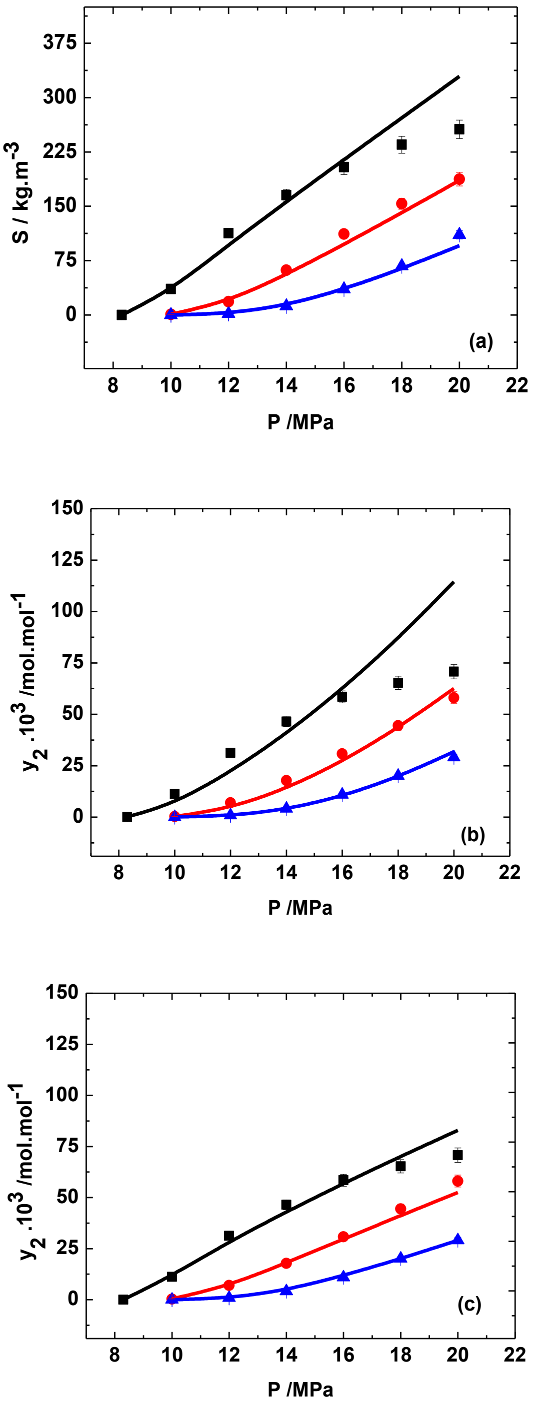

Figure 6.9 Experimental solubility of *N,N*-di-2-ethylhexyl-*iso*-butyramide in supercritical carbon dioxide at different temperatures, (■) 313 K; (●) 323 K; (▲) 333 K; The solid lines represents the model correlations based on (a) Chrastil model (Eq. (2.8)), (b) solution theory based on Wilson activity coefficient model (Eq. (2.13)), (c) association model based on van Laar equation for activity coefficient (Eq. (2.15))

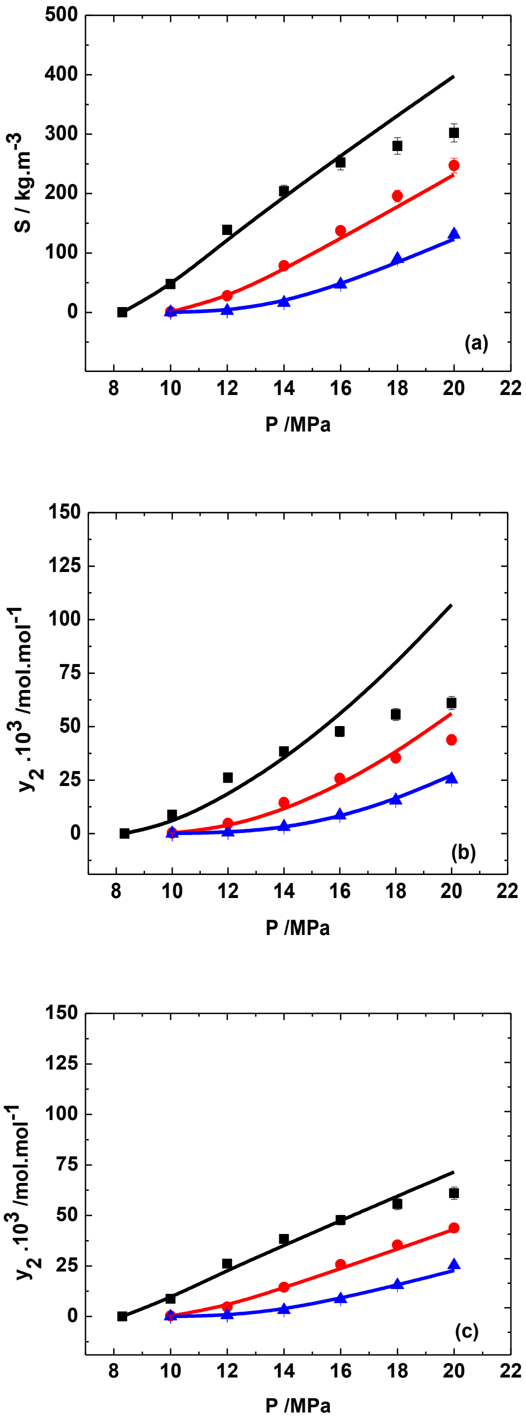

Figure 6.10 Experimental solubility of *N*,*N*-di-2-ethylhexylpivalamide in supercritical carbon dioxide at different temperatures, (■) 313 K; (●) 323 K; (▲) 333 K; The solid lines represents the model correlations based on (a) Chrastil model (Eq. (2.8)), (b) solution theory based on Wilson activity coefficient model (Eq. (2.13)), (c) association model based on van Laar equation for activity coefficient (Eq. (2.15))

6.3 Conclusions

The solubility behavior of linear and branched *N*,*N*-dialkylamides in $SCCO_2$ medium was examined at temperatures, 313 to 333 with pressure varying from 10 to 20 MPa using a flow saturation technique. The solubility increases with the pressure at isothermal conditions. A retrograde behavior in the solubility has been observed with the temperature in the investigated region. The solubility of amides decreases with increase in the carbon number. Experimental solubility data have been correlated using four semi-empirical equations, MT equation, Chrastil equation, solution theory based on Wilson activity coefficient model and association model with van Laar activity coefficient model. The experimental solubility data were found to be self-consistent based on MT equation. The correlation results showed that the association theory based on van Laar activity coefficient model has a good agreement with the experimental solubilities with an AARD of less than 10%. The solubility data of *N*,*N*-dialkyl amides in $SCCO_2$ establish the feasibility of their use as ligands in the extraction of actinides for various applications of nuclear fuel cycle.

Chapter 7

Supercritical fluid extraction studies of actinides from different matrices using modified supercritical carbon dioxide

The application of SFE technique towards recovery of actinides from various matrices has been explored and discussed in this chapter. Actinides such as uranium, thorium and plutonium are to be recovered from aqueous medium to minimize the radiotoxicity on the liquid waste; similarly, separation of uranium from thorium is of importance in thorium fuel cycle; chloride salt waste arising from pyrochemical process contains residual actinides and these actinides have to be removed to reduce radiotoxicity of salt waste and also for the re-use of salt. An attempt has been made in this work to employ $SCCO_2$ containing ligand for recovery of actinides from chloride salt matrix.

Chapter 7 (a)

Supercritical fluid extraction of uranium and thorium from nitric acid medium

7.1.1. Supercritical extraction of uranium from aqueous medium using various organophosphorous compounds

The extraction and recovery of uranium from different matrices is of importance as these ions have many important applications in nuclear fuel cycle. SFE of uranium from nitric acid medium was carried out using $SCCO_2$ containing series of organophosphorous compounds (trialkyl phosphates, dialkylalkyl phosphonates and trialkyl phosphine oxides). These initial studies were carried to identify the potential candidates (ligands) which can be employed in supercritical medium for the recovery of actinides from nitric acid medium.

The results on the SFE of uranium from 4 N HNO_3 medium **(Figure 7.1)** using $SCCO_2$ containing various organophosphorous compounds are given in **Table 7.1.** The co-extraction of water during these experiments can be relatively poor as metal ions are recovered from nitric acid medium, which has higher dielectric constant compared to water. In our studies, the extracted metal ions were directly collected into 0.01 N HNO_3+chloroform mixture and hence, the extraction of water was not examined. Moreover, the solubility water in $SCCO_2$ is relatively lower and is ranging from 4.28 x 10^{-3} to 5.8 x 10^{-3} mole/mol at 313 K &10.13-20.27 MPa [225].

The use of phosphates (TBP, TiAP and THP) resulted in a maximum extraction efficiency of 27 % whereas use of phosphonates (DBBP and DAAP) resulted in an extraction efficiency of 51 and 53 % respectively. There was no significant difference in the extraction behavior of the two phosphonates under these experimental conditions. The extractants, dioctylhydrogen phosphonate and HDEHP provide an extraction of 30 and 66 % respectively for uranium.

Table 7.1 Extraction efficiency of uranium from 4 N nitric acid medium using various organophosphorous compounds

S. No.,	Ligand	Extraction Efficiency[#] (%)
1.	Tributyl phosphate (TBP)	26
2.	Tributyl phosphate*****	51
3.	Tri-*iso*-amyl phosphate (TiAP)	26
4.	Tri-*iso*-amyl phosphate *****	54
5.	Trihexyl phosphate (THP)	27
6.	Trihexyl phosphate *****	57
7.	Diamylamyl phosphonate (DAAP)	56
8.	Dibutylbutyl phosphonate (DBBP)	51
9.	Trioctylphosphine oxide (TOPO)	75
10.	Dioctylhydrogen phosphonate (DOHP)	32
11.	Dioctylphosphine oxide (DPO)	85
12.	*n*-octylphenyl *N*,*N*-di-*iso*-butyl carbamoylmethylphosphine oxide (CMPO)	85
13.	Di-(2-ethylhexyl)phosphoric acid (HDEHP)	66

Experimental conditions: pressure: 30 MPa; temperature: 323 K; $SCCO_2$ flow rate: 2.5 mL/min; sample: uranyl nitrate; sample loaded: 0.01 mmol in 1 mL of 4 N HNO_3, ligand quantity: 0.18 mmol; extraction vessel: 10 mL; static extraction: 1 hour and dynamic extraction: 1 hour.

* Ligand quantity employed: 0.36 mmol; [#]Extraction efficiencies are average of three independent experiments with a relative standard deviation of 5 %.

SFE of uranium with dioctylphosphine oxide has resulted in about 85 % extraction. Use of strong extractants, trioctylphosphine oxide (TOPO) and CMPO resulted in an better extraction efficiency of 74 and 84 % respectively. The extraction efficiency of uranium by CMPO is higher than TOPO although both of them belong to phosphine oxide family. It is likely that TOPO also extracts considerable quantities of acid at 4 M nitric acid through P=O group because of its high basicity, but in the case of CMPO, the P=O is relatively free as the acid prefers C=O group [226], leaving the P=O for the metal . The replacement of long chain octyl group in TOPO with H (DOPO) reduces the crowding on the phosphoryl group around the P=O group thereby allowing the metal to interact with oxygen group of the molecule more effectively, thereby exhibiting higher extraction efficiency, similar to that of CMPO. The present study has shown that phosphine oxides (e.g. CMPO) are stronger extractants compared to phosphonates, which are stronger compared to phosphates.

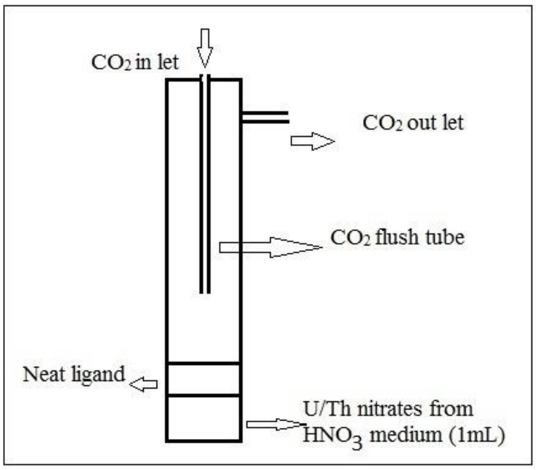

Figure 7.1 Schematic of SFE using 10 mL liquid extraction vessel

7.1.2. Recovery of uranium from nitric acid medium

(a) Recovery of uranium using SCCO_2 containing dialkylalkyl phosphonates

Though CMPO has shown better extraction behavior compared to other organophosphorous compounds, the back stripping efficiency of uranium from Uranium-

CMPO complex is challenging and difficult. Hence, phosphonates were examined as ligands for the recovery (**Table 7.1**) of uranium from aqueous medium. Since both DAAP and DBBP provided comparable recovery, SFE of uranium was studied from nitric acid medium using $SCCO_2$ containing one of the phosphonate, namely, DAAP. The influence of equilibration period on SFE of uranium from HNO_3 medium was studied by performing the extraction with an equilibration (static) period of 15, 30, 45 and 60 min followed by a dynamic extraction for 60 min. Results indicated that increasing equilibration (static) period enhances the extraction efficiency of uranium from HNO_3 medium. For e.g. the extraction efficiencies were found to be 42, 72 and 91 % for an equilibration period of 15, 30 and 45 min respectively. The extraction profile is shown in **Figure 7.2.** This study demonstrated that equilibration period of minimum of 45 min is mandatory; the extraction efficiency did not vary further when the equilibration period was kept beyond this period. These studies established that 45 min. of equilibration period is adequate for the conversion of uranium in to its uranium – DAAP complex.

The influence of dynamic extraction period followed by equilibration was also studied for the U-DAAP system and the extraction profile is shown in **Figure 7.3.** These studies established that about 30 min of dynamic extraction is quite sufficient for the complete transportation of U-DAAP complex into the collection vessel. Though these studies were carried out for only DAAP system, it is quite likely that other organophosphorous ligands will also exhibit similar behavior. However, further studies on the relative solubilities of metal complexes will be useful to understand their relative extraction and transportation behavior.

The effect of temperature (308-328 K) and pressure (10-30 MPa) on the extraction of uranium from 4 N HNO_3 medium was investigated using DAAP as a ligand. These studies have established that increase in pressure resulted in an increase in the extraction efficiency of uranium (**Figure 7.4)**. The extraction efficiencies were found to be 29, 54, 58 and 59 % at 10, 20, 25 and 30 MPa respectively. There was a noticeable increase in the extraction efficiency initially, when the pressure was raised from 10 to 20 MPa; however, the extraction efficiency was more or less constant beyond a pressure of 25 MPa. The density of $SCCO_2$ increases with the pressure, leading to enhanced solubility and extraction of metal complex.

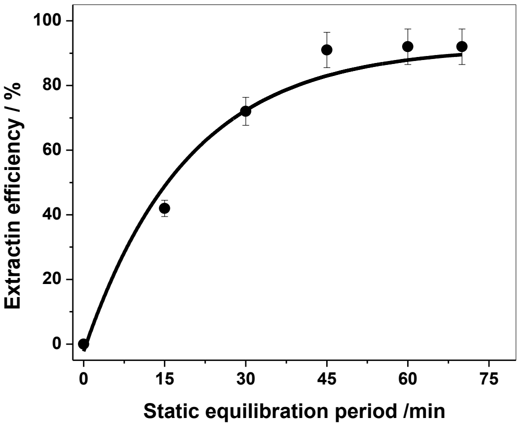

Figure 7.2 Influence of equilibration (static extraction) period on the extraction efficiency of uranium from nitric acid medium using DAAP; Experimental conditions: pressure: 30 MPa; temperature: 323 K; $SCCO_2$ flow rate: 2.5 mL/min; sample: uranyl nitrate; sample loaded: 0.01 mmol in 1 mL of 4 N HNO_3, ligand quantity: 1 mmol; extraction vessel: 10 mL; dynamic extraction: 1 hour.

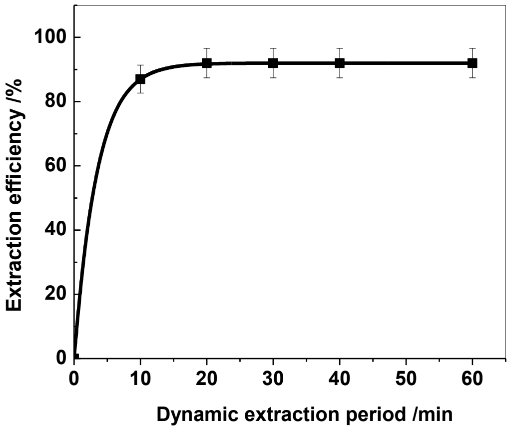

Figure 7.3 Optimization of dynamic extraction period for the extraction of uranium from nitric acid medium using DAAP; Experimental conditions: pressure: 30 MPa; temperature: 323 K; $SCCO_2$ flow rate: 2.5 mL/min; sample: uranyl nitrate; sample loaded: 0.01 mmol in 1 mL of 4 N HNO_3, ligand quantity: 1 mmol; extraction vessel: 10 mL; static extraction: 1 hour.

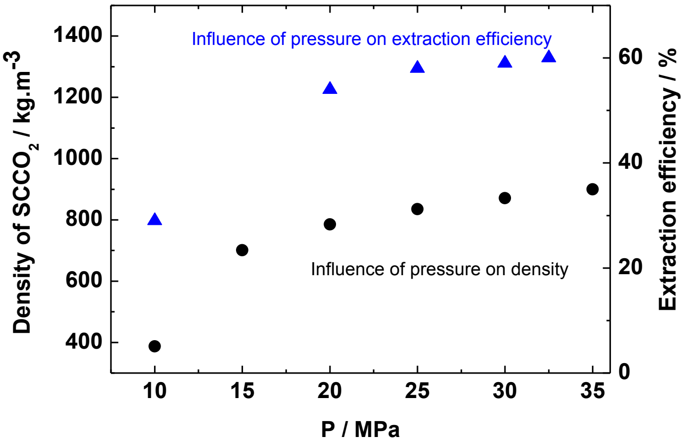

Figure 7.4 Effect of pressure on the extraction of uranium from nitric acid medium using SCCO$_2$ containing DAAP; Experimental conditions: temperature: 323 K; SCCO$_2$ flow rate: 2.5 mL/min; sample: uranyl nitrate; sample loaded: 0.01 mmol in 1 mL of 4 N HNO$_3$, ligand quantity: 0.18 mmol; extraction vessel: 10 mL; static extraction: 45 min and dynamic extraction: 30 min.

In another set of experiments, the pressure was kept constant at 25 MPa and the temperature was varied from 308 to 328 K. The extraction efficiency of uranium as a function of temperature is shown in **Figure 7.5**. The density of SCCO$_2$ will fall with raise in temperature [227] and hence the solubility of analyte is expected to decrease with raise in temperature. The experimental results indicated that there is an increase in the extraction efficiency from 308 to 323 K followed by decrease at 323 K. This could be possibly due to better mass transfer of uranium species from aqueous to SCCO$_2$ phase with raise in temperature, which offset the decrease in the density of SCCO$_2$ with raise in temperature; The better extraction at elevated temperatures also could be due to better volatility of metal solvates, especially the ones which have higher vapor pressures; however at 328 K, there was a marginal decrease in the extraction efficiency, indicating that decrease in the density of SCCO$_2$ phase has been the dominant factor. These studies have established that phosphonate based ligands can be employed for the recovery of uranium from nitric acid medium.

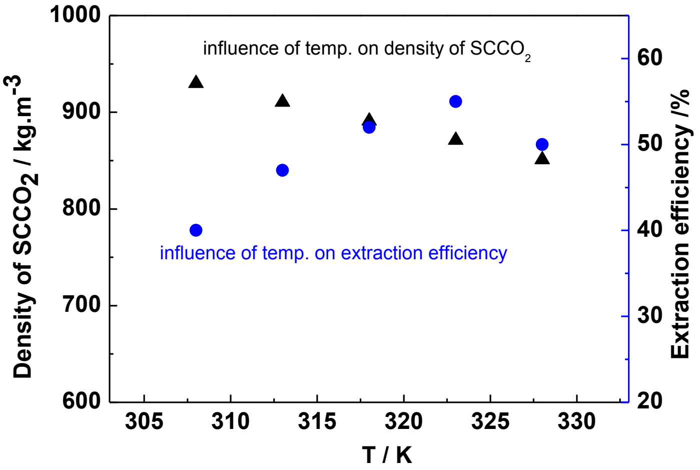

Figure 7.5 Effect of temperature on the extraction of uranium from nitric acid medium using SCCO$_2$ containing DAAP; Experimental conditions: pressure: 25 MPa; SCCO$_2$ flow rate: 2.5 mL/min; sample: uranyl nitrate; sample loaded: 0.01 mmol in 1 mL of 4 N HNO$_3$, ligand quantity: 0.18 mmol; extraction vessel: 10 mL; static extraction: 45 min and dynamic extraction: 30 min.

(b) Recovery of uranium using SCCO$_2$ containing H-phosphonates:

The recovery of uranium from nitric acid medium was also investigated using another phosphonate based ligands, namely, H-Phosphonates. The ligand DOHP was employed for this purpose and the results are shown in **Figure 7.6.** At 4N acidity, the extraction efficiency for uranium was found to be 29 % and the extraction efficiency was found to increase with decreasing acidity i.e. maximum extraction efficiency was observed at lower acidities (0.1 to 1 N). H-phosphonates exists primarily in tautomeric form, in which the phosphorus atom is trivalent and exists in equilibrium with its tetra coordinate penta-valent form [228]. The extraction behavior indicates possibility of two mechanisms in operation; i.e. at lower acidity, extraction of uranium is mainly through cation exchange, typical of acidic extractants and at higher acidities, extraction is mainly through solvation mechanism, which is typical of neutral extractant. Hence it can be concluded that H-phosphonate behaves like bi-functional extractants [228]. Its extraction behavior is also compared with a well-known acidic extractant, HDEHP and the results are shown in **Figure 7.6.** The difference in these two extractants is the arrangement of alkyl chain around the P=O group, both systems have eight carbon alkyl chain but the HDEHP system has branching at second carbon; thus the inductive effect from branched ethyl group adds to basicity of P=O group, thereby increasing the efficiency of extraction of uranium by HDEHP.

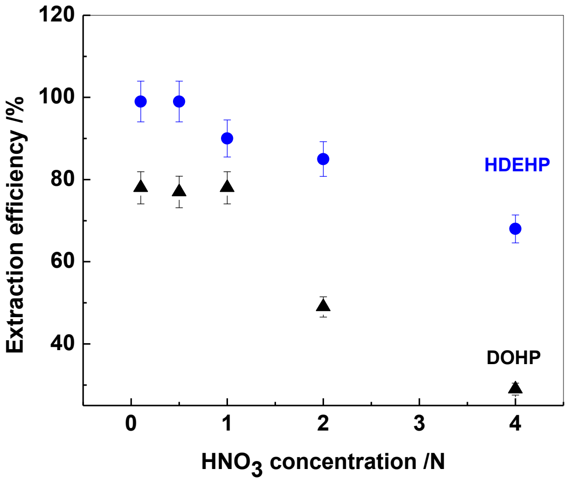

Figure 7.6 Effect of acidity on the extraction of uranium from nitric acid medium with HDEHP and DOHP; Experimental conditions: pressure: 25 MPa; temperature: 323 K; $SCCO_2$ flow rate: 2.5 mL/min; sample: uranyl nitrate; sample loaded: 0.01 mmol in 1 mL of HNO_3, ligand quantity: 0.18 mmol; extraction vessel: 10 mL; static extraction: 1 hour and dynamic extraction: 1 hour.

7.1.3 SFE of uranium and thorium from a mixture

Selective recovery of uranium from thorium matrix (e.g. irradiated ThO_2 fuel) is an important step in the nuclear research programme. In this context, selective extraction of uranium from thorium has been examined using $SCCO_2$ containing (a) trialkyl phosphates, (b) dialkylalkyl phosphonates and (c) trialkylphosphine oxides. These ligands are taken-up as these are traditionally used in solvent extraction experiments.

Recovery from nitric acid medium: The results on the relative extraction of uranium and thorium from 4N HNO_3 medium are represented in **Table 7.2**. Among the ligand employed in the present study, TsBP offers better separation factor and the trend is similar to the results observed with solvent extraction studies [155, 229]. The better separation factor observed with TsBP is due to the branching of substituents in TsBP that cause tri-solvated thorium to be less stable and hence aids in the preferential extraction of uranium over thorium. It is interesting to compare the distribution coefficients of uranium and thorium obtained with TBP and TsBP in solvent extraction conditions [155]. The D value of uranium (tracer) for 1.1M solutions of TBP and TsBP from 3 M nitric acid at 303 K is 24.5 and 37.6 respectively. The D values for thorium under identical conditions with TBP and TsBP are 2.9 and 0.45. The separation factors for uranium-thorium separation with TBP and TsBP are 8.4 and 83.5 respectively. TBP offers lower separation factor than TsBP - because of the branching of substituents in TsBP, which cause tri-solvated thorium to be less stable and hence aids in the preferential extraction of uranium over thorium. Use of phosphonate based molecules (stronger complexing agents than phosphates), resulted in relatively higher extraction of both uranium and thorium under similar experimental conditions. The extraction efficiency of uranium was generally found to be more than that of thorium. Use of stronger extractant e.g. TOPO resulted in the co-extraction of uranium and thorium and the extraction efficiencies were found to be 91 and 87 % for uranium and thorium respectively (**Figure 7.7**).

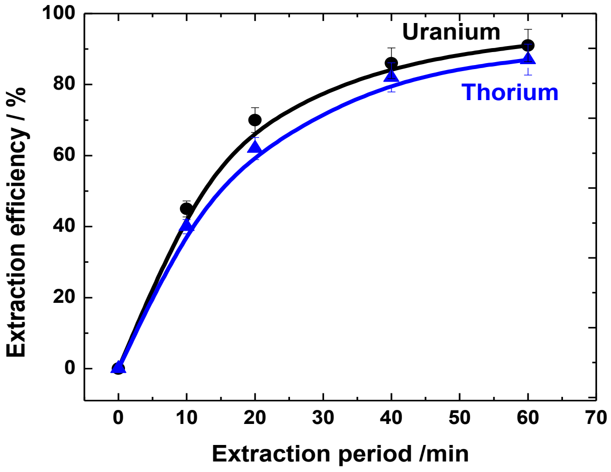

Figure 7.7 SFE of uranium and thorium from nitric acid medium using SCCO$_2$ containing TOPO; Experimental conditions are shown in Table 7.2

Table 7.2 Extraction efficiency of uranyl and thorium nitrates from 4 N nitric acid medium using organophosphorous compounds

S. No.,	Ligand	Extraction efficiency* (%)	
		U	Th
1	Tributyl phosphate (TBP)	74	19
2	Tri-*sec*-butyl phosphate (TsBP)	84	7
3	Tri-*iso*-amyl phosphate (TiAP)	78	38
4	Dibutylbutyl phosphonate (DBBP)	88	45
5	Diamylamyl phosphonate (DAAP)	87	28
6	Trioctylphosphine oxide (TOPO)	91	87

Experimental conditions: temperature: 323 K, pressure: 25 MPa; $SCCO_2$ flow rate: 2.5 mL/min; Sample: uranyl nitrate + thorium nitrate in 4 N HNO_3 medium; sample loaded: 0.01 mmol each; ligand loaded: 0.94 mmol; volume of extraction vessel: 10 mL; static extraction: 1 hour and dynamic extraction: 1 hour; *Extraction efficiencies average of three independent experiments with a relative standard deviation of 5 %

Recovery from solid matrix: Selective extraction of uranium from uranium-thorium nitrate mixture was also examined using $SCCO_2$ containing TBP and TsBP with different co-solvents. In the presence of TBP with methanol as co-solvent uranium and thorium are extracted together and no separation was observed **(Figure 7.8).** Uranyl nitrate forms complex with TBP (as ($UO_2(NO_3)_2.2TBP$)) which acts as Lewis base and the resultant adduct extraction is facilitated by methanol into the CO_2 medium. Similarly, thorium forms $Th(NO_3)_4.3TBP$ which is soluble in the $SCCO_2$ + methanol stream. Both uranium and thorium species were extracted together under these experimental conditions. Use of $SCCO_2$ containing TBP in *n*-hexane/dichloromethane as co-solvent medium resulted in incomplete extraction – however, fractionation of U from Th was observed. The use of co-solvents, dichloromethane as well as *n*-hexane resulted in about 80 % of extraction. Thus the polar co-solvent, methanol provides faster extraction without fractionation whereas non-polar solvents provided marginal fractionation of metal nitrates though the extraction kinetics was slower (**Figure 7.8**). These results indicated that co-solvents play an important role in the extraction / fractionation of metal nitrates.

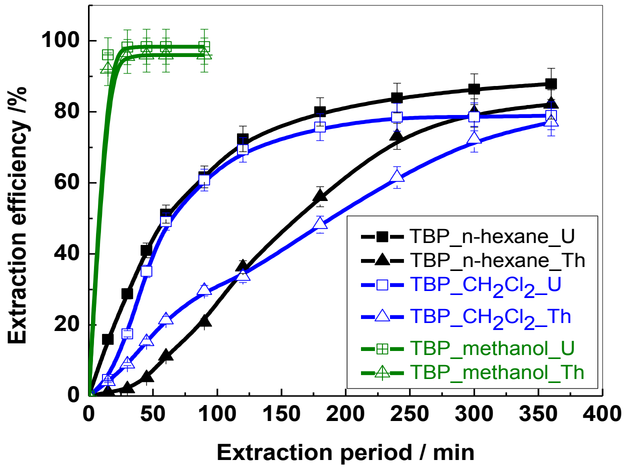

Figure 7.8 SFE of uranyl and thorium nitrates (solid form) using SCCO$_2$ modified with TBP in various co-solvents. Experimental conditions: temperature: 323 K, pressure: 25 MPa; SCCO$_2$ flow rate: 2.5 mL/min; co-solvent flow rate: 0.1 mL/min; ligand concentration: 3 wt% of ligand in a co-solvent; Sample: uranyl nitrate salt + thorium nitrate salt; sample loaded: 100 mg of each salt; volume of extraction vessel: 1 mL; dynamic extraction: 1.5 hours (methanol as co-solvent), 6 hours (*n*-hexane and dichloro methane as co-solvents).

7.1.4 Influence of dielectric constant of co-solvent on the recovery of uranium in SFE experiments

A fundamental study was taken-up to study the influence of co-solvent's dielectric constant on the recovery of uranium from its salt using CMPO as a ligand. Co-solvents having a wide range of dielectric constants ranging from 2 to 33 were employed. The results (**Table 7.3**) indicated that the use of polar co-solvents such as methanol and *iso*-propanol in SCCO$_2$ medium resulted in the complete extraction of uranyl nitrate; the extraction efficiency was drastically reduced when non-polar co-solvents e.g. *n*-hexane were employed. The presence of polar nitrate moieties and six water molecules in the uranyl nitrate hexahydrate demands polar medium (e.g. methanol, *iso*-propanol) for solubilizing the metal nitrates into the SCCO$_2$ medium. The formation of metal solvate depends on the dielectric constant of the medium**.** The polarity of the solvent increases with the dielectric constant of the medium, leading to charge stabilization and solvation in modified $SCCO_2$ medium. Use of $SCCO_2$ containing CMPO in the presence of co-solvent e.g. *n*-hexane has resulted in poor extraction of metal nitrate (< 1%) and extraction of uranium was better with increase in dielectric constant of the medium. Thus extraction efficiency of uranium increases when dielectric constant of the medium.

SFE of externally prepared $UO_2(NO_3)_2$.2CMPO complex was also carried out using $SCCO_2$ with and without co-solvents. These experiments were carried out in order to understand in-situ SFE complexation against pre-prepared metal complexation behavior in supercritical medium. The CMPO metal complex was spiked on to a cellulose matrix and subjected to SFE using neat $SCCO_2$ as well as $SCCO_2$ modified with *n*-hexane / methanol as co-solvents. About 80-90 % extraction was observed with neat $SCCO_2$ as well as $SCCO_2$ with *n*-hexane as the co-solvent whereas complete extraction was observed in the presence of $SCCO_2$ with methanol as a co-solvent (**Table 7.4**). These studies have established that once the complex (metal solvate) is formed, presence of *n*-hexane in the supercritical medium did not prevent extraction of uranium-CMPO solvate.

Table 7.3 Influence of co-solvent on the SFE of uranium using CMPO

S. No.,	**Co-solvent**	**Dielectric constant of co-solvent**	**Uranium extraction* (%)**
1	CH_3OH	32.7	> 99
2	$(CH_3)_2CHCH_2OH$	18.0	> 99
3	$CH_3OH+CH_2Cl_2$	20.8	> 99
4	$(CH_3)_2CHOH$	17.5	> 99
5	CH_2Cl_2	8.93	7
6	$CHCl_3$	4.81	5
7	C_6H_{14}	2.02	< 1

Experimental conditions: temperature: 323 K, pressure: 25 MPa; $SCCO_2$ flow rate: 2.5 mL/min; co-solvent flow rate: 0.1 mL/min; ligand: 3 wt% of CMPO in a co-solvent; Sample: uranyl nitrate salt; sample loaded: 100 mg; volume of extraction vessel: 1 mL; dynamic extraction: 1 hour.

*Extraction efficiencies are average of three independent experiments with a relative standard deviation of less than 5 %

Table 7.4 Extraction efficiency of uranium-CMPO complex in $SCCO_2$ medium

S. No.,	**SFE conditions**	**Uranium extraction* (%)**
1	neat $SCCO_2$	80
2	$SCCO_2$ + *n*-hexane	85
3	$SCCO_2$ + methanol	98

Experimental conditions: temperature: 323 K, pressure: 25 MPa; $SCCO_2$ flow rate: 2.5 mL/min; co-solvent flow rate: 0.1 mL/min; Sample: $UO_2(NO_3)_2.2CMPO$ solvate; sample loaded: 100 mg; volume of extraction vessel: 1 mL; dynamic extraction: 1 hour.

*Extraction efficiencies are average of three independent experiments with a relative standard deviation of 5 %

7.1.5 Conclusions

$SCCO_2$ containing various organophosphorous compounds are employed to understand the ligand strength towards actinides recovery. $SCCO_2$ containing phosphonate was employed for the recovery of uranium from acid medium. $SCCO_2$ containing TsBP resulted in some fractionation of uranium over thorium. The initial studies have established phosphonates and phosphates as the potential candidate materials for recovery of actinides from aqueous medium.

Chapter 7(b)

Supercritical fluid extraction of uranium from representative fission products

SFE of uranium from representative fission products

Selective extraction of actinides from dissolver solution is an important aspect of nuclear fuel reprocessing. Dissolver solution usually contains uranium, plutonium and fission product elements. Hence preferential extraction of uranium from representative fission products (La (III), Ce (III), Pr (III), Nd (III), Cs (I), Sr (II), Ba (II), Zr (IV) and Mo (VI)) has been examined using $SCCO_2$ containing phosphonates and compared with phosphates. Phosphonate and phosphate based ligands are preferred over phosphine oxide based ligands due to easy stripping of actinides in their nitrate form from the actinide-ligand complex. Thus moderately stronger phosphonate based ligands are preferred over very strong phosphine oxide based ligands.

7.2.1. Selective extraction of uranium from representative fission products using TiAP

SFE of uranium and representative fissions products was investigated from 4 N HNO_3 medium using one of the representative phosphate, namely, TiAP as the extractant. Both static and dynamic modes of extraction were carried out. Studies established that a minimum of 45 minutes of static extraction followed by 1 hour of dynamic extraction were required for the complete extraction of uranium from nitric acid medium. The results of extraction of uranium from selected fission products from nitric acid media using TiAP at 323 K and 20 MPa are summarized in **Table 7.5.**

Table 7.5 SFE of uranium from simulated fission products using TiAP

Metal ion		Initial composition (mg)	Extraction efficiency[#] (%)
Uranium	UO_2^{2+}	200	95
Representative fission products	La^{3+}	0.060	<3
	Ce^{4+}	0.100	<3
	Pr^{3+}	0.065	<3
	Nd^{3+}	0.205	<3
	Cs^{+}	0.210	<2
	Ba^{2+}	0.065	<2
	Sr^{2+}	0.120	5
	Zr^{4+}	0.305	8
	Mo^{6+}	0.240	6

Experimental conditions: temperature: 323 K, pressure: 20 MPa; $SCCO_2$ flow rate: 2.5 mL/min; Sample: uranyl nitrate + fission product elements in 4 N HNO_3 medium; sample loaded: as per table; ligand loaded: 500 mg; volume of extraction vessel: 10 mL; static extraction: 1 hour and dynamic extraction: 1 hour

Extraction efficiency is an average of three independent experiments with a relative standard deviation of less than 5%.

The extraction efficiency of uranium was found to be about 95±5%. Metal ions such as lanthanides, Ba (II) and Cs (I) were not extracted under the experimental conditions. The extraction efficiencies for Sr (II), Zr (IV) and Mo (VI) were found to be 5, 8 and 6% respectively. Similar extraction behavior was reported for lanthanides, Cs (I), Sr (II), Ba (II), Zr (IV) and Mo (VI) by employing TBP as a complexing agent [135]. The present study indicated the selective extraction of uranium in the presence of fission products from the nitric acid medium can be achieved using TiAP. The selectivity of uranium from representative fission products is mainly due to their relative differences in distribution ratio values (D_U). The solvent extraction studies reported in the literature indicate that TiAP has higher distribution ratio for uranium over fission products [230, 231]. At 4 N HNO_3 medium, for tracer solution, distribution ratio for uranium is 35.2;

under similar experimental conditions, the distribution ratios for La (III), Ce(III), Nd(III) and Zr (IV) are 0.017, 0.021, 0.033 and 0.44 respectively [231].

The influence of temperature on the extraction efficiency of uranium was investigated at two temperatures 313 and 323 K with pressure varying from 10-25 MPa. The extraction profile is shown in the **Figure 7.9.** The variation of density of $SCCO_2$ under the same experimental conditions is also depicted by the **Figure 7.9**. With increasing temperature from 313 to 323 K, a decrease in the TiAP solubility was observed. The decrease in the solubility is more pronounced at low pressures up to 15 MPa and the same is reflected in the extraction efficiency. These studies indicate that the decrease in the solubility with temperature is responsible for decrease in extraction efficiency of uranium at 323 over 313 K. Beyond 15 MPa, the extraction efficiency was found to be more or less similar at 313 and 323 K.

The effect of pressure on the extraction efficiency was studied at 323 K by varying the pressure from 10-25 MPa (**Figure 7.9**). These results indicated that the extraction efficiency of uranium increases with pressure. An initial steep rise in the extraction efficiency was observed with increasing pressure from 10 to 15 MPa beyond which a tapering the values is noted. The variation in the solubility of TiAP with pressure is also presented in **Figure 7.10**. The extraction efficiency and solubility follows a similar trend with the pressure. The increase in the extraction efficiency of uranium with pressure was also established using various complexing agents [151, 232].

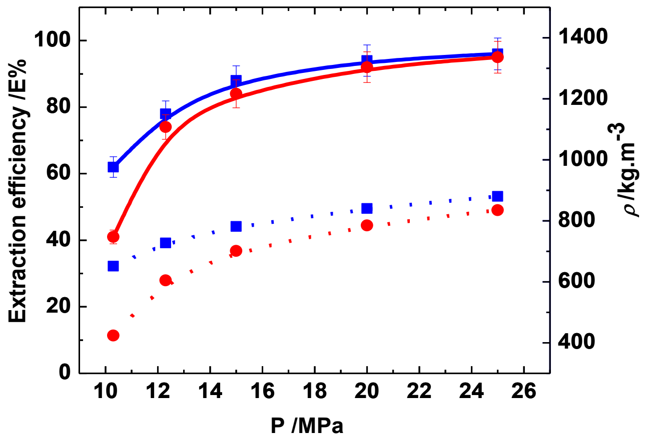

Figure 7.9 Effect of pressure and temperature on the extraction efficiency of uranium from nitric acid medium into SCCO$_2$+TiAP phase with temperature ■, 313 K; ●, 323 K. Solid line represents the variation of extraction efficiency with pressure; dotted line represents the variation of density of SCCO$_2$ with pressure. Experimental conditions: SCCO$_2$ flow rate: 2.5 mL/min; Sample: uranyl nitrate 4 N HNO$_3$ medium; sample loaded: 0.01 mmol each; ligand loaded: 1 mmol; volume of extraction vessel: 10 mL; static extraction: 1 hour and dynamic extraction: 1 hour

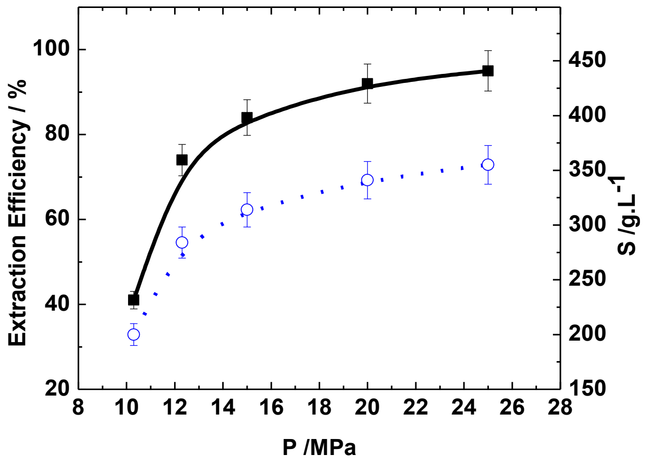

Figure 7.10 Effect of pressure on the extraction efficiency of uranium from nitric acid medium with TiAP; solid line represents the variation of extraction efficiency with pressure; dotted line represents the variation of solubility of TiAP in SCCO$_2$ with pressure. Experimental conditions: temperature: 323 K; SCCO$_2$ flow rate: 2.5 mL/min; Sample: uranyl nitrate 4 N HNO$_3$ medium; sample loaded: 0.01 mmol each; ligand loaded: 1 mmol; volume of extraction vessel: 10 mL; static extraction: 1 hour and dynamic extraction: 1 hour

The influence of extraction period on the SFE of uranium from 4 N HNO_3 medium using TiAP was also studied at 25 MPa and 323 K. One hour static equilibration followed by dynamic extraction was carried out and the extract was collected after every 10 minutes up to 1 hour. The extraction profile is represented by **Figure 7.11** [136]. In the first 20 min extraction period, about 75 % of uranium was extracted. Total extraction of uranium was found to be ~ 95%. The initial extraction rate was faster and subsequently slowed down. In the initial phase of the extraction, a concentration gradient is set-up in the aqueous phase, which decreases with the progress of extraction. These observations indicated that the SFE of uranium from nitric acid medium is mainly diffusion controlled.

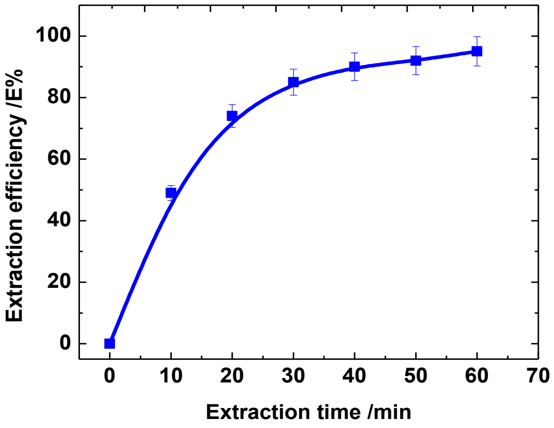

Figure 7.11 Influence of dynamic extraction period on the extraction efficiency of uranium from 4 N HNO_3 medium using $SCCO_2$ containing TiAP; Experimental conditions: pressure: 20 MPa; temperature: 323 K, $SCCO_2$ flow rate: 2.5 mL/min; sample loaded: 0.01 mmol of uranium; ligand loaded: 1 mmol; volume of extraction vessel: 10 mL; static extraction: 1 hour and dynamic extraction: 1 hour

The influence of acidity on the extraction of uranium from representative fission product elements was investigated at 323 K and 20 MPa using TiAP as the extractant. Both static and dynamic modes of extractions were carried out by varying the acidity from 0.1 to 8 N HNO_3. The extraction efficiency of uranium was found to increase with increasing acidity and after passing through a maximum (6 N HNO_3), it starts decreasing

(Figure 7.12). The effect of acidity on the SFE of uranium from nitric acid medium is similar to the trend observed in solvent extraction studies [207].

From Eq. (3.5), increase in the $[NO_3]^-$ in the aqueous phase leads to an increase in the formation of $UO_2(NO_3)_2.2TiAP$ in the supercritical fluid phase. According to the Eq. (3.6), increase in the concentration of $UO_2(NO_3)_2.2TiAP$ in supercritical fluid phase results in higher distribution ratio, leading to higher extraction efficiency. The decrease in the extraction efficiency beyond 6 N HNO_3 can be attributed to the co-extraction of HNO_3 by TiAP to form $TiAP.(HNO_3)$ in supercritical fluid phase. As the acidity increases beyond 6 N HNO_3, there is a competition between HNO_3 and uranium for TiAP to form the corresponding complex in the supercritical fluid phase, leading to decrease in uranium extraction efficiency at > 6N HNO_3.

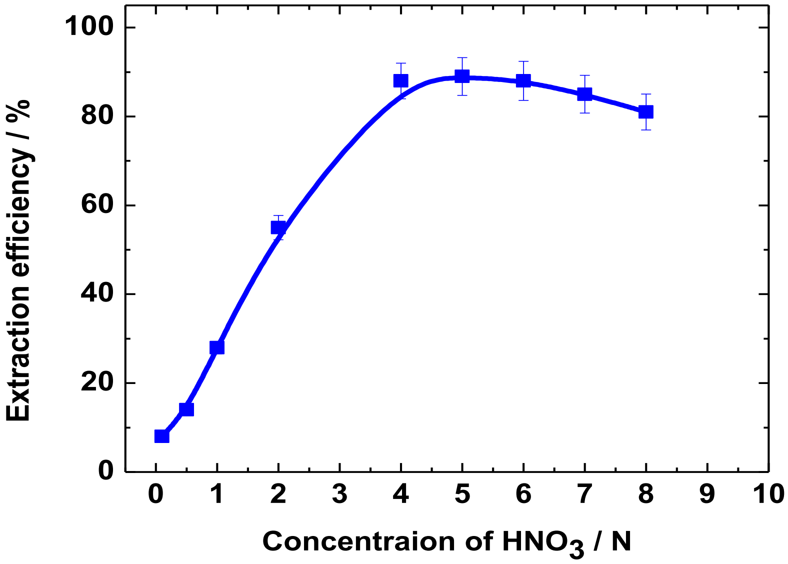

Figure 7.12 Influence of acidity on extraction efficiency of uranium from nitric acid medium using $SCCO_2$ containing TiAP. Experimental conditions: pressure: 20 MPa; temperature: 323 K, $SCCO_2$ flow rate: 2.5 mL/min; Sample: uranyl nitrate; HNO_3 medium; sample loaded: 0.01 mmol of uranium; ligand loaded: 1 mmol; volume of extraction vessel: 10 mL; static extraction: 1 hour and dynamic extraction: 1 hour

7.2.2 Selective extraction of uranium from representative fission products using DAAP

SFE technique was also employed for the recovery of uranium from some of the fission products from nitric acid using DAAP as a ligand. In our initial studies, both DAAP and DBBP were examined for the extraction of uranyl nitrate only from nitric acid medium. The extraction efficiency of uranium was found to be nearly same (**Table 7.3**). Hence, one of the phosphonate, DAAP was employed for the selective extraction of uranyl nitrate in the presence of fission products. Both dynamic and static extractions were carried out. The effect of temperature, pressure and extraction period on the extraction efficiency of uranium was established and the parameters are optimized. SFE of uranium was carried out from aqueous solution to determine the effect of HNO_3 concentration on extraction efficiency of uranium. The concentration of HNO_3 was varied from 0.1 to 6 M at a temperature of 323 K and pressure of 20 MPa. The extraction efficiency of uranium was found to increase with the acidity reaching a maximum at 4 M HNO_3. Therefore, all the experiments were carried out in 4 N HNO_3 medium.

Selective extraction of uranium from fission product elements was observed with DAAP in 4 M HNO_3. The extraction efficiency of uranium was found to be 95% at 323 K and 20 MPa. The extraction efficiencies of uranium and representative fission product elements are reported in **Table 7.6.** Lanthanides, Cs (I) and Sr (II) were not extracted under these experimental conditions. The extraction efficiencies for Zr (IV) and Mo (VI) were found to be about 7-8 %. The separation of uranium from fission products is mainly due to the relative distribution of these metal ions between aqueous and supercritical fluid phase. The distribution coefficients of uranium, lanthanides and other metal ions were measured under solvent extraction conditions in our laboratory [164]. The distribution ratio of uranium (tracer) for 1.1 M solution of DAAP in *n*-dodecane from 4 M nitric acid at 303 K is 66. The distribution ratio for Ba(II), Sr(II), Mo(VI), Ce(IV) and La(III) are found to be <0.1 under these conditions. These studies have established that DAAP in $SCCO_2$ medium can be employed for the selective extraction and recovery of uranium from fission product elements from nitric acid medium.

Table 7.6 Extraction of uranium from representative fission products using $SCCO_2$ containing DAAP at temperature, T and pressure, P[*]

Metal ion	Initial composition (mg)	Extraction efficiency[#] (%)
U (VI)	51.0	95
La (III)	0.015	< 2
Ce (IV)	0.025	< 2
Pr (III)	0.015	< 2
Nd (III)	0.050	< 2
Cs (I)	0.051	< 2
Ba (II)	0.025	< 2
Sr (II)	0.030	< 2
Zr (IV)	0.075	8
Mo (VI)	0.060	7

Experimental conditions: temperature: 323 K, pressure: 20 MPa; $SCCO_2$ flow rate: 2.5 mL/min; Sample: uranyl nitrate + fission product elements in 4 N HNO_3 medium; sample loaded: as per table; ligand loaded: 200 mg; volume of extraction vessel: 10 mL; static extraction: 1 hour and dynamic extraction: 1 hour

[*] Standard uncertainties in u are u(T) = 0.1 K, u(P) = 0.1 MPa

[#] Extraction efficiency is the average of three independent experiments with a relative standard deviation of less than 5%.

7.2.3 Extraction mechanism

The mechanism of extraction of uranium and fission products from aqueous solution is similar to that of solvent extraction. It has been reported that uranium from aqueous medium is extracted as $UO_2(NO_3)_2.2TBP$ into the supercritical phase, which is similar to that observed during conventional solvent extraction studies. The composition of lanthanide and TBP adducts were reported by Laintz *et al.* [126]. Lighter lanthanides are extracted as $Ln(NO_3)_3.3TBP$ and heavier lanthanides are extracted as $Ln(NO_3)_3.2TBP$.

Solvent extraction studies on uranium with TiAP system have established formation of $UO_2(NO_3)_2.2TiAP$ complex, similar to that of uranium-TBP system [230]. Hence, it is assumed that similar complex, $UO_2(NO_3)_2.2TiAP$ is formed during the complexation in supercritical fluid phase. Distribution equations similar to that of TBP could be derived for SFE of uranium using TiAP as a complexing agent. Many equilibrium processes are involved in the extraction and are depicted in **Figure 7.13**.

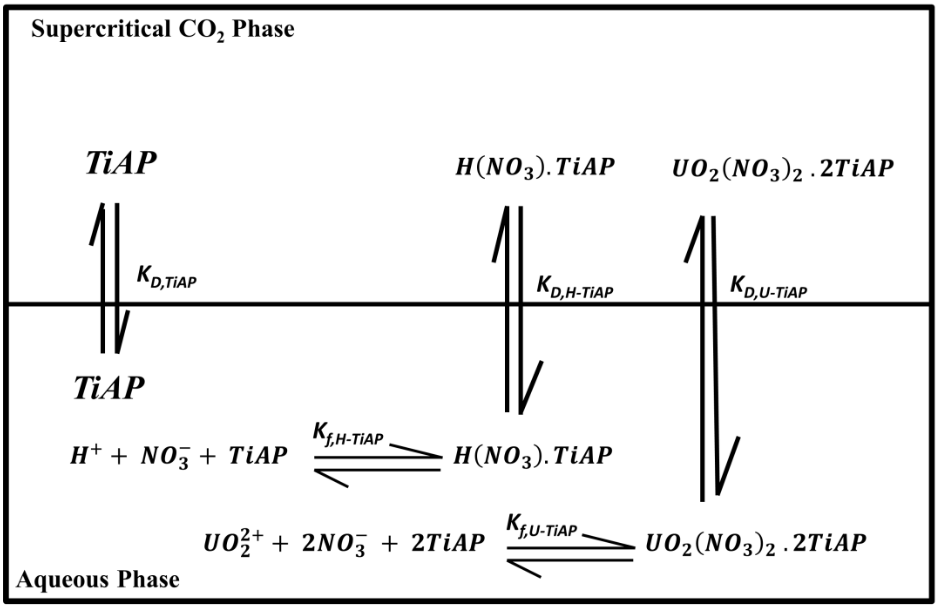

Figure 7.13 Extraction scheme of uranium from nitric acid medium into SCCO$_2$ containing TiAP medium

The possible reaction scheme is as follows:

$$H^+ + NO_3^- + TiAP \Leftrightarrow H(NO_3)TiAP \tag{7.1}$$

$$UO_2^{2+} + 2NO_3^- + 2TiAP \Leftrightarrow UO_2(NO_3)_2 2TiAP \tag{7.2}$$

The extraction mechanism involves (1) distribution of TiAP between aqueous (nitric acid medium) and SCF phase, (2) formation of $UO_2(NO_3)_2.2TiAP$ in the aqueous phase and (3) distribution of $UO_2(NO_3)_2.2TiAP$ complex between nitric acid medium and SCF phase. The overall reaction could be expressed as

$$(UO_2^{2+})_{aq} + 2(NO_3^-)_{aq} + 2(TiAP)_{scf} \overset{K_{ex}}{\Leftrightarrow} (UO_2(NO_3)_2 2TiAP)_{scf} \tag{7.3}$$

where, K_{ex} represents the extraction constant and is given by

$$K_{ex} = \frac{\left[UO_2(NO_3)_2 2TiAP\right]_{scf}}{\left[UO_2^{2+}\right]_{aq} \left[NO_3^-\right]_{aq}^2 \left[TiAP\right]_{scf}^2} \tag{7.4}$$

The distribution ratio of uranium (D_U) between aqueous and supercritical fluid phase is represented as

$$D_U = \frac{\left[UO_2(NO_3)_2 2TiAP\right]_{scf}}{\left[UO_2^{2+}\right]_{aq}} \tag{7.5}$$

From Eq. (7.4) and Eq. (7.5)

$$D_U = K_{ex} \left[NO_3^-\right]_{aq}^2 \left[TiAP\right]_{scf}^2 \tag{7.6}$$

$$\log D_U = \log K_{ex} + 2\log\left[NO_3^-\right]_{aq} + 2\log\left[TiAP\right]_{scf} \tag{7.7}$$

The formation constant of $UO_2(NO_3)_2.2TiAP$ in aqueous phase, $K_{f,U\text{-}TiAP}$ is defined as

$$K_{f,U-TiAP} = \frac{\left[UO_2(NO_3)_2 2TiAP\right]_{aq}}{\left[UO_2^{2+}\right]_{aq} \left[NO_3^-\right]_{aq}^2 \left[TiAP\right]_{aq}^2} \tag{7.8}$$

The phase distribution constants of TiAP, $UO_2(NO_3)_2.2TiAP$ and $H(NO_3)TiAP$ are $K_{D,TiAP,}$, $K_{D,U\text{-}TiAP}$ and $K_{D,HNO3\text{-}TiAP}$ respectively, given by

$$K_{D,TiAP} = \frac{\left[TiAP\right]_{scf}}{\left[TiAP\right]_{aq}} \tag{7.9}$$

$$K_{D,U-TiAP} = \frac{\left[UO_2(NO_3)_2 2TiAP\right]_{scf}}{\left[UO_2(NO_3)_2 2TiAP\right]_{aq}} \tag{7.10}$$

$$K_{D,HNO_3-TiAP} = \frac{\left[(H)NO_3TiAP\right]_{scf}}{\left[(H)NO_3TiAP\right]_{aq}} \tag{7.11}$$

Eq. (7.4) can be rewritten as

$$K_{ex} = \frac{\left[UO_2(NO_3)_2 2TiAP\right]_{scf} \left[UO_2(NO_3)_2 2TiAP\right]_{aq} \left[TiAP\right]_{aq}^2}{\left[UO_2(NO_3)_2 2TiAP\right]_{aq} \left[TiAP\right]_{scf}^2 \left[TiAP\right]_{aq}^2 \left[UO_2^{2+}\right]_{aq} \left[NO_3^-\right]_{aq}^2} \tag{7.12}$$

Using all the equations from Eq. (7.8) to Eq. (7.12), a simplified expression for K_{ex} is obtained,

$$K_{ex} = \frac{K_{D,U-TiAP}\ K_{f,U-TiAP}}{K_{D,TiAP}^2} \tag{7.13}$$

$$\log K_{ex} = \log K_{D,U-TiAP} + \log K_{f,U-TiAP} - 2\log K_{D,TiAP} \tag{7.14}$$

From Eq. (7.7) and Eq. (7.14)

$$\begin{aligned}\log D_U = \log K_{D,U-TiAP} + \log K_{f,U-TiAP} - 2\log K_{D,TiAP} + 2\log\left[NO_3^-\right]_{aq} \\ + 2\log\left[TiAP\right]_{scf}\end{aligned} \tag{7.15}$$

From Eq. (7.15), the extraction efficiency depends on phase distribution constant of TiAP and U-TiAP, formation constant of U-TiAP, acidity of aqueous phase and concentration of TiAP in the SCF phase. Studies have established an increase in the extraction efficiency of uranium with increasing aqueous phase acidity as well as with ligand concentration [154].

Solvent extraction studies on uranium with DAAP have established the formation of $UO_2(NO_3)_2$.2DAAP complex, similar to that of uranium-TiAP system. Therefore, the above mechanism is also applicable for DAAP system.

Chapter 7(c)

Supercritical fluid extraction of uranium and plutonium from pyro chemical salt matrices using trioctylmethylammonium chloride

---

7.3.1 Introduction

Pyrochemical reprocessing is as an alternate to the well-established PUREX process for reprocessing the spent metal fuel. This process involves use of molten salts (LiCl - KCl or NaCl-CsCl) for the separation of actinides from fission products. The electrolyte salt, after processing of few batches, will be loaded with alkali and alkaline earth metals, lanthanide fission products and actinides that are being processed. The electrolyte salt has to be cleansed from residual fission products and actinides, before it can be reused or disposed. Disposal of such molten salts is of great concern and different techniques have been explored in the recent past for the decontamination of molten salts, which can minimize the radioactive waste [174-176]. These techniques generally results in the generation of secondary radioactive waste. In the present study, for the first time, SFE based method has been explored for the recovery of U and Pu from pyrochemical salt matrix using $SCCO_2$ containing appropriate ligand.

Establishing a SFE process for complete recovery of U and Pu from salt matrices, UCl_3-LiCl-KCl, $PuCl_3$-LiCl-KCl and UO_2Cl_2-NaCl-CsCl involves use of basic extractants (e.g. TOMAC) to form ion pair complex and selectively extract the actinides from chloride matrix. Hence $SCCO_2$ containing TOMAC was investigated to achieve the objectives.

7.3.2 Experimental

7.3.2.1 SFE of uranium from pyrochemical salt matrix

The schematic of the SFE apparatus used in the present study is described in **Chapter 2**. SFE of uranium from pyrochemical salt matrix (UCl_3-LiCl-KCl and UO_2Cl_2-NaCl-CsCl) was carried out using modified $SCCO_2$. $SCCO_2$ containing TBP, Acetylacetone (AcAc) and *N*,*N*-di-2-ethylhexylisobutyramide (D2EHIBA) were employed for the recovery of residual uranium from pyrochemical salt matrix using methanol / *n*-propanol as the co-solvents. About 0.1-1 g of UCl_3-LiCl-KCl / UO_2Cl_2-NaCl-CsCl granules or powder and an appropriate amount of neat ligand were loaded on to a 1mL / 10 mL high pressure extraction vessel. The extracts after SFE were collected and estimated for uranium concentration.

7.3.2.2 SFE of uranium from neat uranyl chloride

SFE of neat uranyl chloride (UO_2Cl_2, purity > 98 %) was initially carried out using $SCCO_2$ modified with methanol, TBP and D2EHIBA. About 100 mg of neat UO_2Cl_2 crystals were loaded onto a 1 mL high pressure extraction vessel and dynamic SFE was carried out using $SCCO_2$ containing 0.3 wt% of ligand in methanol. Similarly, 100 mg of UO_2Cl_2 was spiked on to a cellulose matrix and subjected to dynamic SFE using $SCCO_2$ containing different ligands. SFE was carried out under typical experimental conditions viz. Temperature: 323 K, Pressure: 20 MPa with a SC-CO_2 flow rate: 2.5 mL/min and methanol flow rate: 0.1 mL/min.

7.3.2.3 SFE of plutonium from pyrochemical salt matrices

Extraction of plutonium from pyrochemical matrices was carried out using a SFE system, kept in a glove box; SFE system was set-up in a glove box for handling radioactive materials [194]. The glove box facility was developed incorporating modifications required for handling high pressures and isolated electrical connections. Carbon dioxide pump and modifier/ligand pump were placed outside the glove box. The back pressure regulator, thermostat and collection system were placed inside the glove box.

SFE of plutonium from pyrochemical salt matrix ($PuCl_3$-LiCl-KCl) matrix was carried out using $SCCO_2$ containing 3wt% TOMAC in *n*-propanol medium. About 100 mg of salt granules/powder was loaded onto a 1 mL high pressure extraction vessel. Both dynamic and static extractions were carried out using TOMAC. The extract was collected in to a 20 mL of 1:1 *n*-propanol and 0.1N HNO_3 medium. The plutonium content of the extract was assayed by LSC technique.

7.3.3. Results and Discussions

7.3.3.1 Recovery of uranium from pyrochemical salt matrices

$SCCO_2$ containing TBP, AcAc and D2EHIBA were employed for the extraction of uranium from the salt matrix, UO_2Cl_2-NaCl-CsCl. These experiments resulted in an incomplete extraction of uranium from salt matrix and the results are presented in **Table 7.7**. Use of $SCCO_2$ containing methanol / *n*-propanol (without a ligand) resulted in an extraction efficiency of 15 and 20% respectively. The extraction profile for the recovery of uranium form salt matrix using $SCCO_2$ modified with methanol is depicted in **Figure 7.14**. The extraction efficiency with TBP and acid equilibrated TBP was found to be 15 and 20% respectively. The use of $SCCO_2$ containing D2EHIBA resulted in an extraction efficiency of about 25%. Among the ligands employed in the present study, the extraction was found to better with AcAc, with an extraction efficiency of 40%. These results provoked us to investigate the influence of various parameters on the extraction of uranium in the presence of a chloride salt matrix.

Table 7.7 SFE of uranium from pyrochemical salt matrix (UO_2Cl_2-NaCl-CsCl) using modified $SCCO_2$

S. No.,	$SCCO_2$ modified with ligand	Extraction efficiency[#] (%)
1	*n*-propanol	20
2	Methanol	15
3	3 wt% acetyl acetone in methanol	40
4	3 wt% tributyl phosphate in methanol	15
5	3 wt% 8N acid equilibrated TBP in methanol	20
6	3 wt% 8N acid equilibrated TBP – modifier free	20
7	3 wt% 8N acid equilibrated D2EHIBA in methanol	25
8	8N acid equilibrated D2EHIBA – modifier free	20

Experimental conditions: pressure: 20 MPa, temperature: 323 K; $SCCO_2$ flow rate: 2.5 mL/min, co-solvent/modifier flow rate: 0.1 mL/min; ligand: 3 wt% of ligand in co-solvent; sample loaded: 100 mg; extraction vessel: 1 mL; dynamic extraction: 2 hours.

Extraction efficiency is an average of five independent experiments with a relative standard deviation of less than 5%.

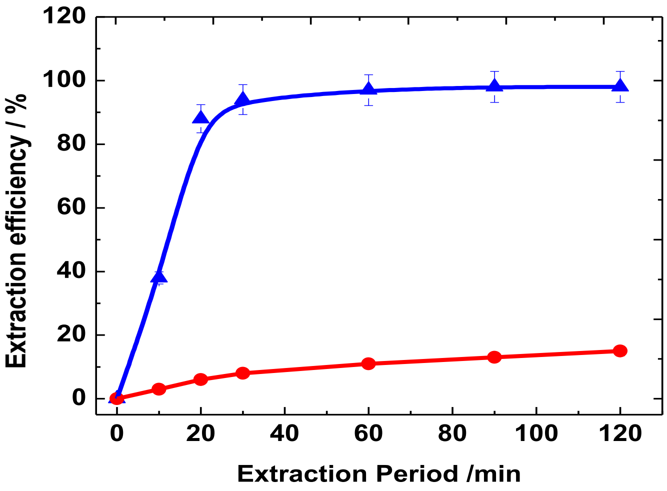

Figure 7.14 SFE of uranium from ●, neat UO_2Cl_2; ▲, pyrochemical salt matrix (UO_2Cl_2-NaCl-CsCl); using $SCCO_2$ modified with methanol; Experimental conditions: pressure: 20 MPa, temperature: 323 K; $SCCO_2$ flow rate: 2.5 mL/min, co-solvent flow rate: 0.1 mL/min; co-solvent: methanol; sample: neat UO_2Cl_2; sample loaded: 100 mg; extraction vessel: 1 mL; dynamic extraction: 2 hours.

Table 7.8 SFE of neat uranyl chloride (UO_2Cl_2) using modified $SCCO_2$

Sample	**Ligand/modifier**	**Extraction period (hours)**	**Extraction efficiency$^{\#}$ (%)**
UO_2Cl_2 crystals	Methanol	1	99
	3% TBP in methanol	2	95
	3% D2EHIBA in methanol	2	85
	3% D2EHIBA in *n*-hexane	4	60
	D2EHIBA modifier free method	4	80
UO_2Cl_2 in cellulose matrix	Methanol	2	80

Experimental conditions: pressure: 20 MPa, temperature: 323 K; $SCCO_2$ flow rate: 2.5 mL/min, co-solvent/modifier flow rate: 0.1 mL/min: ligand: 3 wt% of ligand in co-solvent; sample loaded: 100 mg; extraction vessel: 1 mL; dynamic extraction: 2 hours.

Extraction efficiency is an average of five independent experiments with a relative standard deviation of less than 5%.

7.3.3.2 Extraction uranium from neat UO_2Cl_2

To investigate the incomplete extraction of uranium from actual chloride salt matrix, systematic studies were tak*en*-up. In this connection, SFE of neat UO_2Cl_2 (without matrix) was initially carried out using $SCCO_2$. Results on the SFE of uranium from UO_2Cl_2 crystals and UO_2Cl_2 from cellulose matrix using $SCCO_2$ containing various ligands are presented in **Table 7.8**. $SCCO_2$ modified with methanol resulted in complete extraction of neat UO_2Cl_2 crystals. $SCCO_2$ modified with TBP and D2EHIBA resulted in an extraction efficiency of 95 and 85% respectively. $SCCO_2$ modified with D2EHIBA in the presence of *n*-hexane as co-solvent gave an extraction of 60 % for an extraction period for 4 hours. A modifier free delivery method was also employed for the delivery of ligands into the $SCCO_2$ system, which eliminate the use of co-solvent [233]. The D2EHIBA was delivered into the SFE system using modifier free technique and these experiments resulted in the maximum extraction of 80%. The extraction profiles of uranium from neat UO_2Cl_2 was shown in **Figure 7.14**. In yet another experiment, the extraction of uranium from UO_2Cl_2 from cellulose matrix was also carried out using $SCCO_2$ modified with methanol. An extraction of 80 % was observed for uranium present in the cellulose matrix. The reduction in the extraction efficiency from a cellulose matrix can be attributed to the specific interactions between UO_2Cl_2 and cellulose matrix [146]. The above studies have indicated that the extraction of neat uranyl chloride is feasible with $SCCO_2$ modified with conventional ligands. Therefore, the presence of salt matrix (NaCl and CsCl) played a major role in hindering the extraction process while recovering uranium from a salt matrix.

7.3.3.3 Recovery of uranium from simulated salt matrix (UO_2Cl_2-NaCl-CsCl)

The incomplete extraction of uranium was observed from UO_2Cl_2 in the presence of NaCl-CsCl matrix. In this connection, preliminary experiments were carried by examining the recovery of uranium from a chloride matrix, which was prepared by physically mixing UO_2Cl_2 with NaCl / CsCl. Appropriate quantities of these salts were mixed and grinded prior to SFE. The salt mixture was loaded onto an extraction vessel and SFE was carried out using $SCCO_2$ modified with methanol. The extraction efficiency of uranium was shown in **Table 7.9**. From the above experiments it has been observed that the complete extraction of UO_2Cl_2 was achieved regardless of the NaCl content in the matrix. Thus it can be concluded that NaCl was not playing any significant role in impeding the extraction of UO_2Cl_2 from the UO_2Cl_2-NaCl matrix. Similarly, a series of experiments were carried out with UO_2Cl_2 and CsCl mixture. The extraction efficiency of UO_2Cl_2 in the presence of CsCl is shown in **Table 7.10**. From the above experiments it has been observed that the extraction efficiency of UO_2Cl_2 drops down with increasing CsCl content. Four independent experiments were carried out for each composition and the uncertainty in the extraction efficiency was ± 5%

Table 7.9 Effect of NaCl on the SFE of uranium from a mixture of UO_2Cl_2 – NaCl using $SCCO_2$ containing methanol

S. No.	Amount of UO_2Cl_2 (mg)	Amount of NaCl (mg)	Ratio of UO_2Cl_2 to NaCl	Extraction efficiency[#] (%)
1	25	25	1:1	96
2	25	50	1:2	95
3	25	100	1:4	97
4	25	500	1:20	96
5	25	1250	1:50	98
6	25	2000	1:80	96

Experimental conditions: pressure: 20 MPa, temperature: 323 K; $SCCO_2$ flow rate: 2.5 mL/min, co-solvent: 0.1 mL/min: co-solvent: methanol; sample loaded: 25 mg of UO_2Cl_2; extraction vessel: 10 mL; dynamic extraction: 2 hours.

Extraction efficiency is an average of six independent experiments with a relative standard deviation of less than 5%.

Table 7.10 Effect of CsCl on the SFE of uranium from a mixture of UO_2Cl_2-CsCl using $SCCO_2$ containing methanol

S. No.	Amount of UO_2Cl_2 (mg)	Amount of CsCl (mg)	Ratio of UO_2Cl_2 to CsCl	Extraction efficiency[#] (%)
1	25	25	1:1	90
2	25	50	1:2	78
3	25	125	1:5	<1
4	25	250	1:10	<1
5	25	625	1:25	<1
6	25	1250	1:50	<1

Experimental conditions: pressure: 20 MPa, temperature: 323 K; $SCCO_2$ flow rate: 2.5 mL/min, co-solvent: 0.1 mL/min: co-solvent: methanol; sample loaded: 25 mg of UO_2Cl_2; extraction vessel: 10 mL; dynamic extraction: 2 hours.

Extraction efficiency is an average of six independent experiments with a relative standard deviation of less than 5%.

Based on the above results, it was obvious that CsCl plays a major role in preventing the extraction of uranyl chloride from NaCl-CsCl matrix. This may be due to the formation of no*n*-extractable uranium species in presence of CsCl. The interaction between UO_2Cl_2 and CsCl was studied by IR spectroscopy. The Infrared spectrum of neat UO_2Cl_2, salt mixture (UO_2Cl_2-NaCl and UO_2Cl_2-CsCl) and actual pyrochemical salt

(UO_2Cl_2-NaCl-CsCl) were recorded (**Figure 7.15**). Neat UO_2Cl_2 showed a characteristic band at 947 cm^{-1}, which corresponds to the asymmetric stretching of O=U=O group. Asymmetric stretching at 947 cm^{-1} was observed for UO_2Cl_2 in the presence of sodium chloride. However, in the case of uranyl chloride-cesium chloride mixture, the asymmetric stretch at 947 cm^{-1} was shifted to shorter wave number and split into two bands (911 cm^{-1}& 936 cm^{-1}). These studies revealed there can be interactions between UO_2Cl_2 and cesium chloride when they are mixed. In the case of actual pyrochemical salt UO_2Cl_2-NaCl-CsCl, the asymmetric stretch was observed at much shorter wave number (905 cm^{-1}), indicating stronger interactions between uranyl ion and chloride matrix.

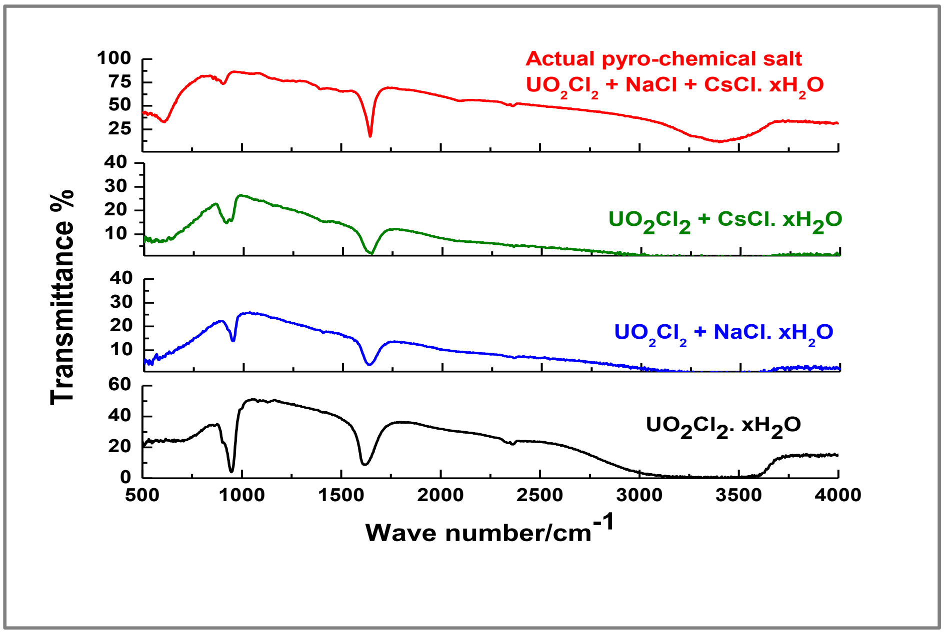

Figure 7.15 Infrared Spectrum of UO_2Cl_2 in presence of salt matrices

7.3.3.4 Recovery of uranium from pyrochemical salt matrices using ionic liquids

Subsequently, ionic liquids such as trioctylmethylammonium chloride (TOMAC), trioctylmethylammonium nitrate (TOMAN) and butylmethylimidazolium chloride (BMIMCL) were introduced into the $SCCO_2$ stream for the extraction of uranium from CsCl matrix. Use of $SCCO_2$ containing TOMAC (equilibrated with 8N HNO_3) resulted in about 95% extraction of uranium. Based on these studies, the extraction of uranium from actual salt matrix (UO_2Cl_2-NaCl-CsCl) was investigated using $SCCO_2$ + TOMAC mixture (**Table 7.11)**. The use of $SCCO_2$ containing 8 N HNO_3 equilibrated TOMAC resulted in the complete extraction of uranium from UO_2Cl_2-NaCl-CsCl. TOMAC is a quaternary ammonium salt and generally it extracts anionic species. The above results indicated the possible presence of uranium in its anionic species in the presence of NaCl-CsCl salt mixture. The above study indicated that the complete extraction of uranium from salt matrix can be achieved with $SCCO_2$ modified with acid equilibrated TOMAC.

Table 7.11 SFE of uranium from pyrochemical salt matrix (UO_2Cl_2-NaCl-CsCl) using $SCCO_2$ modified with 3 wt% ionic liquids in methanol

S. No.,	$SCCO_2$ modified with ionic liquid	Extraction efficiency[#] (%)
1	1-Butyl-3-methylimidazolium chloride	40
2	Trioctylmethylammonium chloride	45
3	Trioctylmethylammonium chloride - 3 stages	60
4	8 N acid equilibrated trioctylmethylammonium chloride	95
5	Trioctylmethylammonium nitrate - 3 stages	65
6	8 N acid equilibrated trioctylmethylammonium nitrate	95

Experimental conditions: pressure: 20 MPa, temperature: 323 K; $SCCO_2$ flow rate: 2.5 mL/min, co-solvent/modifier flow rate: 0.1 mL/min; ligand: 3 wt% of ligand in co-solvent; sample loaded: 100 mg of UO_2Cl_2-NaCl-CsCl; extraction vessel: 1 mL; dynamic extraction: 90 min.

Extraction efficiency is an average of five independent experiments with a relative standard deviation of less than 5%.

7.3.3.5 Optimization of experimental conditions for recovery of uranium

(a) Optimization of HNO_3 concentration

Complete extraction of uranium from salt matrix was obtained with 8 N HNO_3 pre-equilibrated TOMAC as a ligand. A systematic study was carried out to explore the minimum acid concentration requirement for the complete recovery of uranium from the salt matrix. The extraction efficiency of uranium with TOMAC was studied as a function of HNO_3 concentration ranging from 0.1 N to 8 N. $SCCO_2$ modified with neat TOMAC resulted in an extraction efficiency of 45%. With 0.1 N acid equilibrated TOMAC as a ligand, the extraction efficiency was found to be 77%. The extraction efficiency of uranium increases with the acidity and near complete extraction was achieved with 1 N acid equilibrated TOMAC. Beyond 1N acidity, a marginal increase in the extraction efficiency was observed with acid concentration; the extraction behavior is shown in **Figure 7.16.** These studies have shown that $SCCO_2$ containing TOMAC (TOMAC equilibrated with 1 to 2 N HNO_3) is adequate for achieving complete recovery of uranium from chloride salt matrix.

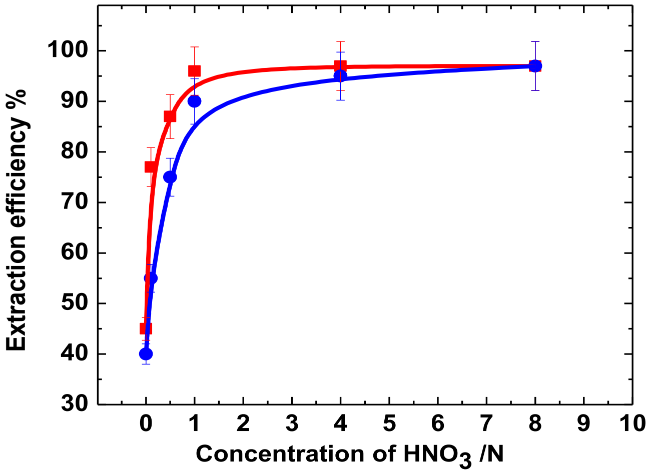

Figure 7.16 Effect of acid concentration on SFE of uranium from salt matrices using $SCCO_2$ modified with ligand; ●, UCl_3-LiCl-KCl; ■, UO_2Cl_2-NaCl-CsCl; Experimental conditions: pressure: 20 MPa, temperature: 323 K; $SCCO_2$ flow rate: 2.5 mL/min, co-solvent/modifier flow rate: 0.1 mL/min; ligand: 3 wt% of acid equilibrated TOMAC in *n*-propanol; sample loaded: 100 mg; ligand loaded: 50 mg; extraction vessel: 1 mL; static extraction: 1 hour and dynamic extraction period: 1 hour.

Optimization of pressure

The effect of pressure on the SFE of uranium from UCl_3-LiCl-KCl / UO_2Cl_2-NaCl-CsCl was studied at three different temperatures, 313, 323 and 333 K with pressure ranging from 10-30 MPa. The extraction profile is shown in **Figure 7.17**. These results indicated that the extraction efficiency of uranium increases with pressure at all isotherms. An initial steep rise in the extraction efficiency was observed with increasing pressure from 10 to 20 MPa, beyond 20 MPa there was no appreciable increase in the extraction. At a constant temperature, the density of $SCCO_2$ increases sharply with pressure, beyond certain pressure a there will be a marginal increase in the density with pressure. The extraction efficiency and $SCCO_2$ density follows a similar trend with the pressure. The increase in the extraction efficiency of uranium with pressure was also established using various complexing agents [151, 232]. The above study indicated that the efficient extraction can be achieved at a pressure of 20 MPa.

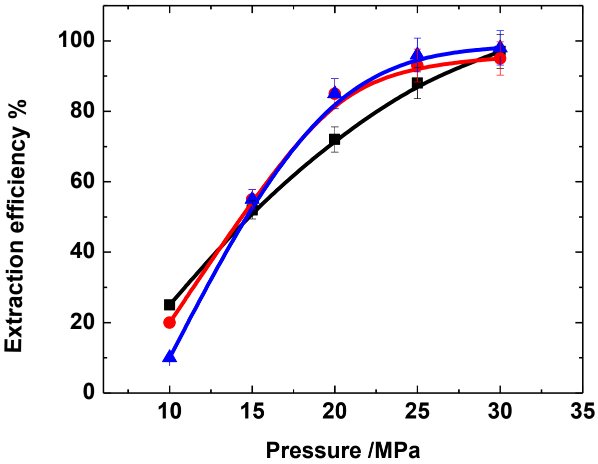

Figure 7.17 Effect of pressure on SFE of uranium from salt matrix (UCl_3-LiCl-KCl) using $SCCO_2$ modified with ligand; ■, 313 K; ●, 323 K; ▲, 333 K; Experimental conditions: temperature: 323 K; $SCCO_2$ flow rate: 2.5 mL/min, co-solvent/modifier flow rate: 0.1 mL/min; ligand: 3 wt% of 1 N HNO_3 equilibrated TOMAC in *n*-propanol; sample loaded: 100 mg; ligand loaded: 50 mg; extraction vessel: 1 mL; static extraction: 1 hour and dynamic extraction period: 1 hour.

Optimization of temperature

To investigate the effect of temperature on the extraction behavior, SFE of uranium from UCl_3-LiCl-KCl / UO_2Cl_2-NaCl-CsCl salt matrix was carried out with acid equilibrated TOMAC at constant pressure, 20 MPa with temperature ranging from 313 to 333 K. The extraction efficiency of uranium as a function of temperature is shown in **Figure 7.18**. The extraction efficiency increases with temperature. At 20 MPa and 313 K, the extraction efficiency of uranium was found to be 70%. With increasing temperature from 313 to 323 K, the extraction efficiency rises to about 87%. When the temperature was further raised to 333 K, only a marginal increase in the extraction efficiency was observed. The increase in the extraction efficiency was more pronounced when temperature was altered from 313 to 323 K. The density of the $SCCO_2$ decreases with raise in temperature, reflecting in the reduction of extraction efficiency at higher temperatures. However in our study, the increase in extraction efficiency at 323– 333 K compared to 313 K is due to better desorption of uranium from the chloride matrix to the modified supercritical CO_2 phase containing ligand, leading to better extraction efficiency.

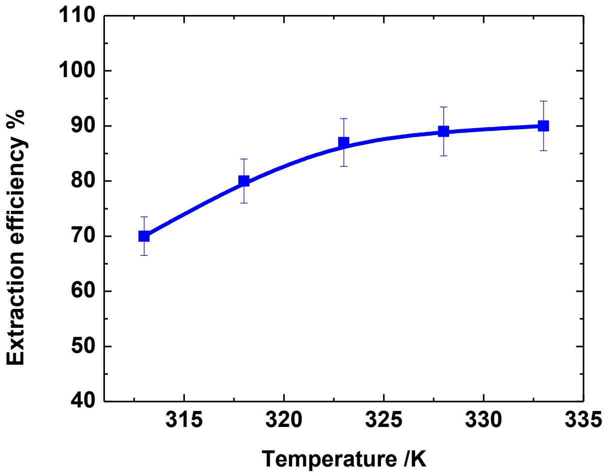

Figure 7.18 Effect of temperature on SFE of uranium from salt matrix (UCl_3-LiCl-KCl) using $SCCO_2$ modified with ligand; Experimental conditions: pressure: 20 MPa; $SCCO_2$ flow rate: 2.5 mL/min, co-solvent/modifier flow rate: 0.1 mL/min; ligand: 3 wt% of 1 N HNO_3 equilibrated TOMAC in *n*-propanol; sample loaded: 100 mg; ligand loaded: 50 mg; extraction vessel: 1 mL; static extraction: 1 hour and dynamic extraction period: 1 hour.

Optimization of co-solvent

Complete extraction of uranium from UCl_3-LiCl-KCl / UO_2Cl_2-NaCl-CsCl was achieved using $SCCO_2$ containing acid equilibrated TOMAC in methanol / *n*-propanol as co-solvents. It is important to study the co-extraction behavior of LiCl, KCl, NaCl and CsCl during the SFE of uranium. In this connection, SFE of chloride salt matrices was carried out using $SCCO_2$ containing acid equilibrated TOMAC in methanol as well as *n*-propanol as co-solvents.

Both static and dynamic extractions were performed. Assay of Li, K, Na and Cs was carried out by Atomic Emission Spectroscopy (**Table 7.12).** With methanol as co-solvent, significant amount of Li (30%) co-extraction was observed from both salt matrices. The co-extraction of Na was about 7% and that of K and Cs was below 2%. The significant co-extraction of Li can be attributed to the solubility of it in methanol. The solubilities of LiCl, NaCl and KCl in methanol at 323 K were reported as 10.32, 0.217 and 0.0588 mol.kg^{-1} [234]. In the case of *n*-propanol as co-solvent, there was no significant carryover of Li (<3%), Na (<0.7), K (<0.2%) and Cs (<0.05%) during SFE experimental conditions. The extraction profile is depicted in **Figure 7.19**. Hence, in the present study, acid equilibrated TOMAC was dissolved in *n*-propanol (co-solvent) and introduced in to the $SCCO_2$ stream for extraction studies.

Table 7.12 Co-extraction of Li, K, Na and Cs during the SFE of pyrochemical salt matrices using $SCCO_2$ containing acid equilibrated TOMAC

S. No.,	Element	Co-extraction efficiency[#] (%)	
		Methanol as a co-solvent	*n*-propanol as a co-solvent
1	Li	30	<3
2	Na	10	<1
3	K	<1	<1
4	Cs	<1	<1

Experimental conditions: pressure: 20 MPa, temperature: 323 K; $SCCO_2$ flow rate: 2.5 mL/min, co-solvent/modifier flow rate: 0.1 mL/min; ligand: 3 wt% of 1 N HNO_3 equilibrated TOMAC in *n*-propanol; sample loaded: 100 mg; ligand loaded: 50 mg; extraction vessel: 1 mL; static extraction: 1 hour and dynamic extraction period: 1 hour.

Extraction efficiency is an average of five independent experiments with a relative standard deviation of less than 5%.

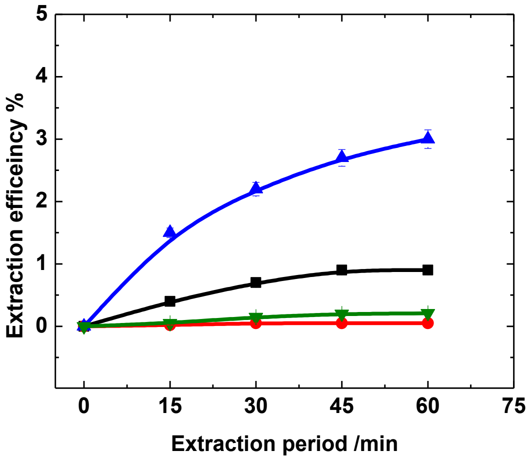

Figure 7.19 Co-extraction behavior of salt matrix during SFE of uranium from salt matrix using SCCO$_2$ containing TOMAC; **▲, Li; ●, Na; ▼, K; ■, Cs;** Experimental conditions: pressure: 20 MPa, temperature: 323 K; SCCO$_2$ flow rate: 2.5 mL/min, co-solvent/modifier flow rate: 0.1 mL/min; ligand: 3 wt% of 1 N HNO$_3$ equilibrated TOMAC in *n*-propanol; sample loaded: 100 mg; ligand loaded: 50 mg; extraction vessel: 1 mL; static extraction: 1 hour and dynamic extraction period: 1 hour.

7.3.3.6 SFE of uranium from pyrochemical salt matrix under optimized conditions

Based on the above optimization studies, SFE of uranium from UCl$_3$-LiCl-KCl / UO$_2$Cl$_2$-NaCl-CsCl salt matrices was carried out; initially dynamic extraction using SCCO$_2$ containing 3wt % of acid equilibrated TOMAC in *n*-propanol medium was carried out. The maximum extraction efficiency was found to be 70% over an extraction period of about 3 h. Latter, a combination of static and dynamic SFE was carried out. In static SFE, salt matrix and TOMAC were kept for 1 h static equilibration at 323 K and 20MPa. Subsequently, the dynamic SFE was carried out at 323 K and 20 MPa with a CO$_2$ flow rate of 2.5 mL/min. Complete extraction of uranium (e.g. 99%) was established in these experiments (**Figure 7.20** & **7.21**).

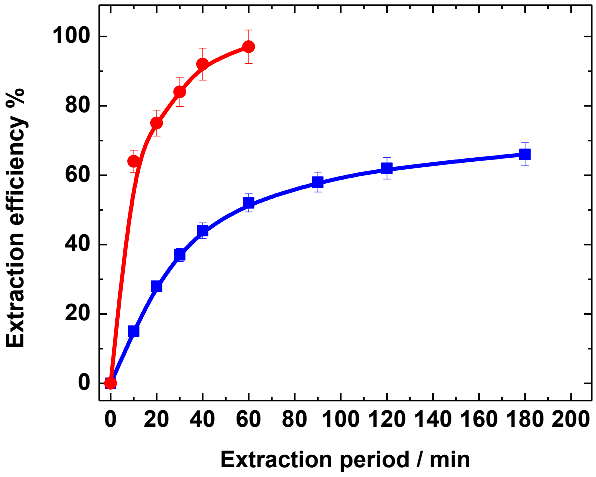

Figure 7.20 SFE of uranium from pyrochemical salt matrix (UO_2Cl_2-NaCl-CsCl) using $SCCO_2$ containing ligand; ●, static followed by dynamic SFE; ■, only dynamic SFE; Experimental conditions: pressure: 20 MPa, temperature: 323 K; $SCCO_2$ flow rate: 2.5 mL/min, co-solvent/modifier flow rate: 0.1 mL/min; ligand: 3 wt% of 1 N HNO_3 equilibrated TOMAC in *n*-propanol; sample loaded: 100 mg; ligand loaded: 50 mg; extraction vessel: 1 mL; static extraction: 1 hour; dynamic extraction period: 1 hour and 3 hours.

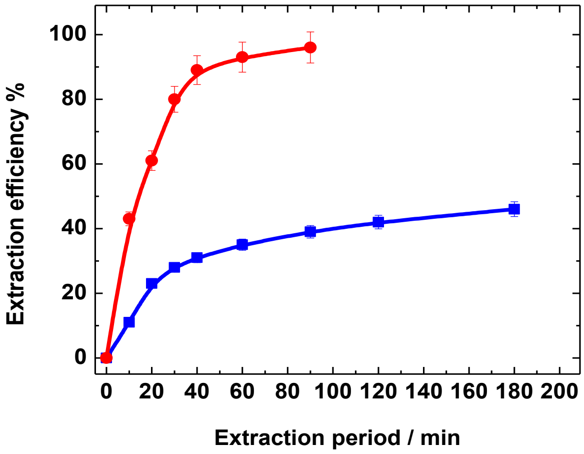

Figure 7.21 SFE of uranium from pyrochemical salt matrix (UCl_3-LiCl-KCl) using $SCCO_2$ containing ligand; ●, static followed by dynamic SFE; ■, only dynamic SFE; Experimental conditions: pressure: 20 MPa, temperature: 323 K; $SCCO_2$ flow rate: 2.5 mL/min, co-solvent/modifier flow rate: 0.1 mL/min; ligand: 3 wt% of 1 N HNO_3 equilibrated TOMAC in *n*-propanol; sample loaded: 100 mg; ligand loaded: 50 mg; extraction vessel: 1 mL; static extraction: 1 hour; dynamic extraction period: 1 hour and 3 hours.

These studies have shown that uranium in chloride salt matrix is possibly present as anionic complexes e.g. $UO_2Cl_4^{2-}$/ UCl_6^{3-}. Such species are extracted by anion exchangers such as quaternary ammonium salts or amines. In the present study TOMAN/TOMAC (quaternary ammonium salt) was employed for the extraction of uranium from the salt matrices. LiCl based melts generally contain uranium in all oxidation states (+3, +4, +5, +6). Dissolution of UO_2Cl_2 / UCl_3 generates $UO_2Cl_4^{2-}$/ UCl_6^{3-} in the NaCl-CsCl and LiCl-KCl mixtures, respectively. SFE of uranium using conventional ligands resulted in poor extraction efficiency provides an additional evidence for possible presence of uranium as $UO_2Cl_4^{2-}$/ UCl_6^{3-} species in the salt matrix. In addition, hexachloro coordinated ions, UCl_6^{2-} and UCl_6^{3-} ions are present in melts containing U(IV) and U(III) ions respectively and the same ions and oxidation states are retained in the quenched melt samples [235-237]. TOMAC reacts with the uranium present as anionic species in the salt matrix and forms U-TOMAC neutral complex. The U-TOMAC complex is soluble in supercritical medium and extracted by $SCCO_2$.

$$\left[2R_4N^+Cl^-\right]_{SCCO_2} + \left[UO_2Cl_4\right]^{2-} \Leftrightarrow \left([R_4N]_2^+\,[UO_2Cl_4]^{2-}\right)_{SCCO_2}$$

$$\left[3R_4N^+Cl^-\right]_{SCCO_2} + \left[UCl_6\right]^{3-} \Leftrightarrow \left([R_4N]_3^+\left[UCl_6\right]^{3-}\right)_{SCCO_2}$$

7.3.3.7 SFE of Pu from pyrochemical salt matrix under optimized conditions

SFE of plutonium from $PuCl_3$-KCl-LiCl matrix was carried out using $SCCO_2$ modified with 1 N HNO_3 equilibrated TOMAC in *n*-propanol. Initially, dynamic extraction was carried out at a CO_2 flow rate of 2.5 mL/min. The extraction kinetics was found to be slow (**Figure 7.22)** and found to be 30% for an extraction period of 3 hours. Under similar experimental conditions, the extraction of uranium from UCl_3-KCl-LiCl was found to be 50%. Generally, kinetics of SFE of plutonium compounds from different matrices are slower compared to that of uranium[140, 148].

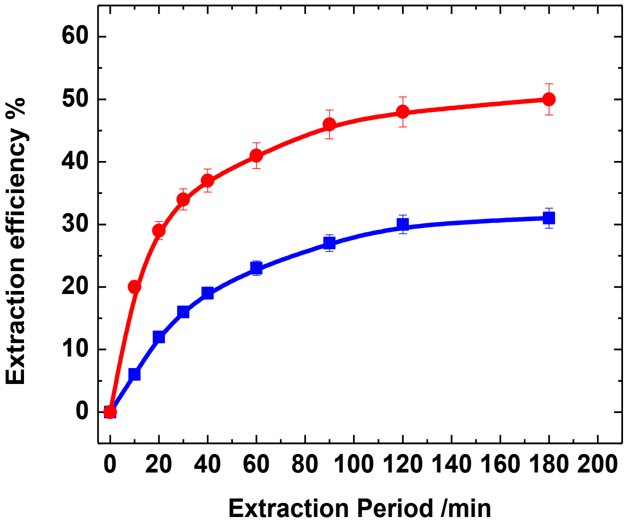

Figure 7.22 SFE of plutonium from pyrochemical salt matrix ($PuCl_3$-LiCl-KCl) using $SCCO_2$ containing ligand; ●, static followed by dynamic SFE; ■, only dynamic SFE; Experimental conditions: pressure: 20 MPa, temperature: 323 K; $SCCO_2$ flow rate: 2.5 mL/min, co-solvent/modifier flow rate: 0.1 mL/min; ligand: 3 wt% of 1 N HNO_3 equilibrated TOMAC in *n*-propanol; sample loaded: 100 mg; ligand loaded: 50 mg; extraction vessel: 1 mL; static extraction: 1 hour; dynamic extraction period: 3 hours.

A combination of static (1 h) followed by dynamic extraction (3 h) were performed for the removal of plutonium form a $PuCl_3$-KCl-LiCl salt matrix. These experiments resulted in a maximum extraction efficiency of 50% (**Figure 7.22**). A maximum of 75 % extraction efficiency of plutonium was established under static equilibration for about 10 hours followed by dynamic extraction for 2 h. These studies have shown that longer equilibration periods are necessary for achieving better recovery of plutonium from chloride salt matrix.

7.3.3.8 SFE of uranium from UCl_3-LiCl-KCl rod

Complete extraction of uranium from UCl_3-LiCl-KCl grains/powder was demonstrated with $SCCO_2$ containing acid equilibrated TOMAC in *n*-propanol. Based on this knowledge, we made an attempt to extract the uranium from UCl_3-LiCl-KCl rod under similar experimental conditions. The cylindrical rod was prepared by drawing the molten salt through a quartz tube. SFE of uranium from matrix made of rod resulted in incomplete extraction of uranium (25%). Subsequently, re-extraction has been carried out on the same rod which was remained in extraction vessel i.e. second time extraction and extraction efficiency was found to be 40%. In similar manner, three stage extractions were performed and maximum extraction found to be 48%.

Table 7.13 Effect of nitric concentration on SFE of uranium from salt matrix (UCl_3-LiCl-KCl) rod using $SCCO_2$ modified with acid equilibrated TOMAC

S. No.,	Concentration of HNO_3 (N)	Extraction efficiency$^{\#}$ (%)
1	1	25
2	2	35
3	4	60
4	8	65
5	10	70

Experimental conditions: pressure: 20 MPa, temperature: 323 K; $SCCO_2$ flow rate: 2.5 mL/min, co-solvent/modifier flow rate: 0.1 mL/min; ligand: 3 wt% of 1 N HNO_3 equilibrated TOMAC in *n*-propanol; sample loaded: 500 mg; ligand loaded: 250 mg; extraction vessel: 10 mL; static extraction: 1 hour; dynamic extraction period: 1 hour.

Extraction efficiency is an average of five independent experiments with a relative standard deviation of 5%.

Latter, extraction of uranium form UCl_3-LiCl-KCl rod was studied as a function of HNO_3 concentration. TOMAC was equilibrated with 1 to 10 N HNO_3 and was employed with $SCCO_2$ and extraction was carried out (**Table 7.13)**. $SCCO_2$ containing 1 N HNO_3 equilibrated TOMAC in *n*-propanol resulted in an extraction efficiency of 25%. With 4N acid equilibrated TOMAC, the extraction efficiency was found to be 60%; a significant increase in the extraction efficiency was observed with increase in acid concentration up to 4 N. Above 4N acidity, there was only a marginal increase in the extraction efficiency. The uranium extraction efficiency was found to be about 70% for $SCCO_2$ containing TOMAC, where the latter was equilibrated with 10 N acid. The uranium present in the peripheral part of the rod was getting extracted and the extraction was found to be diffusion controlled. Subsequently, UCl_3-LiCl-KCl rod was kept for static equilibration over longer duration (48 hours) followed with dynamic extraction (4 hours). These experiments resulted in the recovery of about 90% of the uranium from salt matrix.

7.3.3.9 Semi-preparative scale SFE of uranium from pyrochemical salt matrix

Complete recovery of uranium from chloride salt matrices was demonstrated using $SCCO_2$ containing acid equilibrated TOMAC. All these experiments were carried out using analytical scale SFE system, in which 1 and 10 mL high pressure extraction vessels were used. An attempt was made to scale-up the SFE process for the recovery of actinides. In this context, recovery of uranium from UO_2Cl_2-NaCl-CsCl matrix was carried out using a semi-preparative SFE system (1 L scale extraction vessel) [148]. The semi-preparative system (M/S Inexus, Chennai) consisted of high pressure CO_2 pump capable of delivering carbon dioxide up to 200 g/min, co-solvent pump, high pressure extraction vessel of 1 litre capacity, back pressure regulator and high pressure fraction collection vessel. In the recovery studies, carbon dioxide was delivered with a typical flow rate of 40 g/min while acid equilibrated TOMAC in *n*-propanol was delivered at 1 mL/min. In each experiment about 200-500 g of UO_2Cl_2-NaCl-CsCl salt was loaded onto a 1L high pressure extraction vessel; it was kept at static equilibration (323 K and 20 MPa) for a period of about 4 h followed by a dynamic extraction, for a period of 2 h. SFE was carried out in 6 independent batches. Typical extraction efficiency was found to be about 90% and the overall recovery from 6 independent experiments was found to be 85±5 %. These preliminary studies have established potential use of supercritical fluid for the recovery of actinides and possibility for scaling-up the process.

7.3.4. Conclusions

Supercritical fluid extraction based technique was developed for the extraction of residual uranium and plutonium present in the pyrochemical salt matrix. This study has demonstrated the near complete recovery of uranium from chloride salt matrix using supercritical carbon dioxide modified with trioctylmethylammonium chloride-HNO_3 complex. The extraction efficiency for plutonium was found to be 75%, under similar experimental conditions. The effect of temperature, pressure and HNO_3 concentration on the recovery of actinides was established. The recovery of uranium from chloride salt matrix was also demonstrated using 1 L scale SFE facility. The studies have shown that SFE based technique can provide an excellent alternative to extract and recover actinides from chloride salt matrix with minimum generation of liquid secondary waste.

Chapter 8

Conclusions and discussions

This research work carried out in the thesis attempts to establish methodologies for the development of supercritical fluid based extraction methods for the extraction and recovery of actinides from different matrices. The conclusions drawn based on several investigations that are centralized around this objective are given in this chapter.

8.1 Measurement of solubility of ligands in supercritical carbon dioxide

The solubility of a series of trialkyl phosphates (trimethyl phosphate, triethyl phosphate, tributyl phosphate, triamyl phosphate, tri-*iso*-amyl phosphate and trihexyl phosphate)in $SCCO_2$ medium were experimentally determined for the first time using a flow saturation technique in the temperature range of 313 to 333 K and in the pressure range of 10 to 25 MPa. The solubility decreased with increase in the molecular weight of the trialkyl phosphate. The solubilities of the trialkyl phosphates were in the retrograde region in the temperature and pressure range investigated, similar to the solubility behavior of many organophosphorus compounds. The solubilities were correlated using Chrastil equation, Adachi-Lu model, Mendez-Teja equation, solution model based on Wilson activity coefficient model and association theory with van Laar activity coefficient model. The model parameters of the association model are varied linearly with the carbon number of the trialkyl phosphates and thus can be used to predict the solubilities of a homologous series of trialkyl phosphates.

The more basic extractant, Dialkylalkyl phosphonates (dibutylbutyl phosphonate and diamylamyl phosphonate) were synthesised and their solubilities in $SCCO_2$ medium were determined in the pressure range of 10 to 25 MPa at 313 to 333 K. Being stronger compared to trialkyl phosphates, these ligands can be employed for pre-concentration of actinides from lean streams. Solubilities of dialkylalkyl phosphonates were found to be sufficiently high (0.06 to 0.12 mole/mole) and can be employed ligands in $SCCO_2$ medium. Experimental solubilities were correlated using Chrastil, Mendez-Teja, solution theory with Wilson activity coefficient model and association model based on van Laar activity coefficient model. Comparison among these models revealed that the association model with van Laar activity coefficient model provides better predictions on the solubility behavior.

Solubility of an ionic liquid, trioctylmethylammonium chloride in $SCCO_2$ investigated as these ligands are capable of extracting actinides from chloride salt matrix. Hence solubility of TOMAC was measured at 313,323 and 333 K with pressure varying from 10 to 30 MPa. The solubility of the ionic liquid was found to be low and varies from 10.5×10^{-5} to 12.7×10^{-5} mole/mole. The influence of co-solvents on the solubility of ionic liquid was examined. Addition of polar co-solvents such as methanol and *n*-propanol into the $SCCO_2$ stream results in the enhanced solubility. The influence of temperature, pressure and co-solvent on the solubility of ionic liquid in $SCCO_2$ in the presence of co-solvents has been established. The solubilities of ionic liquid in neat $SCCO_2$ were successfully correlated using four different semi-empirical equations, Chrastil, Mendez-Teja, solution theory and association theory based on activity coefficient models. These studies have established that the ionic liquids in the presence of polar co-solvents can be employed as ligands for the extraction of metal ions.

Solubilities of a series of linear and branched *N*,*N*-dialkyl amides (*N*,*N*-dihexylhexanamide, *N*,*N*-dihexyloctanamide, *N*,*N*-dihexyldecanamide, *N*,*N*-di-2-ethylhexylacetamide, *N*,*N*-di-2-ethylhexyl-*iso*-butyramide and *N*,*N*-di-2-ethylhexylpivalamide) in $SCCO_2$ medium were determined at 313-333 K with pressure ranging from 10-20 MPa to assess their utility as ligand for the extraction of actinides as these compounds have innocuous degradation products on exposure to radiation and completely incinerable in nature. Results indicated that the solubility of amides can be improved by increasing pressure and reducing temperature in the investigated region. The solubilities of amides decreased with the increase in the carbon number. The experimental solubility data was found to be self-consistent with Mendez-Teja (MT) model. The experimental solubilities were correlated using four different models, Chrastil, MT, solution theory using Wilson activity coefficient model and association theory with van Laar activity coefficient model. The correlation results demonstrated that the association theory based on van Laar activity coefficient model was better to predict the solubility data with an average deviation of less than 10%.

8.2 Development of new models for the correlations of ternary solubilities

Two model equations were developed for ternary solubilities ($SCCO_2$ + liquid solute + co-solvent) by using association theory with Wilson and van Laar activity coefficient models. These model equations consist of five and six adjustable parameters and correlate the ternary solubilities of liquids in terms of temperature, pressure, density and co-solvent composition. The solubility of trioctylmethylammonium chloride in $SCCO_2$ in the presence of co-solvents was correlated using the derived equations. The performance of newly derived models was compared with the modified Chrastil equation using corrected Akaike information criteria; the new model equations have successfully correlated the solubilities with an average deviation of less than 8%. The derived models are first of its kind to correlate the liquid solubilities in $SCCO_2$ + co-solvent system.

8.3 Development of supercritical fluid extraction methods for the extraction of actinides

Solubility data of various ligands in $SCCO_2$ medium formed basis for selection of experimental conditions towards development of supercritical fluid based extraction methods for the recovery of actinides from different matrices. A method was developed for the selective extraction of uranium from simulated dissolver solution using $SCCO_2$

containing tri-*iso*-amyl phosphate as well as diamylamyl phosphonate. Our studies indicated that uranium can be selectively extracted from the fission products using modified $SCCO_{2.}$ The effect of pressure, temperature, acidity on extraction of uranium was investigated. These studies have demonstrated that the potential application of $SCCO_2$ containing tri-*iso*-amyl phosphate as well as diamylamyl phosphonate stream for the selective extraction of uranium from different matrices.

Extraction of residual uranium and plutonium from pyrochemical salt matrix (UCl_3-LiCl-KCl, $PuCl_3$-LiCl-KCl and UO_2Cl_2-NaCl-CsCl) was investigated using $SCCO_2$ containing various ligands. Among the ligands employed in the present study, use of $SCCO_2$ containing trioctylmethylammonium chloride resulted in a better recovery of actinides, uranium (95±5%) and plutonium (75±5%). The influence of nature of salt matrix, temperature, pressure, co-solvent and acid concentration was studied for the efficient removal of actinides from salt matrix. The recovery of uranium from salt matrix was also demonstrated using a semi-preparative scale SFE facility with an extraction efficiency of 85±5%. The present work demonstrated that the supercritical fluid based methods can provide an excellent alternative to recover actinides from chloride salt matrix with minimum generation of liquid secondary waste.

$SCCO_2$ containing wide variety of organophosphorous compounds was employed for the extraction of uranyl nitrate and thorium nitrate from solid form. Similarly, the extraction of uranium and thorium from nitric acid medium was also examined. The effect of temperature, pressure, acidity and nature of co-solvent on the selective extraction of uranium from a mixture of uranium and thorium was investigated. $SCCO_2$ containing tri-*sec*-butyl phosphate offered better fractionation of uranium over thorium. These initial studies have also demonstrated the viability of using different organophosphorous compounds in supercritical medium for the recovery of actinides from liquid nuclear waste.

8.4 Future perspectives

The present study of the thesis has been mainly focused on the determination of solubilities of ligands in $SCCO_2$ and their application for the development of supercritical fluid based methods for the extraction and recovery of actinides. All these experiments were carried out by collecting appropriate quantities of ligands, and subsequent estimation of the same using off-line techniques. However, online estimation/detection of the solute concentration can lead to minimization of analysis time. Suitable modification of the existing set-up with a new window for the on-line detection of solute unveils the possibility of measuring the solubilities of wide variety of compounds including metal-ligand complexes.

In the present work, the solubility of neat ligands in $SCCO_2$ medium was examined. Solubility of metal-ligand complex will also play an important role in effecting efficiency of supercritical fluid based methods. Determination of solubilities of metal-ligand complexes is an important assignment, which widens the scope of further applications. Understanding the phase behavior of multicomponent system ($SCCO_2$ + ligand) will be of immense interest as there is no data on available on the critical properties of ligand in supercritical medium. Incorporation of suitable view cell system into high pressure vessel will enable the visual identification of multiple phases at different temperatures and pressures that can provide fundamental understanding of solubility behavior in supercritical fluids.

Supercritical fluid extraction of metal ion involves formation of metal-ligand complexes in $SCCO_2$ medium. Composition of metal-ligand complexes plays a key role in the selective extraction of metal species. Identifying the composition of metal complexes in $SCCO_2$ medium and comparing with the liquid-liquid extraction data will provide the basic understanding of the complexation behavior in $SCCO_2$ phase. These studies can be carried out using a supercritical fluid chromatography (SFC). Separation of various ligands using SFC and correlation of retention times with the solubility behavior may provide suitable insights towards “modeling of solubility behavior”. There is also scope for the development of SFC based method for quantification of actinides with suitable detector with minimum generation of liquid secondary waste. The work carried out in the present thesis provide some insights for the application of supercritical fluid based techniques in nuclear technology and opens-up exciting research opportunities in these areas of research.

References

[1] C.F. Poole, M. Cooke, I.D. Wilson, *Encyclopedia of Separation science*, Academic Press, 2000.

[2] D. Pruett, *Separation science and technology: an ORNL perspective*, in, Oak Ridge National Lab, USA, 1986.

[3] J. Rydberg, C. Musikas, G.R. Choppin, *Solvent extraction principles and practice*, Marcel Dekker, New York, 1992.

[4] P.A. Sewell, B. Clarke, *Chromatographic separations, analytical chemistry by open learning*, John Wiley & Sons, New York, 1987.

[5] P.R. Danesi, Separation of metal species by supported liquid membranes, *Sep. Sci. Technol.* 19 (1984) 857-894.

[6] D.A. Skoog, D.M. West, J.F. Holler, S.R. Crouch, *Fundamentals of Analytical Chemistry*, Thomson-Brooks/Cole, 2004.

[7] M.A. McHugh, V.J. Krukonis, *Supercritical fluid extraction: principles and practice*, 2nd ed., Butterworth-Heinemann, Boston, MA, 1994.

[8] Y. Marcus, A.S. Kertes, *Ion exchange and solvent extraction of metal complexes*, Wiley-Interscience, 1969.

[9] D. Sood, S. Patil, Chemistry of nuclear fuel reprocessing: Current status, *J. Radioanal. Nucl. Chem.* 203 (1996) 547-573.

[10] J.D. Seader, E.J. Henley, *Separation process principles*, John Wiley & Sons, 2005.

[11] B. Raj, H. Kamath, R. Natarajan, P.V. Rao, A perspective on fast reactor fuel cycle in India, *Prog. Nucl. Energy.* 47 (2005) 369-379.

[12] S. David, Future scenarios for fission based reactors, *Nucl. Phys. A* 751 (2005) 429-441.

[13] K.L. Nash, G.J. Lumetta, *Advanced separation techniques for nuclear fuel reprocessing and radioactive waste treatment*, Woodhead Publishing Limited, Cambridge, 2011.

[14] V. Anastasov, M. Betti, F. Boisson, F. Depisch, F. Houlbreque, R. Jeffree, I. Khamis, S. Lattemann, J. Miquel, S. Nisan, Status of minor actinide fuel development, IAEA Nuclear energy series No. NF-T-4.6, (2009).

[15] J. Mathur, M. Murali, K. Nash, Actinide partitioning—a review, *Solvent Extr. Ion Exch.* 19 (2001) 357-390.

[16] P. Anastas, N. Eghbali, Green Chemistry: Principles and Practice, *Chem. Soc. Rev.* 39 (2010) 301-312.

[17] P.T. Anastas, T.C. Williamson, *Green chemistry: frontiers in benign chemical syntheses and processes*, Oxford University Press, USA, 1998.

[18] M.C. Bubalo, S. Vidovic, I.R. Redovnikovic, S. Jokic, Green solvents for green technologies, *J. Chem. Technol. Biotechnol.* 90 (2015) 1631-1639.

[19] P. Pollet, E.A. Davey, E.E. Ureña-Benavides, C.A. Eckert, C.L. Liotta, Solvents for sustainable chemical processes, *Green Chem.* 16 (2014) 1034-1055.

[20] F.M. Kerton, R. Marriott, *Alternative solvents for green chemistry*, Royal Soc. Chem., 2013.

[21] T. Welton, Room-temperature ionic liquids. Solvents for synthesis and catalysis, *Chem. Rev.* 99 (1999) 2071-2084.

[22] J.G. Huddleston, H.D. Willauer, R.P. Swatloski, A.E. Visser, R.D. Rogers, Room temperature ionic liquids as novel media for 'clean'liquid–liquid extraction, *Chem. Commun.* (1998) 1765-1766.

[23] D. Han, K.H. Row, Recent applications of ionic liquids in separation technology, *Molecules* 15 (2010) 2405-2426.

[24] M. Srncik, D. Kogelnig, A. Stojanovic, W. Körner, R. Krachler, G. Wallner, Uranium extraction from aqueous solutions by ionic liquids, *Appl. Radiat. Isot.* 67 (2009) 2146-2149.

[25] J. Dupont, R.F. de Souza, P.A. Suarez, Ionic liquid (molten salt) phase organometallic catalysis, *Chem. Rev.* 102 (2002) 3667-3692.

[26] Y. Xiao, S.V. Malhotra, Diels–Alder reactions in pyridinium based ionic liquids, *Tetrahedron letters* 45 (2004) 8339-8342.

[27] P.T. Anastas, *Green separation processes: fundamentals and applications*, John Wiley & Sons, 2006.

[28] S. Keskin, D. Kayrak-Talay, U. Akman, Ö. Hortaçsu, A review of ionic liquids towards supercritical fluid applications, *J. Supercrit. Fluids* 43 (2007) 150-180.

[29] P. Wasserscheid, W. Keim, Ionic liquids—new "solutions" for transition metal catalysis, *Angew. Chem. Int. Ed.* 39 (2000) 3772-3789.

[30] G. Brunner, Applications of supercritical fluids, *Annu. Rev. Chem. Biomol. Eng.* 1 (2010) 321-342.

[31] Z. Kenz, E. Markocic, M. Leitgeb, M. Primozic, M.K. Hrnviv, M. Skerget, Industrial applications of supercritical fluids: A review, *Energy* 77 (2014) 235-243.

[32] M. Perrut, Supercritical fluid applications: industrial developments and economic issues, *Ind. Eng. Chem. Res.* 39 (2000) 4531-4535.

[33] C.C.d.l. Tour, Effect Obtained by Simultaneous Application of heat and pressure on certain liquids, *Anal. Chem.* 22 (1822) 410.

[34] A. Clifford, T. Clifford, *Fundamentals of supercritical fluids*, Oxford University Press, 1999.

[35] J. Hannay, J. Hogarth, I. On the solubility of solids in gases, *Proc. Royal Soc. Lond.* 30 (1880) 178-188.

[36] Z. Fang, *Rapid production of micro-and nano-particles using supercritical water*, Springer Science & Business Media, 2010.

[37] R.M. Smith, *Supercritical fluid chromatography, RSC chromatography monographs*, Royal Society of Chemistry, 1988.

[38] B. Wenclawiak, *Analysis with supercritical fluids: extraction and chromatography*, Springer, 1992.

[39] M. Mukhopadhyay, *Natural extracts using supercritical carbon dioxide*, CRC press, 2000.

[40] R.C. Narayanan, *Non-catalytic synthesis of biolubricant esters and their solubilities in supercritical fluids*, in: Ph.D., thesis, Indian Institue of Science, Bangalore, 2018.

[41] D. Thiébaut, M. Caude, *Practical Supercritical Fluid Chromatography and Extraction*, Harwood Academic Publishers, 1999.

[42] K.K. Liong, P.A. Wells, N.R. Foster, Diffusion coefficients of long-chain esters in supercritical carbon dioxide, *Ind. Eng. Chem. Res.* 30 (1991) 1329-1335.

[43] H. Iwasaki, M. Takahashi, Viscosity of carbon dioxide and ethane, *J. Chem. Phys.* 74 (1981) 1930-1943.

[44] M. Herrero, J.A. Mendiola, A. Cifuentes, E. Ibanez, Supercritical fluid extraction: Recent advances and applications, *J. Chromatogr. A* 1217 (2010) 2495-2511.

[45] M. Saito, History of supercritical fluid chromatography: instrumental development, *J. Biosci. Bioeng.* 115 (2013) 590-599.

[46] G.P. Blanch, M.M. Caja, M.L. Ruiz del Castillo, G. Santa-María, M. Herraiz, Fractionation of plant extracts by supercritical fluid extraction and direct introduction in capillary gas chromatography using a programmable temperature vaporizer, *J. Chromatogr. Sci.* 37 (1999) 407-410.

[47] T. Madzimbamuto, C. Schwarz, J. Knoetze, Supercritical fractionation of Agathosma (buchu) essential oil. Part I: Measurement of binary phase equilibria, *J. Supercrit. Fluids* 107 (2016) 612-623.

[48] M. Zamudio, C. Schwarz, J. Knoetze, Methodology for process modelling of supercritical fluid fractionation processes illustrated for the separation of

alkane/alcohol isomer mixtures using CO2, *J. Supercrit. Fluids* 104 (2015) 272-280.

[49] M.N. Varma, P.A. Deshpande, G. Madras, Synthesis of biodiesel in supercritical alcohols and supercritical carbon dioxide, *Fuel* 89 (2010) 1641-1646.

[50] J. Jung, M. Perrut, Particle design using supercritical fluids: literature and patent survey, *J. Supercrit. Fluids* 20 (2001) 179-219.

[51] O. Guney, A. Akgerman, Synthesis of controlled-release products in supercritical medium, *AIChE J.* 48 (2002) 856-866.

[52] T. Clifford, K. Bartle, Chemical reactions in supercritical fluids, *ChemInform* 27 (1996).

[53] F. Temelli, O.N. Ciftci, Developing an integrated supercritical fluid biorefinery for the processing of grains, *J. Supercrit. Fluids* 96 (2015) 77-85.

[54] E.H. Zaim, S.G. Nassab, Numerical investigation of laminar forced convection of water upwards in a narrow annulus at supercritical pressure, *Energy* 35 (2010) 4172-4177.

[55] L. Leung, M. Yetisir, W. Diamond, D. Martin, J. Pencer, B. Hyland, H. Hamilton, D. Guzonas, R. Duffey, A next generation heavy water nuclear reactor with supercritical water as coolant, (2011).

[56] C. Schwarz, I. Nieuwoudt, J. Knoetze, Phase equilibria of long chain n-alkanes in supercritical ethane: review, measurements and prediction, *J. Supercrit. Fluids* 46 (2008) 226-232.

[57] C. Schwarz, G. Bonthuys, R. Van Schalkwyk, D. Laubscher, A. Burger, J. Knoetze, Separation of alkanes and alcohols with supercritical fluids. Part II. Influence of process parameters and size of operating range, *J. Supercrit. Fluids* 58 (2011) 352-359.

[58] B.A.S. Machado, C.G. Pereira, S.B. Nunes, F.F. Padilha, M.A. Umsza-Guez, Supercritical fluid extraction using CO2: main applications and future perspectives, *Sep. Sci. Technol.* 48 (2013) 2741-2760.

[59] A.A. Clifford, *Introduction to supercritical fluid extraction in analytical science*, in: E.D. Ramsey (Ed.) Analytical supercritical fluid extraction techniques, Springer Science & Business Media, UK, 2012.

[60] K.E. Laintz, C.M. Wai, C.R. Yonker, R.D. Smith, Extraction of metal Ions from liquid and solid materials by supercritical carbon dioxide, *Anal. Chem.* 64 (1992) 2875-2878.

[61] C.M. Wai, Supercritical fluid extraction of trace metals from solid and liquid materials for analytical applications, *Anal. Sci.* 11 (1995) 165-167.

[62] M. Haruki, F. Kobayashi, M. Okamoto, S.-i. Kihara, S. Takishima, Solubility of β-diketonate complexes for cobalt(III) and chromium(III) in supercritical carbon dioxide, *Fluid Phase Equilib.* 297 (2010) 155-161.

[63] C.M. Wai, S. Wang, Supercritical fluid extraction: metals as complexes, *J. Chromatogr. A* 785 (1997) 369-383.

[64] C. Erkey, Supercritical carbon dioxide extraction of metals from aqueous solutions: a review, *J. Supercrit. Fluids* 17 (2000) 259-287.

[65] R.B. Gupta, J.-J. Shim, *Solubility in supercritical carbon dioxide*, First ed., CRC Press, Boca Raton, Florida, 2006.

[66] J.H. Hildebrand, R.L. Scott, *Regular solutions*, Prentice-Hall, Englewood Cliffs, New Jersey, 1962.

[67] S.R. Allada, Solubility parameters of supercritical fluids, *Ind. En.g Chem. Process. Des. Dev.* 23 (1984) 344-348.

[68] J.C. Giddings, M.N. Myers, L. McLaren, R.A. Keller, High pressure gas chromatography of nonvolatile species, *Science* 162 (1968) 67-73.

[69] M. Saito, Y. Yamauchi, T. Okuyama, *Fractionation by packed-column SFC and SFE: Principles and applications*, VCH Publisher, Inc. USA, 1994.

[70] M. Škerget, Z. Knez, M.a. Knez-Hrnčič, Solubility of solids in sub-and supercritical fluids: a review, *J. Chem. Eng. Data* 56 (2011) 694-719.

[71] R. Dohrn, G. Brunner, High-pressure fluid-phase equilibria: experimental methods and systems investigated (1988–1993), *Fluid Phase Equilib.* 106 (1995) 213-282.

[72] M. Christov, R. Dohrn, High-pressure fluid phase equilibria: experimental methods and systems investigated (1994–1999), *Fluid Phase Equilib.* 202 (2002) 153-218.

[73] R. Dohrn, S. Peper, J.M. Fonseca, High-pressure fluid-phase equilibria: experimental methods and systems investigated (2000–2004), *Fluid Phase Equilib.* 288 (2010) 1-54.

[74] H. Franken, J. Knoetze, C. Schwarz, High-pressure binary phase equilibria, density and dynamic viscosity of 100 & 200 cSt polydimethylsiloxane (PDMS) with supercritical CO 2, *J. Supercrit. Fluids* (2018).

[75] C. Schwarz, Q. Paulse, J. Knoetze, Phase equilibria of methyl esters in supercritical propane, *J. Supercrit. Fluids* 99 (2015) 61-67.

[76] B. Wenclawiak, F. Bickmann, Fluid and supercritical CO2 as eluent in metal chelate chromatography, *Fresenius. J. Anal. Chem.* 319 (1984) 305-305.

[77] R.D. Smith, C.R. Yonker, J.L. Fulton, J.M. Tingey, Organized molecular assemblies in supercritical fluids; metal ion chelates and reverse micelles, *J. Supercrit. Fluids* 1 (1988) 7-14.

[78] K. Laintz, C. Wai, C. Yonker, R. Smith, Solubility of fluorinated metal diethyldithiocarbamates in supercritical carbon dioxide, *J. Supercrit. Fluids* 4 (1991) 194-198.

[79] Y. Meguro, S. Iso, T. Sasaki, Z. Yoshida, Solubility of organophosphorus metal extractants in supercritical carbon dioxide, *Anal. Chem.* 70 (1998) 774-779.

[80] S.H. Page, S.R. Sumpter, S.R. Goates, M.L. Lee, D.J. Dixon, K.P. Johnston, Tri-n-butylphosphate/CO2 and acetone/CO2 phase behaviors and utilities in capillary supercritical-fluid chromatography, *J. Supercrit. Fluids* 6 (1993) 95-101.

[81] Y. Lin, N.G. Smart, C.M. Wai, Supercritical fluid extraction of uranium and thorium from nitric acid solutions with organophosphorus reagents, *Environ. Sci. Technol.* 29 (1995) 2706-2708.

[82] W.J. Schmitt, R.C. Reid, The solubility of paraffinic hydrocarbons and their derivatives in supercritical carbon dioxide, *Chem. Eng. Commun.* 64 (1988) 155-176.

[83] N.G. Smart, T.E. Carleson, S. Elshani, S. Wang, C.M. Wai, Extraction of toxic heavy metals using supercritical fluid carbon dioxide containing organophosphorus reagents, *Ind. Eng. Chem. Res.* 36 (1997) 1819-1826.

[84] S. Wang, S. Elshani, C. Wai, Selective extraction of mercury with ionizable crown ethers in supercritical carbon dioxide, *Anal. Chem.* 67 (1995) 919-923.

[85] W. Wu, J. Zhang, B. Han, J. Chen, Z. Liu, T. Jiang, J. He, W. Li, Solubility of room-temperature ionic liquid in supercritical CO 2 with and without organic compounds, *Chem. Commun.* (2003) 1412-1413.

[86] W. Wu, W. Li, B. Han, T. Jiang, D. Shen, Z. Zhang, D. Sun, B. Wang, Effect of organic cosolvents on the solubility of ionic liquids in supercritical CO2, *J. Chem. Eng. Data* 49 (2004) 1597-1601.

[87] J.P. Coelho, G.P. Naydenov, D.S. Yankov, R.P. Stateva, Experimental measurements and correlation of the solubility of three primary amides in supercritical CO2: acetanilide, propanamide, and butanamide, *J. Chem. Eng. Data* 58 (2013) 2110-2115.

[88] S.-Y. Huang, M. Tang, S.L. Ho, Y.-P. Chen, Solubilities of N-phenylacetamide, 2-methyl-N-phenylacetamide and 4-methyl-N-phenylacetamide in supercritical carbon dioxide, *J. Supercrit. Fluids* 42 (2007) 165-171.

[89] H.S. Yeoh, G.H. Chong, N.M. Azahan, R.A. Rahman, T.S.Y. Choong, Solubility measurement method and mathematical modeling in supercritical fluids, *Eng. J.* 17 (2013) 67-78.

[90] A.N. Sarve, M.N. Varma, S.S. Sonawane, Response surface optimization and artificial neural network modeling of biodiesel production from crude mahua (Madhuca indica) oil under supercritical ethanol conditions using CO2 as co-solvent, *RSC Adv.* 5 (2015) 69702-69713.

[91] S.K. Jha, G. Madras, Neural network modeling of adsorption equilibria of mixtures in supercritical fluids, *Ind. Eng. Chem. Res.* 44 (2005) 7038-7041.

[92] B. Wang, Q. Li, Z. Zhang, J. Yang, Y. Liu, A new model for predicting solute solubility in supercritical fluids based on the Wilson equation, *Korean J. Chem. Eng.* 23 (2006) 131-137.

[93] S.J. Nejad, R. Mohammadikhah, H. Abolghasemi, M.A. Moosavian, M.G. Maragheh, A novel equation of state (EOS) for prediction of solute solubility in supercritical carbon dioxide: experimental determination and correlation, *Can. J. Chem. Eng.* 87 (2009) 930-938.

[94] B.E. Poling, J.M. Prausnitz, J.P. O'Connell, *The properties of gases and liquids*, Fifth ed., McGraw-Hill, New York, 2001.

[95] D.L. Sparks, R. Hernandez, L.A. Estévez, Evaluation of density-based models for the solubility of solids in supercritical carbon dioxide and formulation of a new model, *Chem. Eng. Sci.* 63 (2008) 4292-4301.

[96] R.C. Narayan, G. Madras, Solubilities of n-butyl esters in supercritical carbon dioxide, *J. Chem. Eng. Data* 59 (2014) 3329-3334.

[97] V.M. Rathnam, G. Madras, Experimental determination and development of solution theory based model for the mixture solubilities of 10-undecenoic acid with methyl 10-undecenoate and methyl ricinoleate in supercritical carbon dioxide, *J. Supercrit. Fluids* (2018).

[98] C. Garlapati, G. Madras, New empirical expressions to correlate solubilities of solids in supercritical carbon dioxide, *Thermochim. Acta* 500 (2010) 123-127.

[99] S.N. Reddy, G. Madras, Solubilities of resorcinol and pyrocatechol and their mixture in supercritical carbon dioxide, *Thermochim. Acta* 521 (2011) 41-48.

[100] S.N. Reddy, G. Madras, An association and Wilson activity coefficient model for solubilities of aromatic solid pollutants in supercritical carbon dioxide, *Thermochim. Acta* 541 (2012) 49-56.

[101] J. Chrastil, Solubility of Solids and Liquids in Supercritical Gases, *J. Phys. Chem.* 86 (1982) 3016-3021.

[102] K.D. Bartle, A.A. Clifford, S.A. Jafar, G.F. Shilstone, Solubilities of solids and liquids of low volatility in supercritical carbon dioxide, *J. Phys. Chem. Ref. Data* 20 (1991) 713-757.

[103] J. Mendez-Santiago, A.S. Teja, Solubility of solids in supercritical fluids: consistency of data and a new model for cosolvent systems, *Ind. Eng. Chem. Res.* 39 (2000) 4767-4771.

[104] J.M.D. Valle, J.M. Aguilera, An improved equation for predicting the solubility of vegetable oils in supercritical carbon dioxide, *Ind. Eng. Chem. Res.* 27 (1988) 1551-1553.

[105] C. Garlapati, G. Madras, Solubilities of solids in supercritical fluids using dimensionally consistent modified solvate complex models, *Fluid Phase Equilib.* 283 (2009) 97-101.

[106] N. Lamba, R.C. Narayan, J. Raval, J. Modak, G. Madras, Experimental solubilities of two lipid derivatives in supercritical carbon dioxide and new correlations based on activity coefficient models, *RSC Adv.* 6 (2016) 17772-17781.

[107] G. Burgos-Solórzano, J. Brennecke, M. Stadtherr, Solubility measurements and modeling of molecules of biological and pharmaceutical interest with supercritical CO2, *Fluid Phase Equilib.* 220 (2004) 55-67.

[108] K. Keshmiri, A. Vatanara, Y. Yamini, Development and evaluation of a new semi-empirical model for correlation of drug solubility in supercritical CO2, *Fluid Phase Equilib.* 363 (2014) 18-26.

[109] C.S. Su, Y.P. Chen, Correlation for the solubilities of pharmaceutical compounds in supercritical carbon dioxide, *Fluid Phase Equilib.* 254 (2007) 167-173.

[110] R. Ch, G. Madras, An association model for the solubilities of pharmaceuticals in supercritical carbon dioxide, *Thermochim. Acta* 507 (2010) 99-105.

[111] A.Z. Hezave, M. Lashkarbolooki, A new simple correlation for calculating solubility of drugs in supercritical carbon dioxide, *Journal of Theoretical and Computational Chemistry* 12 (2013) 1350062.

[112] S.N. Reddy, G. Madras, Modeling of ternary solubilities of solids in supercritical carbon dioxide in the presence of cosolvents or cosolutes, *J. Supercrit. Fluids* 63 (2012) 105-114.

[113] S.N. Reddy, G. Madras, A new semi-empirical model for correlating the solubilities of solids in supercritical carbon dioxide with cosolvents, *Fluid Phase Equilib.* 310 (2011) 207-212.

[114] C. Garlapati, G. Madras, Solubilities of hexadecanoic and octadecanoic acids in supercritical CO2 with and without cosolvents, *J. Chem. Eng. Data* 53 (2008) 2913-2917.

[115] C. Garlapati, G. Madras, Solubilities of dodecanoic and tetradecanoic acids in supercritical CO2 with and without entrainers, *J. Chem. Eng. Data* 53 (2008) 2637-2641.

[116] J.C. González, M.R. Vieytes, A.M. Botana, J.M. Vieites, L.M. Botana, Modified mass action law-based model to correlate the solubility of solids and liquids in entrained supercritical carbon dioxide, *J. Chromatogr. A* 910 (2001) 119-125.

[117] X. Ding, Q. Liu, X. Hou, T. Fang, Supercritical Fluid Extraction of Metal Chelate: A Review, *Crit. Rev. Anal. Chem.* 47 (2017) 99-118.

[118] C. Wai, S. Wang, J.-J. Yu, Solubility parameters and solubilities of metal dithiocarbamates in supercritical carbon dioxide, *Anal. Chem.* 68 (1996) 3516-3519.

[119] Y. Lin, C. Wai, Supercritical fluid extraction of lanthanides with fluorinated. beta.-diketones and tributyl phosphate, *Anal. Chem.* 66 (1994) 1971-1975.

[120] R. M'hamdi, J. Bocquet, K. Chhor, C. Pommier, Solubility and decomposition studies on metal chelates in supercritical fluids for ceramic precursor powders synthesis, *J. Supercrit. Fluids* 5 (1992) 55-59.

[121] A.F. Lagalante, B.N. Hansen, T.J. Bruno, R.E. Sievers, Solubilities of copper (II) and chromium (III). beta.-diketonates in supercritical carbon dioxide, *Inorg. Chem.* 34 (1995) 5781-5785.

[122] Y. Lin, C. Liu, H. Wu, H. Yak, C.M. Wai, Supercritical fluid extraction of toxic heavy metals and uranium from acidic solutions with sulfur-containing organophosphorus reagents, *Ind. Eng. Chem. Res.* 42 (2003) 1400-1405.

[123] J.S. Wang, C.M. Wai, Dissolution of precious metals in supercritical carbon dioxide, *Ind. Eng. Chem. Res.* 44 (2005) 922-926.

[124] J. Sunarso, S. Ismadji, Decontamination of hazardous substances from solid matrices and liquids using supercritical fluids extraction: a review, *J. Hazard. Mater.* 161 (2009) 1-20.

[125] F. Lin, D. Liu, S. Maiti Das, N. Prempeh, Y. Hua, J. Lu, Recent progress in heavy metal extraction by supercritical CO2 fluids, *Ind. Eng. Chem. Res.* 53 (2014) 1866-1877.

[126] K.E. Laintz, E. Tachikaw, Extraction of lanthanides from acidic solution using tributyl phosphate modified supercritical carbon dioxide, *Anal. Chem.* 66 (1994) 2190-2193.

[127] O. Tomioka, Y. Enokida, I. Yamamoto, Solvent extraction of lanthanides from their oxides with TBP in supercritical carbon dioxide, *J. Nucl. Sci. Technol.* 35 (1998) 515-516.

[128] L. Sinclair, J. Tester, J. Thompson, R. Fox, The role of water in extraction and separation of rare earth elements in supercritical carbon dioxide, *J. Supercrit. Fluids* 136 (2018) 180-188.

[129] R. Shimizu, K. Sawada, Y. Enokida, I. Yamamoto, Supercritical fluid extraction of rare earth elements from luminescent material in waste fluorescent lamps, *J. Supercrit. Fluids* 33 (2005) 235-241.

[130] T. Vincent, M. Mukhopadhyay, P. Wattal, Direct in situ supercritical fluid extraction of neodymium ion from its oxide using thenoyl tri fluoro acetone–tri butyl phosphate–methanol in carbon dioxide, *J. Supercrit. Fluids* 48 (2009) 230-237.

[131] R.V. Fox, R.D. Ball, P.d.B. Harrington, H.W. Rollins, J.J. Jolley, C.M. Wai, Praseodymium nitrate and neodymium nitrate complexation with organophosphorus reagents in supercritical carbon dioxide solvent, *J. Supercrit. Fluids* 31 (2004) 273-286.

[132] S.N. Joung, S.J. Yoon, S.Y. Kim, K.-P. Yoo, Extraction of lanthanide ions from aqueous solution by modified supercritical CO2: tri-n-butylphosphate+ CO2 and bis-2-ethylhexyl phosphoric acid+ CO2, *J. Supercrit. Fluids* 18 (2000) 157-166.

[133] Y. Lin, R.D. Brauer, K.E. Laintz, C.M. Wai, Supercritical fluid extraction of lanthanides and actinides from solid materials with a fluorinated beta-diketone, *Anal. Chem.* 65 (1993) 2549-2551.

[134] Y. Meguro, S. Iso, Z. Yoshida, Correlation between extraction equilibrium of uranium (VI) and density of CO2 medium in a HNO3/supercritical CO2-tributyl phosphate system, *Anal. Chem.* 70 (1998) 1262-1267.

[135] Y. Meguro, S. Iso, H. Takeishi, Z. Yoshida, Extraction of uranium (VI) in nitric acid solution with supercritical carbon dioxide fluid containing tributylphosphate, *Radiochim. Acta* 75 (1996) 185-191.

[136] A.A. Clifford, S. Zhu, N.G. Smart, Y. Lin, C.M. Wai, Z. Yoshida, Y. Meguro, S. Iso, Modelling of the extraction of uranium with supercritical carbon dioxide, *J. Nucl. Sci. Technol.* 38 (2001) 433-438.

[137] A. Shadrin, V. Kamachev, A. Murzin, D. Shafikov, Extraction of nitric acid and uranyl nitrate by TBP in HFC-134a, *J. Supercrit. Fluids* 42 (2007) 347-350.

[138] Y. Enokida, S.A. El-Fatah, C.M. Wai, Ultrasound-enhanced dissolution of UO2 in supercritical CO2 containing a CO2-philic complexant of tri-n-butylphosphate and nitric acid, *Ind. Eng. Chem. Res.* 41 (2002) 2282-2286.

[139] Y. Meguro, S. Iso, Z. Yoshida, O. Tomioka, Y. Enokida, I. Yamamoto, Decontamination of uranium oxides from solid wastes by supercritical CO2 fluid leaching method using HNO3–TBP complex as a reactant, *J. Supercrit. Fluids* 31 (2004) 141-147.

[140] M. Samsonov, T. Trofimov, S. Vinokurov, S. Lee, B. Myasoedov, C. Wai, Dissolution of actinide oxides in supercritical fluid carbon dioxide, containing various organic ligands, *J. Nucl. Sci. Technol.* 39 (2002) 263-266.

[141] L. Zhu, W. Duan, J. Xu, Y. Zhu, Uranium extraction from TRISO-coated fuel particles using supercritical CO2 containing tri-n-butyl phosphate, *J. Hazard. Mater.* 241 (2012) 456-462.

[142] M. Shamsipur, A.R. Ghiasvand, Y. Yamini, Extraction of uranium from solid matrices using modified supercritical fluid CO2, *J. Supercrit. Fluids* 20 (2001) 163-169.

[143] T. Shimada, S. Ogumo, N. Ishihara, Y. Kosaka, Y. Mori, A study on the technique of spent fuel reprocessing with supercritical fluid direct extraction method (Super-DIREX method), *J. Nucl. Sci. Technol.* 39 (2002) 757-760.

[144] A. Leybros, L. Hung, A. Hertz, D. Hartmann, A. Grandjean, O. Boutin, Supercritical CO2 extraction of uranium from natural ore using organophosphorus extractants, *Chem. Eng. J.* 316 (2017) 196-203.

[145] B.J. Mincher, R.V. Fox, R.G.G. Holmes, R.A. Robbins, C. Boardman, Supercritical fluid extraction of plutonium and americium from soil using thenoyl trifluoroacetone and tributylphosphate complexation, *Radiochim. Acta* 89 (2001) 613-617.

[146] R. Kumar, N. Sivaraman, E.S. Vadivu, T.G. Srinivasan, P.R.Vasudeva Rao, Complete removal of uranyl nitrate from tissue matrix using supercritical fluid extraction, *Radiochim. Acta* 91 (2003) 197-201.

[147] R. Kumar, N. Sivaraman, K. Sujatha, T.G. Srinivasan, P.R.V. Rao, Removal of plutonium and americium from waste matrices by supercritical carbon dioxide extraction, *Radiochim. Acta* 95 (2007) 577-584.

[148] K. Sujatha, K.C. Pitchaiah, N.Sivaraman, T.G.Srinivasan, P.R.V. Rao, Recovery of uranium and plutonium from waste matrices using supercritical fluid extraction, *Am. J. Anal. Chem* 3 (2012) 916-922.

[149] K. Sujatha, K.C. Pitchaiah, N. Sivaraman, K. Nagarajan, T.G. Srinivasan, P.R.V. Rao, Recovery of plutonium from polymeric waste matrices using supercritical fluid extraction, *Desalin. Water Treat.* 52 (2013) 470-475.

[150] D.L. Quach, B.J. Mincher, C.M. Wai, Supercritical fluid extraction and separation of uranium from other actinides, *J. Hazard. Mater.* 274 (2014) 360-366.

[151] A. Rao, P. Kumar, K. Ramakumar, Study of effects of different parameters on supercritical fluid extraction of uranium from acidic solutions employing TBP as co-solvent, *Radiochim. Acta* 96 (2008) 787-798.

[152] P. Kumar, A. Rao, K. Ramakumar, Supercritical fluid extraction of thorium from tissue paper matrix employing β-diketones, *Radiochim. Acta* 97 (2009) 105-112.

[153] A. Rao, P. Kumar, B. Tomar, Supercritical fluid extraction of uranium and thorium employing dialkyl amides, *Sep. Purif. Technol.* 134 (2014) 126-131.

[154] A. Rao, N.V. Rathod, D.D. Malkhede, V.V. Raut, K. Ramakumar, Supercritical carbon dioxide extraction of uranium from acidic medium employing calixarenes, *Sep. Sci. Technol.* 48 (2013) 644-651.

[155] A. Suresh, T.G. Srinivasan, P.R.V. Rao, Extraction of U(VI), Pu(IV) and Th(IV) by some trialkyl phosphates, *Solvent Extr. Ion Exch.* 12 (1994) 727-744.

[156] A. Suresh, T.G. Srinivasan, P.R.V. Rao, The effect of the structure of trialkyl phosphates on their physicochemical properties and extraction behavior, *Solvent Extr. Ion Exch.* 27 (2009) 258-294.

[157] B. Sreenivasulu, A. Suresh, S. Subramaniam, K.N. Sabharwal, N. Sivaraman, K. Nagarajan, T.G. Srinivasan, P.R.V. Rao, Separation of U(VI) and Pu(IV) from Am(III) and trivalent lanthanides with tri-iso-amyl phosphate (TiAP) as the extractant by using an ejector mixer-settler, *Solvent Extr. Ion Exch.* 33 (2015) 120-133.

[158] P.R.V. Rao, Extraction of actinides by trialkly phosphates, *Miner. Process. Extr. Metall. Rev.* 18 (1998) 309-331.

[159] H.A.C. Mckay, J.H. Miles, J.L. Swanson, *The purex process*, in: W.W. Schulz, L.L. Burger, J.D. Navratil (Eds.) Science and technology of tributyl phosphate, CRC Press, Boca Raton, Florida, USA, 1990, pp. 1-9.

[160] W.D. Bond, *The Thorex process*, in: W.W. Schulz, L.L. Burger, J.D. Navratil (Eds.) Science and technology of tributyl phosphate, CRC Press, Boca Raton, Florida, USA, 1990, pp. 225-247.

[161] L.L. Burger, Uranium and plutonium extraction by organophosphorus compounds, *J. Phys. Chem.* 62 (1958) 590-593.

[162] D.C. Madigan, R.W. Cattrall, The extraction of thorium from nitrate solution by dibutyl butyl phosphonate, *J. Inorg. Nucl. Chem.* 21 (1961) 334-338.

[163] B.J. Mincher, L.R. Martin, N.C. Schmitt, Diamylamylphosphonate solvent extraction of Am (VI) from nuclear fuel raffinate simulant solution, *Solvent Extr. Ion Exch.* 30 (2012) 445-456.

[164] C.V.S.B. Rao, T.G. Srinivasan, P.R.V. Rao, Studies on the extraction of actinides by diamylamyl phosphonate, *Solvent Extr. Ion Exch.* 25 (2007) 771-789.

[165] C.V.S.B. Rao, T.G. Srinivasan, P.R.V. Rao, Studies on the extraction of actinides by dibutylbutyl phosphonate, *Solvent Extr. Ion Exch.* 28 (2010) 202-224.

[166] C.V.S.B. Rao, T.G. Srinivasan, P.R.V. Rao, Studies on the extraction of actinides by substituted butyl phosphonates, *Solvent Extr. Ion Exch.* 30 (2012) 262-277.

[167] V. Manchanda, P. Pathak, A.K. Rao, Di (2-Ethylhexyl) Pivalamide (D2EHPVA): A Promising Extractant for Selective Removal of Uranium from High Level Nuclear Waste Solutions, *Solvent Extr. Ion Exch.* 22 (2004) 353-375.

[168] J. Mathur, P. Ruikar, M.B. Krishna, M. Murali, M. Nagar, R. Iyer, Extraction of Np (IV), Np (VI), Pu (IV) and U (VI) with amides, BEHSO and CMPO from nitric acid medium, *Radiochim. Acta* 73 (1996) 199-206.

[169] P. Pathak, L. Kumbhare, V. Manchanda, Structural effects in N, N-dialkyl amides on their extraction behavior toward uranium and thorium, *Solvent Extr. Ion Exch.* 19 (2001) 105-126.

[170] N. Condamines, C. Musikas, The extraction by NN-dialkylamides. II. Extraction of actinide cations, *Solvent Extr. Ion Exch.* 10 (1992) 69-100.

[171] R.L. Stevenson, P.E. Smith, *Fuel reprocessing*, in: S.M. Stoller, R.B. Richards (Eds.) Reactor Handbook, Interscience Publication, New York, 1961.

[172] P.N. Pathak, N,N-Dialkyl amides as extractants for spent fuel reprocessing: an overview, *J. Radioanal. Nucl. Chem.* 300 (2014) 7-15.

[173] A. Rao, B. Tomar, Extraction of thorium employing N, N-dialkyl amide into room temperature ionic liquid followed by supercritical carbon dioxide stripping, *Sep. Purif. Technol.* 161 (2016) 159-164.

[174] V.A. Volkovich, T.R. Griffiths, R.C. Thied, Treatment of molten salt wastes by phosphate precipitation: removal of fission product elements after pyrochemical reprocessing of spent nuclear fuels in chloride melts, *J. Nucl. Mater.* 323 (2003) 49-56.

[175] L. Gray, H. Holcomb, *Recovery of plutonium from molten salt extraction residues*, in, Du Pont de Nemours (EI) and Co., Aiken, SC (USA). Savannah River Plant, 1983.

[176] M.T. Harrison, H.E. Simms, A. Jackson, R.G. Lewin, Salt waste treatment from a LiCl-KCl based pyrochemical spent fuel treatment process, *Radiochim. Acta* 96 (2008) 295-301.

[177] V. Manchanda, P. Pathak, Amides and diamides as promising extractants in the back end of the nuclear fuel cycle: an overview, *Sep. Purif. Technol.* 35 (2004) 85-103.

[178] T. Subramanian, B.P. Reddy, P. Venkatesh, R. Kandan, T. Vandarkuzhali, K. Nagarajan, P.V. Rao, *Studies on the head-end steps for pyrochemical reprocessing of oxide fuels*, in: Proceedings of the Workshop on Pyrochemical Separations, Avignon, France, 2000, pp. 187.

[179] G.M. Kosolapoff, Isomerization of alkylphosphites. III. The synthesis of n-alkylphosphonic acids, *J. Am. Chem. Soc.* 67 (1945) 1180-1182.

[180] E. Coulson, W. Gerrard, H. Hudson, 434. Factors in the formation of isomerically and optically pure alkyl halides. Part IV. The three dealkylation steps in phosphorus trihalide (Cl, Br, I)–alcohol systems, *J. Chem. Soc.* (1965) 2364-2369.

[181] K. Aim, M. Fermeglia, *Solubility of solids and liquids in supercritical fluids*, in: G.H. Hefter, R.P.T. Tomkins (Eds.) The Experimental Determination of Solubilities, John Wiley, Chichester, 2003, pp. 493–555.

[182] D.E. Knox, Solubilities in supercritical fluids, *Pure Appl. Chem.* 77 (2005) 513-530.

[183] H.-D. Sung, J.-J. Shim, Solubility of CI disperse red 60 and CI disperse blue 60 in supercritical carbon dioxide, *J. Chem. Eng. Data* 44 (1999) 985-989.

[184] S. Bristow, B.Y. Shekunov, P. York, Solubility analysis of drug compounds in supercritical carbon dioxide using static and dynamic extraction systems, *Ind. Eng. Chem. Res.* 40 (2001) 1732-1739.

[185] G. Sherman, S. Shenoy, R. Weiss, C. Erkey, A static method coupled with gravimetric analysis for the determination of solubilities of solids in supercritical carbon dioxide, *Ind. Eng. Chem. Res.* 39 (2000) 846-848.

[186] C. Crampon, G. Charbit, E. Neau, High-pressure apparatus for phase equilibria studies: solubility of fatty acid esters in supercritical CO2, *J. Supercrit. Fluids* 16 (1999) 11-20.

[187] A. Hourri, J. St-Arnaud, T. Bose, Solubility of solids in supercritical fluids from the measurements of the dielectric constant: application to CO2–naphthalene, *Rev. Sci. Instrum.* 69 (1998) 2732-2737.

[188] B. Wagner, M. Nishioka, D. Tuma, M. Maiwald, G.M. Schneider, Sample purification for spectroscopic high-pressure investigations by dynamic supercritical fluid extraction, *J. Supercrit. Fluids* 16 (1999) 157-165.

[189] R. Ruivo, A. Paiva, P. Simões, Phase equilibria of the ternary system methyl oleate/squalene/carbon dioxide at high pressure conditions, *J. Supercrit. Fluids* 29 (2004) 77-85.

[190] A. Ferri, M. Banchero, L. Manna, S. Sicardi, An experimental technique for measuring high solubilities of dyes in supercritical carbon dioxide, *J. Supercrit. Fluids* 30 (2004) 41-49.

[191] N. Lamba, R.C. Narayan, J. Modak, G. Madras, Solubilities of 10-undecenoic acid and geraniol in supercritical carbon dioxide, *J. Supercrit. Fluids* 107 (2016) 384-391.

[192] C.A. Lee, M. Tang, S.L. Ho, Y.P. Chen, Solubilities of chlormezanone, metaxalone and methocarbamol in supercritical carbon dioxide, *J. Supercrit. Fluids* 85 (2014) 11-16.

[193] H.S. Ghaziaskar, M. Kaboudvand, Solubility of trioctylamine in supercritical carbon dioxide, *J. Supercrit. Fluids* 44 (2008) 148-154.

[194] V.S. Kumar, R. Kumar, N. Sivaraman, G. Ravisankar, P. Vasudeva Rao, Design and adaptation of a novel supercritical extraction facility for operation in a glove box for recovery of radioactive elements, *Rev. Sci. Instrum.* 81 (2010) 094101.

[195] A. Datta, N. Sivaraman, T.G. Srinivasan, P R Vasudeva Rao, Liquid chromatographic behavior of lanthanides and actinides on monolith supports, *Radiochim. Acta* 99 (2011) 275-283.

[196] H.E. Dobbs, Effect of naphthalene on the quenching of liquid scintillation solutions, *Nature* 197 (1963) 788.

[197] X. Bian, Z. Du, Y. Tang, An improved density-based model for the solubility of some compounds in supercritical carbon dioxide, *Thermochim. Acta* 519 (2011) 16-21.

[198] Y. Adachi, B.C.-Y. Lu, Supercritical fluid extraction with carbon dioxide and ethylene, *Fluid Phase Equilib.* 14 (1983) 147-156.

[199] R.C. Narayan, J.V. Dev, G. Madras, Experimental determination and theoretical correlation for the solubilities of dicarboxylic acid esters in supercritical carbon dioxide, *J. Supercrit. Fluids* 101 (2015) 87-94.

[200] M.D.A. Saldaña, B. Tomberli, S.E. Guigard, S. Goldman, C.G. Gray, F. Temelli, Determination of vapor pressure and solubility correlation of phenolic compounds in supercritical CO2, *J. Supercrit. Fluids* 40 (2007) 7-19.

[201] F. Temelli, Perspectives on supercritical fluid processing of fats and oils, *J. Supercrit. Fluids* 47 (2009) 583-590.

[202] K.H. Kim, Y. Kim, Theoretical studies for the supercritical CO2 solubility of organophosphorous molecules: Lewis acid-base interactions and C−H…O weak hydrogen bonding, *Bull. Korean Chem. Soc.* 28 (2007) 2454-2458.

[203] S.K. Jha, G. Madras, Modeling the solubilities of high molecular weight n-alkanes in supercritical carbon dioxide, *Fluid Phase Equilib.* 225 (2004) 59-62.

[204] R.S. Edmundson, *Dictionary of organophosphorous compounds*, Chapman and Hall Ltd, New York, London, 1988.

[205] K. Paneerselvam, M.P. Antony, T.G. Srinivasan, P.R.V. Rao, Estimation of normal boiling points of trialkyl phosphates using retention indices by gas chromatography, *Thermochim. Acta* 511 (2010) 107-111.

[206] P.R.V. Rao, Z. Kolarik, A review of third phase formation in extraction of actinides by neutral organophosphorus extractants, *Solvent Extr. Ion Exch.* 14 (1996) 955-993.

[207] K.B. Rakesh, A. Suresh, P.R.V. Rao, Extraction and stripping behaviour of tri-iso-amyl phosphate and tri-n-butyl phosphate in n-dodecane with U (VI) in nitric acid media, *Radiochim. Acta* 102 (2014) 619-628.

[208] D.K. Dandge, J.P. Heller, K.V. Wilson, Structure solubility correlations: organic compounds and dense carbon dioxide binary systems, *Ind. Eng. Chem. Prod. Res. Dev.* 24 (1985) 162-166.

[209] O.V. Prezhdo, B. Gawdzik, V.V. Zubkova, V.V. Prezhdo, Molecular structure and electrical properties of some phosphonates, phosphine-oxides and phosphates, *J. Mol. Struct.* 919 (2009) 146-153.

[210] N.R. Foster, G.S. Gurdial, J.S. Yun, K.K. Liong, K.D. Tilly, S.S. Ting, H. Singh, J.H. Lee, Significance of the crossover pressure in solid-supercritical fluid phase equilibria, *Ind. Eng. Chem. Res.* 30 (1991) 1955-1964.

[211] M. Kaboudvand, H.S. Ghaziaskar, Solubility of tridodecylamine in supercritical carbon dioxide, *J. Chem. Eng. Data* 53 (2008) 1841-1845.

[212] Z.-R. Yu, B. Singh, S.S. Rizvi, J.A. Zollweg, Solubilities of fatty acids, fatty acid esters, triglycerides, and fats and oils in supercritical carbon dioxide, *J. Supercrit. Fluids* 7 (1994) 51-59.

[213] X. Lou, H.-G. Janssen, C.A. Cramers, Temperature and pressure effects on solubility in supercritical carbon dioxide and retention in supercritical fluid chromatography, *J. Chromatogr. A* 785 (1997) 57-64.

[214] K. Ohgaki, T. Katayama, Isothermal vapor-liquid equilibrium data for binary systems containing carbon dioxide at high pressures: methanol-carbon dioxide, n-hexane-carbon dioxide, and benzene-carbon dioxide systems, *J. Chem. Eng. Data* 21 (1976) 53-55.

[215] K. Suzuki, H. Sue, M. Itou, R.L. Smith, H. Inomata, K. Arai, S. Saito, Isothermal vapor-liquid equilibrium data for binary systems at high pressures: carbon dioxide-methanol, carbon dioxide-ethanol, carbon dioxide-1-propanol, methane-ethanol, methane-1-propanol, ethane-ethanol, and ethane-1-propanol systems, *J. Chem. Eng. Data* 35 (1990) 63-66.

[216] M.V. da Silva, D. Barbosa, High pressure vapor–liquid equilibrium data for the systems carbon dioxide/2-methyl-1-propanol and carbon dioxide/3-methyl-1-butanol at 288.2, 303.2 and 313.2 K, *Fluid Phase Equilib.* 198 (2002) 229-237.

[217] Y. Koga, Y. Iwai, Y. Hata, M. Yamamoto, Y. Arai, Influence of cosolvent on solubilities of fatty acids and higher alcohols in supercritical carbon dioxide, *Fluid Phase Equilib.* 125 (1996) 115-128.

[218] E. Sahle-Demessie, U. Pillai, S. Junsophonsri, K. Levien, Solubility of organic biocides in supercritical CO2 and CO2+ cosolvent mixtures, *J. Chem. Eng. Data* 48 (2003) 541-547.

[219] S.N. Aki, J.F. Brennecke, A. Samanta, How polar are room-temperature ionic liquids?, *Chem. Commun.* (2001) 413-414.

[220] Z. Huang, S. Kawi, Y. Chiew, Solubility of cholesterol and its esters in supercritical carbon dioxide with and without cosolvents, *J. Supercrit. Fluids* 30 (2004) 25-39.

[221] S.I. Sandler, in: Chemical, biochemical, and engineering thermodynamics, Wiley , India, 2006, 477-478.

[222] P. Kletting, G. Glatting, Model selection for time-activity curves: the corrected Akaike information criterion and the F-test, *J. Med. Phys.* 19 (2009) 200-206.

[223] F. Chang, S.-H. Park, H. Kim, Highly CO2-soluble 5-Amido-8-hydroxyquinoline Chelating Agents for Extraction of Metals in Sc-CO 2, *Bull. Korean Chem. Soc.* 29 (2008) 1327-1331.

[224] T.L. Lemke, *Review of organic functional groups: introduction to medicinal organic chemistry*, Lippincott Williams & Wilkins, 2003.

[225] M. King, A. Mubarak, J. Kim, T. Bott, The mutual solubilities of water with supercritical and liquid carbon dioxides, *J. Supercrit. Fluids* 5 (1992) 296-302.

[226] E. Horwitz, A. Muscatello, D. Kalina, L. Kaplan, The extraction of selected transplutonium (III) and lanthanide (III) ions by dihexyl-N, N-diethylcarbamoylmethylphosphonate from aqueous nitrate media, *Sep. Sci. Technol.* 16 (1981) 417-437.

[227] R. Stryjek, J. Vera, PRSV: An improved Peng—Robinson equation of state for pure compounds and mixtures, *Can. J. Chem. Eng.* 64 (1986) 323-333.

[228] J.P. Guthrie, Tautomerization equilibria for phosphorous acid and its ethyl esters, free energies of formation of phosphorous and phosphonic acids and their ethyl esters, and p K a values for ionization of the P—H bond in phosphonic acid and phosphonic esters, *Can. J. Chem.* 57 (1979) 236-239.

[229] T.H. Siddall, The effects of altering alkyl substituents in trialkyl phosphates on the extraction of actinides, *J. Inorg. Nucl. Chem.* 13 (1960) 151-155.

[230] J.P. Shukla, M.M. Gautam, C.S. Kedari, S.H. Hasan, D.C. Rupainwar, Extraction of uranium (VI), plutonium (IV) and some fission products by tri-iso-amyl phosphate, *J. Radioanal. Nucl. Chem.* 219 (1997) 61-67.

[231] B. Sreenivasulu, A. Suresh, N. Sivaraman, P.R.V. Rao, Solvent extraction studies with some fission product elements from nitric acid media employing tri-iso-amyl phosphate and tri-n-butyl phosphate as extractants, *J. Radioanal. Nucl. Chem.* 303 (2015) 2165-2172.

[232] A. Rao, N.V. Rathod, D.D. Malkhede, V.V. Raut, K.L. Ramakumar, Supercritical carbon dioxide extraction of uranium from acidic medium employing calixarenes, *Sep. Sci. Technol.* 48 (2013) 644-651.

[233] R. Kumar, N. Sivaraman, K. Sujatha, T. Srinivasan, P. Vasudeva Rao, A novel technique for modifier free delivery of ligands for supercritical fluid extraction, *Radiochim. Acta* 97 (2009) 443-451.

[234] M. Li, D. Constantinescu, L. Wang, A. Mohs, J. Gmehling, Solubilities of NaCl, KCl, LiCl, and LiBr in methanol, ethanol, acetone, and mixed solvents and correlation using the LIQUAC model, *Ind. Eng. Chem. Res.* 49 (2010) 4981-4988.

[235] D. Gruen, R. McBeth, Oxidation states and complex ions of uranium in fused chlorides and nitrates, *J. Inorg. Nucl. Chem.* 9 (1959) 290-301.

[236] V. Volkovich, I. May, T. Griffiths, J. Charnock, A. Bhatt, B. Lewin, Structures of chloro-uranium species in molten LiCl–BeCl 2 eutectic: A combined X-ray and electronic absorption spectroscopy study, *J. Nucl. Mater.* 344 (2005) 100-103.

[237] T. Fujii, T. Uda, Y. Iwadate, T. Nagai, A. Uehara, H. Yamana, Raman spectroscopic study of uranyl complex in alkali chloride melts, *J. Nucl. Mater.* 440 (2013) 575-579.

Appendix-1

Characterization of ligands synthesized in the present study

In the present work, eight organophosphorous compounds were synthesized for the solubility and extraction experiments. These compounds are characterized using various techniques such as FT-IR, ^{1}H, ^{13}C, ^{31}P NMR and GC-MS. The infrared spectra of the compounds were recorded in the range 4000 to 500 cm^{-1} using a vertex 70 FT-IR with a resolution of 0.5 cm^{-1}. ^{1}H, ^{13}C, and ^{31}P NMR spectra of the compounds were recorded with BRUKER DMX-400. All ^{1}H chemical shifts were reported are relative to the residual proton resonance in deuterated solvents (298 K, $CDCl_3$). For ^{31}P NMR spectra, H_3PO_4 was used as an external standard. GC-MS analysis was carried out using Perkin-Elmer GC-MS system. The purity for synthesized compounds is ascertained by gas chromatography (GC) system. The compounds are dissolved in *n*-hexane and injected into GC system with N_2 as a carrier gas. Flame ionization detector was used to detect the compounds of interest.

1. Characterization of trialkyl phosphate

1.1 Tri-*sec*-butyl phosphate (TsBP)

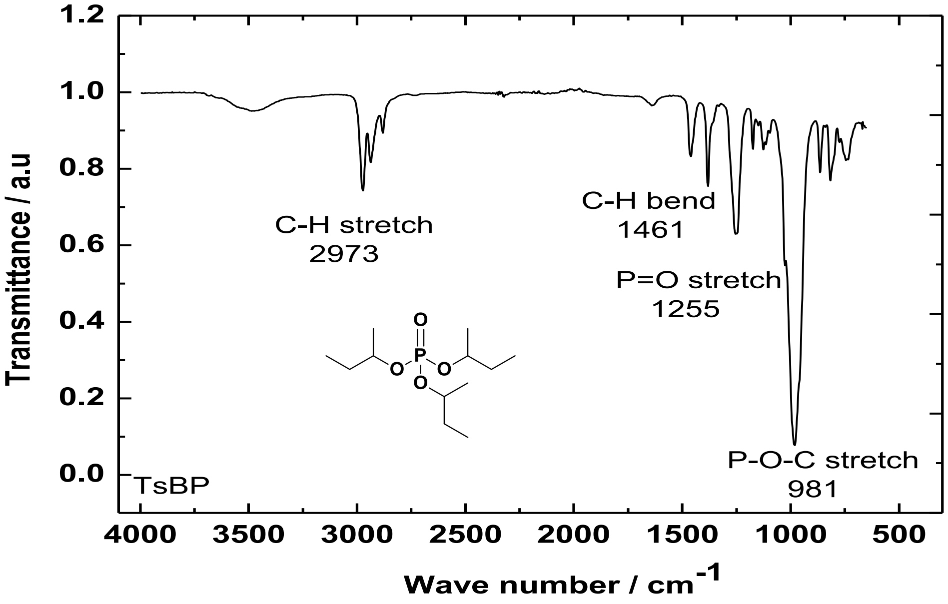

Figure 1 Infrared spectrum of TsBP

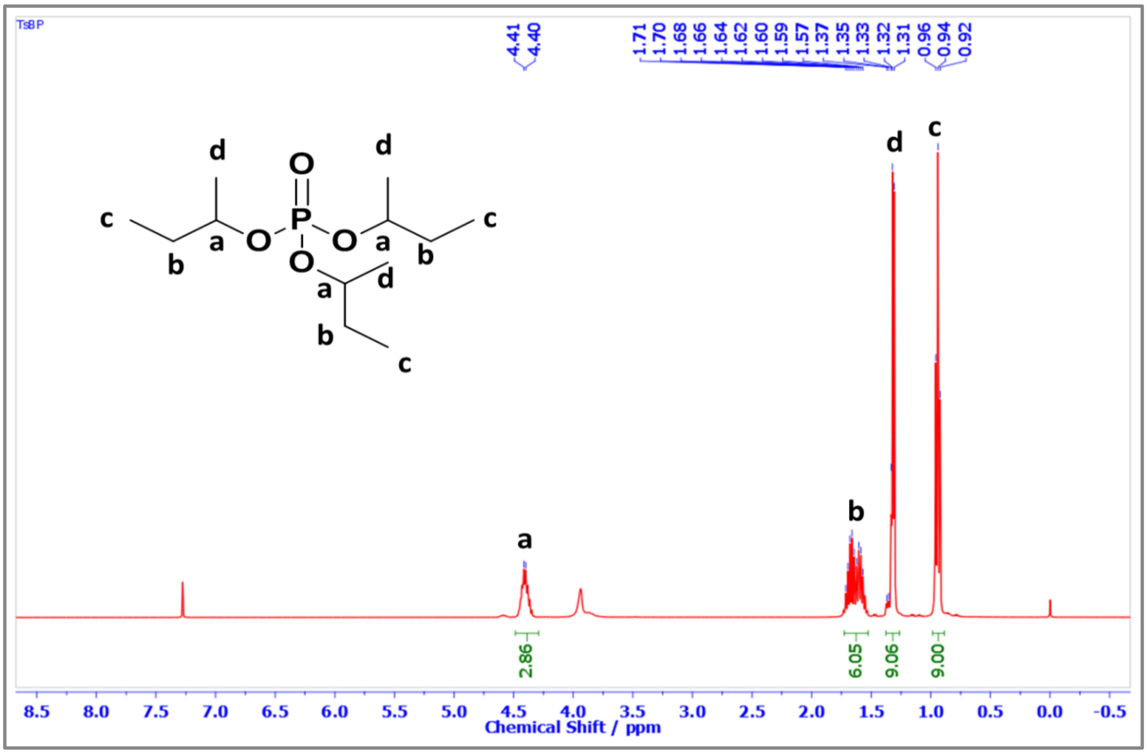

Figure 2 ^{1}H NMR of TsBP

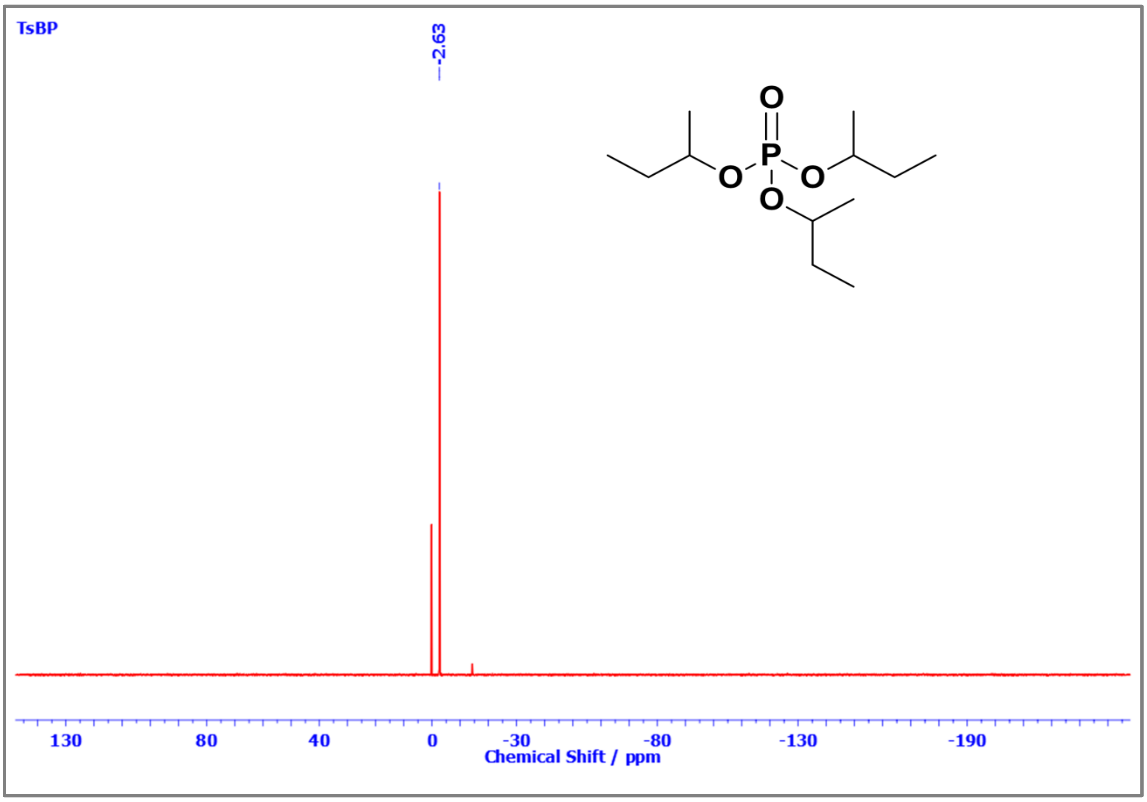

Figure 3 ^{31}P NMR of TsBP

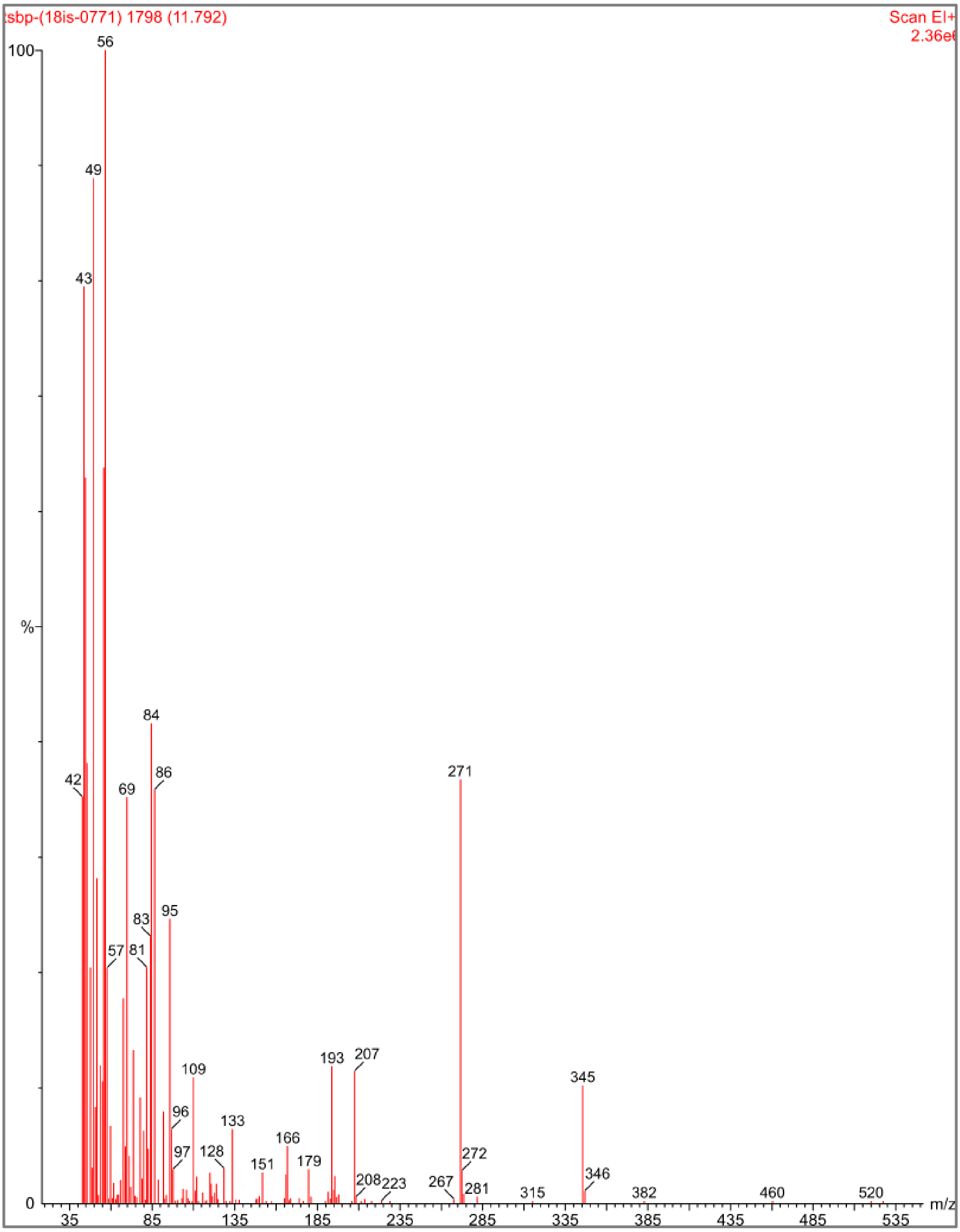

Figure 4 GC-MS spectrum of TsBP

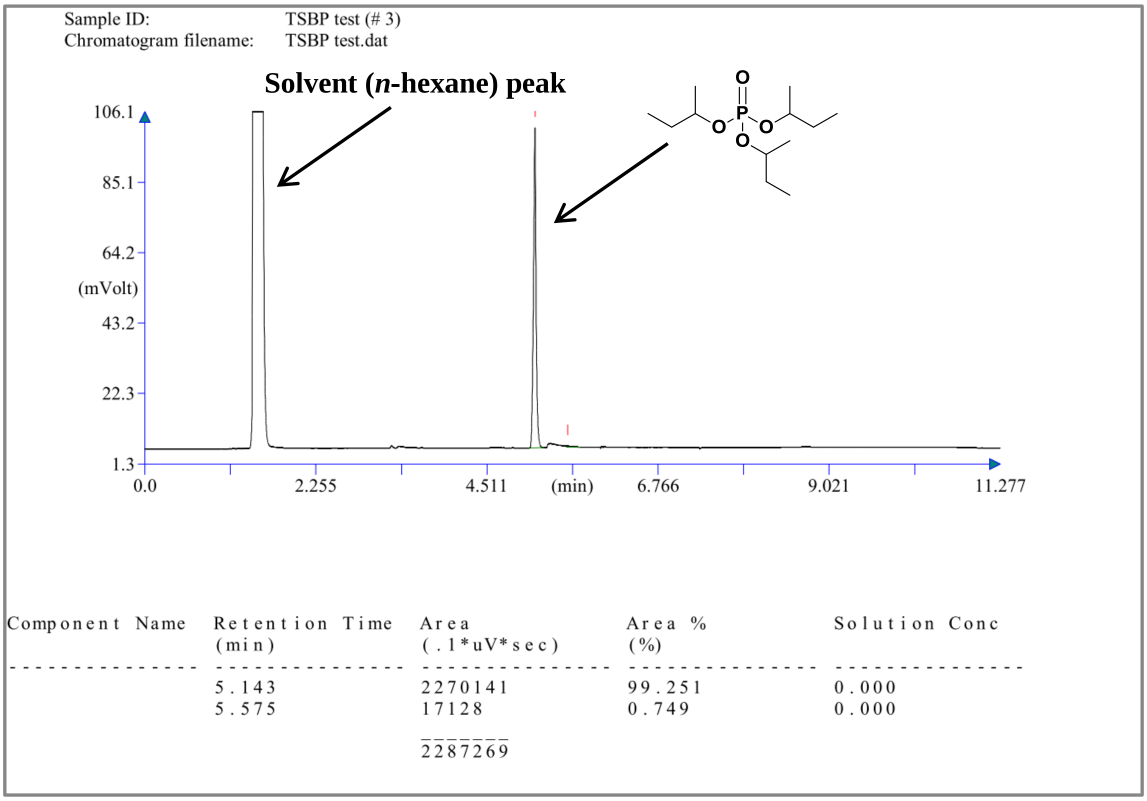

Sample ID: TSBP test (# 3)
Chromatogram filename: TSBP test.dat

```
Component Name   Retention Time   Area            Area %           Solution Conc
                 (min)            (.1*uV*sec)     (%)
---------------  ---------------  ---------------  ---------------  ---------------
                 5.143            2270141          99.251           0.000
                 5.575            17128            0.749            0.000
                                  _______
                                  2287269
```

Figure 5 Gas chromatogram and purity check for TsBP

1.2 Triamyl phosphate (TAP)

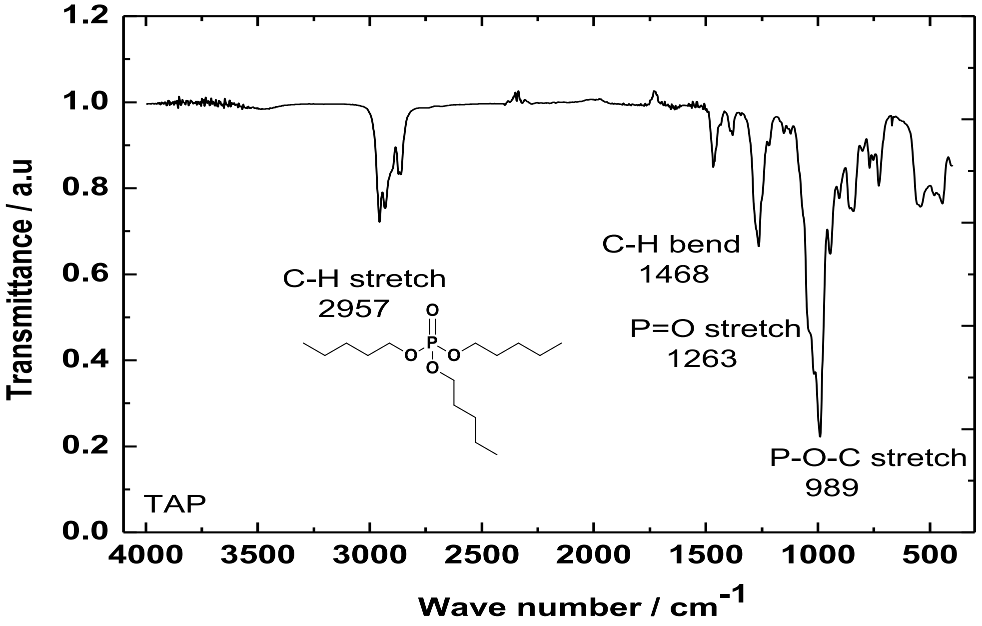

Figure 6 Infrared spectrum of TAP

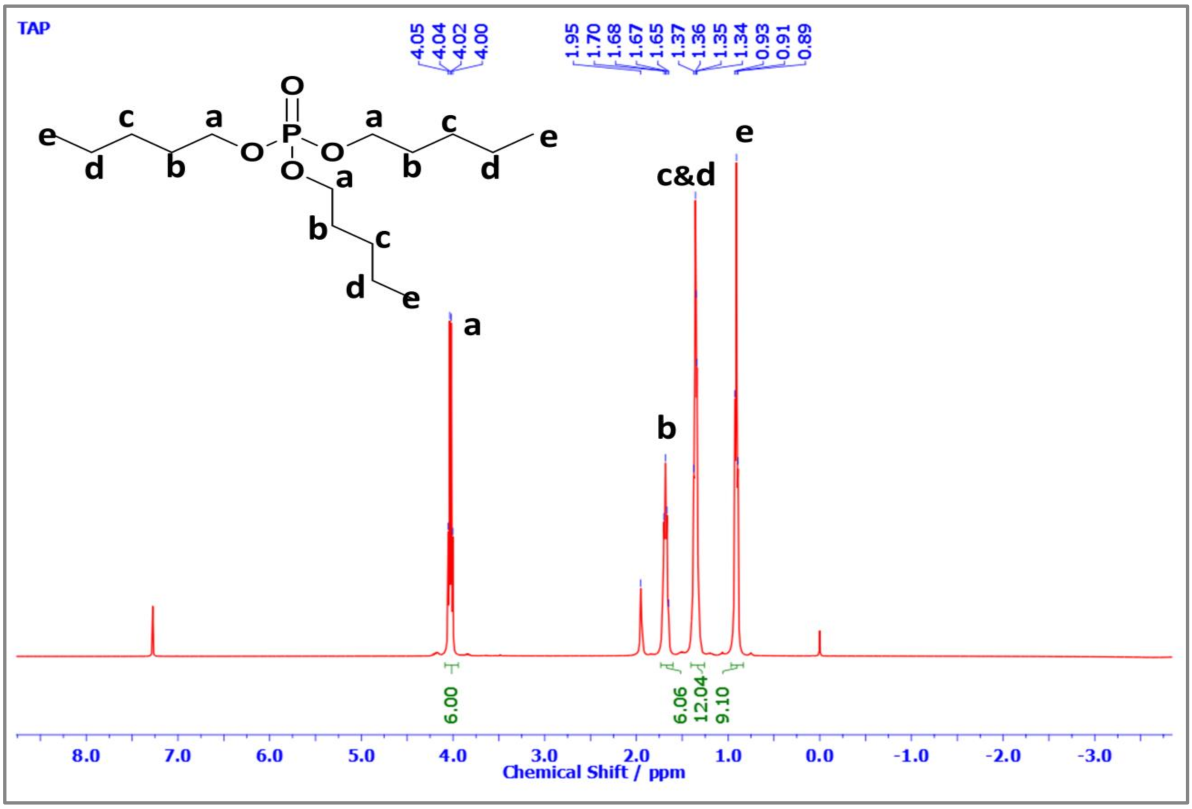

Figure 7 ^{1}H NMR of TAP

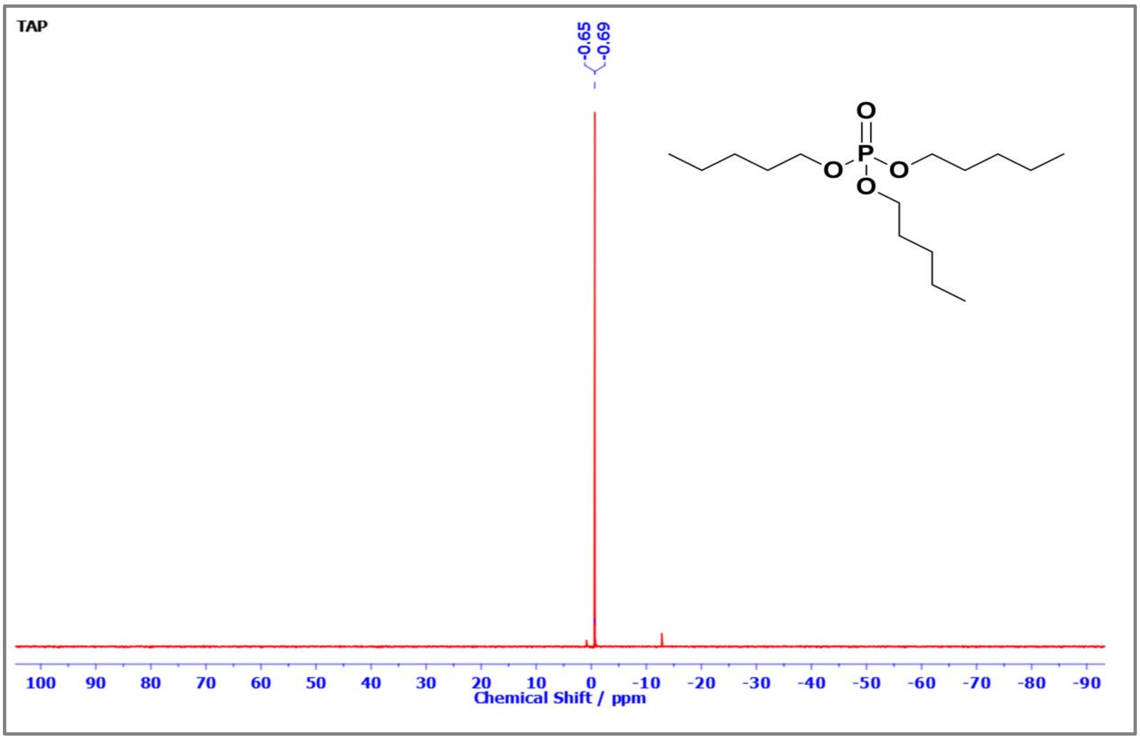

Figure 8 ^{31}P NMR of TAP

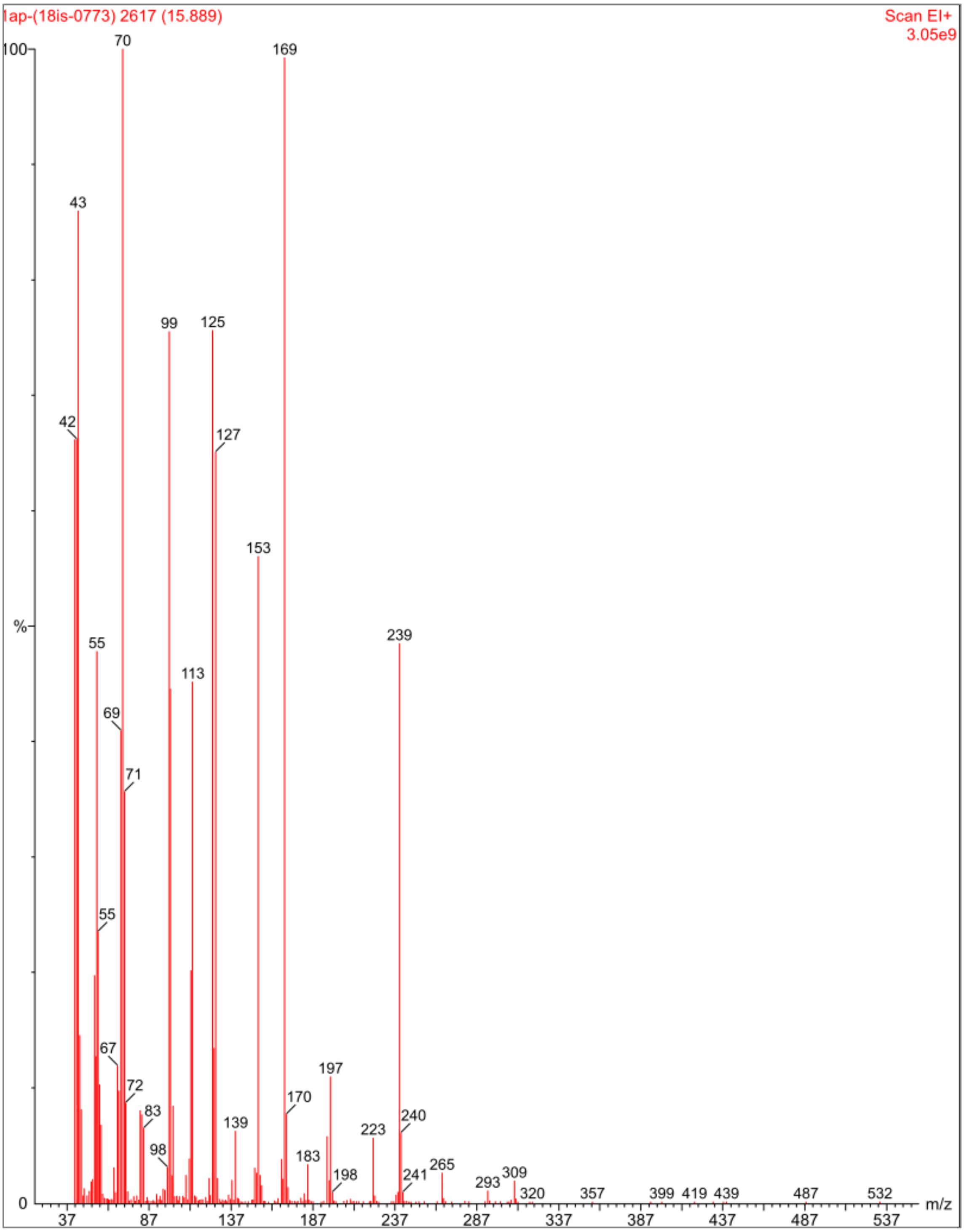

Figure 9 GC-MS spectrum of TAP

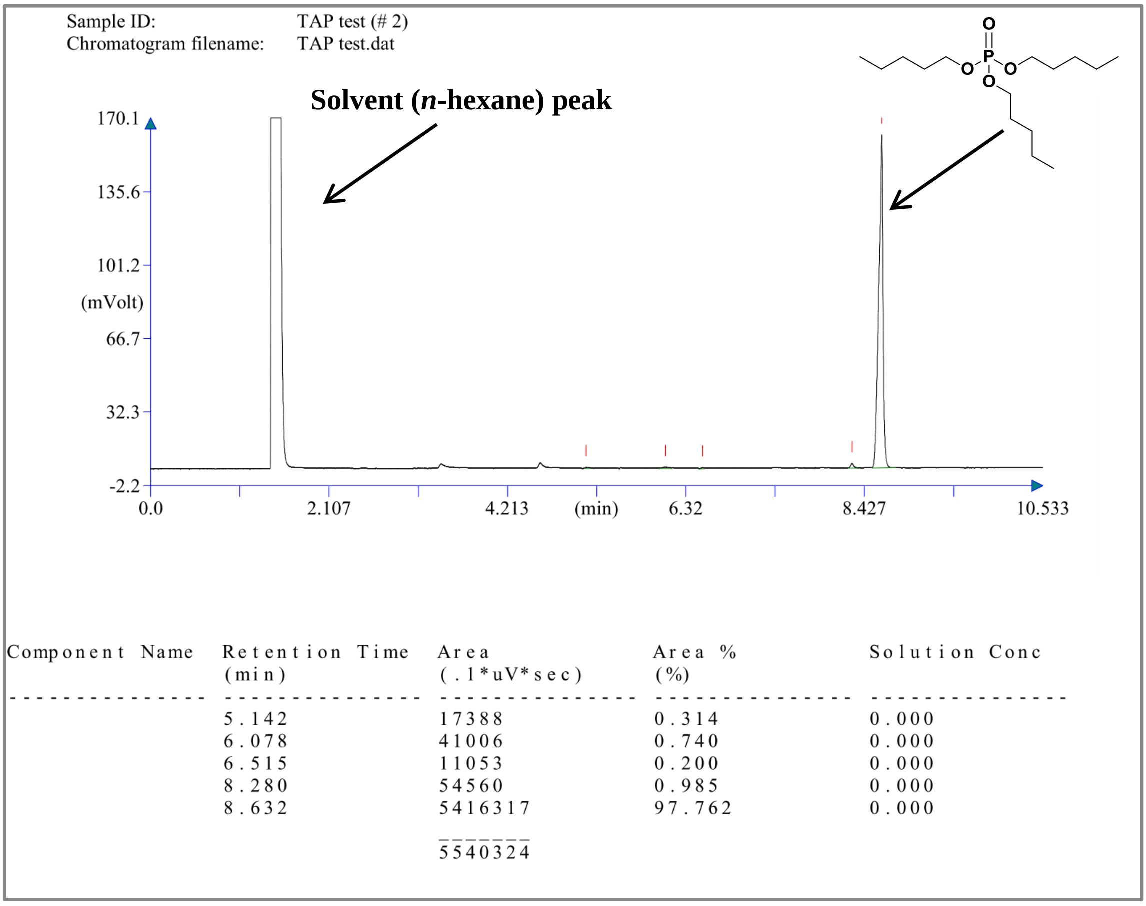

Sample ID: TAP test (# 2)
Chromatogram filename: TAP test.dat

```
Component Name   Retention Time   Area           Area %          Solution Conc
                 (min)            (.1*uV*sec)    (%)
---------------  ---------------  -------------  --------------  ---------------
                 5.142            17388          0.314           0.000
                 6.078            41006          0.740           0.000
                 6.515            11053          0.200           0.000
                 8.280            54560          0.985           0.000
                 8.632            5416317        97.762          0.000
                                  _______
                                  5540324
```

Figure 10 Gas chromatogram and purity check for TAP

1.3 Tri-*iso*-amyl phosphate (TiAP)

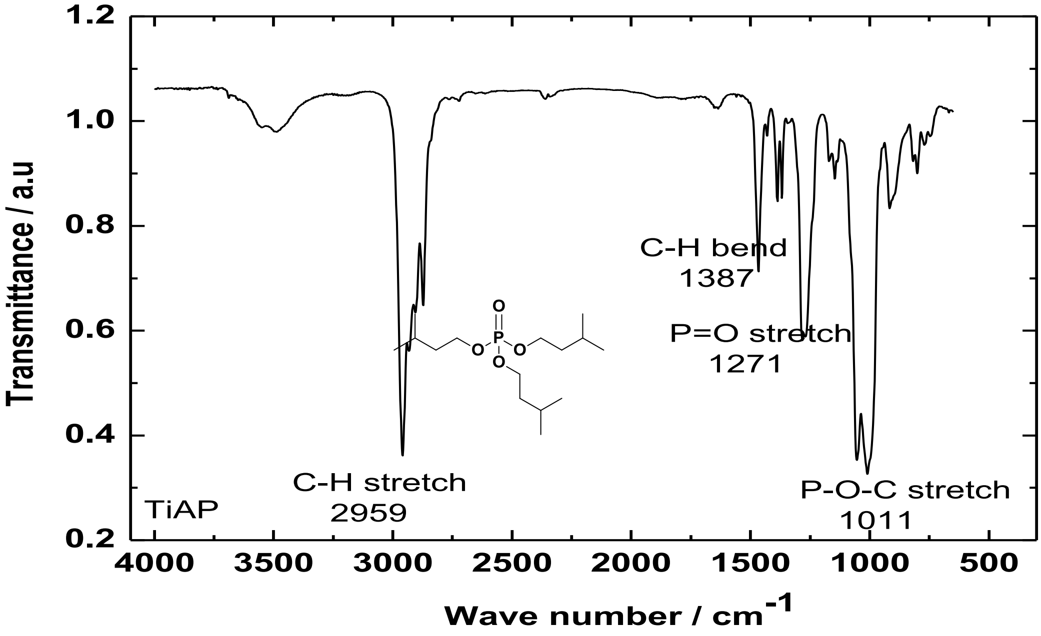

Figure 11 Infrared spectrum of TiAP

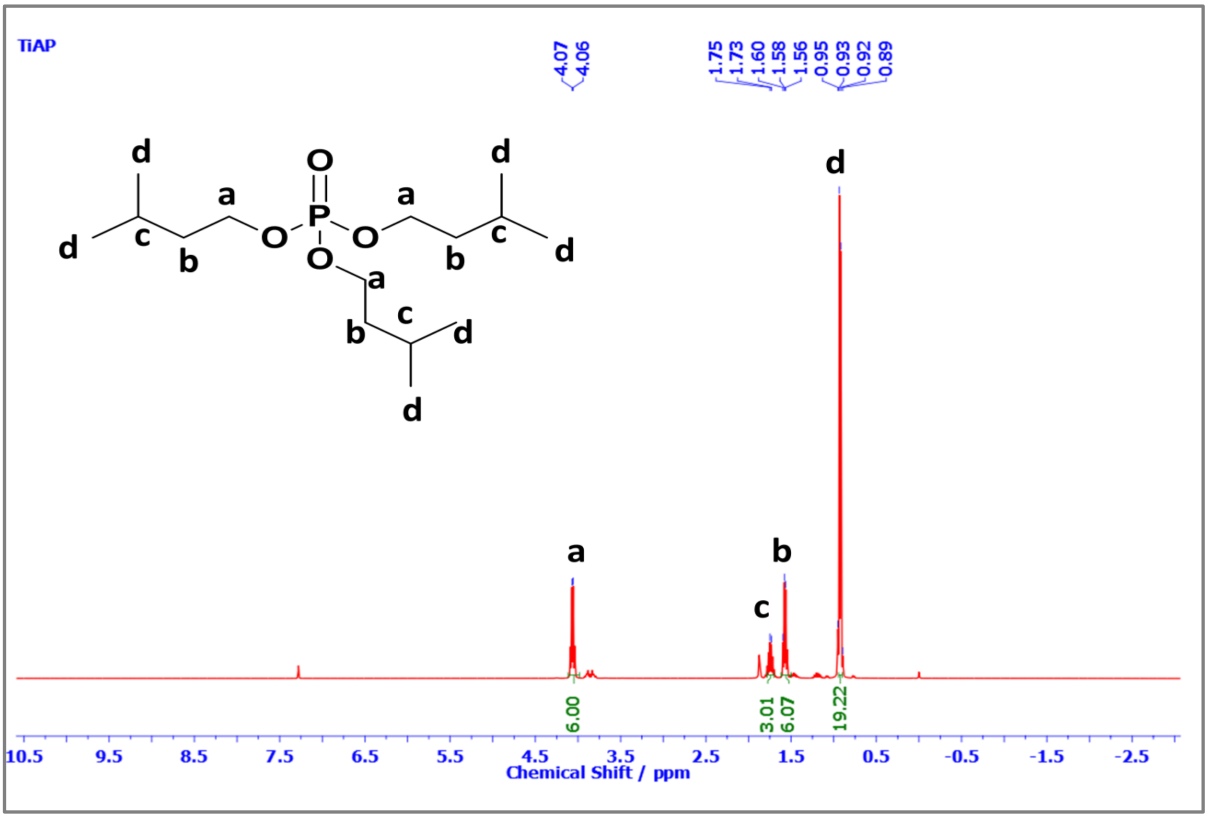

Figure 12 ^{1}H NMR of TiAP

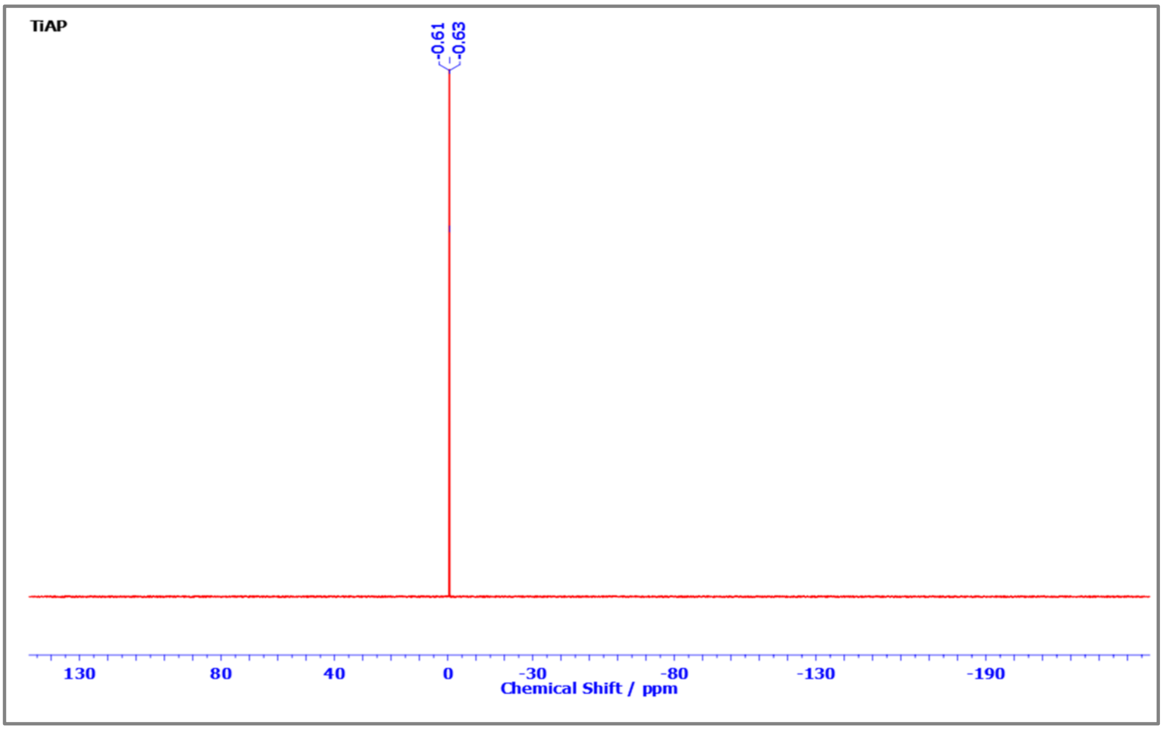

Figure 13 ^{31}P NMR of TiAP

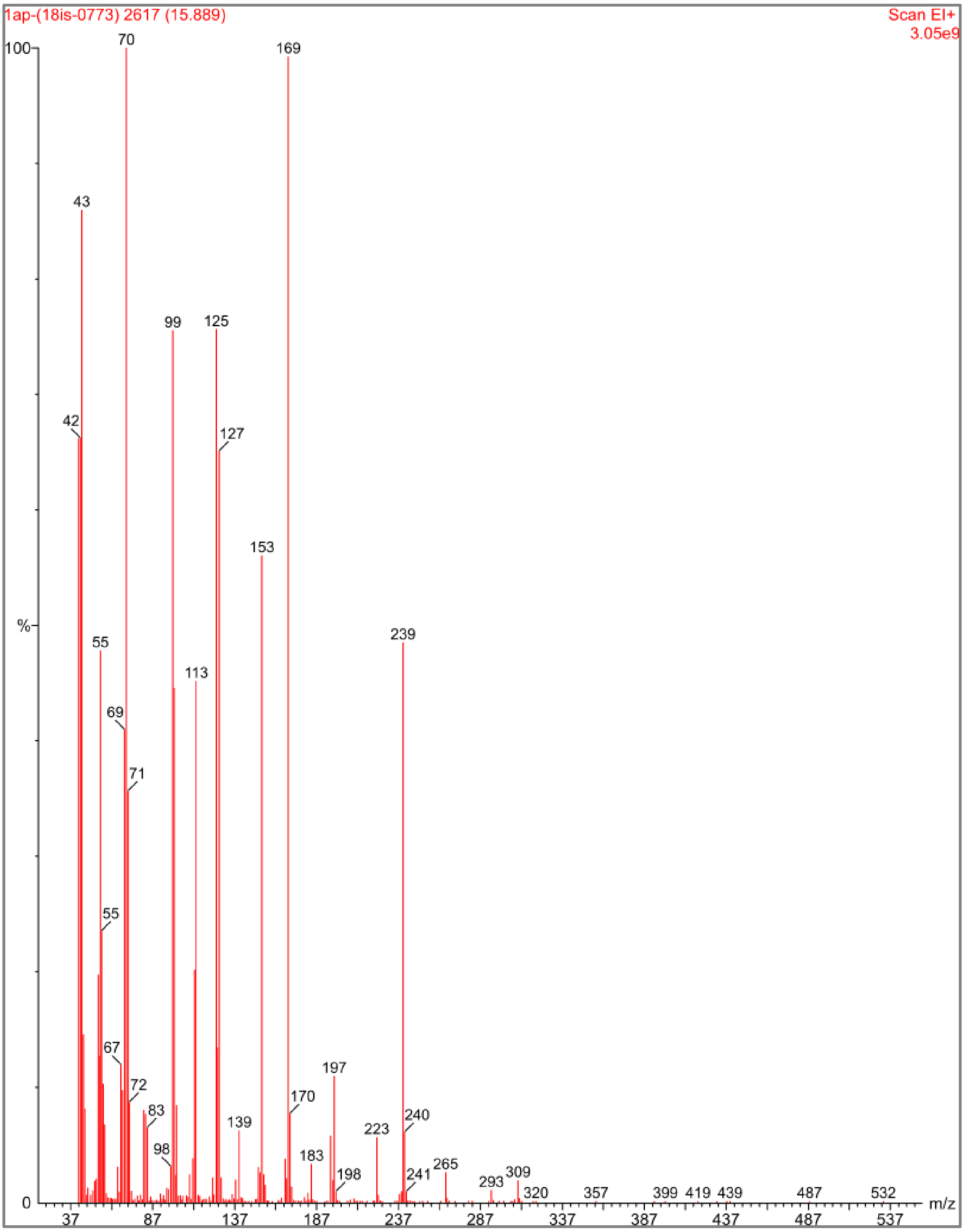

Figure 14 GC-MS spectrum of TiAP

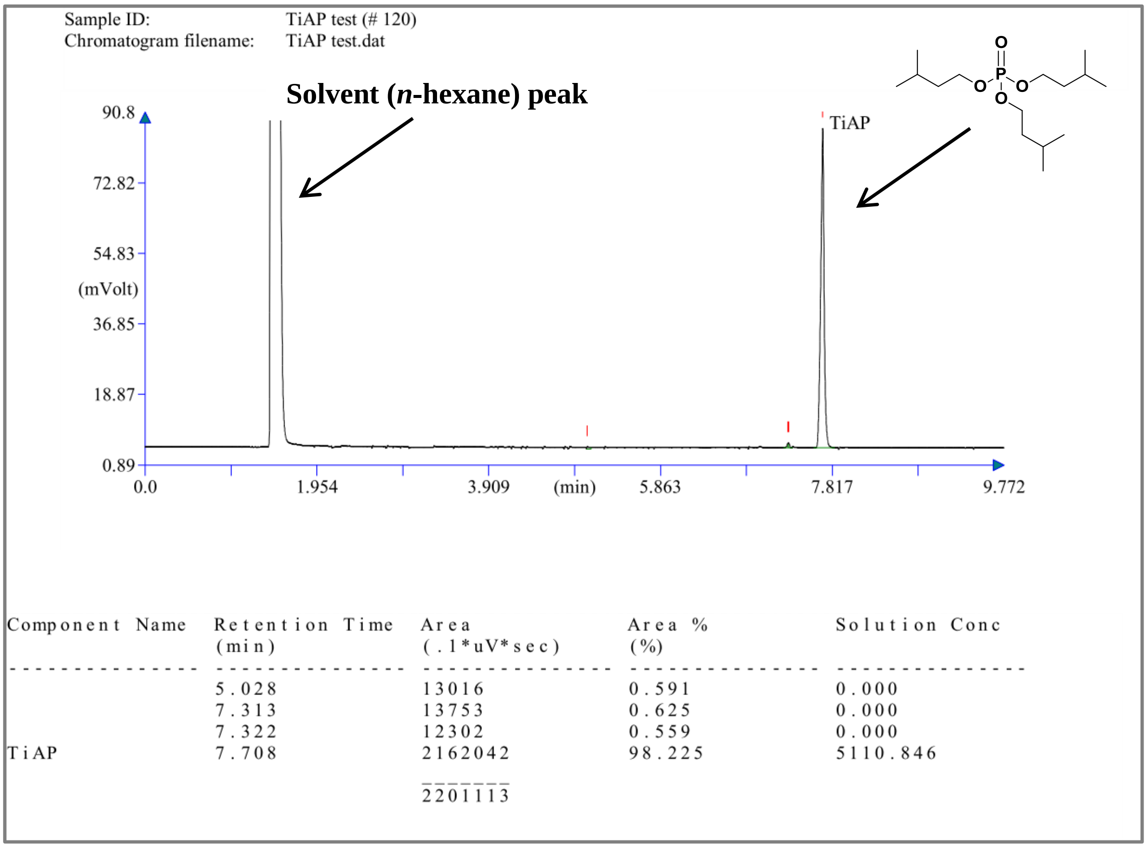

Sample ID: TiAP test (# 120)
Chromatogram filename: TiAP test.dat

```
Component Name   Retention Time   Area              Area %           Solution Conc
                 (min)            (.1*uV*sec)       (%)
---------------  ---------------  ---------------   ---------------  ---------------
                 5.028            13016             0.591            0.000
                 7.313            13753             0.625            0.000
                 7.322            12302             0.559            0.000
TiAP             7.708            2162042           98.225           5110.846
                                  _______
                                  2201113
```

Figure 15 Gas chromatogram and purity check for TiAP

1.4 Trihexyl phosphate (THP)

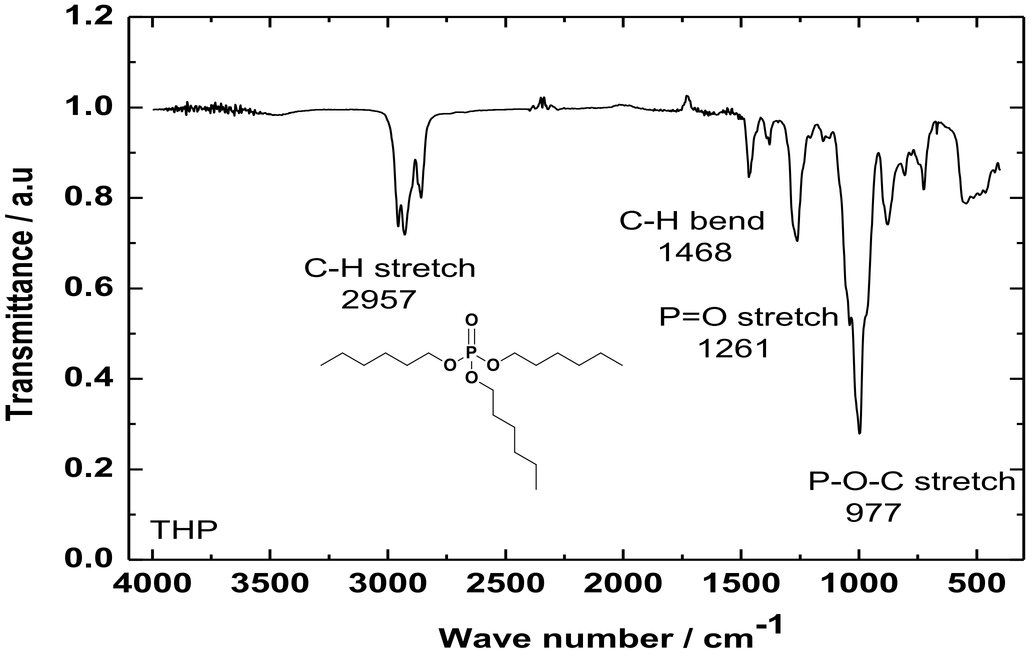

Figure 16 Infrared spectrum of THP

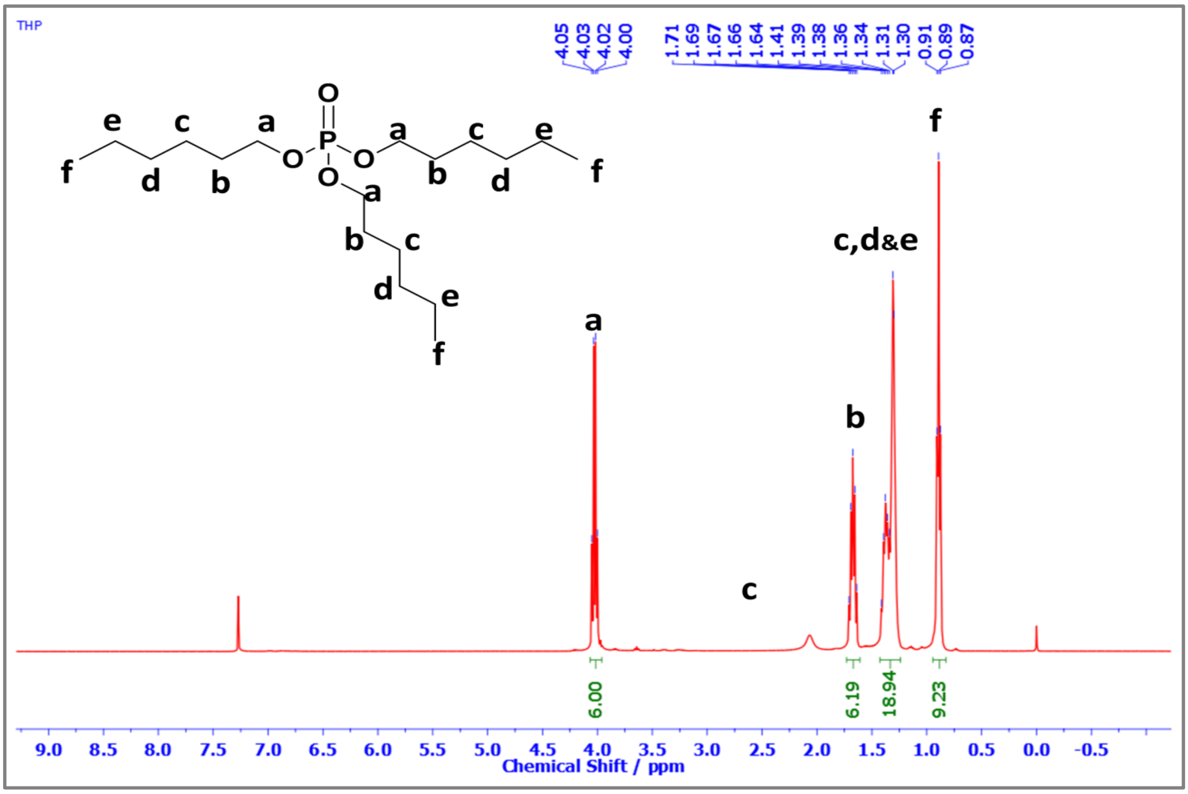

Figure 17 ^{1}H NMR of THP

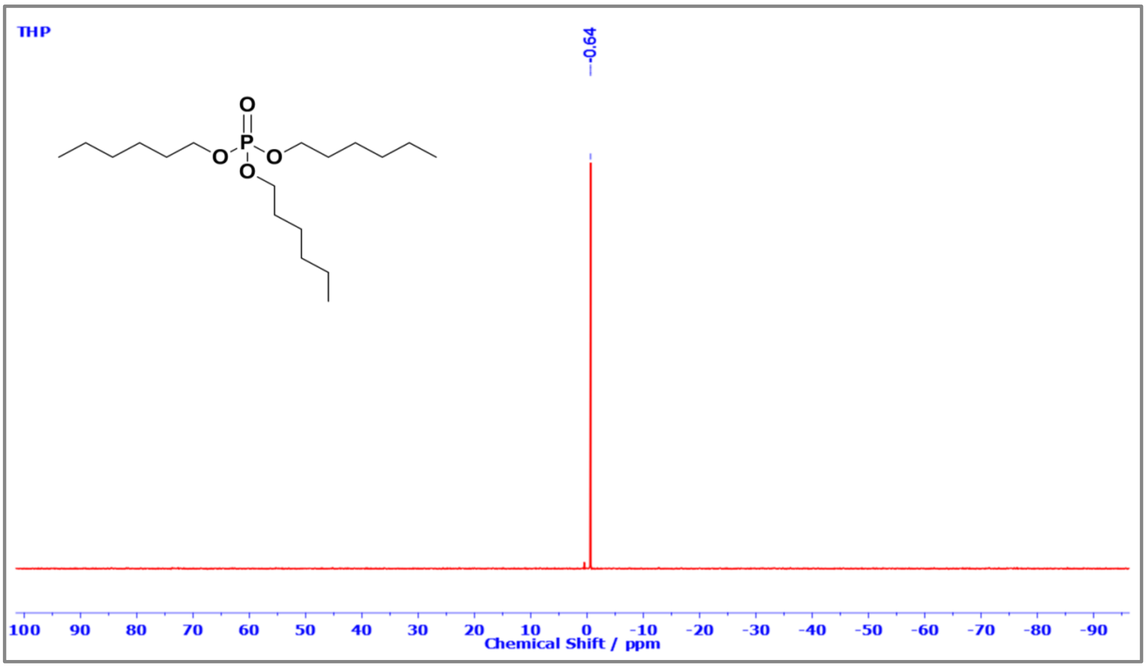

Figure 18 ^{31}P NMR of THP

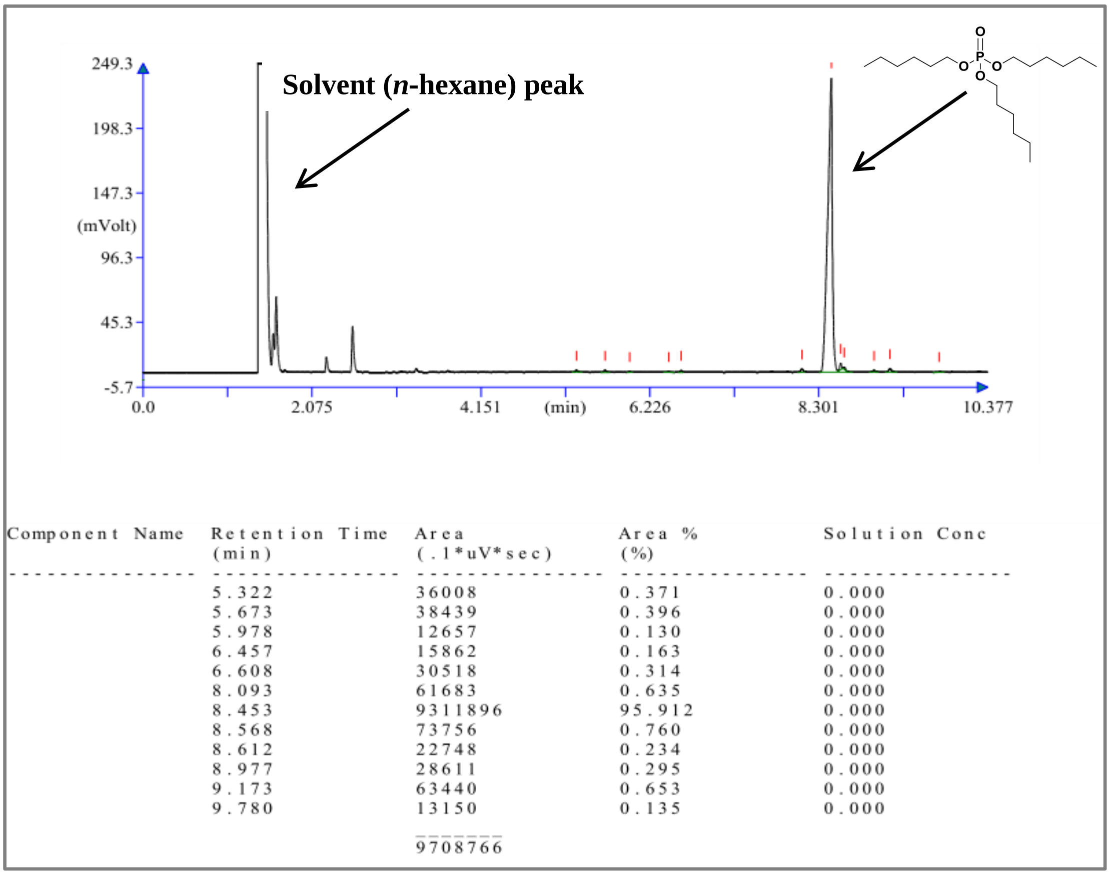

```
Component Name   Retention Time   Area              Area %            Solution Conc
                 (min)            (.1*uV*sec)       (%)
---------------  ---------------  ---------------   ---------------   ---------------
                 5.322            36008             0.371             0.000
                 5.673            38439             0.396             0.000
                 5.978            12657             0.130             0.000
                 6.457            15862             0.163             0.000
                 6.608            30518             0.314             0.000
                 8.093            61683             0.635             0.000
                 8.453            9311896           95.912            0.000
                 8.568            73756             0.760             0.000
                 8.612            22748             0.234             0.000
                 8.977            28611             0.295             0.000
                 9.173            63440             0.653             0.000
                 9.780            13150             0.135             0.000
                                  -------
                                  9708766
```

Figure 19 Gas chromatogram and purity check for THP

2. Characterization of dialkylalkyl phosphonates & dialkylhydrogen phosphonates

2.1 Dibutylbutyl phosphonate (DBBP)

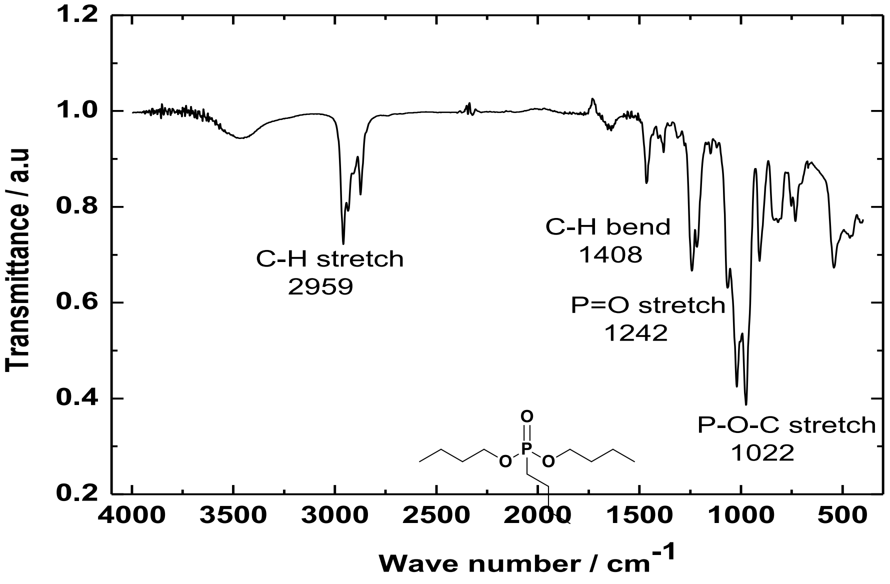

Figure 20 Infrared spectrum of DBBP

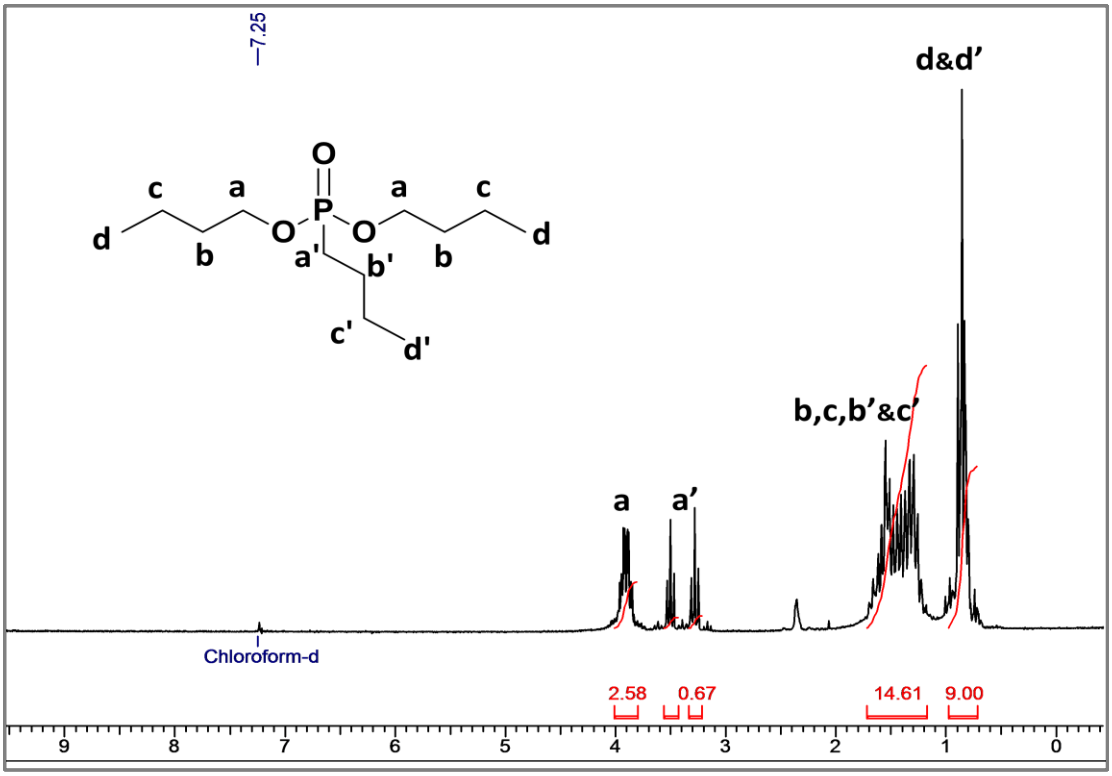

Figure 21 ^{1}H NMR of DBBP

Figure 22 ^{31}P NMR of DBBP

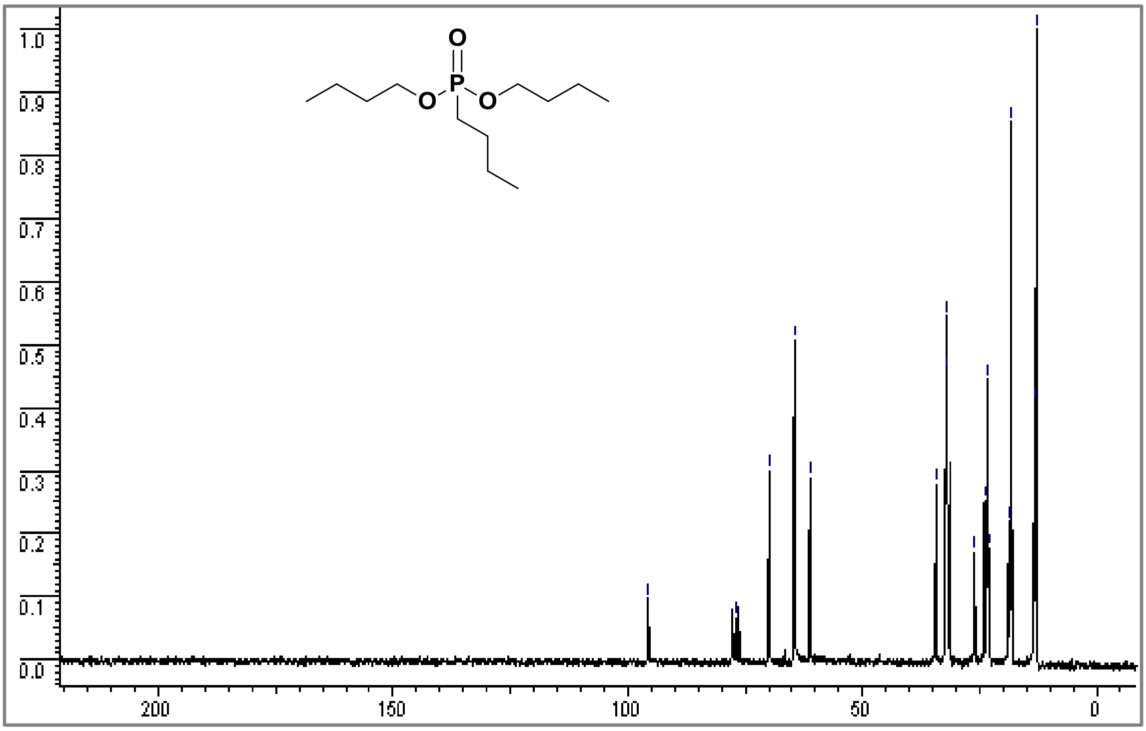

Figure 23 ^{13}C NMR of DBBP

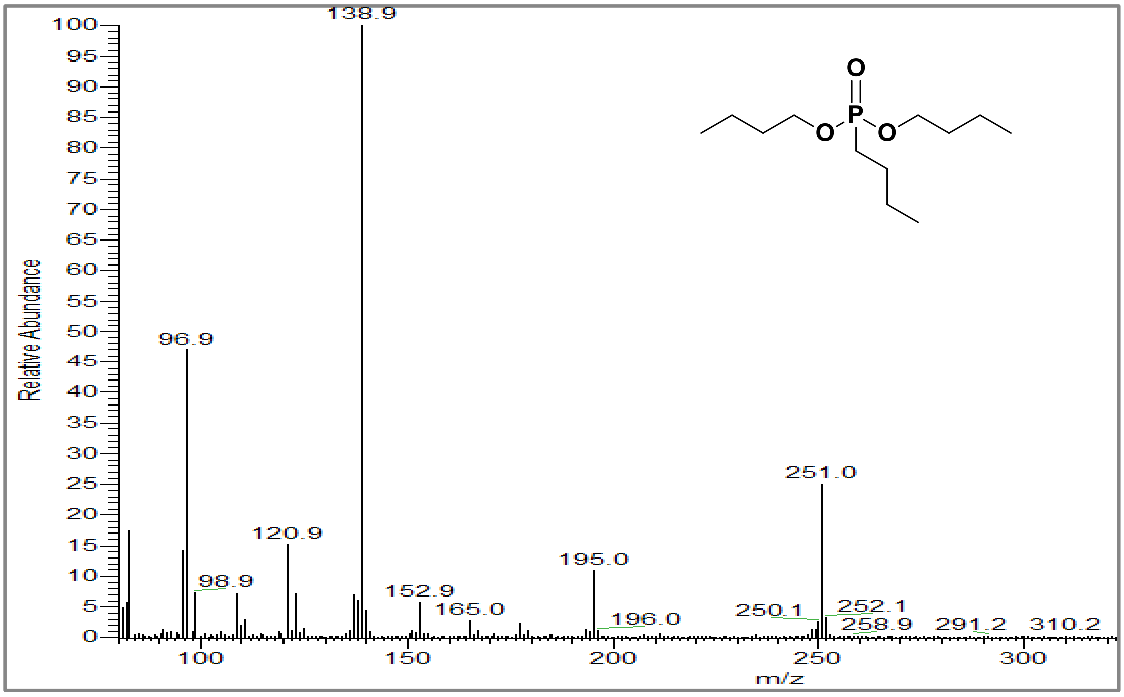

Figure 24 Mass spectrum of DBBP

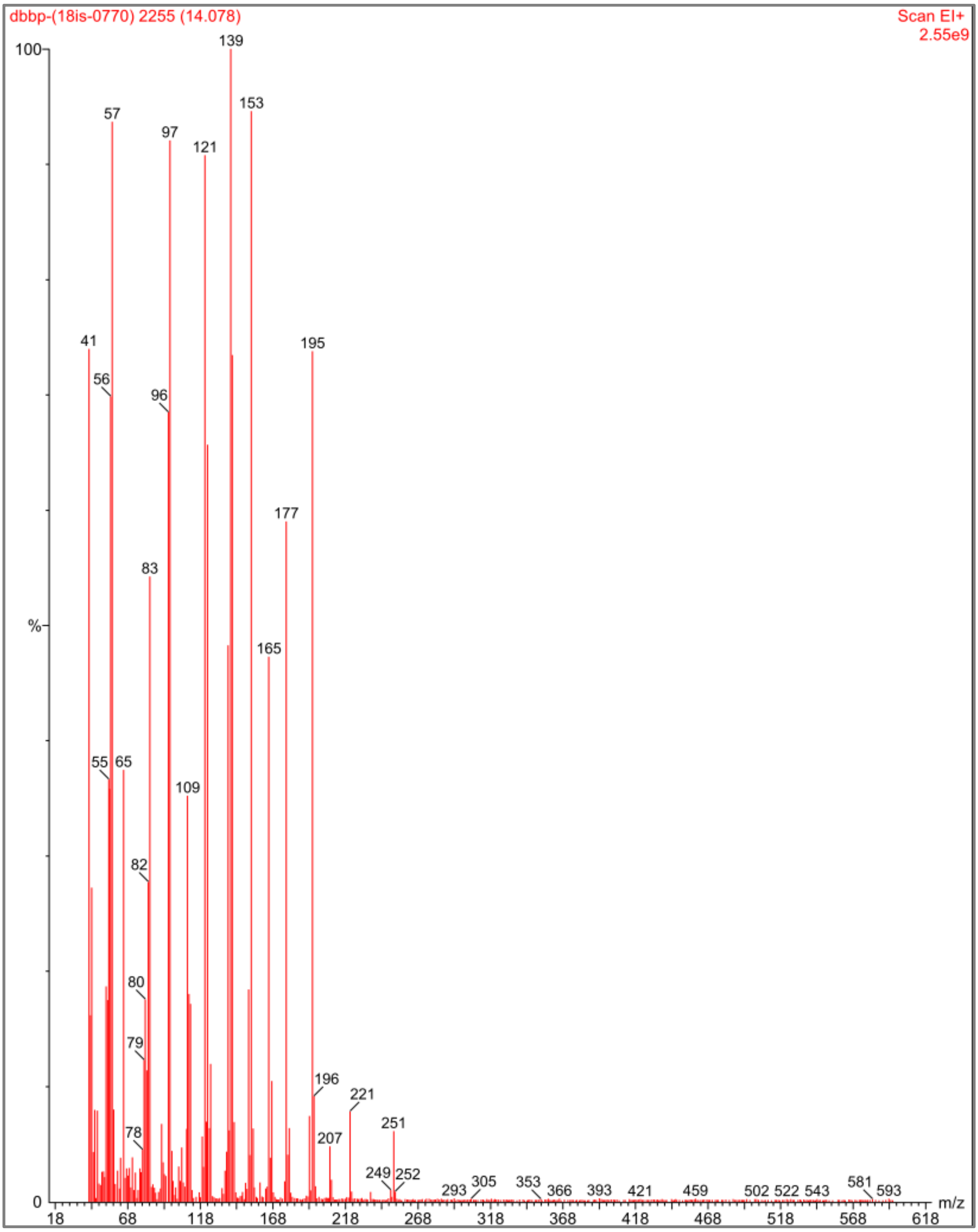

Figure 25 GC-MS spectrum of DBBP

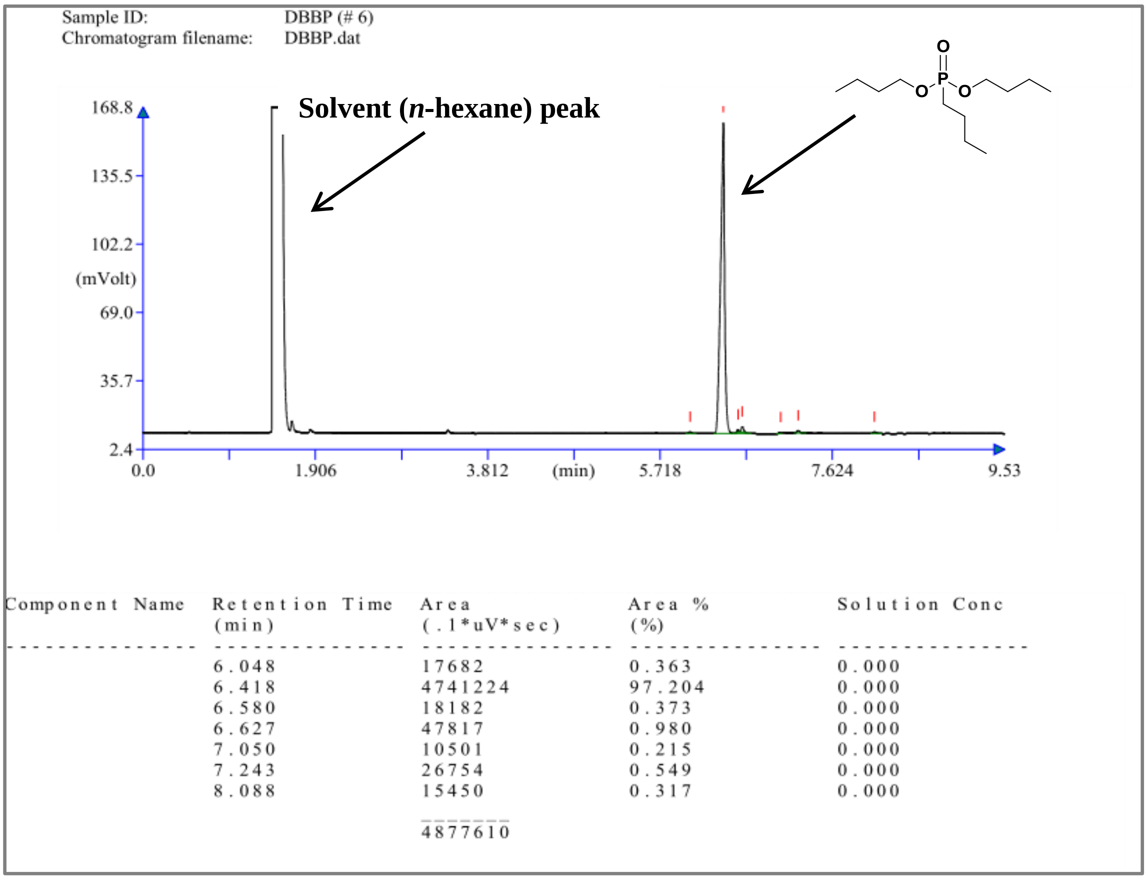

Sample ID: DBBP (# 6)
Chromatogram filename: DBBP.dat

```
Component Name   Retention Time   Area            Area %          Solution Conc
                 (min)            (.1*uV*sec)     (%)
---------------  ---------------  --------------- --------------- ---------------
                 6.048            17682           0.363           0.000
                 6.418            4741224         97.204          0.000
                 6.580            18182           0.373           0.000
                 6.627            47817           0.980           0.000
                 7.050            10501           0.215           0.000
                 7.243            26754           0.549           0.000
                 8.088            15450           0.317           0.000
                                  -------
                                  4877610
```

Figure 26 Gas chromatogram and purity check for DBBP

2.2 Diamylamyl phosphonate (DAAP)

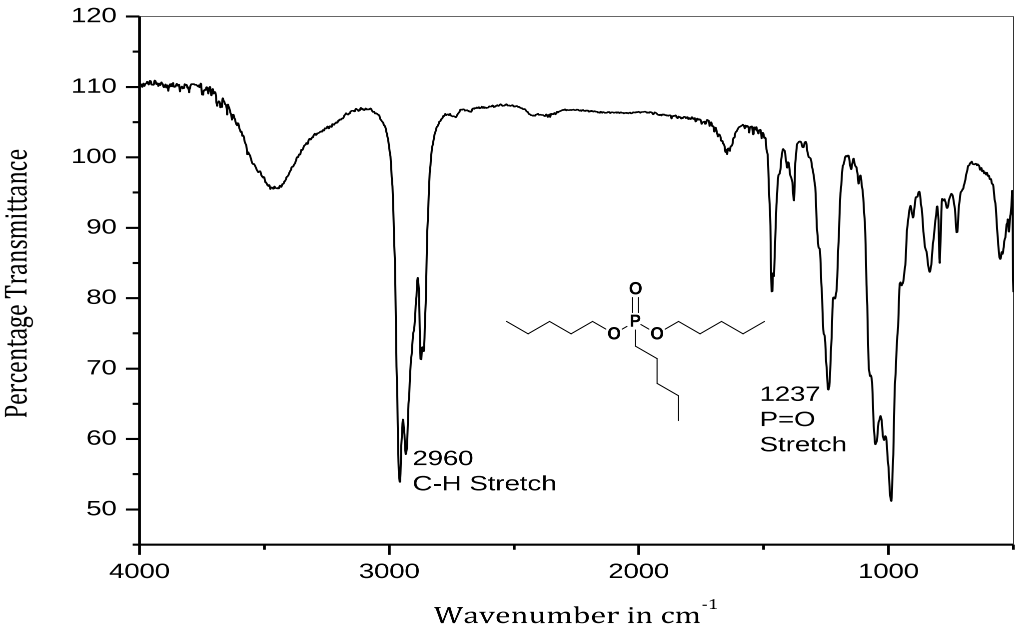

Figure 27 Infrared spectrum of DAAP

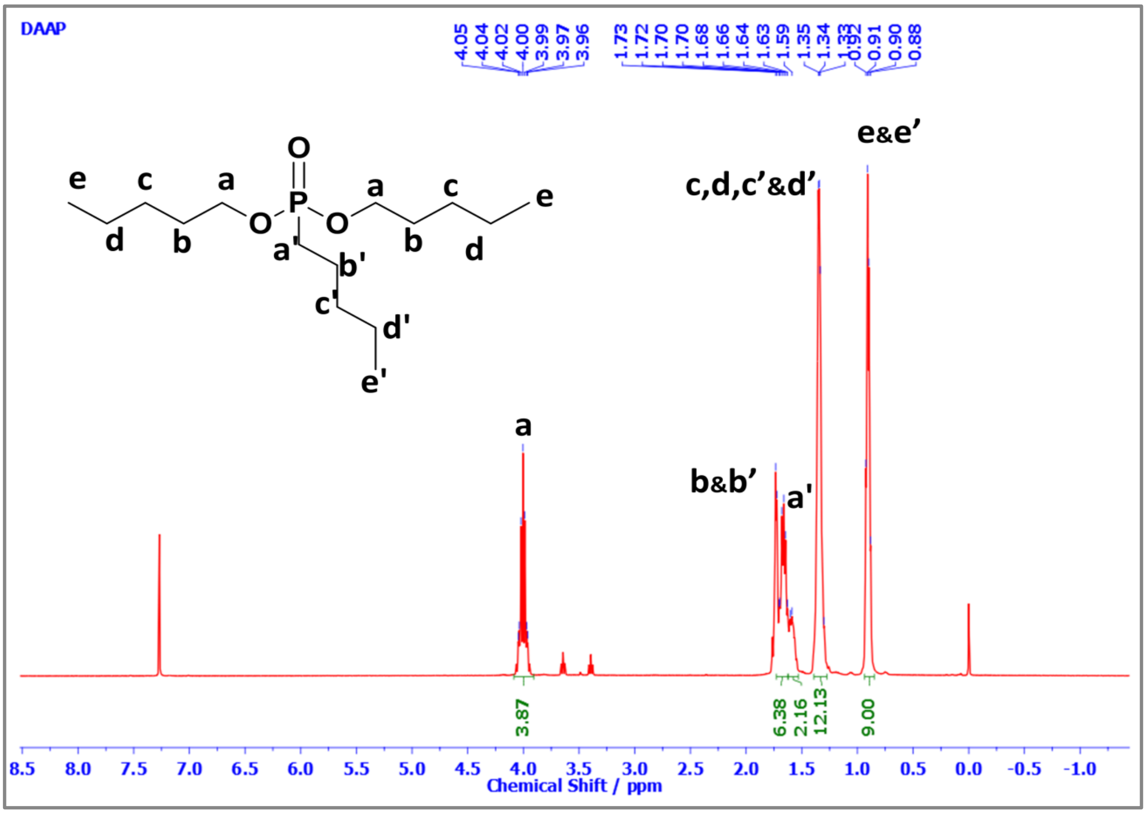

Figure 28 ^{1}H NMR of DAAP

Figure 29 ^{31}P NMR of DBBP

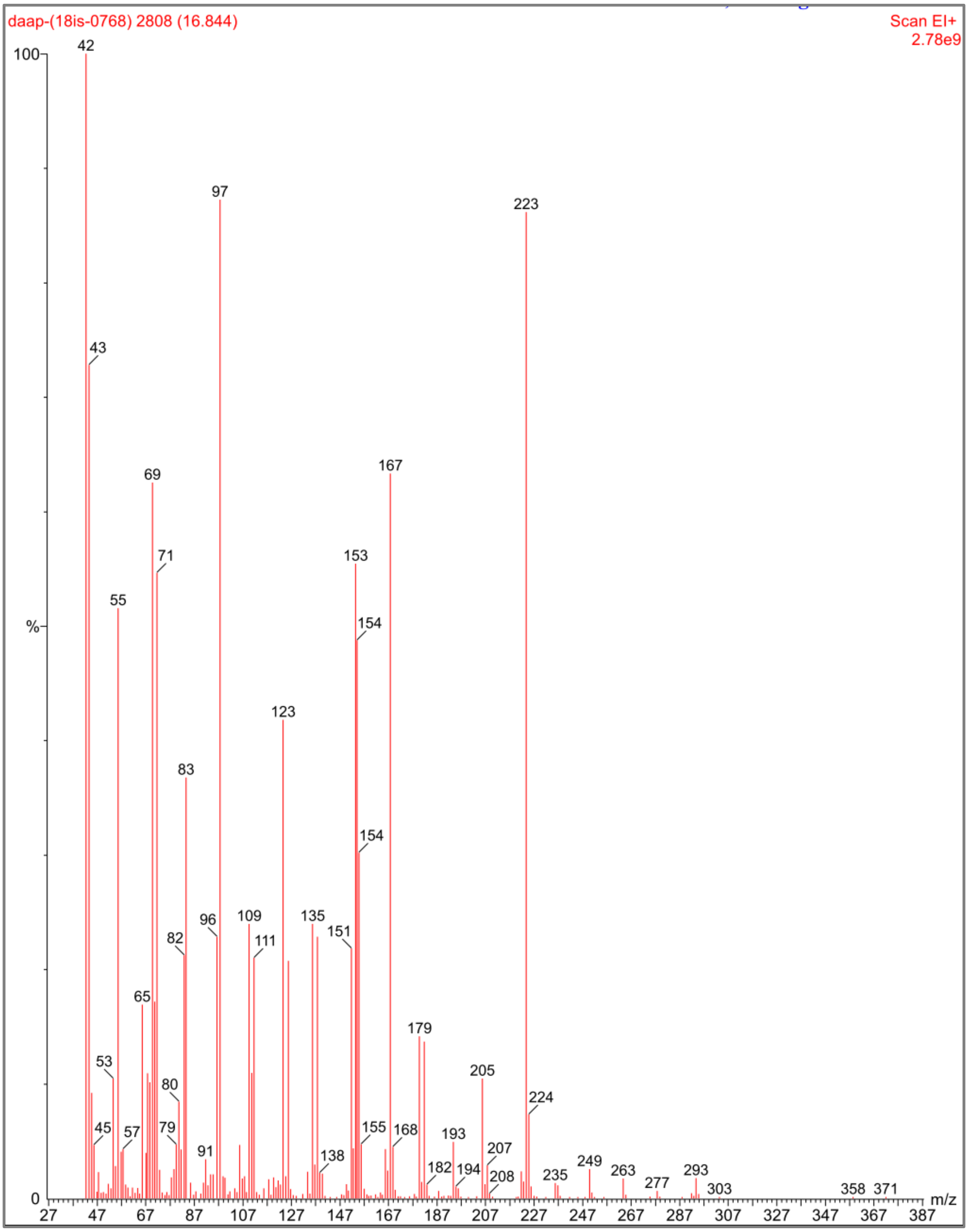

Figure 30 GC-MS spectrum of DAAP

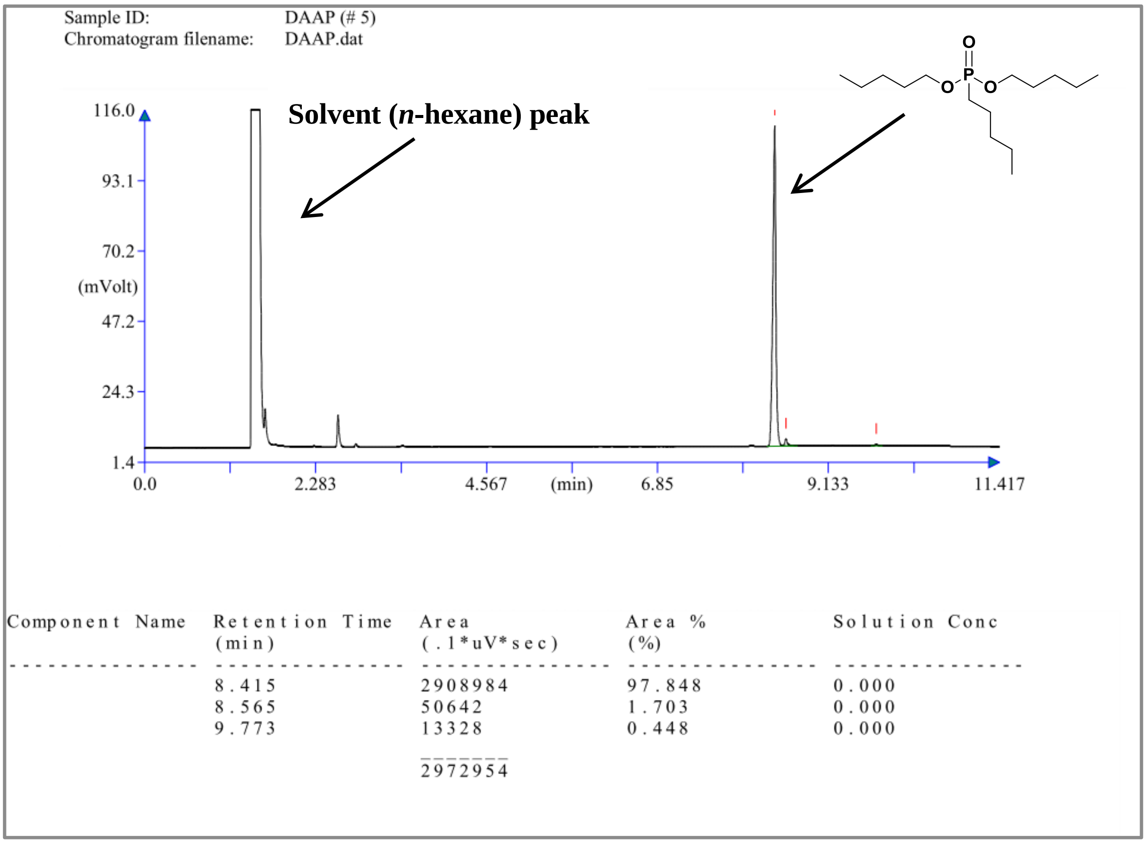

Sample ID: DAAP (# 5)
Chromatogram filename: DAAP.dat

Component Name	Retention Time (min)	Area (.1*uV*sec)	Area % (%)	Solution Conc
	8.415	2908984	97.848	0.000
	8.565	50642	1.703	0.000
	9.773	13328	0.448	0.000
		2972954		

Figure 31 Gas chromatogram and purity check for DAAP

2.3 Dioctylhydrogen phosphonate (DOHP)

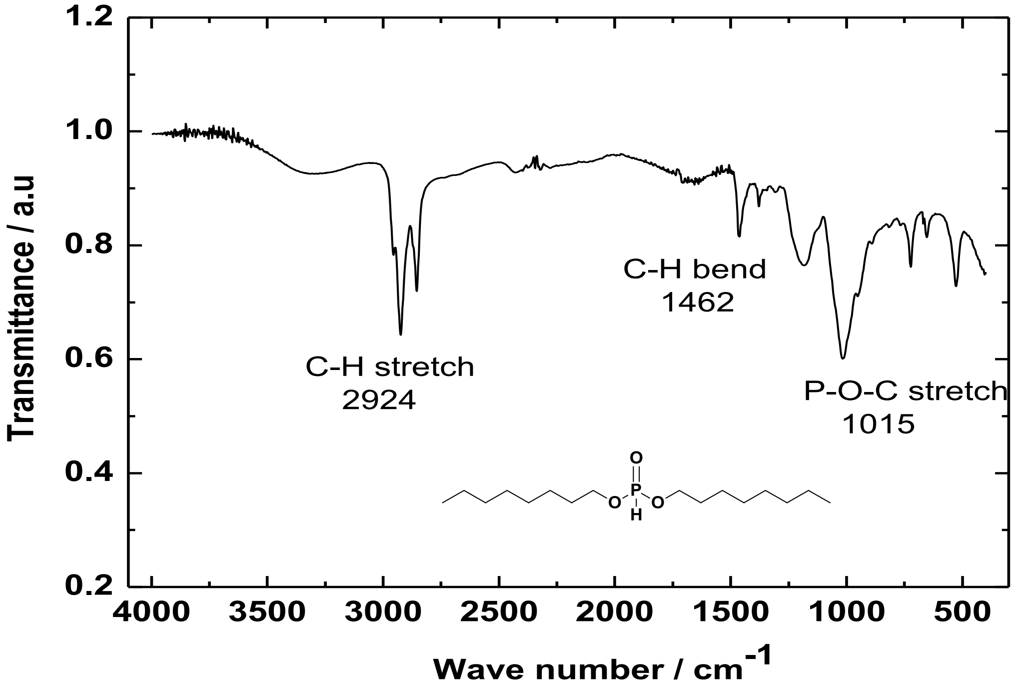

Figure 32 Infrared spectrum of DOHP

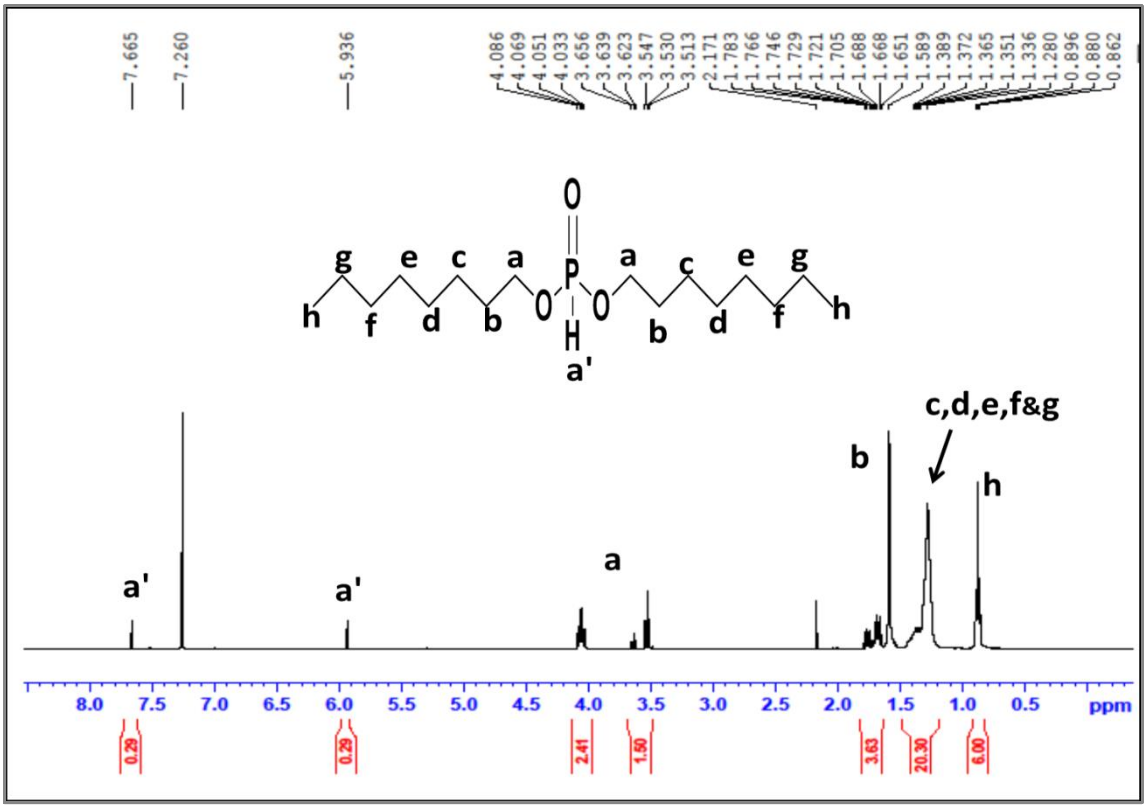

Figure 33 ^{1}H NMR of DOHP

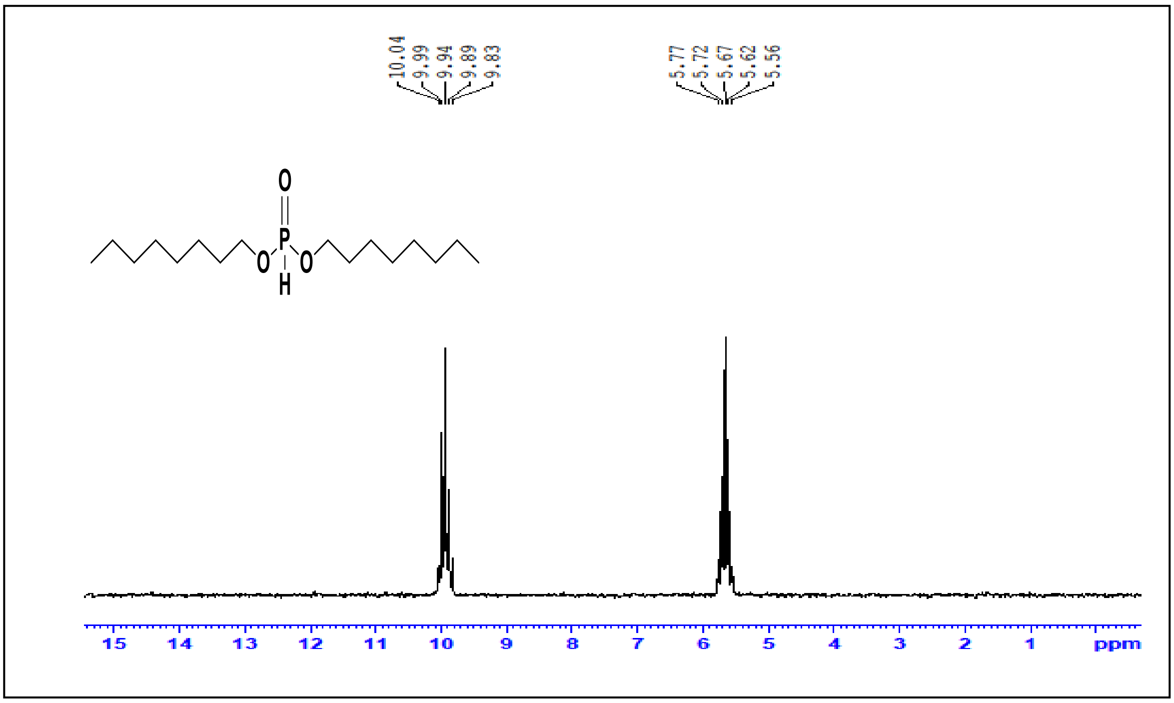

Figure 34 ^{31}P NMR of DOHP

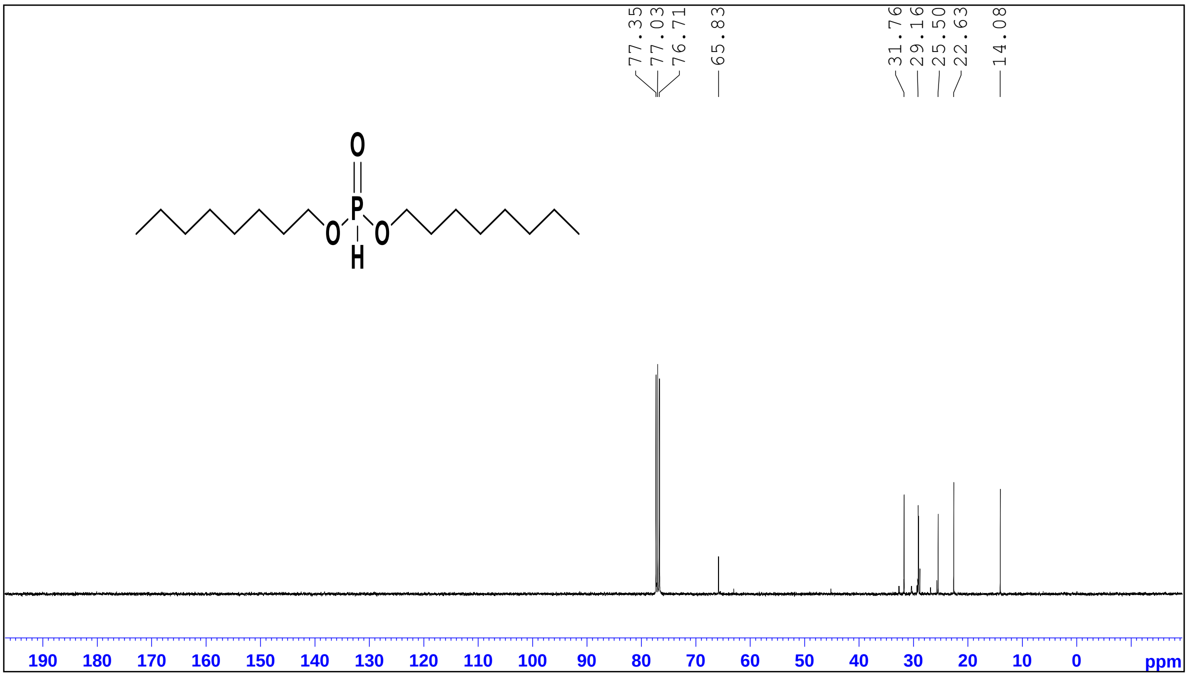

Figure 35 ^{13}C NMR of DOHP

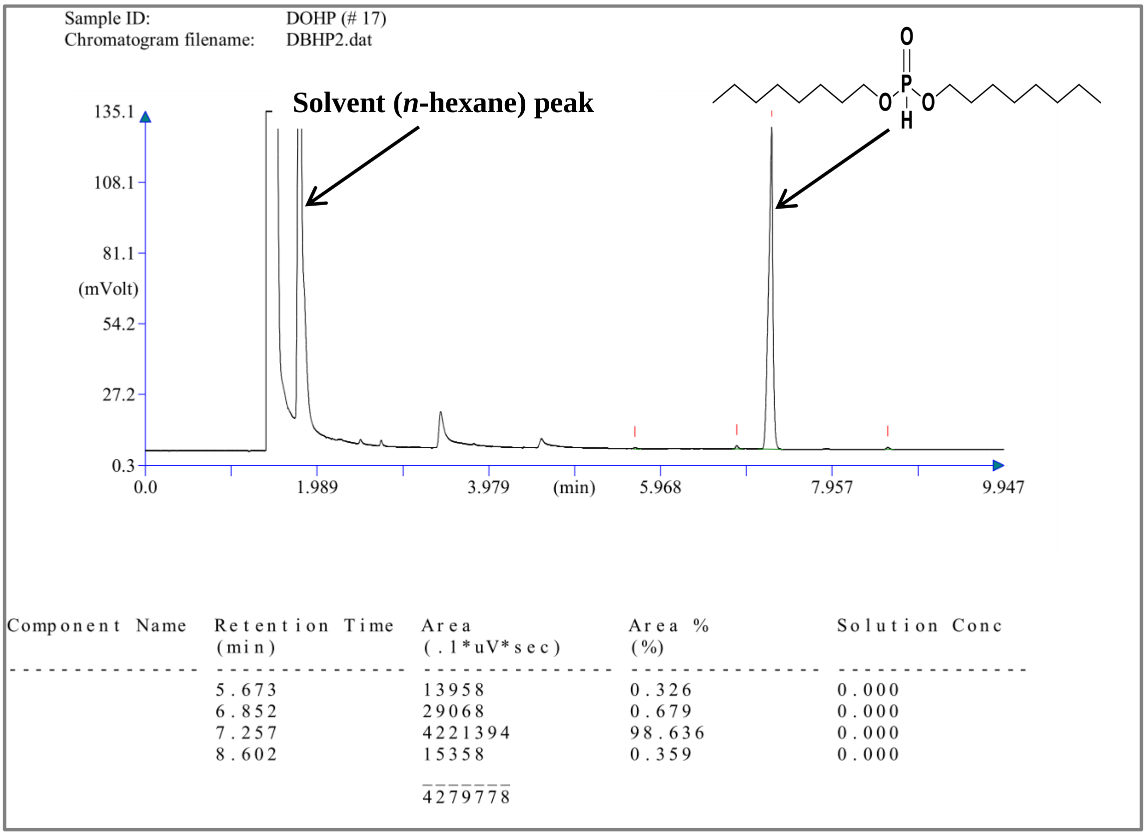
Sample ID: DOHP (# 17)
Chromatogram filename: DBHP2.dat

```
Component Name   Retention Time   Area             Area %           Solution Conc
                 (min)            (.1*uV*sec)      (%)
---------------  ---------------  ---------------  ---------------  ---------------
                 5.673            13958            0.326            0.000
                 6.852            29068            0.679            0.000
                 7.257            4221394          98.636           0.000
                 8.602            15358            0.359            0.000
                                  -------
                                  4279778
```

Figure 36 Gas chromatogram and purity check for DOHP

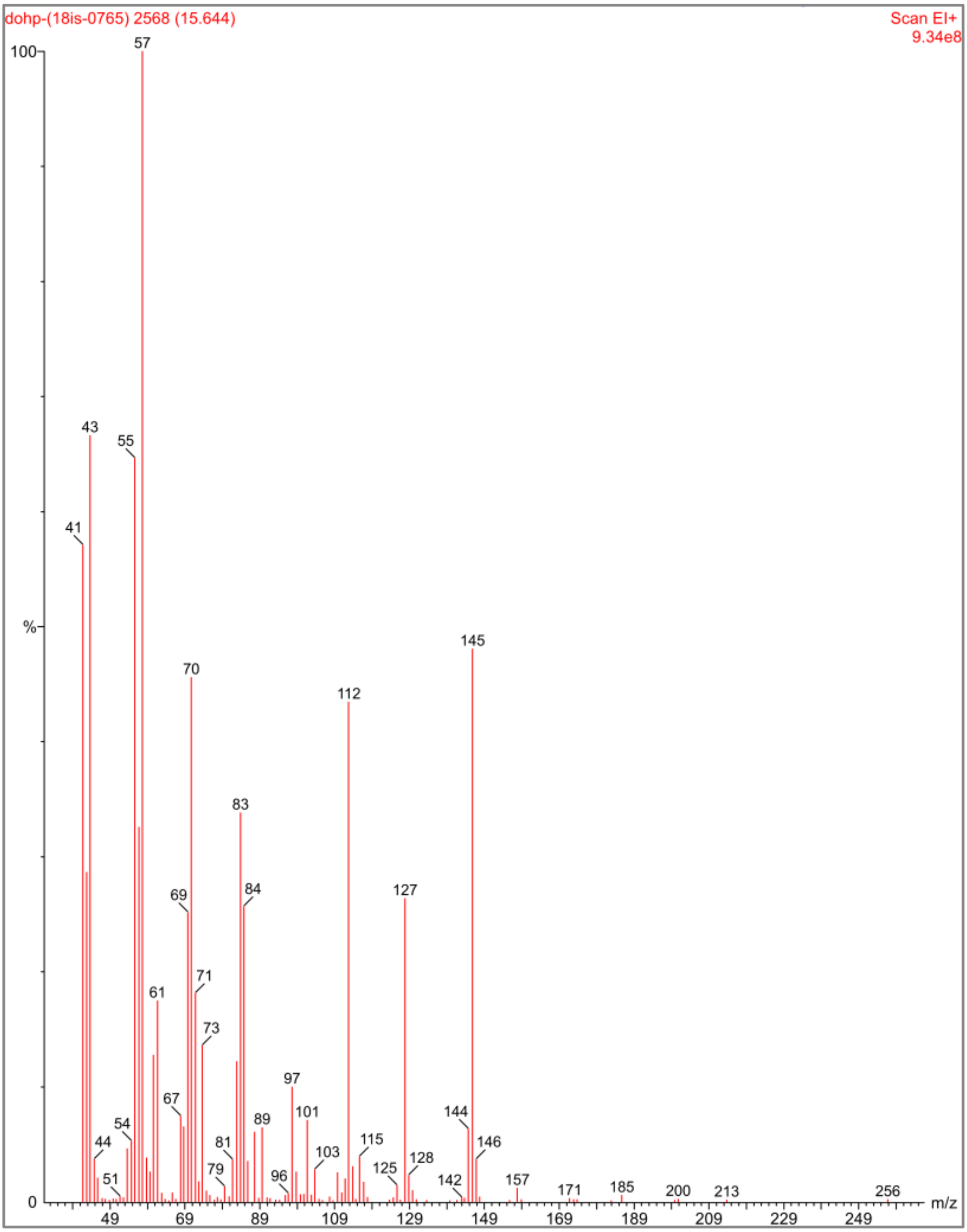

Figure 37 GC-MS spectrum of DOHP

2.4 Dioctylhydrogen phosphine oxide (DOPO)

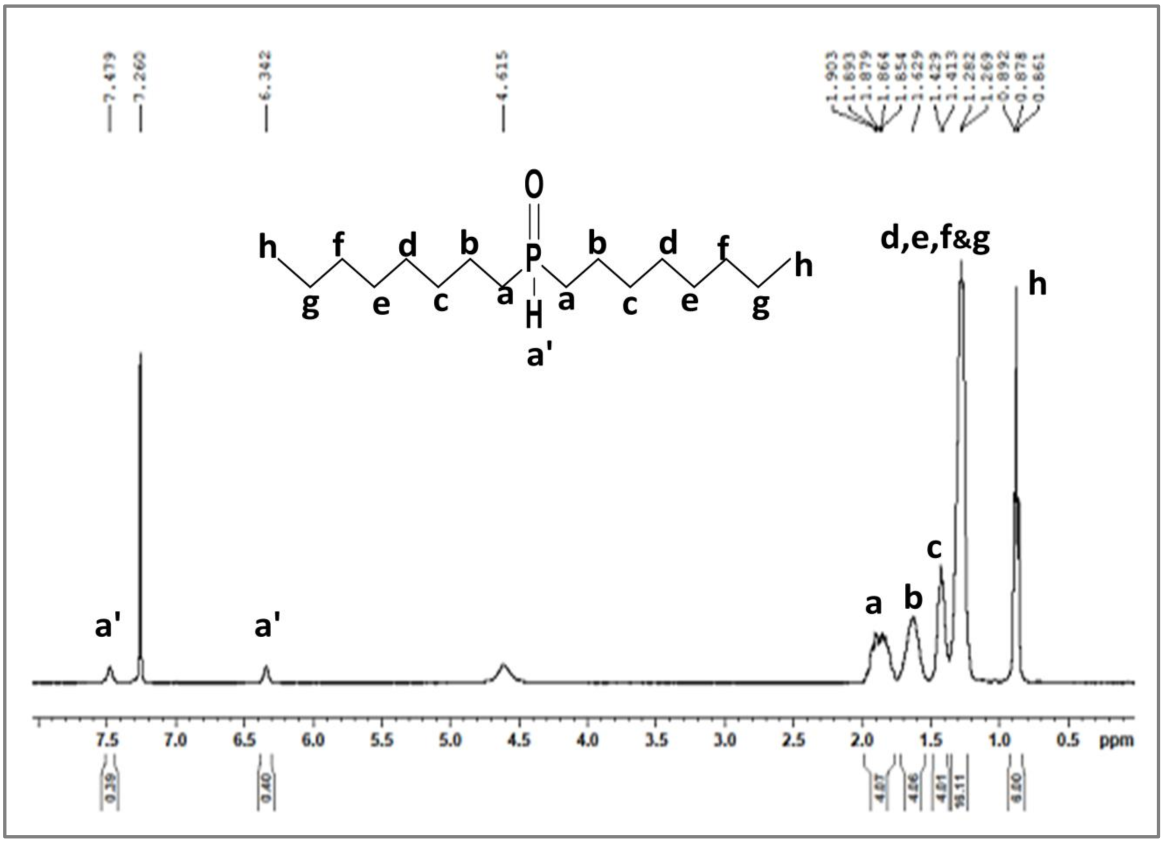

Figure 38 ^{1}H-NMR of DOPO

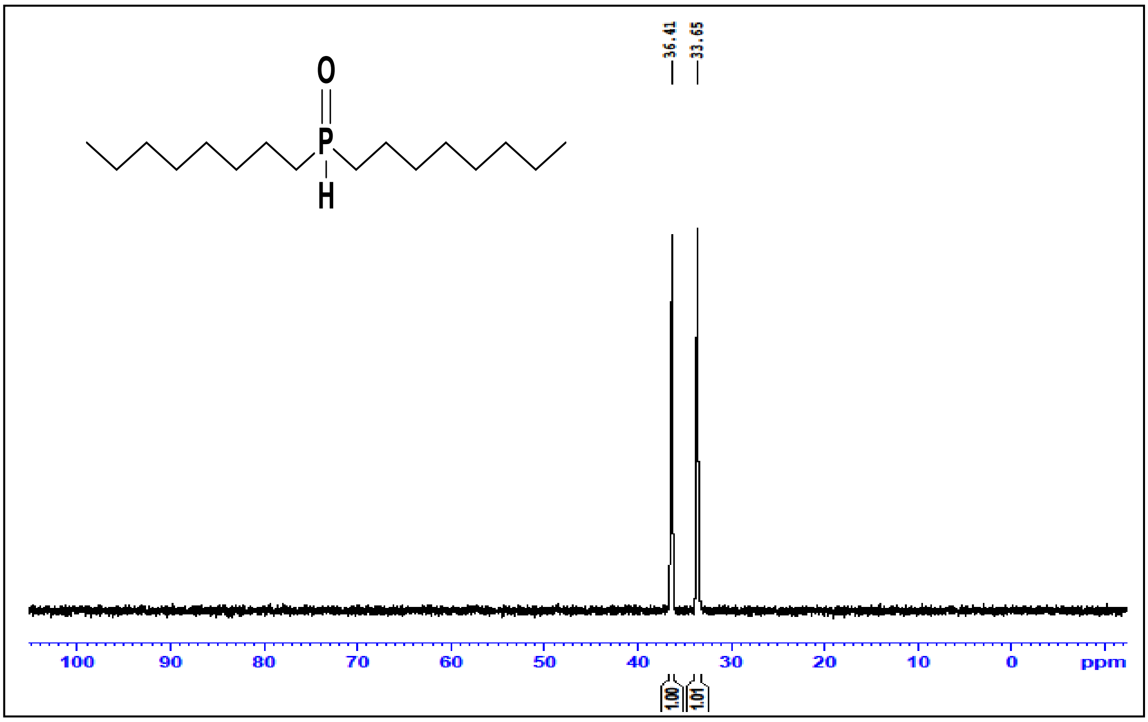

Figure 39 ^{31}P NMR of DOPO

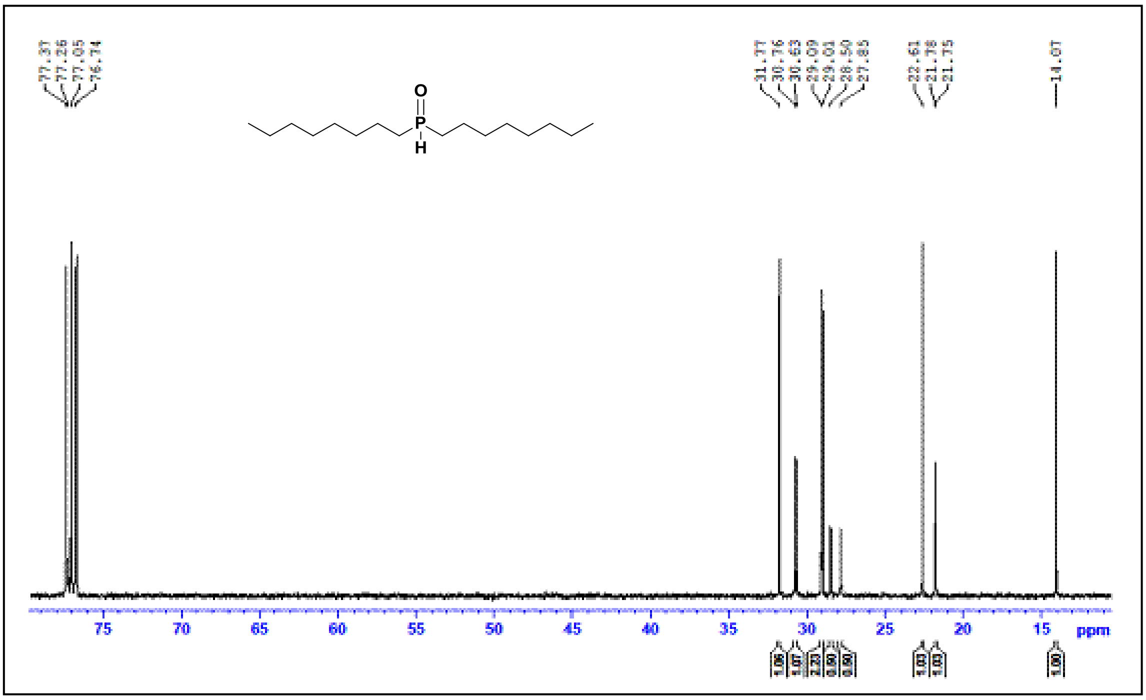

Figure 40 ^{13}C NMR DOPO

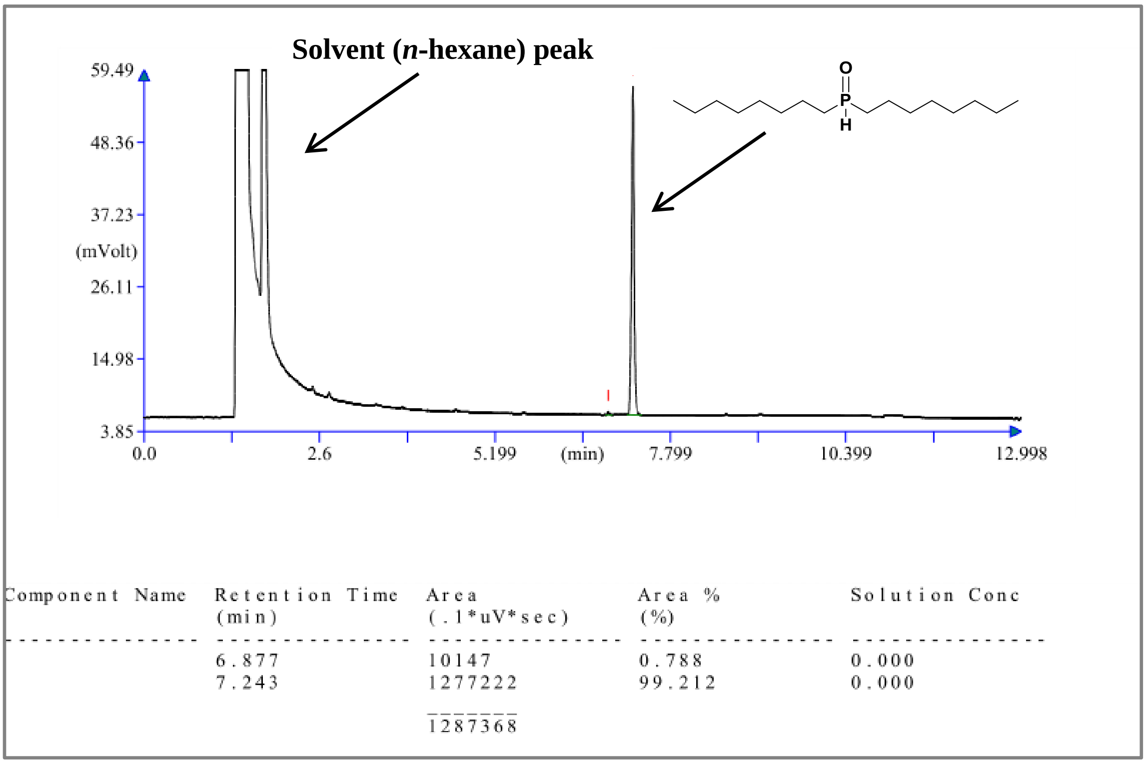

```
Component Name   Retention Time   Area             Area %           Solution Conc
                 (min)            (.1*uV*sec)      (%)
---------------  ---------------  ---------------  ---------------  ---------------
                 6.877            10147            0.788            0.000
                 7.243            1277222          99.212           0.000
                                  _______
                                  1287368
```

Figure 41 Gas chromatogram and purity check for DOPO

Appendix-2

Development of new models to correlate the solubility of liquid solutes in supercritical carbon dioxide in the presence of co-solvent

---

New models

The solubility of solutes in $SCCO_2$ with co-solvent depends on the pressure, temperature, density and co-solvent composition. Semi-empirical models have been developed in the literature for the solubility of solid solutes in $SCCO_2$ modified with a co-solvent using association theory [1, 2]. These equations were developed by assuming each solute molecule is being associated with some molecules of $SCCO_2$ and co-solvent to form a solvato complex. Same concept was adopted for deriving the equations for the solubility of liquid solutes in $SCCO_2$ modified with a co-solvent. The association theory assumes that each solute molecule (A_2) is associated with each co-solvent molecule (A_3) and κ molecules of $SCCO_2$ (A_1) to form a complex denoted by $A_2A_3A_{1\kappa}$,

$$A_2 + A_3 + \kappa A_1 \Leftrightarrow A_2A_3A_{1\kappa} \qquad (1)$$

The equilibrium constant can be expressed in terms of fugacities,

$$K_f = \frac{\left(\hat{f}_{A_2A_3A_{1\kappa}} \Big/ f^*_{A_2A_3A_{1\kappa}} \right)_{SCF}}{\left(\dfrac{\hat{f}_{A_2}}{f^*_{A_2}} \right)_S \left(\dfrac{\hat{f}_{A_1}}{f^*_{A_1}} \right)^{\kappa}_{SCF} \left(\dfrac{\hat{f}_{A_3}}{f^*_{A_3}} \right)_{SCF}} \qquad (2)$$

SCF represents the supercritical phase of carbon dioxide and S represents the pure solute (liquid) phase. f^* is the reference fugacity of the components in their respective phases. The fugacities of the solute and the co-solvent are expressed in terms of activity coefficient to account for the interactions between molecules, while the fugacities of other components are expressed in terms of fugacity coefficient,

$$\hat{f}_i^{SCF} = x_i \gamma_i f_i^l \qquad (3)$$

Where, $i = A_2A_3A_{1\kappa}$, A_2 and A_3.

$$\hat{f}_j = x_j \hat{\phi}_j P \tag{4}$$

Where, j =A$_1$.

$$f_n^* = \phi_n^* \; P^* \tag{5}$$

Where, n = A$_1$, A$_2$, A$_3$ and A$_2$A$_3$A$_{1\kappa}$.

The solute in SCCO$_2$ exists mainly in the associated form, hence $x_{A_2A_3A_{1\kappa}} = x_2$ and $x_{A_3} = x_3$ where x_2 and x_3 represents the mole fraction of the solute and co-solvent in SCCO$_2$. The fugacity of the solute in liquid phase is given by the following expression

$$\hat{f}_2 = \gamma_2^l x_2^l f_2^l \tag{6}$$

γ_2^l and x_2^l are the activity coefficient and mole fraction of solute in the liquid phase respectively. The fugacity of pure solute in liquid phase, f_2^l can be expressed as,

$$f_2^l = P_2^{vap} \phi_{sat} \exp\left(\frac{V_2 (P - P_2^{vap})}{RT} \right) \tag{7}$$

Similarly, the fugacity of co-solvent in SCF phase can be written as,

$$\hat{f}_3 = \gamma_3 x_3 f_3 \tag{8}$$

The pure component (solvent) in SCF phase, f_3 can be expressed as,

$$f_3 = P_3^{vap} \phi_{sat} \exp\left(\frac{V_3 \left(P - P_3^{vap} \right)}{RT} \right) \tag{9}$$

Substituting the equations (3) to (9) in equation (2)

$$K_f = \frac{\left(\dfrac{x_2 \gamma_2 f_{231_\kappa}}{\varphi_{231_\kappa}^* P^*} \right)_{SCF}}{\left(\dfrac{x_2^l \gamma_2^l P_2^{vap} \phi_{sat} \exp\left(\dfrac{V_2 \left(P - P_2^{vap} \right)}{RT} \right)}{\varphi_2^* P^*} \right)_S \left(\dfrac{x_1 \hat{\varphi}_1 P}{\varphi_1^* P^*} \right)^{\kappa} \left(\dfrac{x_3 \gamma_3 P_3^{vap} \phi_{sat} \exp\left(\dfrac{V_3 \left(P - P_3^{vap} \right)}{RT} \right)}{\varphi_3^* P^*} \right)_{SCF}} \tag{10}$$

Eq. (10) can be further simplified by taking the logarithm on both the sides as follows,

$$\ln\left(K_f\right)=\ln\left(x_2\right)+\ln\left(\varphi_{231_\kappa}\big/\varphi^*_{231_\kappa}\right)+(1-k)\ln\left(P\big/P^*\right)-\ln\left(P_2^{sub}\big/P^*\right)+\ln\phi_2^*$$
$$-\frac{V_2\left(P-P_2^{vap}\right)}{RT}-\ln\left(P_3^{vap}\big/P^*\right)-\frac{V_3\left(P-P_3^{vap}\right)}{RT}-\kappa\ln\left(x_1\right)-\ln(\phi_{sat}^2) \quad (11)$$
$$-\kappa\ln\left(\hat{\varphi}_1\big/\varphi_1^*\right)-\ln\left(\gamma_2^l x_2^l\right)-\ln\left(x_3\right)+\ln\left(\gamma_2\big/\gamma_3\right)+\ln\phi_3^*$$

P^* and $\hat{\phi}_i$ are assumed to be reference pressure and reference fugacity coefficient for a particular component. The multiplication of association number and the fugacity coefficient of the solvent in SCF phase can be related to the density of $SCCO_2$ as [3]

$$k\ln\hat{\phi}_1=\rho_1 k\,[2(x_1B_{11}+x_2B_{231_k1})-B] \quad (11a)$$

where, $B=\sum\sum y_i y_j B_{ij}$, B_{ij} is the second virial coefficient (of the pair i-j) of the mixture in $SCCO_2$ phase. For example, B_{231_k1} represents the virial coefficient of the mixture of the solvato complex ($A_2A_3A_{1\kappa}$) and the solvent (A_1). P_2^{vap} and P_3^{vap} can be correlated to the temperature using Antoine equation,

$$\ln P_2^{vap}=A_2-\frac{B_2}{T}\ \text{and}\ \ln P_3^{vap}=A_3-\frac{B_3}{T} \quad (11b)$$

A_2, A_3 and B_2, B_3 in Eq. (11b) are temperature independent constants.

The equilibrium constant can be expressed in terms of heat of solvation as,

$$\ln K_f=\frac{\Delta H_s}{RT}-q_s \quad (11c)$$

ΔH_s is the heat of solvation and q_s is a constant.

From the definition of compressibility factor,

$$Z=\frac{PV_1}{RT}$$

The above equation can also be expressed in terms of molar density (ρ_1) as,

$$\frac{P}{RT} = Z\rho_1$$

On multiplying the above equation by V_2 or V_3 on both the sides,

$\frac{PV_2}{RT} = ZV_2\rho_1$ or $\frac{PV_3}{RT} = ZV_3\rho_1$, these can be further rewritten as,

$$\frac{PV_2}{RT} = Z\frac{\rho_1}{\rho_2} \text{ or } \frac{PV_3}{RT} = Z\frac{\rho_1}{\rho_3} \tag{11d}$$

Z is the compressibility factor that can be expressed using virial equation of state as $Z = (1 + B\rho_1 + C\rho_1^2 + D\rho_1^3 + ...)$. It can be assumed that the solubility is not the function of higher power of density i.e., ρ_B^2, ρ_B^3 etc. Hence these powers in expression for Z have been neglected in the *ln* x_2 expression in Eq. (11). The terms $\frac{P_2^{vap}V_2}{RT}$ and $\frac{P_3^{vap}V_3}{RT}$ are ~ 10^{-6} to10^{-4} and thus can be neglected compared to other terms in Eq. (11). As the solubility of solute in $SCCO_2$ is very small, x_1 is assumed to be nearly equal to 1. Thus, the activity coefficient of solute in SCF phase, γ_2 can be assumed at infinite dilution. Therefore, Eq. (11) can be rewritten as

$$\ln x_2 = \ln x_3 + (k-1)\ln\left(\frac{P}{P*}\right) + \frac{\Delta H_s}{RT} - q_s + k\rho_1(2x_1B_{11} - B) + (A_2 + A_3) - \frac{(B_2 + B_3)}{T}$$
$$-\left(\frac{\phi_{231_k}\phi_1^{*k}}{\phi_{231_k}^*}\frac{\phi_2^*\phi_3^*}{\phi_{sat}^2}\frac{\left(P^*\right)^2}{x_2^l\gamma_2^l}\right) + \rho_1\left(\frac{1}{\rho_2} + \frac{1}{\rho_3}\right) + \ln\frac{\gamma_3}{\gamma_2^\infty} \tag{12}$$

Eq. (12) is the final expression for the solubilities of liquids in supercritical fluids. In Eq. (12), P^* is assumed to be 1 atm. ρ_1, ρ_2 and ρ_3 are the molar densities of solvent, solute and co-solvent, respectively. γ_2^∞ and γ_3 can be expressed using different activity coefficient models. In this work, γ_2^∞ and γ_3 are expressed using Wilson (Case 1) and van Laar activity coefficient models (Case 2).

Case 1: New model based on Wilson activity coefficient model

The activity coefficient of any component 'k' in a multi component mixture is given by the following expression using Wilson activity coefficient model [4],

$$\ln\gamma_k = -\ln\left(\sum_{j=1}^{m} x_j\Lambda_{kj}\right) + 1 - \sum_{j=1}^{m}\frac{x_i\Lambda_{ik}}{\sum_{j=1}^{m} x_j\Lambda_{ij}} \tag{13}$$

Where, $\Lambda_{ij} = \frac{V_j}{V_i}\exp\left(\frac{-\lambda_{ij}-\lambda_{ii}}{RT}\right)$ (13a)

Thus, when i = j, $\Lambda_{ii} = 1$, activity coefficient of the solute can be expressed as,

$$\ln\gamma_2 = -\ln\left(x_1\Lambda_{21} + x_2\Lambda_{22} + x_3\Lambda_{23}\right) + 1 - \left(\frac{x_1\Lambda_{21}}{x_1\Lambda_{11} + x_2\Lambda_{12} + x_3\Lambda_{13}} + \frac{x_2\Lambda_{22}}{x_1\Lambda_{21} + x_2\Lambda_{22} + x_3\Lambda_{23}} + \frac{x_3\Lambda_{32}}{x_1\Lambda_{31} + x_2\Lambda_{32} + x_3\Lambda_{33}}\right) \tag{14}$$

The expression for the infinite dilute activity coefficient of the solute is as follows

$$\ln\gamma_2^{\infty} = -\ln\left(x_1\Lambda_{21} + x_3\Lambda_{23}\right) + 1 - \left(\frac{x_1\Lambda_{21}}{x_1 + x_3\Lambda_{13}} + \frac{x_3\Lambda_{32}}{x_1\Lambda_{31} + x_3}\right) \tag{15}$$

$$x_1\Lambda_{21} > x_3\Lambda_{23} \tag{15a}$$

$$x_1 > x_3\Lambda_{13} \tag{15b}$$

$$x_1\Lambda_{31} > x_3 \tag{15c}$$

Usually a small amount of co-solvent (<5%) is added to increase the solubility of solid in SCCO$_2$, thus the values of Λ_{ij} will be less than 1, hence the above inequalities are considered and equation (15) simplifies to

$$\ln\gamma_2^{\infty} = -\ln\left(x_1\Lambda_{21}\right) + 1 - \left(\Lambda_{21} + \frac{x_3\Lambda_{32}}{x_1\Lambda_{31}}\right) \tag{16}$$

Using Eq. (13) defined in terms of interaction energy parameters, Eq. (16) can be rewritten as,

$$\ln\gamma_2^{\infty} = -\ln\left(x_1\frac{V_1}{V_2}\exp\left(\frac{-(-\lambda_{12}-\lambda_{22})}{RT}\right)\right)+1-\left(\frac{V_1}{V_2}\exp\left(\frac{-(-\lambda_{12}-\lambda_{22})}{RT}\right)+\frac{x_3}{x_1}\frac{V_2}{V_1}\exp\left(\frac{-(\lambda_{13}+\lambda_{33}-\lambda_{12}-\lambda_{22})}{RT}\right)\right) \quad (17)$$

Eq. (17) can be further simplified as,

$$\ln\gamma_2^{\infty} = 1-\ln x_1-\ln V_1+\ln V_2-\frac{(-\lambda_{12}-\lambda_{22})}{RT}-\left(\frac{V_1}{V_2}\exp\left(\frac{-(-\lambda_{12}-\lambda_{22})}{RT}\right)+\frac{x_3}{x_1}\frac{V_2}{V_1}\exp\left(\frac{-(\lambda_{13}+\lambda_{33}-\lambda_{12}-\lambda_{22})}{RT}\right)\right) \quad (17a)$$

Expanding the logarithmic and exponential terms and neglecting the higher oder terms,

$$\ln\gamma_2^{\infty} = 1-\ln x_1-V_1+V_2+\frac{(-\lambda_{12}-\lambda_{22})}{RT}-\frac{V_1}{V_2}+\frac{V_1}{V_2}\frac{(-\lambda_{12}-\lambda_{22})}{RT}-\frac{x_3}{x_1}\frac{V_2}{V_1}+\frac{x_3}{x_1}\frac{V_2}{V_1}\frac{(\lambda_{13}+\lambda_{33}-\lambda_{12}-\lambda_{22})}{RT} \quad (17b)$$

Similarly, an expression for the activity coefficient of co-solvent using Wilson activity coefficient model (Eq. (13)) can be written as,

$$\ln\gamma_3 = -\ln\left(x_1\Lambda_{31}+x_2\Lambda_{32}+x_3\right)+1-\left(\frac{x_1\Lambda_{13}}{x_1+x_2\Lambda_{12}+x_3\Lambda_{13}}+\frac{x_2\Lambda_{23}}{x_1\Lambda_{21}+x_2+x_3\Lambda_{23}}+\frac{x_3}{x_1\Lambda_{31}+x_2\Lambda_{32}+x_3}\right) \quad (18)$$

The solute concentration is very small (order of 10^{-4} to 10^{-5}) in comparison to other terms. Thus, terms involving x_2 are neglected and Eq. (18) can be simplied as,

$$\ln\gamma_3 = 1-\ln\left(x_1\Lambda_{31}+x_3\right)-\left(\frac{x_1\Lambda_{13}}{x_1+x_3\Lambda_{13}}+\frac{x_3}{x_1\Lambda_{31}+x_3}\right) \quad (18a)$$

Applying the inequalities discussed in Eq. (15a), (15b) and (15c),

$$\ln\gamma_3 = 1-\ln\left(x_1\Lambda_{31}\right)-\left(\Lambda_{13}+\frac{x_3}{x_1\Lambda_{31}}\right) \quad (18b)$$

Eq. (18b) can be further expanded in terms of temperature and molar volumes using Eq. (13) as,

$$\ln\gamma_3 = 1-\ln\left(x_1\frac{V_1}{V_3}\exp\left(\frac{-(-\lambda_{13}-\lambda_{33})}{RT}\right)\right)-\left(\frac{V_3}{V_1}\exp\left(\frac{-(-\lambda_{13}-\lambda_{11})}{RT}\right)+\frac{x_3}{x_1}\frac{V_3}{V_1}\exp\left(\frac{(-\lambda_{13}-\lambda_{33})}{RT}\right)\right) \quad (18c)$$

(18c)

Expanding the exponential and logarithmic terms and neglecting the higher order in Eq. (18c),

$$\ln\gamma_3 = 1-\ln x_1 - V_1 + V_3 + \frac{(-\lambda_{13}-\lambda_{33})}{RT} - \frac{V_3}{V_1} - \frac{x_3}{x_1}\frac{V_3}{V_1} + \frac{V_3}{V_1}\frac{(-\lambda_{13}-\lambda_{11})}{RT} - \frac{x_3}{x_1}\frac{V_3}{V_1}\frac{(-\lambda_{13}-\lambda_{33})}{RT} \quad (18d)$$

Eq. (17b) and Eq. (18d) can be expressed in terms of molar densities as,

$$\ln\gamma_2^{\infty} = 1-\ln x_1 - \frac{1}{\rho_1} + \frac{1}{\rho_2} + \frac{(-\lambda_{12}-\lambda_{22})}{RT} - \frac{\rho_2}{\rho_1} + \frac{\rho_2}{\rho_1}\frac{(-\lambda_{12}-\lambda_{22})}{RT} - \frac{x_3}{x_1}\frac{\rho_1}{\rho_2} + \frac{x_3}{x_1}\frac{\rho_1}{\rho_2}\frac{(\lambda_{13}+\lambda_{33}-\lambda_{12}-\lambda_{22})}{RT} \quad (19)$$

$$\ln\gamma_3 = 1-\ln x_1 - \frac{1}{\rho_1} + \frac{1}{\rho_3} + \frac{(-\lambda_{13}-\lambda_{33})}{RT} - \frac{\rho_1}{\rho_3} - \frac{x_3}{x_1}\frac{\rho_1}{\rho_3} + \frac{\rho_1}{\rho_3}\frac{(-\lambda_{13}-\lambda_{11})}{RT} - \frac{x_3}{x_1}\frac{\rho_1}{\rho_3}\frac{(-\lambda_{13}-\lambda_{33})}{RT} \quad (20)$$

Using Eq. (19) and Eq. (20) $\ln\frac{\gamma_3}{\gamma_2^{\infty}}$ is obtained to substitute in Eq. (12) by neglecting the terms $\frac{1}{\rho_3}$ and $\frac{1}{\rho_2}$ as they are small (order of 10^{-5} to 10^{-4}) and x_1~1.

$$\ln\frac{\gamma_3}{\gamma_2^{\infty}} = \left(\frac{1}{\rho_3}-\frac{1}{\rho_2}\right)\left(1-\left(\frac{\rho_1}{\rho_3}+x_3\rho_1\right)\right)+\frac{1}{T}\left(\frac{\lambda_{12}+\lambda_{22}-\lambda_{13}-\lambda_{33}}{R}\right)+\frac{\rho_1}{T}\left(\frac{(-\lambda_{13}-\lambda_{11})}{R\rho_3}-x_3\left(\frac{(-\lambda_{13}-\lambda_{33})}{R\rho_3}\right)\right)$$
$$+\frac{\rho_2}{\rho_1}-\frac{\rho_2}{\rho_1}\frac{(-\lambda_{12}-\lambda_{22})}{RT} \quad (21)$$

In Eq. (21), $\left(\frac{\rho_1}{\rho_3}+x_3\rho_1\right) >> 1$ thus, it can be further simplified as,

$$\ln\frac{\gamma_3}{\gamma_2^{\infty}} = \left(-\frac{\rho_1}{\rho_3^2}+\frac{\rho_1}{\rho_2\rho_3}\right)+x_3\left(\frac{\rho_1}{\rho_2}-\frac{\rho_1}{\rho_3}\right)+\frac{1}{T}\left(\frac{\lambda_{12}+\lambda_{22}-\lambda_{13}-\lambda_{33}}{R}\right)+\frac{\rho_1}{T}\left(\frac{(-\lambda_{13}-\lambda_{11})}{R\rho_3}-x_3\left(\frac{(-\lambda_{13}-\lambda_{33})}{R\rho_3}\right)\right)$$
$$+\frac{\rho_2}{\rho_1}-\frac{\rho_2}{\rho_1}\frac{(-\lambda_{12}-\lambda_{22})}{RT} \quad (21a)$$

Using the condition, $\left(-\frac{\rho_1}{\rho_3^2}+\frac{\rho_1}{\rho_2\rho_3}\right) << x_3\left(\frac{\rho_1}{\rho_2}-\frac{\rho_1}{\rho_3}\right)$, Eq. (21a) can be rewritten as,

$$\ln\frac{\gamma_3}{\gamma_2^{\infty}}=x_3\left(\frac{\rho_1}{\rho_2}-\frac{\rho_1}{\rho_3}\right)+\frac{1}{T}\left(\frac{\lambda_{12}+\lambda_{22}-\lambda_{13}-\lambda_{33}}{R}\right)+\frac{\rho_1}{T}\left(\frac{(-\lambda_{13}-\lambda_{11})}{R\rho_3}-x_3\left(\frac{(-\lambda_{13}-\lambda_{33})}{R\rho_3}\right)\right)$$
$$+\frac{\rho_2}{\rho_1}-\frac{\rho_2}{\rho_1}\frac{(-\lambda_{12}-\lambda_{22})}{RT} \qquad (21b)$$

The expression for the solubility of liquid solute (x_2) in SCCO$_2$ can now be obtained using Eq. (12) and Eq. (21b).

$$\ln x_2=\ln x_3+(k-1)\ln\left(\frac{P}{P*}\right)+\frac{1}{T}\left(\frac{\Delta H_s}{R}-(B_2+B_3)+\frac{\left(\lambda_{12}+\lambda_{22}-\lambda_{13}-\lambda_{33}\right)}{R}\right)$$
$$+\left(\frac{\rho_1}{\rho_2}+\frac{\rho_1}{\rho_3}+x_3\left(\frac{\rho_1}{\rho_2}-\frac{\rho_1}{\rho_3}\right)\right)+k\rho_1(2B_{11}-B)+\frac{\rho_1}{T}\left(\frac{(-\lambda_{13}-\lambda_{11})}{R\rho_3}-x_3\left(\frac{(-\lambda_{13}-\lambda_{33})}{R\rho_3}\right)\right)$$
$$+\left(\frac{\rho_2}{\rho_1}-\frac{1}{T}\left(\frac{\rho_2(-\lambda_{12}-\lambda_{22})}{\rho_1 R}\right)\right)-q_s+(A_2+A_3)-\left(\frac{\phi_{231_k}\phi_1^{*k}}{\phi_{231_k}^{*}}\frac{\phi_2^{*}\phi_3^{*}}{\phi_{sat}^{2}}\frac{\left(P^{*}\right)^2}{x_2^l\gamma_2^l}\right) \qquad (22)$$

Eq. (22) is rearranged as follows

$$\ln x_2=\ln x_3+(k-1)\ln\left(\frac{P}{P*}\right)+\frac{W_1}{T}+\left(\frac{\rho_1}{\rho_2}+\frac{\rho_1}{\rho_3}+x_3\left(\frac{\rho_1}{\rho_2}-\frac{\rho_1}{\rho_3}\right)+kW_2\rho_1\right)$$
$$+\frac{\rho_1}{RT\rho_3}\left(W_3-x_3W_4\right)+\left(\frac{\rho_2}{\rho_1}-\frac{\rho_2}{\rho_1 TR}W_5\right)+W_6 \qquad (23)$$

Where,

$$W_1=\frac{\Delta H_s}{R}-(B_2+B_3)+\frac{\lambda_2''-\lambda_2}{R} \qquad (23a)$$

$$W_2=2B_{11}-B \qquad (23b)$$

$$W_3=-\lambda_{13}-\lambda_{11} \qquad (23c)$$

$$W_4=-\lambda_{13}-\lambda_{33} \qquad (23d)$$

$$W_5=-\lambda_{12}-\lambda_{22} \qquad (23e)$$

$$W_6=A_2+A_3-q_s-\left(\frac{\phi_{231_k}\phi_1^{*k}}{\phi_{231_k}^{*}}\frac{\phi_2^{*}\phi_3^{*}}{\phi_{sat}^{2}}\frac{\left(P^{*}\right)^2}{x_2^l\gamma_2^l}\right) \qquad (23f)$$

Eq. (23) correlates the solubility of liquid solute in $SCCO_2$ + co-solvent system in terms of co-solvent composition, temperature, pressure and density of supercritical fluid. *k* is the association number for SCF, W_1 to W_6 are the temperature independent parameters and ρ_1, ρ_2 and ρ_3 are the molar densities of solvent, solute and co-solvent, respectively.

Case 2: New model based on van Laar activity coefficient model

The activity coefficient for a solute (γ_2) in a ternary mixture using van Laar activity coefficient model can be written as [4],

$$\ln\gamma_2 = \frac{x_3^2 A_{23}\left(\frac{A_{32}}{A_{23}}\right)^2 + x_1^2 A_{21}\left(\frac{A_{12}}{A_{21}}\right)^2 + x_3 x_1\left(\frac{A_{32}}{A_{23}}\right)\left(\frac{A_{12}}{A_{21}}\right)\left(A_{23} + A_{21} - A_{13}\left(\frac{A_{21}}{A_{12}}\right)\right)}{\left(x_2 + x_3\frac{A_{32}}{A_{23}} + x_1\frac{A_{12}}{A_{21}}\right)^2} \quad (24)$$

In Eq. (24),

$$A_{12} = 2q_1 a_{12},\ A_{21} = 2q_2 a_{12} \text{ and } \frac{q_1}{q_2} = \frac{V_1}{V_2} \quad (24a)$$

$$A_{13} = 2q_1 a_{13},\ A_{31} = 2q_3 a_{13} \text{ and } \frac{q_1}{q_3} = \frac{V_1}{V_3} \quad (24b)$$

$$A_{23} = 2q_2 a_{23},\ A_{32} = 2q_3 a_{23} \text{ and } \frac{q_2}{q_3} = \frac{V_2}{V_3} \quad (24c)$$

Where, q_i is the measure of size of component i and a_{ij} denotes the interaction energy between the two components.

Eq. (24) can be written as follows,

$$\ln\gamma_2 = \frac{2q_2\left(x_3^2 a_{23}\left(\frac{V_3}{V_2}\right)^2 + x_1^2 a_{12}\left(\frac{V_1}{V_2}\right)^2 + x_3 x_1\left(\frac{V_3}{V_2}\right)\left(\frac{V_1}{V_2}\right)\left(a_{23} + a_{12} - a_{13}\right)\right)}{\left(x_2 + x_3\frac{V_3}{V_2} + x_1\frac{V_1}{V_2}\right)^2} \quad (25)$$

The concentration of solute in $SCCO_2$ is very small (order of 10^{-5} to 10^{-4}). Thus, the activity coefficient can be considered at infinite dilution and Eq. (25) would reduce to,

$$\ln\gamma_2^{\infty} = \frac{2q_2\left(x_3^2 a_{23}\left(\frac{V_3}{V_2}\right)^2 + x_1^2 a_{12}\left(\frac{V_1}{V_2}\right)^2 + x_3 x_1\left(\frac{V_3}{V_2}\right)\left(\frac{V_1}{V_2}\right)\left(a_{23}+a_{12}-a_{13}\right)\right)}{\left(x_3^2\left(\frac{V_3}{V_2}\right)^2 + x_1^2\left(\frac{V_1}{V_2}\right)^2 + 2x_3 x_1\left(\frac{V_3}{V_2}\right)\left(\frac{V_1}{V_2}\right)\right)} \tag{26}$$

In Eq. (26), $x_3^2\left(\frac{V_3}{V_2}\right)^2 < x_1^2\left(\frac{V_1}{V_2}\right)^2$, thus the first term in the numerator and denominator is neglected in comparison to other terms. After simplification, Eq. (26) can be rewritten as,

$$\ln\gamma_2^{\infty} = \frac{2q_2\left(x_1 a_{12}\frac{V_1}{V_2} + x_3\frac{V_3}{V_2}\left(a_{23}+a_{12}-a_{13}\right)\right)}{\left(x_1\frac{V_1}{V_2} + 2x_3\frac{V_3}{V_2}\right)} \tag{26a}$$

Eq. (26a) can also be written as,

$$\ln\gamma_2^{\infty} = 2q_2\frac{V_2}{x_1 V_1}\left(x_1 a_{12}\frac{V_1}{V_2} + x_3\frac{V_3}{V_2}\left(a_{23}+a_{12}-a_{13}\right)\right)\left(1+2\frac{x_3}{x_1}\frac{V_3}{V_1}\right)^{-1} \tag{26b}$$

Since, $2\frac{V_3}{V_1}\frac{x_3}{x_1} < 1$, the last term in Eq. (26b) is expanded as an infinite binomial series expansion and further simplified by neglecting the higher order terms.

$$\ln\gamma_2^{\infty} = 2q_2 a_{12} + 2q_2\frac{x_3}{x_1}\frac{V_3}{V_1}\left(a_{23}-a_{12}-a_{13}\right) \tag{26c}$$

Similarly, the activity coefficient of the co-solvent in SCF phase can also be written using van Laar activity coefficient model as follows,

$$\ln\gamma_3 = \frac{x_1^2 A_{31}\left(\frac{A_{13}}{A_{31}}\right)^2 + x_2^2 A_{32}\left(\frac{A_{23}}{A_{32}}\right)^2 + x_1 x_2\left(\frac{A_{13}}{A_{31}}\right)\left(\frac{A_{23}}{A_{32}}\right)\left(A_{31}+A_{32}-A_{21}\left(\frac{A_{32}}{A_{23}}\right)\right)}{\left(x_3 + x_1\frac{A_{13}}{A_{31}} + x_2\frac{A_{23}}{A_{32}}\right)^2} \tag{27}$$

Using Eq. (24a) to (24c), Eq. (27) can be modified in terms of molar volumes and interaction energy parameters as,

$$\ln \gamma_3 = \frac{2q_3\left(x_1^2 a_{13}\left(\frac{V_1}{V_3}\right)^2 + x_2^2 a_{23}\left(\frac{V_2}{V_3}\right)^2 + x_1 x_2\left(\frac{V_1}{V_3}\right)\left(\frac{V_2}{V_3}\right)\left(a_{13}+a_{23}-a_{12}\right)\right)}{\left(x_3 + x_1\frac{V_1}{V_3} + x_2\frac{V_2}{V_3}\right)^2} \tag{28}$$

The concentration of solute is very small thus the terms involving x_2 become negligible and Eq. (28) reduces to,

$$\ln \gamma_3 = \frac{2q_3 x_1^2 a_{13}\left(\frac{V_1}{V_3}\right)^2}{\left(x_3 + x_1\frac{V_1}{V_3}\right)^2} \tag{28a}$$

Simplifying Eq. (28a) further using $x_3^2 < x_1^2\left(\frac{V_1}{V_3}\right)^2$,

$$\ln \gamma_3 = 2q_3 x_1 a_{13}\left(1 + 2x_3\frac{V_3}{V_1}\right)^{-1} \tag{28b}$$

Expanding the last term using binomial expansion,

$$\ln \gamma_3 = 2q_3 x_1 a_{13} - 4q_3 a_{13} x_3 x_1 \frac{V_3}{V_1} \tag{28c}$$

Using Eq. (26c) and Eq. (28c), and substituting $x_1 \sim 1$, $\ln\frac{\gamma_3}{\gamma_2^\infty}$ is obtained in terms of molar densities as follows,

$$\ln\frac{\gamma_3}{\gamma_2^\infty} = 2q_3 a_{13} - 2q_2 a_{12} - x_3\frac{\rho_1}{\rho_3}\left(4q_3 a_{13} - 2q_2(a_{23} - a_{12} - a_{13})\right) \tag{29}$$

The expression for the solubility of liquid solute (x_2) in $SCCO_2$ can now be obtained using Eq. (12) and Eq. (29).

$$\ln x_2 = \ln x_3 + (k-1)\ln\left(\frac{P}{P*}\right) + \rho_1\left(\frac{1}{\rho_2} + \frac{1}{\rho_3} - x_3\left(\frac{4q_3 a_{13} - 2q_3\left(a_{23} - a_{12} - a_{13}\right)}{\rho_3}\right) + k(2B_{11} - B)\right)$$
$$+\frac{1}{T}\left(\frac{\Delta H_s}{R} - (B_2 + B_3)\right) - q_s + (A_2 + A_3) - \left(\frac{\phi_{231_k}\phi_1^{*k}}{\phi_{231_k}^*}\frac{\phi_2^*\phi_3^*}{\phi_{sat}^2}\frac{\left(P^*\right)^2}{x_2^l\gamma_2^l}\right) \tag{30}$$

Eq. (30), can be rewritten by grouping the similar terms together as,

$$\ln x_2 = \ln x_3 + (k-1)\ln\left(\frac{P}{P*}\right) + \frac{L_1}{T} + \left(\frac{\rho_1}{\rho_2} + \frac{\rho_1}{\rho_3} - \frac{\rho_1 x_3 L_2}{\rho_3} + k\rho_1 L_3\right) + L_4 \qquad (31)$$

Where,

$$L_1 = \frac{\Delta H_s}{R} - (B_2 + B_3) \qquad (31a)$$

$$L_2 = 4q_3 a_{13} - 2q_3\left(a_{23} - a_{12} - a_{13}\right) \qquad (31b)$$

$$L_3 = 2B_{11} - B \qquad (31c)$$

$$L_4 = A_2 + A_3 - q_s - \left(\frac{\phi_{231_k}\phi_1^{*k}}{\phi_{231_k}^{*}}\,\frac{\phi_2^{*}\phi_3^{*}}{\phi_{sat}^{2}}\,\frac{\left(P^{*}\right)^2}{x_2^l\gamma_2^l}\right) \qquad (31d)$$

Eq. (31) represents a new five parameter model for the solubility of liquid solute in $SCCO_2$ in presence of co-solvents developed using association theory based on the van Laar activity coefficient model.

Reference

[1] S.N. Reddy, G. Madras, A new semi-empirical model for correlating the solubilities of solids in supercritical carbon dioxide with co-solvents, *Fluid Phase Equilib.* 310 (2011) 207-212.

[2] S.N. Reddy, G. Madras, Modeling of ternary solubilities of solids in supercritical carbon dioxide in the presence of co-solvents or cosolutes, *J. Supercrit. Fluids* 63 (2012) 105-114.

[3] C. Jiang, Q. Pan, Z. Pan, Solubility behavior of solids and liquids in compressed gases, *J. Supercrit. Fluids* 12 (1998) 1-9.

[4] S.I. Sandler, in: Chemical, biochemical, and engineering thermodynamics, Wiley , India, 2006, 477-478.

Appendix-3
Results on solubility and extraction experiments

3.1 Results on the solubility measurements

1. Solubility of trimethyl phosphate (TMP) in $SCCO_2$:

T (K)	P (MPa)	Solubility (mol/mol) y_2			Average amount of compound collected in one exp., (mg)	Time of collection (min)
		Exp-1	Exp-2	Exp-3		
313.0	8.3	0.182	0.192	0.190	701	10
313.0	10.3	0.187	0.192	0.195	732	10
313.0	12.3	0.191	0.187	0.195	755	10
313.0	15.0	0.192	0.187	0.197	770	10
313.0	20.0	0.194	0.195	0.189	795	10
313.0	25.0	0.198	0.189	0.196	826	10
323.0	10.3	0.175	0.181	0.185	675	10
323.0	12.3	0.191	0.184	0.193	759	10
323.0	15.0	0.190	0.185	0.196	761	10
323.0	20.0	0.192	0.193	0.187	785	10
323.0	25.0	0.192	0.196	0.187	790	10
333.0	10.3	0.122	0.124	0.121	441	10
333.0	12.3	0.147	0.157	0.155	552	10
333.0	14.0	0.161	0.164	0.169	620	10
333.0	16.0	0.172	0.178	0.182	678	10
333.0	18.0	0.182	0.187	0.178	730	10
333.0	20.0	0.188	0.187	0.181	765	10
333.0	25.0	0.186	0.190	0.183	770	10

CO_2 flow rate at pump head: 0.1 mL/min, pump head temperature: 268 K; Pump head pressure: experimental pressure

2. Solubility of triethyl phosphate (TEP) in $SCCO_2$:

T (K)	P (MPa)	Solubility (mol/mol) y_2			Average amount of compound collected in one exp., (mg)	Time of collection (min)
		Exp-1	Exp-2	Exp-3		
313.0	8.3	0.155	0.162	0.163	750	10
313.0	10.3	0.160	0.165	0.160	800	10
313.0	12.3	0.163	0.165	0.160	815	10
313.0	15.0	0.162	0.159	0.167	820	10
313.0	20.0	0.162	0.169	0.158	830	10
313.0	25.0	0.159	0.166	0.165	830	10
323.0	10.3	0.146	0.148	0.140	710	10
323.0	12.3	0.153	0.157	0.145	756	10
323.0	15.0	0.160	0.158	0.150	805	10
323.0	20.0	0.160	0.162	0.152	820	10
323.0	25.0	0.160	0.164	0.157	835	10
333.0	10.3	0.091	0.095	0.085	415	10
333.0	12.3	0.116	0.120	0.113	550	10
333.0	14.0	0.147	0.146	0.140	725	10
333.0	16.0	0.149	0.155	0.147	745	10
333.0	18.0	0.152	0.152	0.156	766	10
333.0	20.0	0.153	0.159	0.150	781	10
333.0	25.0	0.154	0.160	0.152	795	10

CO_2 flow rate at pump head: 0.1 mL/min, pump head temperature: 268 K; Pump head pressure: experimental pressure

3. Solubility of tributyl phosphate (TBP) in $SCCO_2$:

T (K)	P (MPa)	Solubility (mol/mol) y_2			Average amount of compound collected in one exp., (mg)	Time of collection (min)
		Exp-1	**Exp-2**	**Exp-3**		
313.0	8.3	0.108	0.107	0.100	721	10
313.0	10.3	0.110	0.106	0.115	750	10
313.0	12.3	0.112	0.117	0.109	772	10
313.0	15.0	0.118	0.120	0.111	825	10
313.0	20.0	0.118	0.121	0.112	836	10
313.0	25.0	0.116	0.119	0.110	840	10
323.0	10.3	0.094	0.090	0.091	624	10
323.0	12.3	0.106	0.102	0.100	725	10
323.0	15.0	0.109	0.113	0.101	755	10
323.0	20.0	0.114	0.116	0.110	810	10
323.0	25.0	0.114	0.109	0.117	824	10
333.0	10.3	0.065	0.060	0.062	420	10
333.0	12.3	0.086	0.090	0.085	575	10
333.0	14.0	0.105	0.105	0.097	721	10
333.0	16.0	0.105	0.108	0.100	730	10
333.0	18.0	0.106	0.105	0.109	740	10
333.0	20.0	0.109	0.115	0.105	771	10
333.0	25.0	0.112	0.117	0.105	811	10

CO_2 flow rate at pump head: 0.1 mL/min, pump head temperature: 268 K; Pump head pressure: experimental pressure

4. Solubility of triamyl phosphate (TAP) in $SCCO_2$:

T (K)	P (MPa)	Solubility (mol/mol) y_2			Average amount of compound collected in one exp., (mg)	Time of collection (min)
		Exp-1	**Exp-2**	**Exp-3**		
313.0	8.3	0.095	0.098	0.097	730	10
313.0	10.3	0.096	0.104	0.097	745	10
313.0	12.3	0.096	0.098	0.104	755	10
313.0	15.0	0.099	0.102	0.104	789	10
313.0	20.0	0.103	0.106	0.098	834	10
313.0	25.0	0.105	0.108	0.097	865	10
323.0	10.3	0.093	0.095	0.085	720	10
323.0	12.3	0.097	0.093	0.104	762	10
323.0	15.0	0.097	0.101	0.095	770	10
323.0	20.0	0.102	0.101	0.095	830	10
323.0	25.0	0.103	0.102	0.096	850	10
333.0	10.3	0.015	0.014	0.014	110	10
333.0	12.3	0.056	0.056	0.051	424	10
333.0	14.0	0.094	0.090	0.093	740	10
333.0	16.0	0.094	0.099	0.095	745	10
333.0	18.0	0.093	0.092	0.102	740	10
333.0	20.0	0.094	0.102	0.095	750	10
333.0	25.0	0.096	0.104	0.095	785	10

CO_2 flow rate at pump head: 0.1 mL/min, pump head temperature: 268 K; Pump head pressure: experimental pressure

5. Solubility of trihexyl phosphate (THP) in $SCCO_2$:

T (K)	P (MPa)	Solubility (mol/mol) y_2 Exp-1	Exp-2	Exp-3	Average amount of compound collected in one exp., (mg)	Time of collection (min)
313.0	8.3	0.072	0.076	0.078	610	10
313.0	10.3	0.076	0.085	0.083	658	10
313.0	12.3	0.086	0.083	0.078	758	10
313.0	15.0	0.082	0.087	0.081	730	10
313.0	20.0	0.087	0.086	0.079	794	10
313.0	25.0	0.089	0.086	0.080	830	10
323.0	10.3	0.063	0.067	0.066	510	10
323.0	12.3	0.072	0.073	0.079	604	10
323.0	15.0	0.079	0.083	0.074	700	10
323.0	20.0	0.082	0.078	0.081	742	10
323.0	25.0	0.082	0.079	0.081	784	10
333.0	10.3	0.0050	0.0048	0.0053	122	30
333.0	12.3	0.025	0.024	0.023	224	10
333.0	14.0	0.049	0.046	0.044	442	10
333.0	16.0	0.068	0.062	0.062	592	10
333.0	18.0	0.073	0.072	0.066	650	10
333.0	20.0	0.077	0.076	0.070	688	10
333.0	25.0	0.081	0.076	0.075	748	10

CO_2 flow rate at pump head: 0.1 mL/min, pump head temperature: 268 K; Pump head pressure: experimental pressure

6. Solubility of tri-*iso*-amyl phosphate (TiAP) in $SCCO_2$:

T (K)	P (MPa)	Solubility (mol/mol) y_2 Exp-1	Exp-2	Exp-3	Average amount of compound collected in one exp., (mg)	Time of collection (min)
313.0	8.3	0.081	0.086	0.082	615	10
313.0	10.3	0.084	0.090	0.083	640	10
313.0	12.3	0.086	0.090	0.089	664	10
313.0	15.0	0.086	0.094	0.087	674	10
313.0	20.0	0.091	0.095	0.085	734	10
313.0	25.0	0.093	0.095	0.086	755	10
323.0	10.3	0.083	0.076	0.078	632	10
323.0	12.3	0.084	0.092	0.089	651	10
323.0	15.0	0.084	0.090	0.091	660	10
323.0	20.0	0.089	0.084	0.094	710	10
323.0	25.0	0.092	0.092	0.083	750	10
333.0	10.3	0.014	0.013	0.014	330	30
333.0	12.3	0.067	0.060	0.065	510	10
333.0	14.0	0.078	0.085	0.076	605	10
333.0	16.0	0.083	0.087	0.078	650	10
333.0	18.0	0.086	0.087	0.078	679	10
333.0	20.0	0.086	0.083	0.081	690	10
333.0	25.0	0.090	0.083	0.082	731	10

CO_2 flow rate at pump head: 0.1 mL/min, pump head temperature: 268 K; Pump head pressure: experimental pressure

7. Solubility of dibutylbutyl phosphonate (DBBP) in $SCCO_2$:

T (K)	P (MPa)	Solubility (mol/mol) y_2			Average amount of compound collected in one exp., (mg)	Time of collection (min)
		Exp-1	**Exp-2**	**Exp-3**		
313.0	10.3	0.099	0.100	0.093	625	10
313.0	12.3	0.103	0.103	0.094	655	10
313.0	15.0	0.104	0.106	0.097	672	10
313.0	20.0	0.105	0.106	0.099	694	10
313.0	25.0	0.108	0.102	0.103	726	10
323.0	10.3	0.089	0.096	0.093	555	10
323.0	12.3	0.106	0.108	0.103	680	10
323.0	15.0	0.113	0.111	0.107	740	10
323.0	20.0	0.114	0.115	0.105	761	10
323.0	25.0	0.116	0.110	0.111	784	10
333.0	10.3	0.085	0.087	0.094	525	10
333.0	12.3	0.112	0.110	0.106	720	10
333.0	15.0	0.111	0.118	0.116	725	10
333.0	20.0	0.112	0.118	0.121	745	10
333.0	25.0	0.119	0.115	0.121	810	10

CO_2 flow rate at pump head: 0.1 mL/min, pump head temperature: 268 K; Pump head pressure: experimental pressure

8. Solubility of diamylamyl phosphonate (DAAP) in $SCCO_2$:

T (K)	P (MPa)	Solubility (mol/mol) y_2			Average amount of compound collected in one exp., (mg)	Time of collection (min)
		Exp-1	**Exp-2**	**Exp-3**		
313.0	10.3	0.085	0.084	0.078	650	10
313.0	12.3	0.088	0.091	0.082	685	10
313.0	15.0	0.092	0.090	0.086	726	10
313.0	20.0	0.093	0.091	0.087	744	10
313.0	25.0	0.092	0.087	0.095	751	10
323.0	10.3	0.072	0.069	0.077	541	10
323.0	12.3	0.087	0.094	0.086	675	10
323.0	15.0	0.092	0.091	0.098	724	10
323.0	20.0	0.094	0.098	0.090	740	10
323.0	25.0	0.096	0.099	0.091	784	10
333.0	10.3	0.068	0.072	0.062	512	10
333.0	12.3	0.084	0.090	0.093	645	10
333.0	15.0	0.092	0.096	0.098	729	10
333.0	20.0	0.096	0.099	0.100	772	10
333.0	25.0	0.101	0.104	0.093	831	10

CO_2 flow rate at pump head: 0.1 mL/min, pump head temperature: 268 K; Pump head pressure: experimental pressure

9. Solubility of trioctylmethylammonium chloride (TOMAC) in SCCO$_2$:

T (K)	P (MPa)	Solubility (mol/mol) y_2 x 10^5			Average amount of compound collected in one exp., (mg)	Time of collection (hours)
		Exp-1	Exp-2	Exp-3		
313.0	8.3	1.4	1.5	1.3	18	12
313.0	10.3	6.7	6.2	5.5	75	10
313.0	15.0	9.7	9.1	8.0	65	6
313.0	20.0	9.6	10.4	11.4	78	6
313.0	25.0	11.9	12.8	11.6	89	6
313.0	30.0	11.5	12.9	13.6	96	6
323.0	10.3	2.0	1.8	1.7	24	12
323.0	15.0	5.7	5.5	4.7	64	10
323.0	20.0	7.6	7.4	8.6	98	10
323.0	25.0	9.0	10.2	9.3	71	6
323.0	30.0	10.9	10.6	9.2	75	6
333.0	10.3	0.55	0.65	0.61	20	24
333.0	15.0	3.2	3.7	3.9	46	10
333.0	20.0	4.8	5.0	5.7	65	10
333.0	25.0	6.0	6.9	7.0	49	6
333.0	30.0	7.4	7.2	8.1	57	6

CO$_2$ flow rate at pump head: 0.2 mL/min, pump head temperature: 268 K; Pump head pressure: experimental pressure

10. Solubility TOMAC in SCCO$_2$ in the presence of 1.05 mol % of *n*-hexane as a co-solvent:

T (K)	P (MPa)	Solubility (mol/mol) y_2 x 10^5			Average amount of compound collected in one exp., (mg)	Time of collection (hours)
		Exp-1	Exp-2	Exp-3		
313.0	10.0	6.4	5.6	5.4	70	10
313.0	15.0	9.7	8.7	8.3	65	6
313.0	20.0	11.7	10.0	9.9	80	6
313.0	25.0	11.8	11.4	10.5	82	6
313.0	30.0	12.0	12.4	11.4	85	6
323.0	10.0	1.9	1.6	1.8	25	12
323.0	15.0	4.8	5.2	4.8	68	10
323.0	20.0	7.5	6.6	7.0	95	10
323.0	25.0	9.0	7.5	9.1	72	6
323.0	30.0	9.7	11.0	9.9	78	6

CO$_2$ flow rate at pump head: 0.2 mL/min, pump head temperature: 268 K; Pump head pressure: experimental pressure

11. Solubility TOMAC in SCCO$_2$ in the presence of 2.1 mol % of *n*-hexane as a co-solvent:

T (K)	P (MPa)	Solubility (mol/mol) y_2 x 10^5			Average amount of compound collected in one exp., (mg)	Time of collection (hours)
		Exp-1	Exp-2	Exp-3		
313.0	10.0	7.1	8.0	8.4	80	10
313.0	15.0	11.9	11.6	10.8	82	6
313.0	20.0	13.7	14.0	12.9	96	6
313.0	25.0	15.1	14.7	14.0	108	6
313.0	30.0	15.8	15.2	14.8	114	6
323.0	10.0	2.4	2.8	2.6	30	12
323.0	15.0	7.4	7.6	6.4	85	10
323.0	20.0	8.6	9.8	10.3	102	10
323.0	25.0	11.0	12.4	12.8	78	6
323.0	30.0	14.2	13.7	13.0	102	6

CO$_2$ flow rate at pump head: 0.2 mL/min, pump head temperature: 268 K; Pump head pressure: experimental pressure

12. Solubility TOMAC in SCCO$_2$ in the presence of 4.2 mol % of *n*-hexane as a co-solvent:

T (K)	P (MPa)	Solubility (mol/mol) y_2 x 10^5			Average amount of compound collected in one exp., (mg)	Time of collection (hours)
		Exp-1	Exp-2	Exp-3		
313.0	10.0	9.1	9.6	10.0	104	10
313.0	15.0	12.6	13.0	12.0	84	6
313.0	20.0	13.4	14.2	14.5	96	6
313.0	25.0	14.1	14.5	15.3	102	6
313.0	30.0	14.7	15.1	16.0	108	6
323.0	10.0	4.2	4.0	4.9	58	12
323.0	15.0	7.7	8.3	8.1	90	10
323.0	20.0	10.1	10.6	10.9	121	10
323.0	25.0	12.4	13.1	13.3	91	6
323.0	30.0	13.1	13.8	14.0	96	6

CO$_2$ flow rate at pump head: 0.2 mL/min, pump head temperature: 268 K; Pump head pressure: experimental pressure

13. Solubility TOMAC in SCCO$_2$ in the presence of 1.05 mol % of *n*-propanol as a co-solvent:

T (K)	P (MPa)	Solubility (mol/mol) y_2 x 10^5			Average amount of compound collected in one exp., (mg)	Time of collection (hours)
		Exp-1	Exp-2	Exp-3		
313.0	10.0	8.8	8.2	9.2	60	6
313.0	15.0	21	22	18	48	2
313.0	20.0	28	26	24	64	2
313.0	25.0	34	40	37	80	2
313.0	30.0	38	45	46	88	2
323.0	10.0	1.8	2.2	2.0	24	12
323.0	15.0	10	12	12	96	6
323.0	20.0	23	19	22	54	2
323.0	25.0	26	29	28	60	2
323.0	30.0	30	38	33	72	2

CO$_2$ flow rate at pump head: 0.2 mL/min, pump head temperature: 268 K; Pump head pressure: experimental pressure

14. Solubility TOMAC in SCCO$_2$ in the presence of 2.1 mol % of *n*-propanol as a co-solvent:

T (K)	P (MPa)	Solubility (mol/mol) y_2 x 10^5			Average amount of compound collected in one exp., (mg)	Time of collection (hours)
		Exp-1	Exp-2	Exp-3		
313.0	10.0	20	24	24	46	2
313.0	15.0	59	52	49	64	1
313.0	20.0	81	86	93	94	1
313.0	25.0	102	114	116	121	1
313.0	30.0	130	132	120	156	1
323.0	10.0	4.2	4.8	4.6	70	10
323.0	15.0	34	30	28	78	2
323.0	20.0	55	63	66	62	1
323.0	25.0	106	90	88	128	1
323.0	30.0	120	113	125	140	1

CO$_2$ flow rate at pump head: 0.2 mL/min, pump head temperature: 268 K; Pump head pressure: experimental pressure

15. Solubility TOMAC in SCCO$_2$ in the presence of 4.2 mol % of *n*-propanol as a co-solvent:

T (K)	P (MPa)	Solubility (mol/mol) y_2 x 10^5			Average amount of compound collected in one exp., (mg)	Time of collection (min)
		Exp-1	Exp-2	Exp-3		
313.0	10.0	114	110	104	136	60
313.0	15.0	232	225	236	135	30
313.0	20.0	328	335	329	195	30
313.0	25.0	403	449	435	243	30
313.0	30.0	488	480	401	299	30
323.0	10.0	16.3	15.5	13.4	38	120
323.0	15.0	107	117	123	125	60
323.0	20.0	211	230	240	125	30
323.0	25.0	340	365	375	205	30
323.0	30.0	436	450	433	516	30

CO$_2$ flow rate at pump head: 0.2 mL/min, pump head temperature: 268 K; Pump head pressure: experimental pressure

16. Solubility TOMAC in SCCO$_2$ in the presence of 1.05 mol % of methanol as a co-solvent:

T (K)	P (MPa)	Solubility (mol/mol) y_2 x 10^5			Average amount of compound collected in one exp., (mg)	Time of collection (hours)
		Exp-1	Exp-2	Exp-3		
313.0	10.0	9.9	10.4	11.1	66	6
313.0	15.0	24	23	27	55	2
313.0	20.0	35	35	29	80	2
313.0	25.0	40	46	42	94	2
313.0	30.0	50	46	52	120	2
323.0	10.0	2.4	2.8	2.5	27	10
323.0	15.0	14.1	12.5	12.4	32	2
323.0	20.0	25	22	23	58	2
323.0	25.0	35	30	33	82	2
323.0	30.0	43	44	37	102	2

CO$_2$ flow rate at pump head: 0.2 mL/min, pump head temperature: 268 K; Pump head pressure: experimental pressure

17. Solubility TOMAC in $SCCO_2$ in the presence of 2.1 mol % of methanol as a co-solvent:

T (K)	P (MPa)	Solubility (mol/mol) y_2 x 10^5			Average amount of compound collected in one exp., (mg)	Time of collection (hours)
		Exp-1	Exp-2	Exp-3		
313.0	10.0	30	27	25	70	2
313.0	15.0	65	70	77	74	1
313.0	20.0	104	108	102	126	1
313.0	25.0	150	139	149	160	1
313.0	30.0	163	175	170	211	1
323.0	10.0	7.1	6.2	5.9	82	10
323.0	15.0	39	33	35	45	1
323.0	20.0	65	78	68	76	1
323.0	25.0	110	95	105	131	1
323.0	30.0	114	131	135	135	1

CO_2 flow rate at pump head: 0.2 mL/min, pump head temperature: 268 K; Pump head pressure: experimental pressure

18. Solubility TOMAC in $SCCO_2$ in the presence of 4.2 mol % of methanol as a co-solvent:

T (K)	P (MPa)	Solubility (mol/mol) y_2 x 10^5			Average amount of compound collected in one exp., (mg)	Time of collection (min)
		Exp-1	Exp-2	Exp-3		
313.0	10.0	96	102	103	110	60
313.0	15.0	298	313	323	175	30
313.0	20.0	418	440	450	251	30
313.0	25.0	535	563	572	325	30
313.0	30.0	608	636	656	375	30
323.0	10.0	17	19	18.6	40	120
323.0	15.0	137	140	148	160	60
323.0	20.0	268	281	289	320	60
323.0	25.0	404	424	433	246	30
323.0	30.0	495	520	530	305	30

CO_2 flow rate at pump head: 0.2 mL/min, pump head temperature: 268 K; Pump head pressure: experimental pressure

19. Solubility of *N*,*N*-dihexylhexanamide (DHHA) in $SCCO_2$:

T (K)	P (MPa)	Solubility (mol/mol) y_2			Average amount of compound collected in one exp., (mg)	Time of collection (min)
		Exp-1	Exp-2	Exp-3		
313.0	8.0	0.055	0.051	0.050	21	600
313.0	10.0	12.8	12.5	11.6	84	10
313.0	12.0	32	34	32	216	10
313.0	14.0	60	56	59	421	10
313.0	16.0	76	74	69	544	10
313.0	18.0	89	91	97	652	10
313.0	20.0	97	103	107	720	10
323.0	10.0	0.35	0.38	0.39	55	240
323.0	12.0	5.8	6.1	6.4	114	30
323.0	14.0	16.9	18.7	18.3	113	10
323.0	16.0	33	30	32	226	10
323.0	18.0	47	51	50	328	10
323.0	20.0	60	64	66	428	10
333.0	10.0	0.07	0.06	0.07	26	600
333.0	12.0	0.65	0.72	0.69	51	120
333.0	14.0	4.3	4.7	4.7	76	30
333.0	16.0	10.0	10.7	10.9	201	30
333.0	18.0	22	21	20	148	10
333.0	20.0	29	28	30	200	10

CO_2 flow rate at pump head: 0.1 mL/min, pump head temperature: 268 K; Pump head pressure: experimental pressure

20. Solubility of *N*,*N*-dihexyloctanamide (DHOA) in $SCCO_2$:

T (K)	P (MPa)	Solubility (mol/mol) y_2			Average amount of compound collected in one exp., (mg)	Time of collection (min)
		Exp-1	Exp-2	Exp-3		
313.0	10.0	8.7	8.2	8.4	62	10
313.0	12.0	19.8	18.9	18.4	144	10
313.0	14.0	32	33	31	238	10
313.0	16.0	40	38	42	302	10
313.0	18.0	46	45	49	352	10
313.0	20.0	50	51	54	388	10
323.0	10.0	0.25	0.27	0.26	108	600
323.0	12.0	4.4	4.2	4.1	94	30
323.0	14.0	13	12.2	12	95	10
323.0	16.0	23	21	22	170	10
323.0	18.0	28	28	26	210	10
323.0	20.0	34	32	31	258	10
333.0	10.0	0.045	0.043	0.047	45	1440
333.0	12.0	0.54	0.52	0.54	139	360
333.0	14.0	2.6	2.8	2.9	114	60
333.0	16.0	8.7	8.0	7.9	64	10
333.0	18.0	14.2	13.4	13.0	105	10
333.0	20.0	19	18.8	18.4	142	10

CO_2 flow rate at pump head: 0.1 mL/min, pump head temperature: 268 K; Pump head pressure: 9experimental pressure

21. Solubility of *N*,*N*-dihexyldecanamide (DHDA) in $SCCO_2$:

T (K)	P (MPa)	Solubility (mol/mol) y_2			Average amount of compound collected in one exp., (mg)	Time of collection (min)
		Exp-1	Exp-2	Exp-3		
313.0	8.0	0.01	0.0099	0.011	16	1440
313.0	10.0	1.9	1.7	1.8	91	60
313.0	12.0	4.3	4.6	4.7	96	30
313.0	14.0	8.0	7.4	7.5	63	10
313.0	16.0	13.1	12.4	12.1	105	10
313.0	18.0	19.1	19.8	20.2	155	10
313.0	20.0	28.5	27.9	27.6	235	10
323.0	10.0	0.052	0.050	0.48	35	720
323.0	12.0	1.2	1.1	1.1	60	60
323.0	14.0	3.3	3.2	3.1	78	30
323.0	16.0	6.0	5.7	6.1	72	15
323.0	18.0	10.3	9.8	9.5	83	10
323.0	20.0	13.3	13.6	13.9	107	10
333.0	10.0	0.0050	0.049	0.0054	12	1440
333.0	12.0	0.10	0.09	0.09	60	720
333.0	14.0	0.71	0.67	0.65	101	180
333.0	16.0	2.3	2.2	2.1	54	30
333.0	18.0	4.3	3.9	4.0	105	30
333.0	20.0	6.3	6.6	6.9	153	30

CO_2 flow rate at pump head: 0.1 mL/min, pump head temperature: 268 K; Pump head pressure: experimental pressure

22. Solubility of *N*,*N*- di-2-ethylhexylacetamide (D2EHAA) in $SCCO_2$:

T (K)	P (MPa)	Solubility (mol/mol) y_2			Average amount of compound collected in one exp., (mg)	Time of collection (min)
		Exp-1	Exp-2	Exp-3		
313.0	8.0	0.17	0.16	0.16	38	360
313.0	10.0	23	22	21	151	10
313.0	12.0	54	50	49	370	10
313.0	14.0	69	74	68	485	10
313.0	16.0	84	80	86	605	10
313.0	18.0	91	86	93	665	10
313.0	20.0	97	96	91	721	10
323.0	10.0	0.67	0.64	0.65	52	120
323.0	12.0	9.6	9.1	9.0	63	10
323.0	14.0	31	29	31	209	10
323.0	16.0	53	54	49	370	10
323.0	18.0	64	62	68	455	10
323.0	20.0	73	75	78	524	10
333.0	10.0	0.11	0.10	0.10	53	720
333.0	12.0	1.6	1.5	1.5	63	60
333.0	14.0	9.5	9.0	8.8	63	10
333.0	16.0	18.3	19.7	20	123	10
333.0	18.0	35	38	38	240	10
333.0	20.0	48	52	53	340	10

CO_2 flow rate at pump head: 0.1 mL/min, pump head temperature: 268 K; Pump head pressure: experimental pressure

23. Solubility of *N,N*-di-2-ethylhexyl-*iso*-butyramide (D2EHiBA) in SCCO$_2$:

T (K)	P (MPa)	Solubility (mol/mol) y_2 Exp-1	Exp-2	Exp-3	Average amount of compound collected in one exp., (mg)	Time of collection (min)
313.0	8.0	0.062	0.059	0.058	31	720
313.0	10.0	11.5	11.2	10.9	82	10
313.0	12.0	33	30	31	240	10
313.0	14.0	44	47	48	335	10
313.0	16.0	55	58	60	425	10
313.0	18.0	67	62	67	526	10
313.0	20.0	67	72	74	530	10
323.0	10.0	0.36	0.35	0.33	92	360
323.0	12.0	7.3	7.0	6.8	53	10
323.0	14.0	18	18.2	17.3	134	10
323.0	16.0	32	32	30	239	10
323.0	18.0	43	44	46	326	10
323.0	20.0	60	59	56	468	10
333.0	10.0	0.063	0.058	0.058	64	1440
333.0	12.0	0.91	0.82	0.80	76	120
333.0	14.0	4.3	4.2	4.4	66	20
333.0	16.0	10.5	11.0	11.2	77	20
333.0	18.0	21	20	19	155	10
333.0	20.0	28	28	30	210	10

CO$_2$ flow rate at pump head: 0.1 mL/min, pump head temperature: 268 K; Pump head pressure: experimental pressure

24. Solubility of *N,N*- di-2-ethylhexylpivalamide (D2EHPVA) in SCCO$_2$:

T (K)	P (MPa)	Solubility (mol/mol) y_2 Exp-1	Exp-2	Exp-3	Average amount of compound collected in one exp., (mg)	Time of collection (min)
313.0	8.0	0.035	0.035	0.033	19	720
313.0	10.0	9.0	8.6	8.5	67	10
313.0	12.0	25	27	26	195	10
313.0	14.0	40	38	36	310	10
313.0	16.0	48	50	45	380	10
313.0	18.0	58	57	54	470	10
313.0	20.0	62	64	58	511	10
323.0	10.0	0.29	0.26	0.28	81	360
323.0	12.0	4.9	4.7	4.5	37	10
323.0	14.0	14.9	14.3	14.0	114	10
323.0	16.0	25	27	26	195	10
323.0	18.0	36	36	33	288	10
323.0	20.0	43	45	46	335	10
333.0	10.0	0.030	0.031	0.028	36	1440
333.0	12.0	0.58	0.54	0.55	52	120
333.0	14.0	3.0	3.3	3.2	67	30
333.0	16.0	8.9	8.4	8.2	68	10
333.0	18.0	16.1	15.3	15.1	125	10
333.0	20.0	26	25	24	205	10

CO$_2$ flow rate at pump head: 0.1 mL/min, pump head temperature: 268 K; Pump head pressure: experimental pressure

3.2 Results on the extraction experiments

3.2.1 Results on extraction of actinides from different matrices - Data for various plots represented in Chapter – 7

Figure 7.2		**Figure 7.3**	
Static equilibration period (min)	**Extraction efficiency (%)**	**dynamic equilibration period (min)**	**Extraction efficiency (%)**
15	42	10	87
30	72	20	92
45	91	30	92
60	92	40	92
70	92	60	92

Figure 7.4			**Figure 7.5**		
Pressure (MPa)	**Extraction efficiency (%)**	**SCCO$_2$ density (kg.m^{-3})**	**Temperature (K)**	**Extraction efficiency (%)**	**SCCO$_2$ density (kg.m^{-3})**
10	29	386.77	308	40	929.68
15	--	701.08	313	47	910.47
20	54	785.16	318	52	890.90
25	58	834.84	323	55	871.03
30	59	871.03	328	50	850.86
32.5	60	--			
35	--	899.77			

Figure 7.6			**Figure 7.7**		
HNO$_3$ concentration (N)	**Extraction efficiency (%)**		**Extraction period (min)**	**Extraction efficiency (%)**	
	DOHP	**HDEHP**		**Th**	**U**
0.1	78	99	10	40	45
0.5	77	99	20	62	70
1	78	90	40	82	86
2	49	85	60	87	91
4	29	68			

Figure 7.8						
Extraction period (min)	**Extraction efficiency (%)**					
	Th			**U**		
	TBP/CH$_3$OH	**TBP/CH$_2$Cl$_2$**	**TBP/C$_6$H$_{14}$**	**TBP/CH$_3$OH**	**TBP/CH$_2$Cl$_2$**	**TBP/C$_6$H$_{14}$**
15	92	4	1	96	5	16
30	96	9	2	98	17	29
45	96	15	5	98	35	41
60	96	21	11	98	49	51
90	-	30	21	-	61	62
120	-	34	36	-	69	72
180	-	48	56	-	76	80
240	-	61	73	-	78	84
300	-	72	80	-	79	86
360	-	77	82	-	79	88

Figure 7.9

Pressure (MPa)	313		323	
	Extraction efficiency (%)	$SCCO_2$ density ($kg.m^{-3}$)	Extraction efficiency (%)	$SCCO_2$ density ($kg.m^{-3}$)
10.3	62	651.49	41	423.74
12.3	78	727.57	74	604.62
15	88	781.32	84	701.08
20	94	840.61	92	785.16
25	96	880.15	95	834.89

Figure 7.10

Pressure (MPa)	Extraction efficiency (%)	Solubility (g/L)
10.3	41	200
12.3	74	284
15	84	314
20	92	341
25	95	355

Figure 7.11

Extraction time (min)	Extraction efficiency (%)
10	49
20	74
30	85
40	90
50	92
60	95

Figure 7.12

Conc. of HNO_3 (N)	Extraction efficiency (%)
0.1	8
0.5	14
1	28
2	55
4	80
5	85
6	88
7	85
8	81

Figure 7.14

Extraction period (min)	Extraction efficiency (%)	
	neat UO_2Cl_2	UO_2Cl_2-NaCl-CsCl
10	38	3
20	88	6
30	94	8
60	97	11
90	98	13
120	98	15

Figure 7.16

Conc. of HNO_3 (N)	Extraction efficiency (%)	
	UCl_3-LiCl-KCl	UO_2Cl_2-NaCl-CsCl
0.1	55	77
0.5	75	87
1	90	96
4	95	97
8	97	97

Figure 7.17

Pressure (MPa)	Extraction efficiency (%)		
	313 K	323 K	333 K
10	25	20	10
15	52	55	55
20	72	85	85
25	88	93	96
30	97	95	98

Figure 7.18

Temperature (K)	Extraction efficiency (%)
313	70
318	80
323	87
328	89
333	90

Figure 7.20

Extraction period (min)	Extraction efficiency (%)	
	Dynamic	Static+ dynamic
10	15	64
20	28	75
30	37	84
40	44	92
60	52	97
90	58	-
120	62	-
180	66	-

Figure 7.21

Extraction period (min)	Extraction efficiency (%)	
	Dynamic	Static+ dynamic
10	11	43
20	23	61
30	28	80
40	31	89
60	35	93
90	39	96
120	42	-
180	46	-

Figure 7.22

Extraction period (min)	Extraction efficiency (%)	
	Dynamic	Static+ dynamic
10	6	20
20	12	35
30	16	46
40	19	55
60	23	62
90	27	68
120	30	73
180	32	79

3.2.2 Analysis of metal ions using high pressure liquid chromatography (HPLC)

In the present study, uranium and thorium extracts resulting from supercritical fluid extraction (SFE) from different matrices was carried out using HPLC technique. The amount of metal ions extracted during the SFE process is estimated by injecting an aliquot into HPLC and comparing with standards (briefly described in **Chapter 2.7**). The reverse phase HPLC column was examined for its performance by separation of benzene and toluene **(Figure 3.1**). A mobile phase consisting of 50/50 vol% water/methanol was employed to separate the benzene and toluene. Benzene and toluene were monitored at 254 nm by using a UV-Visible detector. The capacity factors (k) separation factor (α), resolution (Rs) and number of theoretical plates ((N), 10 cm column) were measured and given the **Table 3.1**. The results indicated the good performance of the C_{18} support. The peaks are symmetrical with minimum "tailing".

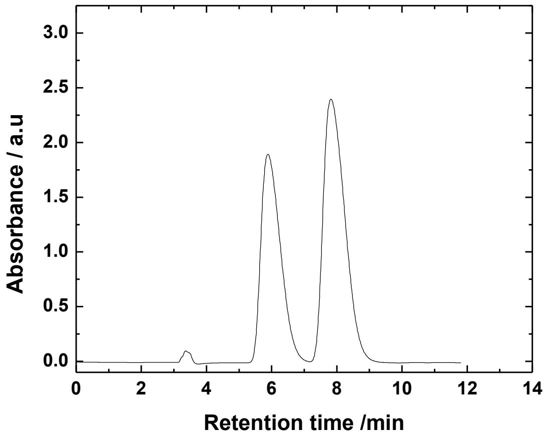

Figure 3.1 Separation of Benzene and Toluene by HPLC; column: 10 cm, 5 µm; mobile phase: 50/50 vol% water/methanol; flow rate of mobile phase: 1 mL/min sample: benzene + toluene; sample injected: 20 µL; temperature: 303 K;

Table 3.1 Separation factor for benzene and toluene

Retention time (t_R)		**k**		**α**	**R_S**	**N**
Benzene t_{RB}	**Toluene t_{RT}**	**Benzene k_B**	**Toluene k_T**			
9.2 min	11.2min	1.75	2.33	1.33	2.78	3708

Estimation of uranium/thorium/lanthanides:

A series of standard solutions of uranium / thorium / lanthanides were prepared by diluting their stock solutions respectively. The standards were injected into the HPLC system and corresponding chromatograms were recorded (**Figure 3.2, 3.3, 3.4 and 3.5**). The peak area of the standards were measured and used to prepare calibration curve. The peak area of the standards was plotted against the concentration of the standards. The calibration curves for both uranium and thorium were shown **Figure 3.6** and **3.7** respectively. The extracts containing metal ions are injected into HPLC system and corresponding peak-area was determined. From the peak area and calibration curve, the concentration of metal ions in the extract was analyzed. For uranium/thorium analysis, 0.1 M α-HIBA was employed as a mobile phase. After elution of uranium/thorium form the column, the metal ion was mixed with post column reagent (Arsenazo (III)) and the complex was monitored at 655 nm using a UV-Visible detector.

In case of samples containing both uranium and thorium, 0.1 M α-HIBA (pH=3.5) was employed to separate uranium and thorium. The complexation of uranyl ion with α-HIBA can result in the formation of different species such as $[UO_2(IBA)]^+$, $[UO_2(IBA)_2]$, $[UO_2(IBA)_3]^+$. similarly, thorium can form $[Th(IBA)]^{3+}$, $[Th(IBA)_2]^{2+}$,$[Th(IBA)_3]^+$,$[Th(IBA)_4]$. The probability of formation of different species is dependent on pH and α -HIBA concentration. From **Figure 3.5**, it was observed that at pH=3.5, thorium is eluted at 2.7 min followed by uranium at 6.1 min. Higher retention for uranyl ion at is due to the species, $[UO_2(IBA)_3]^+$ which has 3 HIBA molecules and hence results in strong hydrophobic interaction with C_{18} support. The lower retention of Th(IV) compared to U(VI) is due to the possible formation of anionic species e.g. $[Th(IBA)_4(OH)_2]^{2-}$, which is expected to have a lower retention time on C_{18}column. For lanthanides separation, a mixture of CSA + α-HIBA was employed as mobile phase.

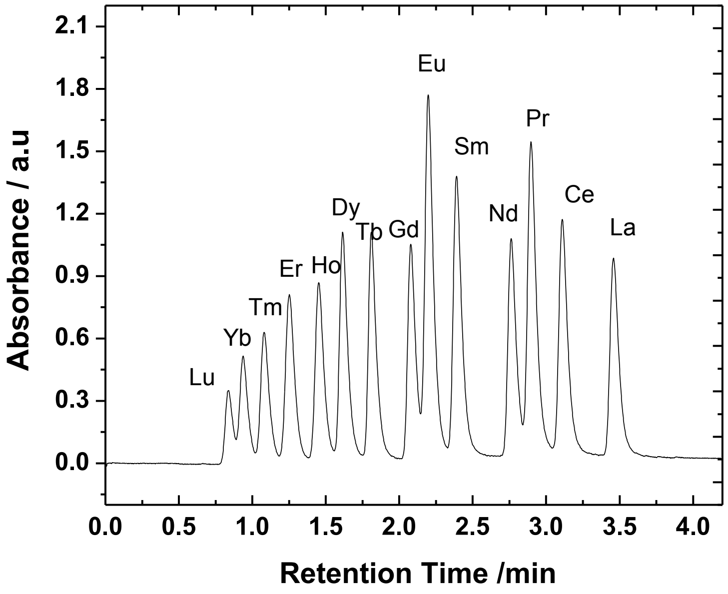

Figure 3.2 Gradient Separation of lanthanides on a Reprosil gold column; column: 3 cm, 1.8µm; mobile phase (A) 0.05M CSA + 0.05M α-HIBA (pH=3.8); (B) 0.05M CSA + 0.1M α-HIBA (pH=4.0); flow rate of mobile phase: 3 mL/min; Sample: Lanthanides (50ppm) in 0.01N HNO_3; sample injected: 5µL; temperature: 303 K.

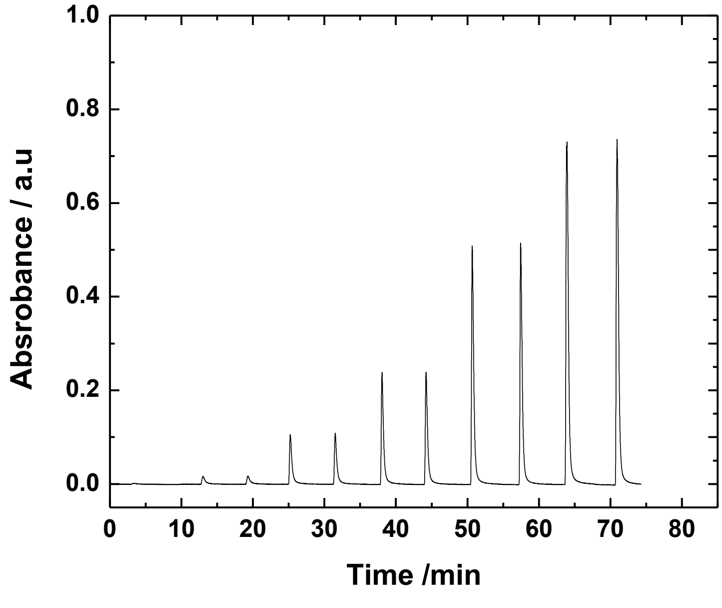

Figure 3.3 Chromatogram of a series of uranium standards; column: 10 cm, 5 µm; mobile phase: 0.1 M α-HIBA; Flow rate of mobile phase: 2 mL/min; post column reagent: Arsenazo (III), sample: uranium in 0.01N HNO_3; sample injected: 20 µL; temperature: 303 K;

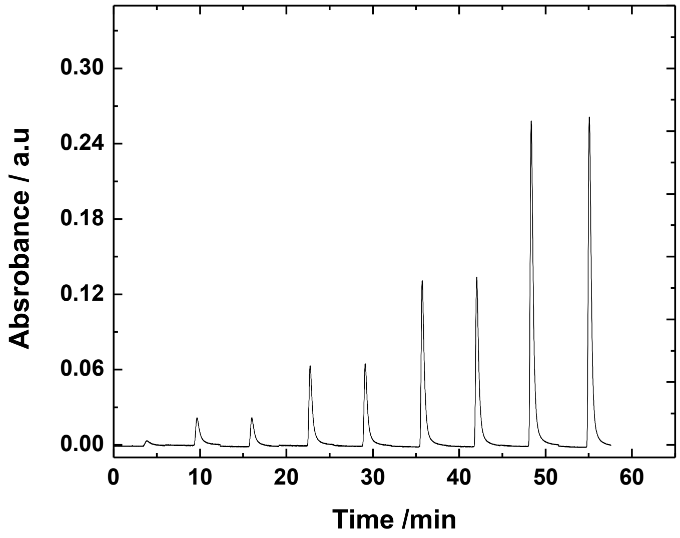

Figure 3.4 Chromatogram of a series of thorium standards; column: 10 cm, 5 µm; mobile phase: 0.1 M α-HIBA; flow rate of mobile phase: 2 mL/min; post column reagent: Arsenazo (III), sample: uranium in 0.01N HNO_3; sample injected: 20 µL; temperature: 303 K;

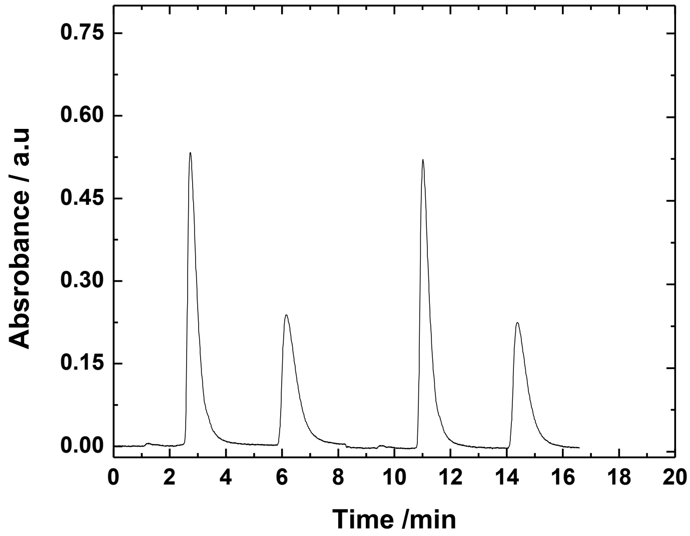

Figure 3.5 Chromatogram for uranium + thorium standard; column: 10 cm, 5 µm; mobile phase: 0.1 M α-HIBA (pH=3.5); flow rate of mobile phase: 2 mL/min; post column reagent: Arsenazo (III), sample: uranium in 0.01N HNO_3; sample injected: 20 µL; temperature: 303 K;

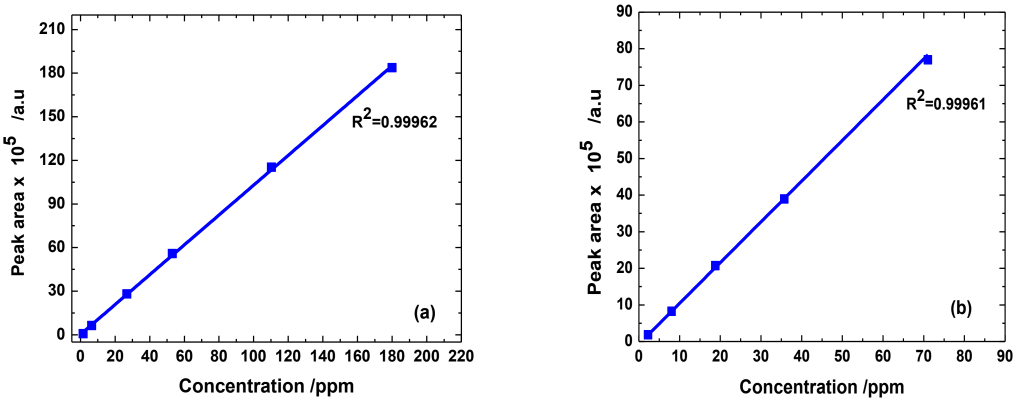

Figure 3.6 Calibration curve for (a) uranium and (b) thorium

3.3 Analysis of plutonium by liquid scintillation counting (LSC) technique

Liquid scintillation counting (LSC) technique was used for plutonium analysis in both aqueous and organic medium. Liquid scintillation cocktail is prepared by mixing appropriate quantities of naphthalene (10%), PPO (0.7%), POPOP (0.03%) and TOPO (4%) in 1,4-dioxane.

Chemical	Role in LSC
1,4-dioxane	Primary solvent
2,5-diphenyloxazole (PPO)	Primary scintillator
1,4-di-2-(5- phenyloxazolyl)benzene (POPOP)	Wavelength shifter
Naphthalene	Complexing agent
Tri-*n*-octylphosphine oxide (TOPO)	Primary solvent

The LSC system was calibrated using standard plutonium solution. Known amount of standard solution of plutonium (plutonium in 1 M HNO_3) was added to cocktail and measured the α-activity of the solution. Blank solutions were prepared in the same way, except that the plutonium containing solution was replaced with 1 M HNO_3. 1 μg of plutonium (^{239}Pu) in the cocktail gives ~ 1,60,000 counts/min. 1 mL of SFE extract containing plutonium was added to cocktail and measured for its α-activity. Based on the activity of the extract and the activity of standard plutonium solution, the concentration of plutonium is estimated.